

JSCSEN 75(4)423–594(2010)

# Journal of the Serbian Chemical Society

ersion  
lectronic

**VOLUME 75**

**No 4**

**BELGRADE 2010**

Available on line at



[www.shd.org.rs/JSCS/](http://www.shd.org.rs/JSCS/)

The full search of JSCS  
is available through

**DOAJ** DIRECTORY OF  
OPEN ACCESS  
JOURNALS

[www.doaj.org](http://www.doaj.org)



**Organic Chemistry**

- B. Tamami, A. N. Shirazi and K. Parvanak Borujeni: Poly styrene-supported aluminum chloride as an efficient and reusable catalyst for condensation of indole with various carbonyl compounds ..... 423

**Biochemistry and Biotechnology**

- M. M. Poša and K. N. Kuhajda: Influence of bile acids on the adsorption of lidocaine and verapamil in an *in vitro* experiment ..... 433
- R. S. Verma, R. K. Verma, A. Chauhan and A. K. Yadav: Changes in the essential oil composition of *Majorana hortensis* Moench. cultivated in India during plant ontogeny..... 441
- M. S. Milašinović, M. M. Radosavljević and Lj. P. Dokić: Effects of autoclaving and pululanase debranching on the resistant starch yield of normal maize starch ..... 449

**Inorganic Chemistry**

- P. S. Zhao, X. Wang, F. F. Jian, J. L. Zhang and H. L. Xiao: Crystal engineered acid–base complexes with 2D and 3D hydrogen bonding systems using *p*-hydroxybenzoic acid as the building block ..... 459
- D. Singh and K. Kumar: Macrocyclic complexes: synthesis and characterization ..... 475

**Theoretical Chemistry**

- S. Erić, M. Kalinić, A. Popović, H. Makić, E. Civić and M. Bektašević: The importance of the accuracy of the experimental data for the prediction of solubility ..... 483

**Physical Chemistry**

- R. F. de Farias and C. Airoidi: Hexamethylenetetramine reaction with graphite oxide (GO) as a strategy to increase the thermal stability of GO: synthesis and characterization of a compound ..... 497

**Electrochemistry**

- L. Wang, S. Chen, B. Yuan, F. Meng, J. Wang, C. Wang and L. Li: Digital holographic reconstruction detection of localized corrosion arising from scratches ..... 505

**Analytical Chemistry**

- R. M. Baošić, A. D. Radojević and Ž. Lj. Tešić: Prediction of the retention of  $\beta$ -diketonato complexes in TLC systems on silica gel by quantitative structure–retention relationships ..... 513

**Chemical Engineering**

- Z. Arsenijević, Ž. Grbavčić, B. Grbić, N. Radić, R. Garić-Grulović, S. Miletić, G. Savčić and B. Đorđević: Fluidized bed combustion of pesticide-manufacture liquid wastes..... 523

**Materials**

- R. E. Sabzi, K. Rezapour and N. Samadi: Polyaniline–multi-wall-carbon nanotube nanocomposites as a dopamine sensor ..... 537

**Environmental**

- V. K. Gochev, Z. I. Velkova and M. S. Stoytcheva: Hexavalent chromium removal by waste mycelium of *Aspergillus awamori* ..... 551
- M. B. Ninković, R. D. Petrović and M. D. Laušević: Removal of organochlorine pesticides from water using virgin and regenerated granular activated carbon ..... 565
- D. Marinović, M. Stojanović and D. Popović: Purification of waters and elimination of organochlorine insecticides by means of active coal ..... 575

**EuCheMS News**

- B. Karlberg, P. Worsfold and J. E. T. Andersen: European Analytical Column no. 38 from the Division of Analytical Chemistry (DAC) of the European Association for Chemical and Molecular Sciences (EuCheMS), January 2010 ..... 587



*J. Serb. Chem. Soc.* 75 (4) 423–431 (2010)  
JSCS–3975

Journal of  
the Serbian  
Chemical Society

JSCS@tmf.bg.ac.rs • www.shd.org.rs/JSCS

UDC 678.746+546.62'131:544.478+547.756

Original scientific paper

## Polystyrene-supported aluminum chloride as an efficient and reusable catalyst for condensation of indole with various carbonyl compounds

BAHMAN TAMAMI<sup>1\*</sup>, AMIR NASROLAHI SHIRAZI<sup>1</sup>  
and KAVEH PARVANAK BORUJENI<sup>2</sup>

<sup>1</sup>Department of Chemistry, Shiraz University, Shiraz 71454 and  
<sup>2</sup>College of Science, Shahrekord University, Shahrekord 115, Iran

(Received 31 August 2009, revised 8 February 2010)

**Abstract:** Crosslinked poly styrene-supported aluminum chloride (PS–AlCl<sub>3</sub>) is a stable, recyclable and environmental friendly heterogeneous catalyst for the condensation of indole with aldehydes and ketones to afford diindolymethanes. In addition, PS–AlCl<sub>3</sub> shows satisfactory selectivity in the reaction of mixtures of an aldehyde and a ketone with indole. Although AlCl<sub>3</sub> is a water sensitive, corrosive and environmentally harmful compound, PS–AlCl<sub>3</sub> is a stable and water-tolerant species. The mild reaction conditions, short reaction times, easy work-up, high to excellent yields, chemoselectivity, reuse of the catalyst for at least ten times without significant change in its catalytic activity, low cost, and easy preparation and handling of the polymeric catalyst are obvious advantages of the present method.

**Keywords:** bis-indolymethanes; indole; polystyrene; aluminum chloride.

### INTRODUCTION

Indole and its corresponding compounds have been identified as an important category of heterocyclic compounds in medicinal chemistry.<sup>1,2</sup> Among different indole derivatives, diindolymethanes are known as a privileged group because of their representation in natural products<sup>3</sup> and extensive applications in pharmaceuticals.<sup>4</sup> Diindolymethanes, which are found in marine sponges,<sup>5,6</sup> are effective in the prevention of cancer due to their ability to modulate cancer-causing estrogen metabolites.<sup>7</sup> Synthetically, the reaction of indole with aldehydes or ketones produces azafulvanium salts, which further react with another indole molecule to form bis-indolymethanes.<sup>8</sup> A great number of methods have been reported in the literature for the preparation of bis-indolymethanes in which protic acids,<sup>9</sup> as well as Lewis and other acids, such as LiClO<sub>4</sub>,<sup>10</sup> montmoril-

\* Corresponding author. E-mail: tamami@chem.susc.ac.ir  
doi: 10.2298/JSC090831026T



Ionite K10,<sup>11</sup> HClO<sub>4</sub> (TP P),<sup>12</sup> CeCl<sub>3</sub>·7H<sub>2</sub>O,<sup>13</sup> Amberlyst-15,<sup>14</sup> KHSO<sub>4</sub>,<sup>15</sup> zeo-karb-225,<sup>16</sup> poly indole salt,<sup>17</sup> La(PFO)<sub>3</sub>,<sup>18</sup> PEG-supported sulfonic acid,<sup>19</sup> ZrOCl<sub>2</sub>·8H<sub>2</sub>O/silica gel<sup>20</sup> and heteropolyacids,<sup>21,22</sup> are employed. Ionic liquids in conjugation with In(OTf)<sub>3</sub> or FeCl<sub>3</sub>·6H<sub>2</sub>O<sup>23</sup> were also reported to be useful media for this transformation. Although these methods were appropriate, many of them are associated with several drawbacks, including the requirement of large or stoichiometric amount of catalysts due to their deactivation by the nitrogen-containing reactants, low yields, long reaction time, expensive catalysts, exhausting work-up and the generation of environmentally perilous waste material as a result of the required extraction procedures.

Due to their wide range of biological, industrial and synthetic applications, the preparation of bis-indolylmethanes has received renewed attention of researchers interested in the discovery of improved protocols. In continuation of ongoing research on the use of heterogeneous polystyrene-supported aluminum chloride as a Lewis acid catalyst in organic reactions<sup>24–26</sup>, herein this polymeric catalyst is introduced for the efficient electrophilic substitution of indole with a variety of carbonyl compounds.

#### EXPERIMENTAL

All chemicals were purchased from Merck or Fluka. Polystyrene (8 % divinylbenzene, prepared *via* suspension polymerization using polyvinylpyrrolidone 90 K as the suspension agent, grain size range: 0.25–0.6 mm) was obtained from the Iran Polymer and Petrochemical Institute. All products are known compounds and were identified by comparison of their physical and spectral data with those of authentic samples. The capacity of the catalyst was determined by the Mohr titration method and atomic absorption technique using a Philips atomic absorption instrument. Reaction monitoring and purity determination of the products were accomplished by TLC on silica-gel polygram SILG/UV254 plates. The IR spectra were recorded on a Shimadzu FTIR-8300 spectrophotometer,  $\nu_{\max}$  in cm<sup>-1</sup>. The <sup>1</sup>H-NMR (250 MHz) and <sup>13</sup>C-NMR (62.5 MHz) were recorded on a Bruker Advanced DPX-250, FT-NMR spectrometer,  $\delta$  in ppm. The mass spectra were recorded on a Shimadzu GC MS-QP 1000 EX instrument. Microanalyses were performed on a Perkin-Elmer 240-B microanalyzer. Melting points were recorded on a Büchi B-545 apparatus in open capillary tubes.

##### *Preparation of PS-AlCl<sub>3</sub>*

Anhydrous AlCl<sub>3</sub> (4.5 g) was added to polystyrene (8 % divinylbenzene, 3.5 g) in carbon disulfide (25 mL) as the reaction medium. The mixture was stirred using a magnetic stirrer under reflux condition for 50 min, cooled and then water (40 mL) was cautiously added to hydrolyze the excess AlCl<sub>3</sub>. The mixture was stirred until the deep orange color disappeared and the polymer became light yellow. The polymer beads were filtered and washed with water (350 mL) and then with acetone and diethyl ether. The polymer was dried in a vacuum oven for 12 h at room temperature. The capacity of the polymeric catalyst based on its chloride content was 0.40 mmol AlCl<sub>3</sub>/g catalyst.<sup>24–26</sup>

##### *General procedure for the condensation of carbonyl compounds with indole*

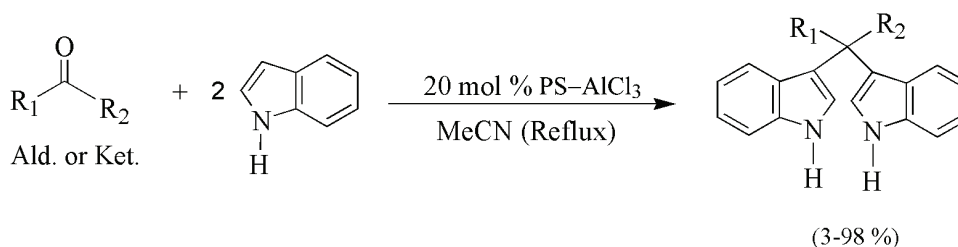
In a round bottom flask (25 mL) equipped with a condenser and a magnetic stirrer, a solution of the required carbonyl compound (1.0 mmol) and indole (2.0 mmol) in 10 mL MeCN

was prepared. PS-AlCl<sub>3</sub> (0.20 mmol) was added to the solution and the reaction mixture was stirred magnetically under reflux conditions. The progress of the reaction was followed by TLC. After completion of the reaction, the catalyst was filtered off and washed with Et<sub>2</sub>O (2×15 mL) and the filtrate concentrated on a rotary evaporator under reduced pressure to give the desired product. When required, the products were purified by column chromatography so as to afford the pure bis-indolylmethanes. The spent catalyst from different experiments was washed with Et<sub>2</sub>O, dried and used again.

#### RESULTS AND DISCUSSION

PS-AlCl<sub>3</sub> was prepared by addition of anhydrous AlCl<sub>3</sub> to polystyrene (8 % divinylbenzene) in carbon disulfide under reflux conditions. The Mohr titration method<sup>27</sup> and the atomic absorption technique were employed to determine the capacity. The capacity of the polymeric catalyst was 0.40 mmol AlCl<sub>3</sub> per gram of catalyst. Although AlCl<sub>3</sub> is a water sensitive, corrosive and environmentally harmful compound, PS-AlCl<sub>3</sub> is a stable and water tolerant species (as a bench-top catalyst). This catalyst is easy to prepare, stable, storable in air for a long time without any change, easily recycled and reused without appreciable loss of activity.

In order to optimize the reaction conditions, PS-AlCl<sub>3</sub> was employed as the catalyst for the condensation of indole and benzaldehyde in different solvents, *i.e.*, MeCN, THF, CH<sub>2</sub>Cl<sub>2</sub>, EtOH, toluene, Et<sub>2</sub>O and cyclohexane. Acetonitrile proved to be the best medium. It was found that 0.20:1.0:2.0 mmol ratio of catalyst/benzaldehyde/indole was sufficient to obtain the desired diindolylmethanes in 95 % yield within 1 h under reflux conditions (Scheme 1).



Scheme 1.

Next, (PS-AlCl<sub>3</sub>)-catalyzed electrophilic substitution reactions of indole with a variety of aldehydes and ketones were performed to better understand the generality of this method (Table I).

As can be seen in Table I (entries 1–16), aromatic, aliphatic and heterocyclic aldehydes underwent electrophilic substitution reaction with indole effectively to afford a wide range of substituted diindolylmethanes. Substrates with an electron-withdrawing substituent gave excellent yields in comparison with those carrying an electron-donating group, but the difference in time was not significant (entries 2–10). Both *o*-substituted and *p*-substituted aromatic aldehydes gave high yields. It was also found that the reaction of terephthalaldehyde (entry 16) with 4

equivalents of indole proceeded rapidly under similar conditions to afford *p*-bis-(diindolylmethyl)benzene in high yield (Scheme 2).

TABLE I. PS-AlCl<sub>3</sub> catalyzed synthesis of diindolylmethane derivatives (all reactions were performed under reflux in CH<sub>3</sub>CN. Ratio of catalyst/carbonyl compound/indole was 0.20:1.0:2.0)

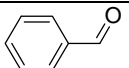
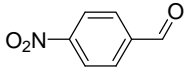
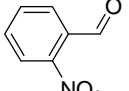
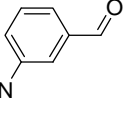
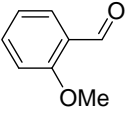
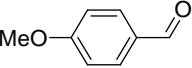
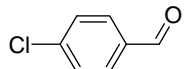
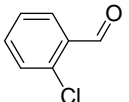
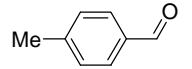
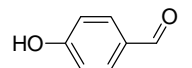
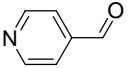
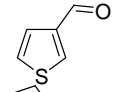
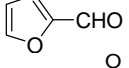
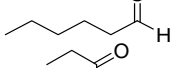
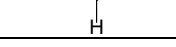

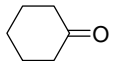
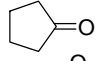
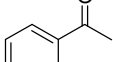
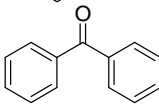
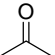
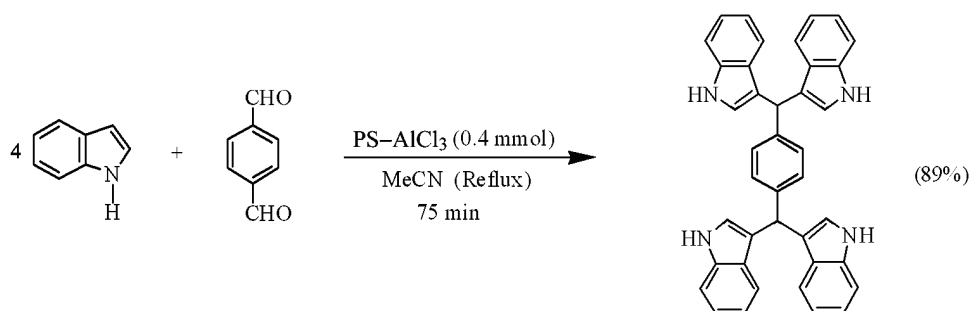
Entry	Carbonyl compound <sup>a</sup>	Time, min	Yield, % <sup>b</sup>	References for known compounds
1		60	95	28
2		80	98	16
3		80	90	28
4		65	93	29
5		75	85	18
6		75	89	28
7		80	93	28
8		30	83	28
9		50	89	10
10		55	85	17
11		75	89	29
12		65	90	30
13		80	87	28
14		120	79	10
15		120	75	15

TABLE I. Continued

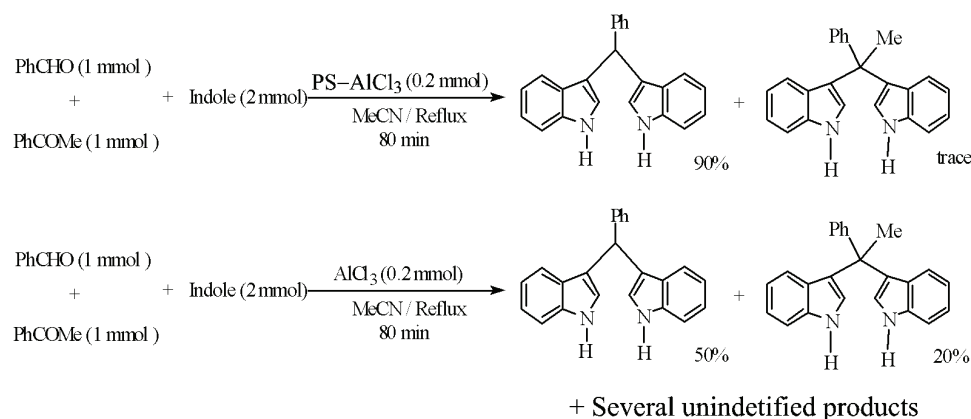
Entry	Carbonyl compound <sup>a</sup>	Time, min	Yield, % <sup>b</sup>	References for known compounds
16		75	89	28
17		150	76	28
18		200	65	28
19		220	3	28
20		240	0	–
21		240	55	31

<sup>a</sup>All products are known compounds and were identified by comparison of their physical and spectral data with those of the corresponding authentic sample; <sup>b</sup>isolated yields



Ketones required a longer reaction time and were obtained in moderate yields (entries 17–21). This striking difference in reactivity prompted an investigation of the applicability of the present method for the chemoselective electrophilic substitution reaction of indole with aldehydes and ketones. Thus, equimolar mixtures of aldehydes and ketones were allowed to react with indole in the presence of PS-AlCl<sub>3</sub>. As shown in Scheme 3, the catalyst was able to discriminate between aldehydes and ketones. The observed chemoselectivity of PS-AlCl<sub>3</sub> makes it suitable for the selective reaction of aldehydes in the presence of keto carbonyl functions and hence it can be employed in the synthesis of complex molecules by multistep processes. The chemoselectivity of PS-AlCl<sub>3</sub> toward aldehydes and ketones is presumably due to its mild catalytic activity and also to the difference in bulkiness of the carbonyl compounds. It is noteworthy that PS-AlCl<sub>3</sub> showed a higher chemoselectivity than that of AlCl<sub>3</sub> in the reaction of indole with a mix-

ture of aldehyde and ketones (Scheme 3). This is probably due to the higher reactivity of  $\text{AlCl}_3$ , *i.e.*, stronger Lewis acidity, and therefore lower selectivity.



Scheme 3.

Representative spectral data of some of the obtained compounds are given below.

*3,3'-(Phenylmethylene)bis-1H-indole (entry 1)*. Pink solid. Yield: 95 %; m.p. 141–143 °C (Lit.<sup>28</sup> 140–142 °C). IR (K Br,  $\text{cm}^{-1}$ ): 3402, 3051, 1618, 1600.  $^1\text{H-NMR}$  (250 MHz,  $\text{CDCl}_3$ ,  $\delta$  / ppm): 5.86 (1H, *s*, C–H), 6.66 (2H, *s*, C–H), 7.11 (2H, *t*, ArH,  $J = 6.9$  Hz), 7.14–7.22 (3H, *m*, ArH), 7.28–7.31 (2H, *m*, ArH), 7.35–7.42 (6H, *m*, ArH), 7.93 (2H, *broad NH*).  $^{13}\text{C-NMR}$  (60 MHz;  $\text{CDCl}_3$ ,  $\delta$  / ppm): 31.6, 110.9, 111.9, 118.4, 119.5, 121.2, 124.0, 126.3, 127.1, 128.5, 128.6, 137.0, 145.2.

*3,3'-[(2-Nitrophenyl)methylene]bis-1H-indole (entry 3)*. Yellow solid. Yield: 90 %; m.p. 140–142 °C (Lit.<sup>28</sup> 139–141 °C).  $^1\text{H-NMR}$  (250 MHz;  $\text{CDCl}_3$ ,  $\delta$  / ppm): 5.24 (1H, *s*, ArCH), 6.55 (2H, *s*, ArH), 7.10–7.87 (12H, *m*, ArH), 8.36 (2H, *broad d*,  $2 \times \text{NH}$ ,  $J = 8.6$  Hz).  $^{13}\text{C-NMR}$  (60 MHz,  $\text{CDCl}_3$ ,  $\delta$  / ppm): 34.9, 111.5, 111.6, 119.5, 120.7, 121.9, 122.2, 124.3, 126.8, 129.6, 131.2, 132.6, 134.2, 136.8, 149.7.

*3,3'-(2-Furanylmethylene)bis-1H-indole (entry 13)*. Brown solid. Yield: 87 %; m.p. 317–319 °C (Lit.<sup>28</sup> 316–318 °C). IR (KBr,  $\text{cm}^{-1}$ ): 3410, 1712, 1450.  $^1\text{H-NMR}$  (250 MHz,  $\text{CDCl}_3$ ,  $\delta$  / ppm): 5.97 (1H, *s*, ArCH), 6.90 (2H, *s*, ArH), 7.08–7.43 (11H, *m*, ArH), 8.00 (2H, *broad*,  $2 \times \text{NH}$ ).  $^{13}\text{C-NMR}$  (60 MHz,  $\text{CDCl}_3$ ,  $\delta$  / ppm): 34.8, 106.5, 110.2, 111.3, 112.2, 118.0, 119.3, 119.7, 121.7, 124.3, 126.3, 135.9, 142.0.

*3,3',3'',3'''-(1,4-Phenylenedimethyldiyne)tetrakis-1H-indole (entry 16, Scheme 2)*. Pink solid. Yield: 89 %; m.p. 193 °C (dec.) (Lit.<sup>28</sup>, 191 °C).  $^1\text{H-NMR}$  (250 MHz,  $\text{CDCl}_3$ ,  $\delta$  / ppm): 5.87 (2H, *s*, ArCH), 6.54 (4H, *s*, ArH), 7.09–7.18



(8H, *m*, ArH), 7.28–7.41 (12H, *m*, ArH), 8.14 (4H, *broad*, 4×NH). <sup>13</sup>C-NMR (60 MHz, CDCl<sub>3</sub>, δ / pp m): 30.7, 111.8, 117.9, 118.1, 119.4, 121.1, 124.0, 126.6, 127.9, 137.0, 142.7.

The feasibility of recycling the catalyst was also examined. After completion of the reaction of indole with benzaldehyde, the polymer was filtered and washed with diethyl ether, dried in a vacuum oven at room temperature for 12 h and re-used for the reaction of indole with the same or different aldehydes. As is shown in Table II, the efficiency of the recycled catalyst had not changed appreciably after ten cycles.

TABLE II. Comparison of the efficiencies of the recycled catalyst in the condensation of indole with benzaldehyde within 60 min

Entry	No. of cycles	Yield, % <sup>a</sup>
10		95
21		90
32		90
43		90
54		85
65		85
76		85
87		85
98		85
109		85

<sup>a</sup>Isolated yields

A comparison of the efficiency of the PS–AlCl<sub>3</sub> catalyst with some of those reported in the literature is given in Table III. As can be seen, in addition to having the general advantages attributed to polymeric supported catalysts, PS–AlCl<sub>3</sub> has a good efficiency compared to many of the other reported catalysts. The present procedure is superior in comparison with BF<sub>3</sub>, Et<sub>2</sub>O or AlCl<sub>3</sub> catalysts employed in the reaction of acetone with indole, which are reported to lead to the production of several unidentified products.<sup>32–36</sup>

TABLE III. Comparison of the efficiencies of a number of different reported catalysts with that of PS–AlCl<sub>3</sub> in the condensation of indole with benzaldehyde

Entry	Cataly	st/solvent	Time, min	Yield, % <sup>a</sup>	Ref.
1	PS–AlCl	<sub>3</sub> /CH <sub>3</sub> CN	60	95	–
2	In(OTf)	<sub>3</sub> /CH <sub>3</sub> CN	25	71	23
3	LiClO	<sub>4</sub> /CH <sub>3</sub> CN	120	80	10
4	ZrOCl	<sub>2</sub> ·8H <sub>2</sub> O, solvent-free	<del>80</del>		20
5	La(PFO)	<sub>3</sub> /CH <sub>3</sub> CN	30	90	18
6	PPh	<sub>3</sub> ·HClO <sub>4</sub> /CH <sub>3</sub> CN	30	61	12
7	AIPW	<sub>12</sub> O <sub>40</sub> /CH <sub>3</sub> CN	15	92	21
8	Zeokarb-225/CH	<sub>3</sub> CN	450	95	16

<sup>a</sup>Isolated yields

## CONCLUSIONS

In conclusion, a highly efficient polymer-supported catalyst has been introduced for the reaction of indole with carbon yl compounds, to afford diindolylmethanes in good to excellent yields. Although  $\text{AlCl}_3$  is a water sensitive, corrosive and environmentally harmful compound,  $\text{PS-AlCl}_3$  is a stable and water tolerant species. The mild reaction conditions, short reaction times, easy work-up, high to excellent yields, chemoselectivity, reuse of the catalyst for at least ten times without significant change in its catalytic activity, low cost, and easy preparation and handling of the polymeric catalyst are the obvious advantages of the present method.

*Acknowledgements.* We gratefully acknowledge the partial support of this study by the Shiraz University and the Shahrekord University Research Council. In addition, the help of Mr. Gh. R. Nejabat in this work is appreciated.

## ИЗВОД

АЛУМИНИЈУМ-ХЛОРИД НА ПОЛИСТИРЕНСКОМ НОСАЧУ КАО ЕФИКАСАН И  
ВИШЕКРАТНО УПОТРЕБЉИВ КАТАЛИЗАТОР У РЕАКЦИЈИ КОНДЕНЗАЦИЈЕ  
ИНДОЛА И РАЗЛИЧИТИХ КАРБОНИЛНИХ ЈЕДИЊЕЊА

BAHMAN TAMAMI<sup>1</sup>, AMIR NASROLAHI SHIRAZI<sup>1</sup> и KAVEH PARVANAK BORUJENI<sup>2</sup>

<sup>1</sup>Department of Chemistry, Shiraz University, Shiraz 71454 и <sup>2</sup>College of Science,  
Shahrekord University, Shahrekord 115, Iran

Алуминијум-хлорид везан за умрежени полистирен ( $\text{PS-AlCl}_3$ ) је стабилан хетероген катализатор, подложен рециклирању и није штетан по животну средину. Ефикасан је као катализатор у реакцији кондензације индола са алдехидима и кетонима, при чему се добијају дииндолилметани.  $\text{PS-AlCl}_3$  показује задовољавајућу селективност у реакцијама индола са смешом алдехида и кетона. Без обзира на то што је  $\text{AlCl}_3$  осетљив према води, корозиван и штетан према животној средини,  $\text{PS-AlCl}_3$  је стабилан и отпоран на присуство воде. Благо реакциони услови, кратко реакционо време, лака обрада реакционе смеше, висок до одличан принос реакција, хемоселективност, могућност вишеструке употребе катализатора до 10 пута без уочљивог губитка каталитичких својстава, ниска цена и лакоћа у припреми и руковању полимерног катализатора, очигледне су предности описаног поступка.

(Примљено 31. августа 2009, ревидирано 8. фебруара 2010)

## REFERENCES

1. R. J. Sundberg, *The Chemistry of Indoles*, Academic Press, New York, 1996
2. S. Hibino, T. Chozi, *Nat. Prod. Rep.* **18** (2001) 66
3. S. A. Morris, R. J. Anderson, *Tetrahedron* **46** (1990) 715
4. A. Ramirez, S. Garcia-Rubio, *Curr. Med. Chem.* **10** (2003) 1891
5. F. Y. Miyake, K. Yakushijin, D. A. Horne, *Org. Lett.* **4** (2002) 941
6. B. Jiang, C. G. Yang, J. Wang, *J. Org. Chem.* **67** (2002) 1396
7. J. J. Michnovicz, H. L. Bradlow, in *Food Phytochemicals for Cancer Prevention 1: Fruits and Vegetables*, M. J. Huang, T. Osawa, C. T. Ho, R. T. Rosen, Eds., American Chemical Society, Washington DC, 1994, pp. 282–293

8. W. A. Remers, R. K. Browns, in *The Chemistry of Heterocyclic Compounds*, Vol. 25, Part I, W. J. Houlihan, Ed., John Wiley and Sons, New York, 1972, p. 1
9. M. Roomi, S. MacDonald, *Can. J. Chem.* **48** (1970) 139
10. J. S. Yadav, B. V. S. Reddy, C. V. S. R. Murthy, G. Mahesh Kumar, C. Madan, *Synthesis* (2001) 783
11. M. Chakrabarty, N. Ghosh, R. Basak, Y. Harigaya, *Tetrahedron Lett.* **43** (2002) 4075
12. R. Nagarajan, P. T. Perumal, *Synth. Commun.* **32** (2002) 105
13. C. C. Silveira, S. R. Mendes, F. M. Libero, E. J. Lenardao, G. Perin, *Tetrahedron Lett.* **54** (2009) 6060
14. C. Ramesh, J. Baneree, R. Pal, B. Das, *Adv. Synth. Catal.* **345** (2003) 557
15. R. Nagarajan, P. T. Perumal, *Chem. Lett.* **33** (2004) 288
16. C. J. Magesh, R. Nagarajan, M. Karthik, *Appl. Catal. A* **266** (2004) 1
17. S. Palaniappan, A. John, *J. Mol. Catal. A* **242** (2005) 168
18. L. Wang, J. H. Han, T. Sheng, J. Z. Fan, X. Tang, *Synlett* (2005) 337
19. S. R. Sheng, Q. Y. Wang, Y. Ding, X. L. Liu, M. Z. Cai, *Catal. Lett.* **128** (2009) 413
20. H. Firouzabadi, N. Iranpoor, M. Jafarpour, A. Ghaderi, *J. Mol. Catal. A* **253** (2006) 249
21. N. Azizi, L. Torkian, M. R. Saidi, *J. Mol. Catal. A* **275** (2007) 109
22. H. Firouzabadi, N. Iranpoor, A. A. Jafari, *J. Mol. Catal. A* **244** (2006) 168
23. S.-J. Ji, M.-F. Zhou, D.-G. Gu, Z.-Q. Jiang, T. P. Loh, *Eur. J. Org. Chem.* (2004) 1584
24. B. Tamami, K. Parvanak Borujeni, *Tetrahedron Lett.* **45** (2004) 715
25. B. Tamami, K. Parvanak Borujeni, *Synth. Commun.* **34** (2004) 65
26. B. Tamami, K. Parvanak Borujeni, *Catal. Commun.* **8** (2007) 1191
27. I. M. Kolthoff, E. B. Sandell, *Textbook of Quantitative Inorganic Analysis*, 3<sup>rd</sup> ed., Macmillan Company, New York, 1965, p. 451
28. A. Hasaninejad, A. Zare, H. Sharghi, K. Niknam, M. Shekouhy, *Arkivoc*, Part xiv, 2007, 39
29. G. V. M. Sharma, J. J. Reddy, P. S. Lakshmi, P. R. Krishna, *Tetrahedron Lett.* **45** (2004) 7729
30. V. T. Kamble, K. R. Kadam, N. S. Joshi, D. B. Muley, *Catal. Commun.* **8** (2007) 498
31. J. T. Li, H. J. Dai, W. Z. Xu, T. S. Li, *Ultrasonics Sonochem.* **13** (2006) 24
32. A. Chatterjee, S. Manna, J. Banerji, C. Pascard, T. Prange, J. Shoolery, *J. Chem. Soc. Perkin Trans. 1* (1980) 553
33. J. Banerji, A. Chatterjee, S. Manna, C. Pascard, T. Prange, J. Shoolery, *Heterocycles* **15** (1981) 325
34. E. Roder, *Arch. Pharm.* **305** (1972) 96
35. E. Roder, *Arch. Pharm.* **305** (1972) 117
36. W. Noland, M. Venkiteswaren, C. Richards, *J. Org. Chem.* **26** (1961) 4241.





*J. Serb. Chem. Soc.* 75 (4) 433–440 (2010)  
JSCS–3976

Journal of  
the Serbian  
Chemical Society

JSCS@tmf.bg.ac.rs • www.shd.org.rs/JSCS

UDC 547.93+541.183:57.04:547.933

Original scientific paper

## Influence of bile acids on the adsorption of lidocaine and verapamil in an *in vitro* experiment

MIHALJ M. POŠA<sup>1\*</sup> and KSENIJA N. KUHAJDA<sup>2#</sup>

<sup>1</sup>Department of Pharmacy, Faculty of Medicine, University of Novi Sad, Hajduk Veljkova 3, 21000 Novi Sad and <sup>2</sup>Department of Chemistry, Faculty of Sciences, University of Novi Sad, Trg D. Obradovića 3, 21000 Novi Sad, Serbia

(Received 10 August, revised 6 October 2009)

**Abstract:** The work is concerned with the influence of the structure of bile acids (cholic, deoxycholic, chenodeoxycholic, and their keto derivatives) on the *in vitro* adsorption of lidocaine and verapamil from an aqueous phase to rat's intestine membrane. Transport of lidocaine from an aqueous medium to the rat's intestine membrane was significantly increased ( $p < 0.05$ ) only by 7-ketodeoxycholic acid, whereas an analogous increase in verapamil transport was produced only by cholic acid. It appeared that, of all the tested bile acids, these two acids form the most stable complexes (by hydrogen bonds) with the respective drug.

**Keywords:** lidocaine; verapamil; bile acids.

### INTRODUCTION

Bile acids belong to a special group of surface active molecules, so-called amphiphilic molecules. They are planar polar molecules in which the hydrophobic and hydrophilic surfaces are separated.<sup>1–4</sup> Thanks to this property, bile acids show several pharmacological features, such as relaxation of smooth muscles of the endothelium,<sup>5</sup> lowering of the glucose blood level<sup>6</sup> and the like. In addition, bile acids exhibit a promotive effect in the action of some drugs (insulin, quinidine, morphine, *etc.*).<sup>6,7</sup>

In previous investigations,<sup>8</sup> 7-ketodeoxycholic and 12-ketochenodeoxycholic acids, as well as cholic acid, showed promotive effects on the anesthetic action of lidocaine in infiltrational tail anesthesia of rats. <sup>1</sup>H-NMR measurements<sup>9</sup> showed that lidocaine in deuterated chloroform forms hydrogen-bond complexes with some bile acids (keto derivatives of cholic, deoxycholic and chenodeoxycholic acids). Kinetic studies revealed a positive correlation between the forma-

\* Corresponding author. E-mail: junposam@eunet.rs

# Serbian Chemical Society member.

doi: 10.2298/JSC080810029P



tion constant of the bile acid–lidocaine complexes and the promotive action of the bile acids on the transfer of lidocaine from an aqueous phase to chloroform (model of cell membrane) if the bile acids were present in the organic phase (pretreatment model).<sup>9</sup> In the mechanism of the promotive action of bile acids on the transport of drugs through the cell membrane, their interaction with membrane phospholipids plays an important role.<sup>10,11</sup>

In view of the above facts, the aim of this work was to investigate the effect of bile acids (cholic, deoxycholic and chenodeoxycholic, and their keto derivatives) (Fig. 1, Table I) on the transfer of lidocaine from an aqueous phase to the membrane of rat intestine (*in vitro*) pretreated with the corresponding bile acid solution. Namely, the objective was to establish whether bile acids exhibit the same structure–activity relationship as in the transfer of lidocaine from an aqueous phase to chloroform, *i.e.*, how well can chloroform model a biological membrane. In addition, the aim was to examine the action of bile acids on the transport of verapamil to the rat intestine membrane. Namely, in contrast to the lidocaine molecule, which has one proton-donor group (amide group) and one proton-acceptor group (tertiary amine group), the verapamil molecule has only proton-acceptor groups (methoxy, nitrile and tertiary amine groups). The application of verapamil may indicate the importance of hydrogen bonds in the formation of bile acid complexes, and thus in the promotive action of bile acids.

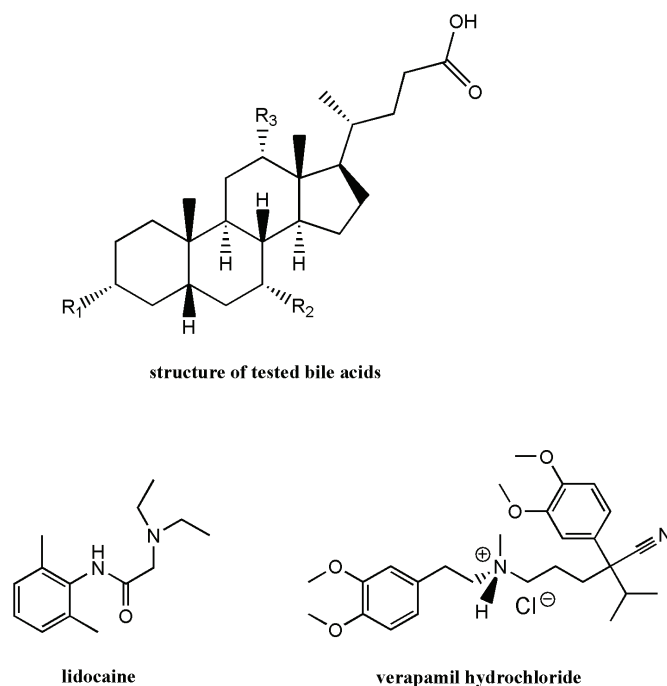


Fig. 1. Structures of tested bile acids and lidocaine and verapamil hydrochloride.

TABLE I. The tested bile acids

Position of hydroxyls and keto groups (Fig. 1)	Bile acid
$R_1 = R_2 = R_3 = OH$	3 $\alpha$ ,7 $\alpha$ ,12 $\alpha$ -trihydroxy-5 $\beta$ -cholanoic acid (cholic acid)
$R_1 = R_3 = OH$ ; $R_2 = H$	3 $\alpha$ ,12 $\alpha$ -dihydroxy-5 $\beta$ -cholanoic acid (deoxycholic acid)
$R_1 = R_2 = OH$ ; $R_3 = H$	3 $\alpha$ ,7 $\alpha$ -dihydroxy-5 $\beta$ -cholanoic acid (chenodeoxycholic acid)
$R_1 = R_3 = OH$ ; $R_2 = O$	3 $\alpha$ ,12 $\alpha$ -dihydroxy-7-keto-5 $\beta$ -cholanoic acid (7-ketodeoxycholic acid)
$R_1 = R_2 = OH$ ; $R_3 = O$	3 $\alpha$ ,7 $\alpha$ -dihydroxy-12-keto-5 $\beta$ -cholanoic acid (12-ketochenodeoxycholic acid)
$R_3 = OH$ ; $R_1 = R_2 = O$	12 $\alpha$ -hydroxy-3,7-diketo-5 $\beta$ -cholanoic acid
$R_1 = OH$ ; $R_2 = R_3 = O$	3 $\alpha$ -hydroxy-7,12-diketo-5 $\beta$ -cholanoic acid (7,12-diketolithocholic acid)
$R_1 = R_2 = R_3 = O$	3,7,12-triketo-5 $\beta$ -cholanoic acid
$R_1 = OH$ ; $R_3 = O$ ; $R_2 = H$	3 $\alpha$ -hydroxy-12-keto-5 $\beta$ -cholanoic acid (12-ketodeoxylithocholic acid)
$R_1 = R_3 = O$ ; $R_2 = H$	3,12-diketo-5 $\beta$ -cholanoic acid
$R_1 = OH$ ; $R_2 = O$ ; $R_3 = H$	3 $\alpha$ -hydroxy-7-keto-5 $\beta$ -cholanoic acid (7-ketolithocholic acid)
$R_1 = R_2 = O$ ; $R_3 = H$	3,7-diketo-5 $\beta$ -cholanoic acid

## EXPERIMENTAL

*Material*

Cholic, deoxycholic and chenodeoxycholic acids (Sigma, New Zealand, 98 %) were used as the starting compounds for the synthesis of their keto derivatives. The syntheses of keto derivatives of all the three bile acids, and their transformation to sodium salts were performed as described in previous articles.<sup>1,3,4</sup>

*Determination of the influence of sodium salts of bile acids on the in vitro adsorption of lidocaine and verapamil in the small intestine*

The small intestine (5 cm) was taken from an ether-anesthetized Wistar rat and prepared according to Al-Salami *et al.*<sup>12</sup> Then, the intestine was cut into small pieces and placed in Tyrode solution (pH 7.4  $H_2PO_4^-/HPO_4^{2-}$ ) containing the dissolved sodium salt of a bile acid, so that the bile acid concentration was identical to the critical micellar concentration<sup>3,4</sup> (the control was Tyrode solution without bile acid). The intestine was soaked in Tyrode solution with bile acid for 24 h under a constant flow of oxygen and stirring (50 rpm) – this phase of the experiment served to pretreat the intestine with bile acid. Subsequently, the intestine was removed from the bile acid solution and washed with Tyrode solution (25 ml). Then, the intestine pieces were transferred to Tyrode solution containing either lidocaine hydrochloride (10 ml, 40 mM) or verapamil hydrochloride (10 ml, 40 mM) and left in contact with the given drug (magnetic stirrer, 50 rpm) for 5 min. After that, a sample of the solution (750  $\mu$ l) was taken to determine spectrophotometrically the concentration of the tested drug (the blank was Tyrode solution, Agilent 8453). Lidocaine was measured at a wavelength of 263 nm and verapamil at 280 nm, using the corresponding calibration graph.

*Data treatment*

The results were treated (paired-samples *t*-test) using the SPSS10.0 package for Windows.

## RESULTS AND DISCUSSION

In pharmacodynamic investigations of the promotive action of bile acids on drug transport, it is customary to treat experimental animals first with the bile acid and then with the drug.<sup>6,7,13</sup> Hence, the test of the influence of bile acids on the resorption of lidocaine and verapamil in the intestine membrane was preceded by treatment with solutions of the sodium salts of bile acids and the decrease in the concentration of the tested drug was measured after 5 min. Namely, the effect of the tested bile acid on the drug concentration in the solution after intestine soaking for 10 min did not differ from that for the blank, as the greatest change in the drug concentration occurred in the first 5 min.

The concentrations of the tested drugs measured 5 min after the application in the *in vitro* experiment are given in Table II, from which it can be seen that a higher degree of resorption after 5 min was registered for verapamil in the control experiment than for lidocaine, which could be expected based on the higher lipophilicity of verapamil (lidocaine,  $\log P = 2.26$ ; verapamil,  $\log P = 3.45$ ).<sup>14,15</sup> The decrease in the lidocaine concentration was significant in the presence of 7-ketodeoxycholic acid. Namely, lidocaine and 7-ketodeoxycholic acid form a hydrogen-bonded complex with a larger formation constant ( $K = 14.22 \text{ dm}^3 \text{ mol}^{-1}$ ) compared to the other tested bile acids, the complex formation constants of which are in the range  $1\text{--}9 \text{ dm}^3 \text{ mol}^{-1}$ .<sup>9</sup> A significant decrease in the verapamil concentration was evidenced when the intestine membrane was pretreated with sodium cholate. Namely, in contrast to lidocaine, the verapamil molecule contains only proton-acceptor groups (methoxy, nitrile and tertiary amine groups), which means that verapamil forms hydrogen-bonded complexes with those bile acids which

TABLE II. Concentrations of tested drugs measured 5 min after application in the *in vitro* experiment (starting concentrations:  $c$  (lidocaine) = 40mM;  $c$  (verapamil) = 40 mM)

Bile acid	$c(\text{lidocaine})^a / \text{mM}$	$c(\text{verapamil})^a / \text{mM}$
Control	35.12±4.74	31.78±3.31
Deoxycholic	31.70±4.09	28.38±3.52
Chenodeoxycholic	32.02±3.50	28.91±4.12
Cholic	30.17±3.98	25.80±3.19 <sup>b</sup>
12-Ketolithocholic	34.09±2.61	32.00±2.50
3,12-Diketo-5 $\beta$ -cholanoic	36.00±2.50	34.36±4.41
7-Ketolithocholic	30.84±5.47	30.51±2.98
3,7-Diketo-5 $\beta$ -cholanoic	33.98±7.04	32.37±4.60
12-Ketochenodeoxycholic	29.42±6.80	31.36±2.52
7-Ketodeoxycholic	27.76±6.30 <sup>b</sup>	30.90±2.76
7,12-Diketolithocholic	33.00±2.98	32.84±2.71
12 $\alpha$ -Hydroxy-3,7-diketo-5 $\beta$ -cholanoic	34.73±4.00	31.93±2.16
3,7,12-Triketo-5 $\beta$ -cholanoic	32.90±3.75	33.25±3.04

<sup>a</sup>Each value represents mean  $\pm$  *sd* ( $n = 7$ ); <sup>b</sup>values which are significantly different ( $p < 0.05$ ) from the corresponding control



have hydroxyl groups. It is evident from Table II that the greatest effect on the decrease of verapamil concentration in the aqueous phase was induced by cholic acid, followed by deoxycholic acid and then by chenodeoxycholic acid. Namely, cholic acid molecule has three hydroxyl groups on the  $\alpha$  side of the steroid skeleton, which form a binding region for the proton-acceptor groups of the verapamil molecule. As can be seen from Fig. 2, the 2-cyano-2-(3,4-dimethoxyphenyl)-2-isopropyl-ethyl segment (region) of the verapamil molecule fits the triangle formed by the three OH groups of cholic acid and hence this bile acid forms the most stable complex with verapamil. The molecules of deoxycholic and chenodeoxycholic acids have smaller numbers of hydroxyl groups; hence, their interaction with verapamil is less pronounced. The bile acids whose molecules contain only keto groups, such as 3,7,12-triketo-5 $\beta$ -cholanoic, 3,12-diketo-5 $\beta$ -cholanoic and 3,7-diketo-5 $\beta$ -cholanoic acids, do not affect verapamil transport since they, like verapamil, have only proton-acceptor groups.

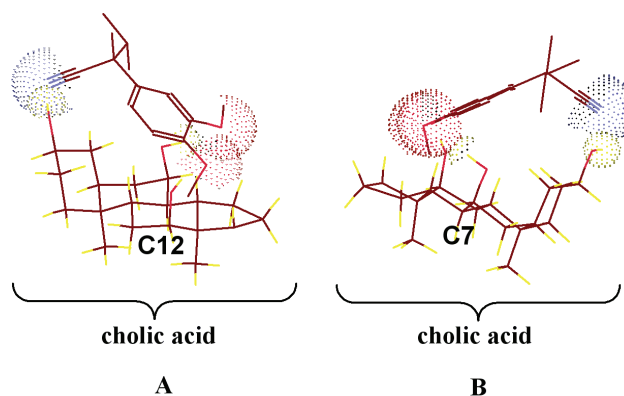


Fig. 2. Hydrogen-bonded complex formed between verapamil and cholic acid; the proton-acceptor groups: methoxy, nitrile and tertiary amine groups coincide sterically with the triangle formed by the three hydroxyl groups of cholic acid (A-view from C12 of cholic acid; B-view from C7 of cholic acid).

In order to form a complex with lidocaine (1:1 stoichiometry), a bile acid should have in its molecular structure either two OH groups or one keto (or carbonyl group from COOH) and one OH group at an appropriate mutual distance (from 4.4 to 5.5 Å).<sup>9</sup> Of the tested bile acids, 7-ketodeoxycholic acid provoked the strongest decrease of the lidocaine concentration. Namely, the molecule of this bile acid may bind with lidocaine in three different ways involving 1:1 stoichiometry (Fig. 3). At the same time, because of steric repulsions, 7-ketodeoxycholic acid can bind only one molecule of lidocaine; however, the complex 7-ketodeoxycholic acid–lidocaine (1:1) can be realized *via* three microstates. The same structural analysis shows that the other tested bile acids form their complexes with lidocaine *via* one microstate only. In other words, formation of the

complex 7-ketodeoxycholic acid–lidocaine (1:1) is three times more probable than the formation of such a complex with the other bile acids.

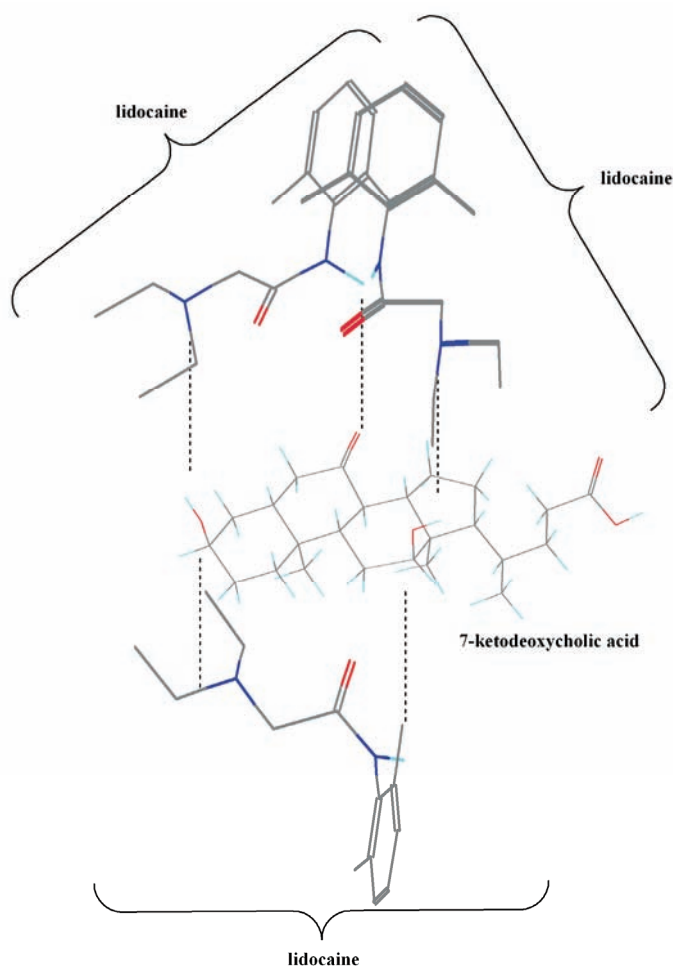


Fig. 3. Possible interactions (hydrogen bonds) between lidocaine and 7-ketodeoxycholic acid.

Deoxycholic and chenodeoxycholic acids, as markedly hydrophobic molecules,<sup>4</sup> induced no significant increase in the resorption of lidocaine (Table II).

Based on this experiment, it can be concluded that the formation of a mixed micelle of cell membrane phospholipids from the small intestine with a hydrophobic bile acid does not influence resorption of the tested drug, that is, no “holes” are formed in the cell membrane. However, in order to have a faster drug resorption, the cell membrane should form a complex with the drug, which then becomes more hydrophobic (Fig. 4). Namely, only the unprotonated lipophilic form

of lidocaine or verapamil is able to penetrate the cell membrane.<sup>14,15</sup> In the cell membrane, the corresponding drug and bile acid can form hydrogen-bonded complexes (such complexes between lidocaine and bile acids in chloroform were proven by NMR measurements<sup>9</sup>) which then shifts the ionization equilibrium (aqueous solution) to the formation of molecular lidocaine or verapamil (Fig. 4).

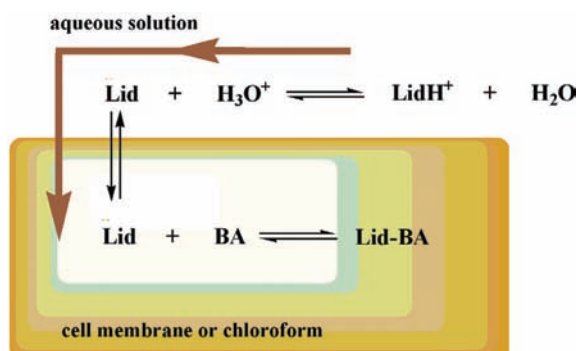


Fig. 4. General mechanism proposed for the promotive action of bile acids (BA) on the increase of resorption of lidocaine and verapamil. Lid-BA = hydrogen-bonded complex.

From Table II, it can also be seen that structural differences in the bile acids influenced lidocaine transfer from the aqueous medium to the membrane, and that this effect was not the same as when this drug was transferred to chloroform.<sup>9</sup> Namely, in the transfer of lidocaine to chloroform, each of the tested bile acids showed a promotive effect with respect to control at a significance of  $p < 0.01$ . On the other hand, if the transfer lidocaine to the small intestine is considered, then only 7-ketodeoxycholic acid showed a significant promotive action.

#### CONCLUSIONS

The transport of lidocaine from an aqueous medium to the intestine membrane is significantly increased ( $p < 0.05$ ) by 7-ketodeoxycholic acid, whereas verapamil transport is influenced by cholic acid. Namely, of all the tested bile acids, these two acids form the most stable hydrogen-bonded complexes with the corresponding drug.

*Acknowledgment.* This work was supported by the Ministry of Science and Technological Development of the Republic of Serbia (Project No. 142005B).

#### ИЗВОД

#### УТИЦАЈ ЖУЧНИХ КИСЕЛИНА НА АДСОРПЦИЈУ ЛИДОКАИНА И ВЕРАПАМИЛА У *IN VITRO* ЕКСПЕРИМЕНТУ

МИХАЉ М. ПОША<sup>1</sup> и КСЕНИЈА Н. КУХАЈДА<sup>2</sup>

<sup>1</sup>Каџедра за фармацију, Медицински факултет, Универзитет у Новом Саду, Хајдук Вељкова 3, 21000 Нови Сад и <sup>2</sup>Департаман за хемију, ПМФ, Универзитет у Новом Саду, Трг Д. Обрадовића 3, 21000 Нови Сад

Циљ овог рада је да се испита утицај структуре жучних киселина (холна, деоксихолна и хенодеоксихолна киселина као и њихови кето-деривати) на адсорпцију лидокаина и верапа-

мила из водене фазе у зид танког црева пацова *in vitro*. Пре испитивања адсорпције одговарајућих лекова цревна мембрана је третирана раствором жучних киселина чије су концентрације одговарале њиховим критичним мицеларним концентрацијама. Од свих испитиваних жучних киселина једино је 7-кетодооксихолна имала знатан утицај ( $p < 0.05$ ) на адсорпцију лидокаина из водене фазе у зид танког црева. На адсорпцију верапамила у зид танког црева једино је холна киселина имала знатан утицај ( $p < 0.05$ ). Сматра се да је овакав ефекат наведених жучних киселина на адсорпцију испитиваних лекова последица формирања комплекса са максималним бројем водоничних веза између жучних киселина и верапамила односно лидокаина.

(Примљено 10. августа, ревидирано 6. октобра 2009)

#### REFERENCES

1. A. Roda, A. F. Hofmann, K. J. Mysels, *J. Biol. Chem.* **258** (1983) 6362
2. M. Calabresi, P. Andreozzi, M. La Camillo, *Molecules* **12** (2007) 1731
3. M. Poša, S. Kevrešan, M. Mikov, V. Ćirin-Novta, C. Sârbu, K. Kuhajda, *Colloids Surf., B* **59** (2007) 179
4. M. Poša, S. Kevrešan, M. Mikov, V. Ćirin-Novta, K. Kuhajda, *Colloids Surf., B* **64** (2008) 151
5. M. A. Dopico, V. J. Walsh, J. Singer, *J. Gen. Physiol.* **119** (2002) 251
6. M. Mikov, J. P. Fawcett, *Bile Acids*, Medishet Publisher, Geneva, 2007, p. 177
7. M. Mikov, S. Kevrešan, K. Kuhajda, V. Jakovljević, V. Vasović, *Pol. J. Pharmacol.* **56** (2004) 267
8. M. Poša, S. Kevrešan, M. Mikov, V. Ćirin-Novta, K. Kuhajda, *Eur. J. Drug Metab. Pharmacokinet.* **32** (2007) 109
9. M. Poša, V. Guzsvány, J. Csanádi, S. Kevrešan, K. Kuhajda, *Eur. J. Pharm. Sci.* **34** (2008) 281
10. G. S. Gordon, A. C. Moses, R. D. Silver, J. R. Flier, M. C. Carey, *Proc. Natl. Acad. Sci. USA* **82** (1985) 7419
11. C. L. Bowe, L. Mokhtarzadeh, P. Venkatesen, S. Babu, H. Axelrod, M. J. Sofia, R. Karkarla, T. Y. Chan, J. S. Kim, H. J. Lee, G. L. Amidon, S. Y. Choe, S. Walker, D. Kahne, *Proc. Natl. Acad. Sci. USA* **94** (1997) 12218
12. H. Al-Salami, G. Butt, I. G. Tucker, M. Mikov, *Methods Find. Exp. Clin. Pharmacol.* **30** (2008) 107
13. V. Vasović, A. Vukmirović, M. Poša, M. Mikov, A. Rašković, V. Jakovljević, *Eur. J. Drug Metab. Pharmacokinet.* **31** (2006) 311
14. S. Offermans, W. Rosenthal, *Molecular Pharmacology*, Springer, Berlin, 2004, p. 562
15. J. G. Hardman, L. E. Limbrid, *Godman & Gilman's The Pharmacological Basis of Therapeutics*, McGraw and Hill, New York, 2001, p. 370.



*J. Serb. Chem. Soc.* 75 (4) 441–447 (2010)  
JSCS–3977

## Changes in the essential oil composition of *Majorana hortensis* Moench. cultivated in India during plant ontogeny

RAM S. VERMA\*, RAJESH K. VERMA, AMIT CHAUHAN and AJAI K. YADAV

Central Institute of Medicinal and Aromatic Plants, Resource Centre Purara,  
P.O. – Gagrigole, Bageshwar, Uttrakhand-263688, India

(Received 14 August, revised 7 October 2009)

**Abstract:** The essential oil content and composition of “sweet marjoram” (*Majorana hortensis* Moench.) cultivated in the Kumaon region of the western Himalayas was studied at different ages of the crop. The samples were taken after 60, 90, 120 and 150 days of transplanting. The essential oil contents varied from 0.20 to 0.70 %. The essential oil was analyzed by GC and GC–MS. Twenty eight components, representing 96.53–98.44 % of the oil, were identified. The major essential oil constituents, viz., *cis*-sabinene hydrate (37.05–47.49 %), terpinen-4-ol (14.45–16.22 %) and *trans*-sabinene hydrate (5.81–6.97 %) showed considerable variation in their concentrations in relation to crop age.

**Keywords:** *Majorana hortensis*; Lamiaceae; crop age; essential oil content; GC–MS.

### INTRODUCTION

*Majorana hortensis* Moench. commonly known as “sweet marjoram” is a member of the family Lamiaceae. It is a perennial herb native to Cyprus and eastern Mediterranean countries.<sup>1</sup> The plant is propagated by seeds and tender stem cuttings. This plant is characterized by a strong, sweet, spicy pleasant odour. The leaves are used fresh or dried and are highly esteemed as a condiment for seasoning food products. The aerial parts of the plants are used for the isolation of oil, which has many uses in the flavour, perfumery and pharmaceutical industries. In the food industry, it is mainly used as a spice in sausages, but its use in baked goods, processed vegetables, condiments, soups, snack foods and gravies has also been reported.<sup>2</sup> In addition to this, marjoram is well known for its medicinal<sup>3</sup> and insecticidal values.<sup>4</sup> The plant is also reported to possess anticancer,<sup>5</sup> antioxidant<sup>6</sup> and antifungal properties.<sup>7,8</sup>

The essential oil composition of marjoram was investigated by a number of workers in different countries<sup>9–19</sup> but it has been the subject of limited invest-

\* Corresponding author. E-mail: rswaroop1979@yahoo.com  
doi: 10.2298/JSC090814023V

tigation from India.<sup>20,21</sup> The time of harvest or harvesting stage, in general, is in close relation to the yield and quality of the essential oil and it varies from place to place and from plant to plant.<sup>22–25</sup> Therefore, it is essential to determine the proper harvesting time for aromatic plants to obtain a better yield and quality of the essential oil. A review of the literature revealed that there are no reports on the effect of crop age on the yield and composition of the essential oil of *M. hortensis* from the western Himalayas, India. Therefore, in the present investigation, the essential oils obtained from crops of different age were compared for yield and chemical composition.

## EXPERIMENTAL

### *Plant material*

*M. hortensis* rooted cuttings were transplanted in the experimental field of the Central Institute of Medicinal and Aromatic Plants (CIMAP), Resource Centre, Purara, Uttarakhand, on the 15<sup>th</sup> December, 2007, and the crop was raised following normal agricultural practices. Sampling was started after 60 days (early vegetative stage) following transplanting and then taken every month at 30 days interval until 150 days (flowering stage). The soil pH, organic carbon, available nitrogen, available phosphorus and available potassium of the experimental site were 6.5, 0.35 %, 175, 7 and 135 kg ha<sup>-1</sup>, respectively. The site is located between the coordinates 28°60' to 31°29' N, 77°49' to 80°60' E and at an altitude of 1250 m in Kattiyur Valley. Climatologically, the site falls into a sub-temperate zone (1200–1700 m) of the western Himalaya, with the monsoon usually breaking in June and continuing up to September. A voucher specimen of the plant was deposited in the Herbarium of CIMAP, Resource Centre, Purara.

### *Isolation of the essential oils*

Freshly harvested samples were immediately subjected to hydro-distillation in a Clevenger type apparatus for 3 h for extraction of the essential oil. The oils were collected, dehydrated with anhydrous sodium sulphate, measured and kept cool in the dark prior to analysis.

### *Gas chromatography (GC)*

GC analyses of the oil samples was realised using either a Perkin-Elmer Auto XL GC or a Nucon gas chromatograph model 5765 equipped with FIDs and two different stationary phases, PE-5 (50 m×0.32 mm, 0.25 µm film coating) and BP-20 (coated with a Carbowax 20M, 30 m×0.32 mm×0.25 µm film thickness) fused silica capillary columns, respectively. Hydrogen was the carrier gas at a flow rate of 1.0 mL/min. The temperature of the columns was programmed from 100 to 280 °C at 3 °C/min (for the PE-5) and from 70 to 230 °C at 4 °C/min (for the BP-20). The injector and detector temperatures were 220 and 300 °C on the PE-5 and 200 and 230 °C on the BP-20 columns, respectively. The injection volume was 0.02 µL neat and the split ratio was 1:30.

### *Gas chromatography – mass spectrometry (GC–MS)*

The GC–MS spectra were recorded on a Perkin-Elmer Auto System XL GC coupled to a turbo mass spectrometer, using a fused silica capillary column, PE-5 (50 m×0.32 mm, film thickness 0.25 µm). The column temperature was programmed 100–280 °C at 3 °C /min,

using helium as the carrier gas at a constant pressure of 69 kPa. The MS conditions were: EI mode, 70 eV; ion source temperature, 250 °C.

#### Identification of compounds

The identification was realised based on the retention time, the Kovats Index, an MS Library search (NIST & Wiley), the *n*-alkane (C<sub>9</sub>–C<sub>22</sub>) hydrocarbon pattern (Nile, Italy) and by comparing the mass spectra with MS literature data.<sup>26,27</sup> The relative amounts of the individual components were calculated based on the GC peak areas without using correction factors.

### RESULTS AND DISCUSSION

The essential oil yield and terpenoids composition together with the crop age/phenological stage are presented in Table I. The *M. hortensis* crop harvested at 150 days, flowering stage, produced a higher yield of essential oil (0.70 %) than those harvested at 120 days (flower initiation; 0.66 %), 90 days (late vegetative stage; 0.32 %) and 60 days (early vegetative stage; 0.20 %). Apparently, the dynamics of the essential oil content in marjoram is metabolically regulated during the vegetative and flowering stages of crop growth. In most aromatic plants, the essential oil preferentially accumulates during the flowering stage, probably due to its ecological role in attracting pollinators and as a defence mechanism. A similar variation in the essential oil content was registered for other aromatic crops.<sup>23–25</sup> Twenty-eight compounds, comprising 96.53–98.44 % of the total, were identified with the help of GC and GC–MS (Table I). The chemical formulae of the major components, compounds **1–3**, are shown in Fig. 1.

TABLE I. Composition (%) of the essential oil of Sweet marjoram (*Majorana hortensis* Moench.) at different ages/stages from India (t = trace (<0.1 %))

Compound <sup>a</sup>	K <sup>b</sup>	K <sup>c</sup>	Phenological stage/crop age <sup>d</sup> , days				Detection <sup>e</sup>
			EVS	LVS	FI	FS	
			60	90	120	150	
$\alpha$ -Pinene	1022	935	1.03	0.85	0.73	1.35	A,B,C
$\beta$ -Pinene	1105	980	0.12	0.10	0.06	0.09	A,B
Sabinene	1119	974	4.59	4.98	5.01	7.64	A,B,C
$\beta$ -Myrcene	1163	989	1.05	1.30	1.44	2.22	A,B
$\alpha$ -Terpinene	1177	1021	2.01	2.89	2.81	5.85	A,B
Limonene	1194	1030	0.99	1.07	0.99	1.51	A,B
1,8-Cineole	1204	1035	0.96	1.16	0.80	0.86	A,B
$\gamma$ -Terpinene	1244	1062	4.06	5.20	5.77	8.66	A,B,C
( <i>E</i> )- $\beta$ -Ocimene	1244	1047	0.27	0.23	–	–	A,B
<i>p</i> -Cymene	1271	1025	2.81	1.13	0.64	0.52	A,B,C
$\alpha$ -Terpinolene	1079	1090	0.96	1.15	1.19	2.33	A,B
3-Octanol	–	993	0.64	0.67	0.15	t	A,B
1-Octen-3-ol	1411	978	t	0.16	–	t	A,B
<i>trans</i> -Sabinene hydrate <sup>†</sup>	1463	1068	6.08	5.81	6.12	6.97	A,B
Camphor	1506	1146	0.38	0.52	1.48	0.42	A,B,C
<i>cis</i> -Sabinene hydrate <sup>†</sup>	–	1097	44.90	47.89	44.79	37.05	A,B
Linalool	1538	1098	1.30	1.20	1.27	0.81	A,B,C

TABLE I. Continued

Compound <sup>a</sup>	<i>KI</i> <sup>b</sup>	<i>KI</i> <sup>c</sup>	Phenological stage/crop age <sup>d</sup> , days				Detection <sup>e</sup>
			EVS	LVS	FI	FS	
			60	90	120	150	
Linalyl acetate	–	1257	0.16	0.06	0.04	0.04	A,B
Bornyl acetate	1558	1285	–	–	t	t	A,B
$\beta$ -Caryophyllene	1594	1419	2.04	1.56	2.11	1.18	A,B
Terpinen-4-ol	1604	1177	14.45	14.76	16.22	15.36	A,B
$\alpha$ -Humulene	1669	1462	0.24	0.20	0.26	0.17	A,B
$\alpha$ -Terpineol	1701	1188	2.88	3.28	3.85	3.68	A,B
Piperitone	–	1252	2.84	1.87	1.67	0.50	A,B
Geraniol	1830	1237	0.61	0.40	t	t	A,B,C
$\beta$ -Caryophyllene oxide	1995	1584	1.16	t	t	0.76	A,B
Thymol	2209	1313	–	–	–	t	A,B
Carvacrol	2243	1315	–	–	–	t	A,B
Class composition							
Monoterpene hydrocarbons	–	–	15.08	17.77	18.0	29.65	–
Oxygenated monoterpenes	–	–	74.56	76.95	76.24	65.69	–
Sesquiterpene hydrocarbons	–	–	2.28	1.76	2.37	1.35	–
Aliphatic compounds	–	–	0.64	0.83	0.15	t	–
Phenolic monoterpenes	–	–	2.81	1.13	0.64	0.52	–
Others	–	–	1.16	t	t	0.76	–
Total terpenoids/ %	–	–	96.53	98.44	97.40	97.97	–
Oil content/ % of fresh weight	–	–	0.2	0.32	0.66	0.70	–

<sup>a</sup>Compounds are listed in the order of elution from a polar column (BP-20); <sup>b</sup>*KI* literature (BP-20); <sup>c</sup>*KI* calculated (PE-5); <sup>d</sup>EVS = early vegetative stage, LVS = late vegetative stage, FI = flower initiation and FS = flowering stage (bloom); <sup>e</sup>A = Kovats index, B = GC-MS, C = co-injection with authentic sample; <sup>f</sup>cis/trans related to methyl vs. isopropyl groups

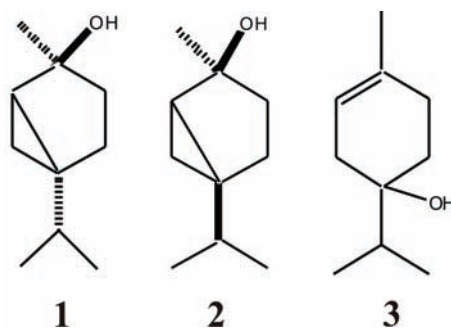


Fig. 1. The chemical formulae of the major components identified in the essential oil.



The obtained results clearly indicate that there were considerable variations in the qualitative composition of the oils obtained from crops of different ages. The oils were dominated by oxygenated monoterpenes (65.69–76.95 %) with the maximum at 90 (late vegetative stage) and 120 days (flower initiation). On the other hand, monoterpene hydrocarbons were found to be increased with advancement of the crop age (15.08–29.65 %) and attained the maximum at 150 days (flowering stage). The major components of these oils were *cis*-sabinene hydrate (**1**, 37.05–47.89 %), *trans*-sabinene hydrate (**2**, 5.81–6.97 %), terpinen-4-ol (**3**, 14.45–16.22 %), sabinene (4.59–7.64 %),  $\alpha$ -terpinene (2.01–5.85 %),  $\gamma$ -terpinene (4.06–8.66 %) and  $\alpha$ -terpineol (2.88–3.85 %). The percent of *cis*-sabinene hydrate (47.89 %) and 3-octanol (0.67 %) were found to be higher in 90-day followed by in 60-day old crops (44.90 and 0.64 %, respectively), while their lowest percent were recorded at the flowering stage, *i.e.*, after 150 days (37.05 % and trace, respectively). However, the amount of terpinen-4-ol and  $\alpha$ -terpineol reached higher values during the flower initiation stage, *i.e.*, at 120 days (16.22 and 3.85 %, respectively) and started to decline as the flowering advanced. The amounts of *trans*-sabinene hydrate (6.97 %),  $\alpha$ -pinene (1.35 %), sabinene (7.64 %), myrcene (2.22 %),  $\alpha$ -terpinene (5.85 %), limonene (1.51 %),  $\gamma$ -terpinene (8.66 %) and  $\alpha$ -terpinolene (2.33 %) were higher at 150 days than at any other crop age. Furthermore, the registered percents of  $\beta$ -pinene (0.12 %), (*E*)- $\beta$ -ocimene (0.27 %), *p*-cymene (2.81 %), linalool (1.30 %), linalyl acetate (0.16 %), piperitone (2.84 %), geraniol (0.61 %) and  $\beta$ -caryophyllene oxide (1.16 %) were relatively higher in the crop harvested after 60 days after transplanting.

The experiments performed under controlled as well as under field conditions indicated the influence of environmental factors, such as light, temperature, *etc.* on the monoterpene metabolism of aromatic crops, which resulted in marked variations in their essential oil compositions.<sup>28–31</sup> Therefore, these variations in the essential oil content and composition of *M. hortensis* might be due to variation in enzyme levels and their pool sizes in response to changing weather conditions during different months.

#### CONCLUSIONS

The sweet marjoram grown in the hilly tracks of northern India belongs to the *cis*-sabinene hydrate chemotype. Based on the essential oil content, the flowering stage (150 days) could be considered as the best harvesting time for sweet marjoram, but the flavour compounds of marjoram consist mainly of light oxygenated compounds; reports concerning this oil always refer to *cis*-sabinene hydrate,<sup>32</sup> the content of which was lowest at day 150. Therefore, it is judicious to harvest and distil *M. hortensis* crop at the flower initiation stage, *i.e.*, at day 120 under the sub-temperate conditions of north India in order to obtain a good yield of quality oil.

*Acknowledgements.* The authors are grateful to the Director, CIMAP, Lucknow (UP), India, for continuous encouragement and providing the necessary facilities. The authors are also thankful to CSIR for providing the financial support.

## ИЗВОД

ПРОМЕНА САСТАВА ЕТАРСКОГ УЉА ТОКОМ РАСТА БИЉКЕ  
*Majorana hortensis* Moench. ИЗ ИНДИЈЕ

RAM S. VERMA, RAJESH K. VERMA, AMIT CHAUHAN и AJAI K. YADAV

*Central Institute of Medicinal and Aromatic Plants, Resource Centre Purara,  
P.O. – Gagrigole, Bageshwar, Uttrakhand-263688, India*

Испитиван је састав етарског уља „слатког мајорана“ (*Majorana hortensis* Moench.) гајеног у области Кумаон у западним Хималајима, у различитим периодима раста. Узорци су сакупљани после 60, 90, 120 и 150 дана од пресађивања. Количина етарског уља у биљци је варијала од 0,20 до 0,70 %. Етарско уље је анализирано методама GC и GC-MS. Идентификовано је двадесет осам састојака који су чинили укупно 96,53–98,44 % етарског уља. Главни састојци етарског уља су били *cis*-сабинен-хидрат (37,05–47,49 %), терпинен-4-ол (14,45–16,22 %) и *trans*-сабинен-хидрат (5,81–6,97 %). Њихов удео се знатно мењао са старењем биљке.

(Примљено 14. августа, ревидирано 7. октобра 2009)

## REFERENCES

1. J. H. Ietswaart, *A taxonomic revision of the genus Origanum (Labiatae)*, Leiden University Press, Leiden, 1980
2. *Fenaroli's handbook of flavour ingredients Vol. 1: Natural flavours*, 3<sup>rd</sup> ed., G. A. Burdock, Ed., CRC Press, Boca Raton, FL, 1995
3. A. Chevallier, *The encyclopaedia of medicinal plants*, Dorling Kindersley, London, 1996
4. M. A. Abbassy, S. A. M. Abdelgaleil, R. Y. A. Rabie, *Ent. Exp. Appl.* **131** (2009) 225
5. J. L. Hartwell, *Lloydia*, **32** (1969) 247
6. A. H. El-Ghorab, A. F. Mansour, K. F. El-Massry, *Flavour Fragrance J.* **19** (2004) 54
7. A. F. Afifi, A. E. Dowidar, *J. Physiol. Sci.* **3** (1976) 81
8. J. S. Pruthi, *Spice and condiments: chemistry, microbiology, technology*, Academic Press, New York, 1980, p. 221
9. B. M. Lawrence, *Perfum. Flavor.* **14** (1989) 29
10. I. Nykanen, *Z. Lebensm. Unters. Forsch.* **183** (1986) 267
11. M. E. Komaitis, N. Infanti-Papatragianni, E. Melissari-Panagiotou, *Food Chem.* **45** (1992) 117
12. K. H. C Baser, N. Kirimer, G. Tumen, *J. Essent. Oil Res.* **5** (1993) 577
13. R. R. Vera, J. Chan Ming, *Food Chem.* **66** (1999) 143
14. E. Sarer, J. J. C. Scheffer, A. B. Svedsen, *Planta Med.* **46** (1982) 236
15. E. A. Omer, H. E. Ouda, S. S. Ahmed, *J. Herbs Spices Med. Plants* **2** (1994) 9
16. A. M. Refaat, *Ph.D. Thesis*, Faculty of Agriculture, Ain Shams University, Cairo, 1988, p. 163
17. N. Arnold, B. Bellomaria, G. Valentini, *J. Essent. Oil Res.* **5** (1993) 71
18. G. Circella, C. Franz, J. Novak, H. Resh, *Flavour Fragrance J.* **10** (1995) 371
19. J. Novak, J. Langbehn, F. Pank, C. M. Franz, *Flav. Fragr. J.* **17** (2002) 175

20. A. C. Mishra, K. S. Negi, P. Suneja, M. L. Maheshwari, *Indian Perfum.* **48** (2004) 41
21. G. R. Mallavarapu, R. N. Kulkarni, S. Ramesh, *Indian Perfum.* **37** (1993) 81
22. S. D. Bharadwaj, L. J. Srivastava, *Indian Perfum.* **28** (1984) 38
23. S. K. Lattoo, R. S. Dhar, A. K. Dhar, P. R. Sharma, S. G. Agarwal, *Flavour Fragrance J.* **21** (2006) 817
24. S. Maric, M. Maksimovic, M. Milos, *J. Essent. Oil Res.* **18**, (2006) 178
25. M. Moghaddam, R. Omidbiagi, *J. Essent. Oil Res.* **19** (2007) 18
26. W. Jennings, T. Shibamoto, *Qualitative analysis of flavour and fragrance volatiles by glass capillary gas chromatography*, Academic Press, New York, 1989
27. R. P. Adams, *Identification of essential oil components by Gas chromatography/quadrupole mass spectroscopy*, Allured Publishing Corp., Carol Stream, IL, 2001
28. R. J. Clark, R. C. Menary, *Aust. J. Plant Physiol.* **7** (1980) 685
29. D. E. Lincoln, J. H. Langenheim, *Biochem. Syst. Ecol.* **6** (1978) 21
30. B. Voirin, N. Brun, C. Bayet, *Phytochemistry* **29** (1990) 749
31. S. Halva, L. E. Craker, J. E. Simon, D. J. Charles, *J. Herbs Spices Med. Plants* **1** (1992) 47
32. S. Nitz, H. Kollmannsberger, M. Punkert, *Chem. Mikrobiol. Technol. Lebensm.* **14** (1992) 108.





*J. Serb. Chem. Soc.* 75 (4) 449–458 (2010)  
JSCS–3978

## Effects of autoclaving and pullulanase debranching on the resistant starch yield of normal maize starch

MARIJA S. MILAŠINOVIĆ<sup>1\*</sup>, MILICA M. RADOSAVLJEVIĆ<sup>1</sup> and LJUBICA P. DOKIĆ<sup>2</sup>

<sup>1</sup>Maize Research Institute, Zemun Polje, Slobodana Bajića 1, Belgrade-Zemun and  
<sup>2</sup>Faculty of Technology, University of Novi Sad, Bul. Cara Lazara 1, Novi Sad, Serbia

(Received 4 September, revised 2 November 2009)

**Abstract:** In this study, resistant starch (RS), type 3, was prepared by the autoclaving and debranching of normal maize starch isolated from a selected ZP genotype. The objectives of this study were to optimize both starch autoclaving and debranching with pullulanase (PromozymeBrewQ) for the production of RS. Autoclaving at 120 °C (30 min) increased the RS content of all samples, whereas freezing at –20 °C did not have an obvious effect on the RS contents. The highest RS yield in the autoclaved starch samples was 7.0 % after three autoclaving–cooling cycles. After pullulanase debranching at 50 °C and retrogradation at 4 °C, the RS yields ranged from 10.2 to 25.5 % in all samples (depending on the hydrolysis time). Debranched starch samples with a maximum RS yield of 25.5 % were obtained after a debranching time of 24 h. This study showed that starch from the selected ZP maize genotype is suitable for pullulanase treatment and RS preparation but that additional studies with a greater number of different treatments (incubation time/temperature) are necessary to manipulate and promote crystallization and enhance RS formation.

**Keywords:** maize starch; autoclaving; debranching; pullulanase; resistant starch.

### INTRODUCTION

There is considerable interest in the nutritional implications of resistant starch (RS) in foods. The term “resistant starch” was used to designate mainly enzyme-resistant retrograded amylose but was expanded to all forms of starch that escape digestion and absorption in the small intestines.<sup>1</sup> The positive effect of RS in nutrition is based on the results of the fermentation process during which short chain fatty acids, primarily acetates, propionates and butyrates, are produced. They directly affect the large intestine by decreasing the pH value, which prevents the growth of pathogenic micro-organisms, and increasing the potential for mineral absorption. Fatty acids stimulate colonic blood flow and increase nutrient

\* Corresponding author. E-mail: mmilasinovic@mrizp.rs  
doi: 10.2298/JSC090904027M

flow.<sup>2–5</sup> Besides physiological benefits in human, RS has been reported to have potential as a unique ingredient that can yield high-quality foods. For example, application tests of RS showed improved crispness and expansion in certain products and better mouth feel, colour and flavour as compared with products produced with traditional, insoluble fibres.<sup>6</sup>

Resistant starch can result from a highly retrograded amylose fraction, the quantity formed being directly proportional to the amylose content of the starch.<sup>7</sup> This type of RS has been classified as RS type 3 (RS3). The degree of RS formation in foods depends not only on the type of included starch and the adopted processing conditions but is also influenced by the duration and conditions of storage.<sup>8</sup>

RS3 is produced by gelatinization, which is a disruption of the granular structure by heating starch with an excess of water, and retrogradation, a slow recrystallization of starch components (amylose and amylopectin) upon cooling or dehydration. The generation of RS3 after this hydrothermal treatment is due to increased interaction between starch components. It has been shown that, after debranching of starch, the linear chains can contribute to a high RS content. In addition, partial acid hydrolysis and debranching of amylopectin are very effective in generating RS from various starches.<sup>9–11</sup> The advantages of debranching over mild acid hydrolysis include a shorter processing time, better processing control and higher RS yields.

Among different resistant starches, retrograded resistant starch (RS3) has great commercial importance, since its crystalline polymorphs exhibit an endothermic transition from 120 to 165 °C<sup>12,13</sup> that typically survives most, but not all, food-processing conditions. RS3 was initially hypothesized as a crystalline state of amylose double helices.<sup>14</sup> Later, the non-crystalline part of retrograded starch was also found to be enzyme resistant.<sup>15,16</sup>

Although starches from diverse plants may be utilized, maize is the world's most abundant source that provides the majority of substrates used in the preparation of starch hydrolysates. Starch granules are quite resistant to penetration by both water and hydrolytic enzymes, due to the formation of hydrogen bonds within the same molecule and with other neighbouring molecules. However, these inter- and intra-hydrogen bonds can become weak as the temperature of the suspension is raised. As normal maize starch contains both linear amylose and branched amylopectin with short and long chains of different sizes, our approach was to degrade it through physical and enzymatic treatments to attenuate starch digestion properties. In the present study, debranching using pullulanase was applied to produce a sample with linear, low molecular weight and recrystallizable polymer chains. Debranching enzymes, such as pullulanase, rapidly hydrolyze only the  $\alpha$ -1,6-glucosidic bonds, releasing a mixture of long and shorter unit chains from the parent amylopectin molecule. In theory, a fast and efficient enzyme hyd-

rolysis requires pre-swelling the starch in water and full starch gelatinization. The objectives of this work were to check the possibility of RS production from normal maize starch from the selected ZP genotype and to optimize both starch autoclaving and debranching with pullulanase (PromozymeBrewQ) for RS production.

## EXPERIMENTAL

### *Materials*

Commercial maize starch was obtained from a local producer ("Jabuka", Pančevo, Serbia). Normal maize starch was isolated from the genotype ZP 434. Commercial debranching enzyme, pullulanase (PromozymeBrewQ, 400 PUN/ml) from *Bacillus acidipullulyticus* was obtained from Novozymes (Bagsvaerd, Denmark). One Pullulanase Unit Novo (PUN) is defined as the amount of enzyme that hydrolyzes pullulan, liberating reducing carbohydrates with a reducing power equivalent to one  $\mu\text{mol}$  glucose per minute under standard conditions. The resistant starch assay kit was purchased from Megazyme International Ireland Ltd. (Wicklow, Ireland).

### *Starch isolation*

Starch from maize grain (ZP 434) was isolated by applying a 100-g laboratory maize wet-milling procedure.<sup>17</sup> The moisture, ash, crude protein and crude fat contents of the starch were determined using the oven method,<sup>18</sup> the AOAC method,<sup>19</sup> the microKjeldahl method<sup>19</sup> and the Soxhlet method,<sup>19</sup> respectively. The amylose content was determined by a rapid colorimetric method.<sup>20</sup>

### *Resistant starch production by autoclaving and cooling*

The samples were prepared by suspending 10 % and 20 % (w/v) of maize starch in 1000 ml of water. The suspensions were heated in a boiling water bath for 15 min with stirring and then transferred to an autoclave (Sutjeska, Belgrade, Serbia). The autoclaving conditions were: pressure, 1.1 bar, temperature, 120 °C, autoclaving time, 30 min and vessel volume, 60 dm<sup>3</sup>. After autoclaving, the samples were stored at 4 °C for 24 h. The samples were subjected to three autoclaving-cooling cycles. After the third cycle, the sample was divided in two; one part was stored at 4 °C and the other at -20 °C for 24 h. After each cycle, the RS was determined.

### *Conditions for enzymatic debranching of maize starch*

Prior to starch debranching, the optimal concentration of pullulanase was determined.

A maize starch suspension (20 %, w/v) was gelatinized on a boiling water bath for 15 min under stirring. This gel was autoclaved at 120 °C for 30 min and then the gel was re-dissolved in distilled water to obtain a 10% (w/v) gel solution. The gel was cooled to 50 °C and pullulanase at different concentrations (0.25, 0.5, 1.0, 2.0 and 4.0 %, calculated on dry starch weight) was added. The mixture was incubated with constant stirring for 24 h. Samples were taken out at different times and the reducing sugars (DE value) were determined by the Luff-Schoorl method (ISO 5377:1981).<sup>21</sup> At least three replicates for each hydrolysis time were conducted and good reproducibility was achieved since the differences between the triplicate measurements were less than 10 %.

### *Resistant starch production by starch debranching*

Normal maize starch isolated from the genotype ZP 434 was debranched using an enzyme in concentration of 2 % (calculated on dry starch weight), which was determined as optimal concentration. The maize starch gel was prepared as described in the previous section

and the reaction time was varied (1, 3, 5, 7, 9, 11 and 24 h); after these times, the samples were heated at 95 °C for 20 min, cooled down to room temperature and stored for 24 h at 4 °C or –20 °C. The samples were dried at 40 °C and stored in closed glass containers.

#### *Resistant starch determination*

The RS content in the starch modifications was determined by an enzymatic method (AOAC 2002.02).<sup>22</sup> The samples were incubated with pancreatic  $\alpha$ -amylase and amyloglucosidase (AMG) for 16 h at 37 °C, during which time the non-resistant starch was solubilised and hydrolyzed to glucose by the combined action of the two enzymes. The reaction was terminated by the addition of an equal volume of ethanol and the RS was recovered as a pellet on centrifugation. This was then washed twice with ethanol (50 % v/v), and centrifuged. The RS in the pellet was dissolved in 2 M KOH by vigorously stirring on an ice-water bath. This solution was neutralized with acetate buffer and the starch was quantitatively hydrolyzed to glucose with AMG. The glucose was quantified with glucose oxidase/peroxidase reagent (GOPOD), which gave a measure of the RS content of the sample.

#### *Statistical analysis*

The results are expressed by means of values  $\pm$  standard error of three separate determinations. The data reported for the effects of autoclaving on the formation of RS was assessed by analyses of variance (ANOVA) and the Duncan multiple test was used to identify any significant differences at the  $P < 0.05$  level between the means. The analyses were conducted using the statistical software package Statistica 8.1. (StatSoft Inc., USA).

## RESULTS AND DISCUSSION

#### *Proximate composition*

The basic properties of the starch samples used in this study are given in Table I. The commercial maize starch “Jabuka” and “ZP 434” did not significantly differ in their amylose content but they differed slightly in their ash and contents of crude protein and crude fat.

TABLE I. The properties of native starch samples (“Jabuka” and “ZP 434”)

Starch sample	Amylose, %	Moisture, %	Ash, %	Crude protein, %	Crude fat, %
“Jabuka”	26.5 $\pm$ 0.4	10.4 $\pm$ 0.2	0.10 $\pm$ 0.02	0.30 $\pm$ 0.05	0.10 $\pm$ 0.02
“ZP 434”	26.0 $\pm$ 0.3	8.4 $\pm$ 0.1	0.01 $\pm$ 0.00	0.26 $\pm$ 0.04	0.05 $\pm$ 0.00

Normal maize starch was chosen for this study because of its abundance and a low price compared with high amylose maize starches. Previously, it was found that there were not significant differences in the physicochemical characteristics between starches of different dent ZP maize genotypes.<sup>23</sup> The genotype ZP 434 ranks among the top hybrids produced in Serbia. Due to the limited quantity of starch isolated from “ZP 434”, commercial maize starch “Jabuka” was used in order to identify the optimum debranching conditions for RS formation. In the further steps, only starch from the selected maize genotype was used.



### Starch autoclaving

The formation of resistant starch type 3 (RS3) depends on many factors, *e.g.*, pH, temperature, incubation time, storage time, number of heating and cooling cycles, starch type, *etc.* The amylose content and the amount of water are directly correlated to the yield of resistant starch.<sup>2</sup> The gelatinization of starch granules during heat processing strongly influences their susceptibility to enzymatic hydrolysis. Even for starches with normal amylose levels, it is recognized that cooking at >100 °C can increase the RS3 yield. Repeated heat/moisture treatments are associated with a decrease in the hydrolysis limit of pancreatic  $\alpha$ -amylase and the increased RS3 formation.<sup>2</sup>

The effects of autoclaving and storage temperatures on the formation of resistant starch from normal maize starch ZP 434 are presented in Tables II and III, respectively. In this study, the starch concentration (10 % or 20 %) in the suspension did not significantly affect the RS yields but the number of autoclaving–cooling cycles did. After three autoclaving–cooling cycles, the RS yields increased by 2.1 % for both starch concentrations.

TABLE II. Effect of autoclaving at 120 °C on resistant starch formation from normal maize starch

Starch content in suspension, %	Autoclaving cycle	Resistant starch, %
10	I	4.8 <sup>c</sup> ± 0.2
	II	6.8 <sup>a</sup> ± 0.1
	III	6.9 <sup>a</sup> ± 0.1
20	I	4.9 <sup>c</sup> ± 0.1
	II	5.9 <sup>b</sup> ± 0.3
	III	7.0 <sup>a</sup> ± 0.2

<sup>a,b,c</sup> Means within a column followed by different letters are significantly different ( $P < 0.05$ )

TABLE III. Effect of storage temperatures (4 and –20 °C) on resistant starch formation from autoclaved and debranched starches

Sample	Resistant starch, %	
	<i>t</i> / °C	
	4	–20
Autoclaved sample	7.0 ± 0.2	6.9 ± 0.1
Debranched sample (1 h)	10.2 ± 0.3	9.8 ± 0.1
Debranched sample (24 h)	25.5 ± 0.5	24.9 ± 0.2

Escarpa *et al.*<sup>24</sup> standardized the hydrothermal process in starch gelatinization, and they reported the RS content ranged from 7.6 for waxy starch (0 % amylose) to 36.4 % for purified amylose. These authors found that the RS yield increased with increasing amylose content in the starches under study. The differences in the results found in this study and those determined by other researchers might be due to the source of the starch and the conditions applied for the RS

preparation. Sievert and Pomeranz<sup>12</sup> determined RS values between 2.5 and 21.3 % for diverse starch sources, and with the Berry method,<sup>25</sup> the RS values ranged between 2.8 and 31 %.<sup>13</sup> Autoclaved wheat starch possessed 9 % RS compared with less than 1 % in uncooked wheat starch.<sup>26</sup> The autoclaved wheat starch contained 6.2 % RS (of dry matter); this increased to 7.8 % after 3 further boiling/cooling cycles.<sup>27</sup>

Generally, the content of resistant starch increases during storage, especially during low-temperature storage. Cold storage seems to support an increase in the RS content. In this study, the storage conditions (4 or  $-20$  °C) did not significantly affect the formation of RS of either autoclaved or debranched samples. These findings are in accordance with the results obtained by Hasjim and Jane,<sup>28</sup> who found that freezing at  $-20$  °C had little or no effect on the RS content of acid-modified starch samples.

#### *Effect of enzyme concentration on starch debranching*

An increased degree of debranching would enable the chains to align and aggregate and hence form perfectly crystalline structures, thereby leading to the formation of more RS.<sup>29</sup> Berry<sup>25</sup> reported that debranching of potato amylopectin with pullulanase before subjecting it to heating and cooling cycles substantially increased the RS3 content; this was attributed to an increase in the content of linear starch chains resulting from debranching.

As shown in Fig. 1, commercial maize starch “Jabuka” debranched with 4 % pullulanase exhibited the highest reducing value, followed by starch samples debranched with 2, 1, 0.5 and 0.25 % pullulanase. In the cases of 2 and 4 % en-

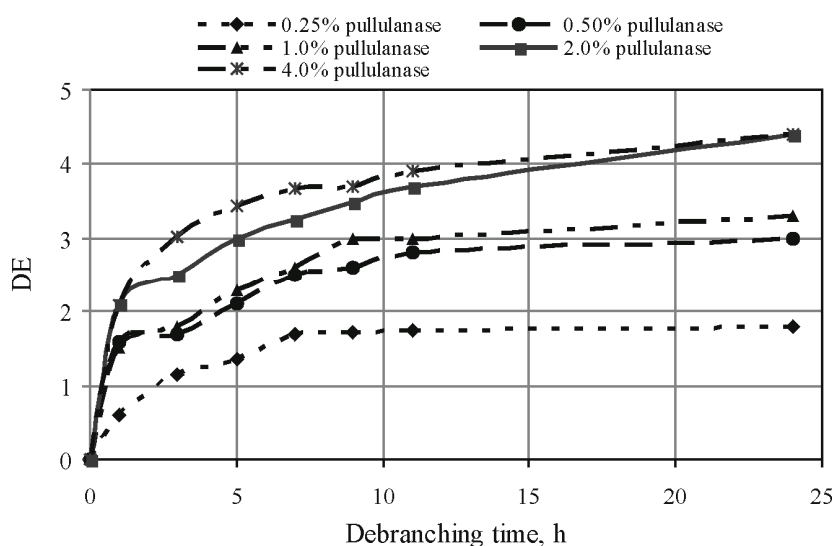


Fig. 1. Optimization of maize starch debranching; DE represents dextrose equivalent.

zyme, the reducing values resulting after 1 h of hydrolysis were not statistically different. The addition of the higher amount of enzyme did not result in complete debranching, thus a concentration of 2 % was used for starch debranching in this work. This result is in agreement with the findings of Hizukuri *et al.*<sup>30</sup> who reported that isoamylase and pullulanase initially degraded potato amylose rapidly and then approached constant values on prolonged incubation with a large amount of enzyme.

The kinetics of starch debranching in a 2-L-reactor (Fig. 1) showed that after 9 h and longer, the glucose concentration was constant (for the lowest enzyme concentration) or slightly higher (for higher enzyme concentrations); however, starch debranching was performed for 11 and 24 h. After debranching for different times (seven samples), the starch solution was heated at 95 °C to deactivate the enzyme and RS was obtained.

#### *Resistant starch content*

Seven debranching times (1, 3, 5, 7, 9, 11 and 24 h) were applied to study the effect of debranching time on the content of RS (Fig. 2). A gradual increase in the RS content of the maize starch samples was observed with increasing debranching time, some of which were significant. Native maize starch from the genotype ZP 434 had a very low RS content (0.60 %) compared to the debranched samples. The RS content increased significantly from 0.60 to 25.0 % after 11 h of debranching. After a total debranching time of 24 h, the RS content slightly increased to 25.5 %. The RS content measured after 5 h was 18 %, showing that 70 % of the totally obtained resistant starch was produced during this time. When the content of debranched starch increased, higher amounts of short starch chains were produced. These linear fragments can contribute to starch retrogradation

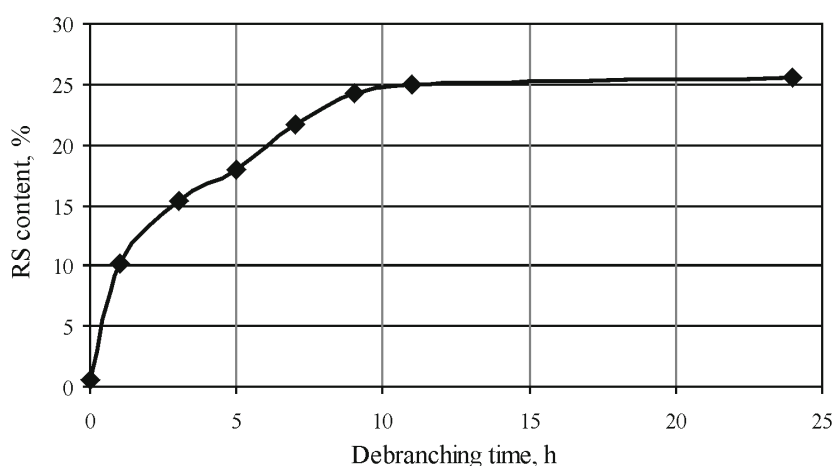


Fig. 2. Effect of debranching time on RS formation.

and decreased enzymatic susceptibility of starch, with the concomitant increasing in the RS content.

The RS contents of all debranched samples were significantly ( $P < 0.05$ ) higher compared to their respective autoclaved samples (control). Debranching was performed at 50 °C after which the samples were dried at 40 °C. The debranching and drying conditions were suitable for RS3 formation.

The content of amylose (37 %) determined after debranching corresponds well with findings reported by Escarpa *et al.*<sup>24</sup> who used potato starch with a similar amylose/amylopectin ratio as in the present samples. As can be seen in Fig. 2, the RS content after 5 h of debranching was 18 % compared to 18.2 % reported by Escarpa *et al.*<sup>24</sup> These authors observed increased RS yields when the amylose content in the studied starches was higher. Recently, the results of Ozturk *et al.*<sup>31</sup> indicated that 48 h of debranching of high amylose maize starches was suitable for RS formation. The results of González-Soto *et al.*<sup>32</sup> demonstrated that debranching of banana starch with pullulanase (Promozyme D) for 5 h was sufficient to obtain a high RS level (18 %). In another study,<sup>25</sup> an RS content of up to 46.8 % was determined in potato amylopectin after debranching, drying and heat processing. The differences in the results found in this study and those determined by other researchers might be due to the source of the starch and the conditions used for the RS preparation.

Based on the obtained results, it can be concluded that a high level of debranching occurred during the first 11 h of debranching; thus, an 11-hour debranching with pullulanase was sufficient to obtain a high RS level.

#### CONCLUSIONS

Autoclaving at 120 °C (30 min) increased the RS content in all samples, whereas freezing at -20 °C had no obvious effect on the RS contents. The highest RS yield in the autoclaved starch samples was 7.0 % after three autoclaving-cooling cycles. After debranching of starch with pullulanase at 50 °C and subsequent retrogradation at 4 °C, RS yields ranging from 10.2 to 25.5 % were found in all samples (depending of the hydrolysis time). The RS determination showed that starch debranched for 24 h had the highest RS level and that approximately 70 % of the starch had been hydrolyzed after 5 h. An enzyme concentration of 2 % was sufficient for starch debranching, giving the highest amount of liberated glucose. Debranching of maize starch for 11 h was sufficient to obtain a high content of RS in the products.

This study showed that the selected starch from the ZP maize genotype was susceptible for pullulanase treatment and RS preparation but additional studies with a greater number of different treatments (incubation time/temperature) are necessary to manipulate and promote crystallization and hence enhance RS formation.

## ИЗВОД

## УТИЦАЈ ОБРАДЕ У АУТОКЛАВУ И ХИДРОЛИЗЕ ПУЛУЛАЗОМ НА ПРИНОС РЕЗИСТЕНТНОГ СКРОБА ИЗ НОРМАЛНОГ КУКУРУЗНОГ СКРОБА

МАРИЈА С. МИЛАШИНОВИЋ<sup>1</sup>, МИЛИЦА М. РАДОСАВЉЕВИЋ<sup>1</sup> И ЉУБИЦА П. ДОКИЋ<sup>2</sup><sup>1</sup>Институт за кукуруз „Земун Поље“, Слободана Бајића 1, Београд-Земун и <sup>2</sup>Технолошки факултет, Универзитет у Новом Саду, Бул. Цара Лазара 1, Нови Сад

У овом раду, резистентан скроб (РС), тип 3, припремљен је обрадом у аутоклаву и хидролизом са пулулазозом из нормалног кукурузног скроба који је изолован из одабраног ЗП генотипа кукуруза. Предмет истраживања је био да се изврши оптимизација третмана обраде у аутоклаву и хидролизе пулулазозом (PromozymeBrewQ) у циљу добијања РС-а. Обрада у аутоклаву на 120 °C (30 min) је утицала на повећање садржаја РС-а у свим узорцима, док температура чувања од -20 °C није имала утицаја на његов садржај. Највећи принос РС-а у аутоклавираним узорцима скроба је био 7,0 % након три циклуса обрада у аутоклаву-хлађење. Након хидролизе пулулазозом на 50 °C и ретроградације на 4 °C принос РС-а у свим узорцима се кретао од 10,2 до 25,5 % (зависно од времена хидролизе). Хидролизоване узорци скроба са максималним приносом РС-а од 25,5 % одређени су након 24 часа инкубације. Ово истраживање показује да је скроб из одабраног ЗП генотипа кукуруза погодан за хидролизу пулулазозом и добијање РС-а, али су неопходна даља истраживања са већим бројем различитих третмана (време/температура инкубације) у циљу побољшања процеса кристализације и повећања приноса РС-а.

(Примљено 4. септембра, ревидирано 2. новембра 2009)

## REFERENCES

1. J. H. Cumming, H. N. Englyst, *Trends Food Sci. Technol.* **2** (1991) 99
2. S. G. Haralampu, *Carbohydr. Polym.* **41** (1999) 285
3. M. M. Champ, *J. AOAC Int.* **87** (2004) 749
4. P. J. Tomasik, *Chemical and functional properties of food saccharides*, CRC Press LLC, Boca Raton, FL, 2004, p. 325
5. D. L. Topping, P. M. Clifton, *Physiol. Rev.* **81** (2001) 1031
6. P. Yue, S. Waring, *Food Aust.* **50** (1998) 615
7. G. Annison, D. L. Topping, *Ann. Rev. Nutr.* **14** (1994) 297
8. L. Goñi, E. García-Diz, F. Mañas, F. Saura-Calixto, *Food Chem.* **56** (1996) 445
9. J. Brumovsky, D. B. Thompson, *Cereal Chem.* **78** (2001) 680
10. S. G. Haralampu, A. Gross, US Patent 5849090 (1998) Bedford, Ma, Opta Food Ingredients, Inc.
11. J. M. King, S. Y. Tan, US Patent Application 20050089624 (2005)
12. D. Sievert, Y. Pomeranz, *Cereal Chem.* **66** (1989) 342
13. Y. Pomeranz, *Eur. J. Clin. Nutr.* **46** (Suppl. 2) (1992) S63
14. J.-L. Jane, J. Robyt, *Carbohydr. Res.* **132** (1984) 105
15. C. S. Berry, K. l'Anson, M. J. Miles, V. J. Morris, P. L. Russell, *J. Cereal Sci.* **8** (1988) 203
16. D. Sievert, Z. Czuchajowska, Y. Pomeranz, *Cereal Chem.* **68** (1991) 86
17. S. R. Eckhoff, S. K. Singh, B. E. Zehr, K. D. Rausch, E. J. Fox, A. K. Mistry, A. E. Haken, Y. X. Niu, S. H. Zou, P. Buriak, M. E. Tumbleson, P. L. Keeling, *Cereal Chem.* **73** (1996) 54
18. D. Pearson, *The chemical analysis of foods*, Longman Group, London, 1976

19. AOAC, *Official method of analysis*, 17<sup>th</sup> ed., Association of Official Analytical Chemists, Washington D.C., 1990
20. S. J. McGrance, H. J. Cornell, C. J. Rix, *Starch* **50** (1998) 158
21. ISO 5377:1981, *Starch hydrolysis products – Determination of reducing power and dextrose equivalent-Lane and Eynon constant titre method*, Geneva, Switzerland, 1981
22. AOAC, *Official method of analysis*, 17<sup>th</sup> ed., Association of Official Analytical Chemists, Washington D.C., 2002
23. M. Milasinovic, M. Radosavljevic, Lj. Dokic, J. Jakovljevic, J. Kapusniak, J.-L. Jane, in *Proceeding of International Congress on Food Technology, Quality and Safety*, XVI Symposium of Cereal-Bread, Novi Sad, Serbia, 2007, p. 107
24. A. Escarpa, M. C. González, E. Mañas, L. García-Diz, F. Saura-Calixto, *J. Agric. Food Chem.* **44** (1996) 924
25. C. S. Berry, *J. Cereal Sci.* **4** (1986) 301
26. M. Siljestrom, N. G. Asp, *Z. Lebensm. Unters. Forsch.* **4** (1985) 1
27. I. Bjorck, M. Nyman, P. Pedersen, M. Siljestrom, N. G. Asp, B. O. Eggum, *J. Cereal Sci.* **6** (1987) 159
28. J. Hasjim, J.-L. Jane, in *AACC International Annual Meeting*, Orlando, FL, 2005
29. H. S. Guraya, C. James, E. T. Champagne, *Starch/Stärke* **53** (2001) 64
30. S. Hizukuri, Y. Takeda, M. Yasuda, *Carbohydr. Res.* **94** (1981) 205
31. S. Ozturk, H. Koxsel, K. Kahraman, P. K. W. Ng, *Eur. Food Res. Technol.* **229** (2009) 115
32. R. A. González-Soto, E. Agama-Acevedo, J. Solorza-Feria, R. Rendón-Villalobos, L. A. Bello-Pérez, *Starch/Stärke* **56** (2004) 495.



*J. Serb. Chem. Soc.* 75 (4) 459–473 (2010)  
JSCS–3979

## Crystal engineered acid–base complexes with 2D and 3D hydrogen bonding systems using *p*-hydroxybenzoic acid as the building block

PU SU ZHAO\*, XIAN WANG, FANG FANG JIAN, JUN LI ZHANG and HAI LIAN XIAO

*New Materials and Function Coordination Chemistry Laboratory, Qingdao University of Science and Technology, Qingdao Shandong 266042, P. R. China*

(Received 16 April, revised 21 September 2009)

**Abstract:** *p*-Hydroxybenzoic acid (*p*-HOBA) was selected as the building block for self-assembly with five bases, *i.e.*, diethylamine, *tert*-butylamine, cyclohexylamine, imidazole and piperazine, and generation of the corresponding acid–base complexes **1–5**. Crystal structure analyses suggest that proton transfer from the carboxyl hydrogen to the nitrogen atom of the bases can be observed in **1–4**, while only in **5** does a solvent water molecule co-exist with *p*-HOBA and piperazine. With the presence of O–H...O hydrogen bonds in **1–4**, the deprotonated *p*-hydroxybenzoate anions (*p*-HOBAA<sup>–</sup>) are simply connected each other in a head-to-tail motif to form one-dimensional (1D) arrays, which are further extended to distinct two-dimensional (2D) (for **1** and **4**) and three-dimensional (3D) (for **2** and **3**) networks *via* N–H...O interactions. While in **5**, neutral acid and base are combined pair-wise by O–H...N and N–H...O bonds to form a 1D tape and then the 1D tapes are sequentially combined by water molecules to create a 3D network. Some interlayer or intralayer C–H...O, C–H... $\pi$  and  $\pi$ ... $\pi$  interactions help to stabilize the supramolecular buildings. Melting point determination analyses indicate that the five acid–base complexes are not the ordinary superposition of the reactants and they are more stable than the original reactants.

**Keywords:** hydrogen bonding; crystal structure; supramolecular; *p*-hydroxybenzoic acid.

### INTRODUCTION

Organic crystals built from acid–base complexes have received considerable attention in the predictable assembly of supramolecular architectures.<sup>1–7</sup> One of the important ways is the use of self-organization of small molecules with N–H...O, O–H...O and other weak intermolecular interactions to create one-, two-, and three-dimensional (1D, 2D, and 3D) networks in crystalline solids.<sup>8,9</sup> Recent

\* Corresponding author. E-mail: zhaopusu@163.com  
doi: 10.2298/JSC090416011Z

studies were focused on the host networks with space to create materials for molecular storage and catalysis.<sup>10–12</sup> In the context of designing specific arrays, aromatic acid molecules attract great interest because of their importance in crystal engineering, due to their ability to form strong and directional hydrogen bond,<sup>12</sup> whereby the number of carboxylic groups and the different placement of the carboxylic group on the aromatic ring may lead to variable hydrogen-bonding fashions and architectures. For example, 3,5-dinitrobenzoic acid, terephthalic acid, trimelic acid and benzene-1,2,4,5-tetracarboxylic acid were successfully employed as building blocks to construct various hydrogen-bond supramolecules.<sup>1,13–15</sup> Among numerous aromatic acids, *p*-hydroxybenzoic acid (*p*-HOBA) is a typical monocarboxylic acid. Although a dimer can be formed by *p*-HOBA itself,<sup>16</sup> using this synthon with organic bases, such as pyridine,<sup>17</sup> pyrrolidine,<sup>18</sup> benzylamine,<sup>19</sup> *N,N*-dimethylbenzylamine,<sup>19</sup> *N*-methylbenzylamine,<sup>19</sup> and (*S*)-1-ethylphenylamine,<sup>20</sup> more organic crystals were reported. In early reports,<sup>18,19</sup> *p*-hydroxybenzoic acid (*p*-HOBA) was always deprotonated as the *p*-hydroxybenzoate anion (*p*-HOBA<sup>−</sup>) and the corresponding organic bases were always protonated, which means an increase of the hydrogen bond acceptor sites in *p*-HOBA and the increase of the hydrogen bond donor sites in the organic bases. Thus, the numbers and varieties of the hydrogen bond between *p*-HOBA and the organic bases will increase, which will finally form rich hydrogen bonding systems and help in the building of multiple hydrogen-bond networks. With this in mind, *p*-hydroxybenzoic acid (*p*-HOBA) was chosen as a building block to construct organic crystals with various organic bases. It is imaginable that combinations of the *p*-HOBA molecule with different organic bases will exhibit variable hydrogen bonding modes and interesting networks. Herein, the synthesis and the molecular structures, as well as the supramolecular structures of complexes formed by *p*-HOBA with the organic bases of diethylamine, *tert*-butylamine, cyclohexylamine, imidazole and piperazine are described.

## EXPERIMENTAL

### *Materials and methods*

All employed chemicals were of analytical reagent grade purchased from Sinopharm Chemical Reagent Co. Ltd., P. R. China, and used directly without further purification. Elemental analyses for carbon, hydrogen and nitrogen were performed using a Perkin-Elmer 240C elemental instrument. The melting points were determined on a Yanaco MP-500 melting point apparatus. The IR spectra were recorded in the wavenumber range 4000–400 cm<sup>−1</sup> using KBr pellets on a Nicolet 170SX spectrophotometer.

### *Synthesis of the compounds*

[*p*-HOBA<sup>−</sup>]-[protonated diethylamine] (**1**). *p*-HOBA (276 mg, 2.00 mmol) was dissolved in a mixture of water (10.0 mL) and ethanol (10.0 mL) with stirring and then transferred into a straight glass tube. Diethylamine (0.20 mL, 2.0 mmol) was carefully layered onto it. Colorless block crystals were observed on the tube wall after 2 days.



[*p*-HOBAA<sup>-</sup>]-[protonated *tert*-butylamine] (**2**). *p*-HOBA (276 mg, 2.00 mmol) was dissolved in a mixture of water (10.0 mL) and ethanol (10.0 mL) with stirring and then transferred into a straight glass tube. *tert*-Butylamine (0.21 mL, 2.0 mmol) was carefully layered onto it. Colorless block crystals were observed on the tube wall after 3 days.

[*p*-HOBAA<sup>-</sup>]-[protonated cyclohexylamine] (**3**). The same procedure as for **1** was applied except cyclohexylamine (0.23 mL, 2.0 mmol) was used instead of diethylamine and colorless block crystals were obtained after 2 days.

[*p*-HOBAA<sup>-</sup>]-[protonated imidazole] (**4**). *p*-HOBA (276 mg, 2.00 mmol) and imidazole (136 mg, 2.00 mmol) were dissolved in a mixture of water (10.0 mL) and ethanol (10.0 mL) under stirring. Upon slow evaporation of the solvents at room temperature, colorless block single crystals suitable for X-ray analysis were obtained after 4 days.

[*p*-HOBA]-[piperazine]·[H<sub>2</sub>O] (**5**). *p*-HOBA (276 mg, 2.00 mmol) and piperazine (172 mg, 2.00 mmol) were dissolved in a mixture of water (10.0 mL) and ethanol (10.0 mL) under stirring. Upon slow evaporation of the solvents at room temperature, colorless block single crystals suitable for X-ray analysis were obtained after 4 days.

#### Single-crystal X-ray diffraction studies

The diffraction data for **1–5** were collected on an Enraf-Nonius CAD-4 diffractometer with graphite-monochromated Mo K $\alpha$  radiation ( $\lambda = 0.71073 \text{ \AA}$ ,  $T = 293 \text{ K}$ ) in the  $\omega$ -scan mode. The structures were solved by direct methods and refined by least squares on  $F^2$  using the SHELXTL<sup>21</sup> software package. All non-hydrogen atoms were anisotropically refined. The positions of the hydrogen atom were fixed geometrically at calculated distances and allowed to ride on the parent carbon atoms. The molecular graphics were plotted using SHELXTL. Atomic scattering factors and anomalous dispersion corrections were taken from the International Tables for X-ray Crystallography.<sup>22</sup> Further detailed information of the crystallographic data and structural analysis for **1–5** are listed in Table I.

TABLE I. Crystal data and structure refinement summary for compounds **1–5**

Property	<b>1</b>	<b>2</b>	<b>3</b>	<b>4</b>	<b>5</b>
Empirical formula	C <sub>11</sub> H <sub>17</sub> NO <sub>3</sub>	C <sub>11</sub> H <sub>17</sub> NO <sub>3</sub>	C <sub>13</sub> H <sub>19</sub> NO <sub>3</sub>	C <sub>10</sub> H <sub>10</sub> N <sub>2</sub> O <sub>3</sub>	C <sub>9</sub> H <sub>13</sub> NO <sub>4</sub>
$M_r$	211.26	211.26	237.29	206.20	199.20
Crystal size, mm	0.24×0.20×0.16	0.24×0.22×0.18	0.22×0.20×0.18	0.26×0.18×0.14	0.22×0.20×0.16
Crystal system	Orthorhombic	Mono clinic	Monoclinic	Mono clinic	Monoclinic
Space group	<i>Pbca</i>	<i>P2<sub>1</sub>/c</i>	<i>P2<sub>1</sub>/c</i>	<i>P2<sub>1</sub>/c</i>	<i>P2<sub>1</sub>/c</i>
$a / \text{Å}$	12.176(2)	6.8300(14)	6.1820(12)	9.6160(19)	6.6120(13)
$b / \text{Å}$	10.728(2)	9.2790(19)	14.184(3)	10.587(2)	11.898(2)
$c / \text{Å}$	17.666(4)	19.831(4)	15.038(3)	11.075(5)	12.442(3)
$\alpha / ^\circ$	90	90	90	90	90
$\beta / ^\circ$	90	99.58(3)	99.74(3)	118.93(2)	92.48(3)
$\gamma / ^\circ$	90	90	90	90	90
$V / \text{Å}^3$	2307.6(8)	1239.3(4)	1299.6(5)	986.8(5)	977.9(3)
$Z$	8	4	4	4	4
$\rho_{\text{calcd}} / \text{g cm}^{-3}$	1.216	1.132	1.213	1.388	1.353
$F(000)$	912	456	512	432	424
$\mu / \text{mm}^{-1}$	0.088	0.082	0.086	0.105	0.107

TABLE I. Continued

Property	1	2	3	4	5
$\theta$ Range, °	2.31–26.95	2.08–26.96	1.99–27.01	2.42–26.96	2.37–26.97
Completeness to $\theta$ , %	98.2	99.3	97.5	97.9	97.1
Range of $h, k, l$	–14/14, –12/0, –21/0	0/8, 0/11, –23/23	0/7, –16/16, –17/17	0/11, –12/0, –14/12	0/7, 0/14, –14/14
Reflections collected/unique	4815/2468	2899/2677	5895/2766	2232/2109	2245/2071
$R_{\text{int}}$	0.0789	0.0391	0.0735	0.0268	0.0215
Data/restraints/ /parameters	2468/0/205	2677/0/149	2766/0/167	2109/0/137	2071/1/140
GOF on $F^2$	0.946	1.046	0.997	1.063	1.073
Final $R$ indices ( $I > 2\sigma(I)$ )	$R_1 = 0.0432,$ $wR_2 = 0.0847$	$R_1 = 0.0567,$ $wR_2 = 0.1456$	$R_1 = 0.0527,$ $wR_2 = 0.1273$	$R_1 = 0.0388,$ $wR_2 = 0.1039$	$R_1 = 0.0551,$ $wR_2 = 0.1662$
$R$ indices (all data)	$R_1 = 0.1610,$ $wR_2 = 0.1100$	$R_1 = 0.0883,$ $wR_2 = 0.1700$	$R_1 = 0.1307,$ $wR_2 = 0.1604$	$R_1 = 0.0641,$ $wR_2 = 0.1150$	$R_1 = 0.0672,$ $wR_2 = 0.1766$
Extinction coefficient	0.0112(12)	0.59(3)	0.018(3)	0.022(3)	0.074(11)
Peak, hole $\text{e}\text{\AA}^{-3}$	0.124, –0.114	0.217, –0.294	0.227, –0.261	0.219, –0.185	0.615, –0.662

## RESULTS AND DISCUSSION

*Preparation of compounds 1–5*

Since *p*-HOBA is only slightly soluble in water but well soluble in ethanol, and the organic bases used in this work easily dissolve in ethanol, a mixture of water and ethanol was used as the solvent, thus successfully giving the expected single-crystals. All crystallizations of *p*-HOBA and different organic bases were carried out in a 1:1 ratio, considering the acid–base reaction stoichiometric ratio. For preparation of **1**, **2** and **3**, since selected bases of diethylamine, *tert*-butylamine and cyclohexylamine are all liquids with densities smaller than those of the mixed  $\text{H}_2\text{O}-\text{C}_2\text{H}_5\text{OH}$  solution, they were carefully layered onto the mixed solvents. Three test tubes were used to facilitate the slow diffusion and desired single-crystals in all cases were obtained. For the preparation of **4** and **5**, *p*-HOBA was mixed directly with equivalent bases of imidazole or piperazine in  $\text{H}_2\text{O}-\text{C}_2\text{H}_5\text{OH}$  solutions, which were allowed to evaporate at ambient condition to give the final crystalline products.

*Analytical and spectral data for the synthesized compounds*

[*p*-HOBA<sup>−</sup>] $\cdot$ [protonated diethylamine] (**1**). M.p. 215 °C; An. al. Calcd. for  $\text{C}_{11}\text{H}_{17}\text{NO}_3$  ( $M_r = 211.26$ ): C, 62.5; H, 8.1; N, 6.6 %. Found: C, 62.4; H, 8.0; N, 6.5 %. IR (KBr,  $\text{cm}^{-1}$ ): 3421 *m*, 2993 *vs*, 2770 *vs*, 2658 *vs*, 2484 *vs*, 1626 *vs*, 1501 *vs*, 1377 *vs*, 1279 *vs*, 1160 *s*, 1091 *m*, 857 *s*, 784 *vs*, 701 *m*, 617 *s*.

[p-HOBAA<sup>-</sup>][protonated tert-butylamine] (**2**). M.p 260 °C; Anal. Calcd. for C<sub>11</sub>H<sub>17</sub>NO<sub>3</sub> (*M<sub>r</sub>* = 211.26): C, 62.5; H, 8.1; N, 6.6 %. Found: C, 62.3; H, 8.0; N, 6.45 %. IR (KBr, cm<sup>-1</sup>): 3418 *m*, 3103 *vs*, 3017 *vs*, 2829 *vs*, 2735 *s*, 2626 *s*, 2535 *m*, 1605 *vs*, 1502 *vs*, 1394 *vs*, 1287 *vs*, 1164 *s*, 1099 *m*, 856 *m*, 792 *m*, 703 *w*, 619 *m*.

[p-HOBAA<sup>-</sup>][protonated cyclohexylamine] (**3**). M.p. 220 °C; Anal. Calcd. for C<sub>13</sub>H<sub>19</sub>NO<sub>3</sub> (*M<sub>r</sub>* = 237.29): C, 65.8; H, 8.1; N, 5.9 %. Found: C, 65.7; H, 7.9; N, 5.7 %. IR (KBr, cm<sup>-1</sup>): 3420 *m*, 2938 *vs*, 2858 *s*, 2654 *vs*, 2572 *m*, 2141 *m*, 1597 *vs*, 1501 *vs*, 1439 *vs*, 1376 *vs*, 1276 *vs*, 1233 *vs*, 1156 *s*, 1091 *s*, 1030 *s*, 922 *w*, 892 *m*, 842 *s*, 788 *s*, 701 *w*, 644 *w*, 616 *m*.

[p-HOBAA<sup>-</sup>][protonated imidazole] (**4**). M.p. 224 °C; Anal. Calcd. for C<sub>10</sub>H<sub>10</sub>N<sub>2</sub>O<sub>3</sub> (*M<sub>r</sub>* = 206.20): C, 58.2; H, 4.9; N, 13.6 %. Found: C, 58.0; H, 4.6; N, 13.35 %. IR (KBr, cm<sup>-1</sup>): 3427 *s*, 3161 *vs*, 2922 *s*, 2803 *s*, 2689 *s*, 2026 *w*, 1598 *vs*, 1607 *vs*, 1542 *s*, 1390 *vs*, 1245 *vs*, 1160 *m*, 1128 *m*, 1049 *m*, 844 *s*, 780 *s*, 753 *m*, 697 *w*, 624 *m*.

[p-HOBA][piperazine][H<sub>2</sub>O] (**5**). M.p. 235 °C; Anal. Calcd. for C<sub>9</sub>H<sub>13</sub>NO<sub>4</sub> (*M<sub>r</sub>* = 199.20): C, 54.3; H, 6.6; N, 7.0 %. Found: C, 54.1; H, 6.4; N, 6.9%. IR (cm<sup>-1</sup>): 3132 *vs*, 3016 *vs*, 2773 *m*, 2497 *m*, 1611 *vs*, 1545 *s*, 1398 *vs*, 1271 *m*, 1228 *m*, 1165 *m*, 1095 *s*, 980 *m*, 856 *m*, 783 *m*, 697 *w*, 625 *m*.

#### Molecular and supramolecular structure of **1**

The hydrogen bonds for **1** are listed in Table II, together with the hydrogen-bond information for **2–5**. Some C–H... $\pi$  and  $\pi$ ... $\pi$  interactions for **1–5** are listed in Table III.

TABLE II. Hydrogen bond lengths (Å) and angles (°) for compounds **1–5**

Compound	D–H...A	Symmetry code	D...A	$\angle$ D–H...A
<b>1</b>	O(1)–H(2)...O(3)	$-1/2+ x, y, 1/2-z$	2.6404	169.25
	N(1)–H(4)...O(2)	$-1/2+x, 1/2-y, -z$	2.8764	140.49
	N(1)–H(4)...O(3)	$-1/2+ x, 1/2-y, -z$	3.0353	154.77
	N(1)–H(10)...O(2)	$1/2-x, -1/2+y, z$	2.7307	171.82
<b>2</b>	N(1)–H(1)...O(2)	–	2.8351	168.63
	N(1)–H(2)...O(2)	$1-x, 1-y, -z$	2.8422	161.42
	N(1)–H(3)...O(1)	$2-x, -1/2+y, 1/2-z$	2.7945	174.50
	O(3)–H(3B)...O(1)	$1-x, 1/2+y, 1/2-z$	2.6209	163.31
<b>3</b>	C(3)–H(3A)...O(3)	$1-x, 1/2+y, 1/2-z$	3.2161	130.00
	N(1)–H(1)...O(1)	$1-x, -y, 1-z$	2.8436	169.53
	N(1)–H(2)...O(2)	$-x, -y, 1-z$	2.8297	178.11
	N(1)–H(3)...O(2)	$1+x, y, z$	2.8752	155.38
	O(3)–H(3A)...O(1)	$-x, 1/2+y, 1/2-z$	2.6227	171.57
<b>4</b>	C(9)–H(9A)...O(3)	$x, 1/2-y, 1/2+z$	3.2757	144.49
	N(1)–H(1B)...O(1)	–	3.0681	120.62
<b>5</b>	N(1)–H(1B)...O(2)	–	2.6888	177.11
	N(2)–H(2B)...O(1)	$x, -1/2+y, 1/2-z$	2.7580	154.02
	O(3)–H(3A)...O(1)	$-x, 1/2+y, 1/2-z$	2.6394	169.18

TABLE II. Continued

Compound	D-H...A	Symmetry code	D...A	∠D-H...A
<b>4</b>	C(9)-H(9A)···O(3) 1+	$x, -1+y, z$	3.2810	138.77
	C(10)-H(10A)···O(2)	$x, 1/2-y, -1/2+z$	3.0467	119.88
<b>5</b>	O(2)-H(1)···N(1)	$x, 1/2-y, 1/2+z$	2.7446	154.23
	N(1)-H(1B)···O(3)	—	2.6270	88.21
O(1)-H(2)···O(1W)	$-1+x, 1/2-y, -1/2+z$	2.7190	169.69	
O(1W)-H(3)···O(2)	$1-x, 1/2+y, 1/2-z$	2.8184	158.14	
O(1W)-H(4)···O(3)	—	2.8126	168.19	

TABLE III. Data about C-H... $\pi$  and  $\pi$ ... $\pi$  interactions for compounds **1–5**

Cpd.	C-H	... $\pi$ or $\pi$ ... $\pi$ Sy	mmetry code	C...Cg <sup>a</sup> or Cg...Cg distance, Å	Perpendicular distance between planes of the rings, Å	∠C-H...Cg, °
<b>1</b>	C(8)-H(1)···Cg(1)	$-1/2+$	$x, y, 1/2-z$	3.600	—	122.20
	C(9)-H(6)···Cg(1) <sup>b</sup>	—	—	3.522	—	97.91
	C(9)-H(7)···Cg(1)	—	—	3.522	—	117.07
	C(8)-H(17)···Cg(1)	$-1/2+$	$x, y, 1/2-z$	3.600	—	97.07
<b>2</b>	C(9)-H(9B)···Cg(1)	—	$x, 1+y, z$	4.095	—	165.60
<b>3</b>	C(14)-H(14B)···Cg(1)	—	—	3.624	—	128.72
<b>4</b>	Cg(1)···Cg(1)	1-	$x, -y, 1-z$	3.808	3.525	—
	Cg(1)···Cg(2) <sup>c</sup>	1-	$x, 1-y, 1-z$	3.762	3.576	—
	Cg(2)···Cg(1)	1-	$x, 1-y, 1-z$	3.762	3.451	—
<b>5</b>	C(8)-H(8B)···Cg(2)	—	—	3.788	—	147.40

<sup>a</sup>Cg denotes a center of an aromatic ring; in **1**, **2** and **3**; <sup>b</sup>Cg(1) denotes the phenyl ring; in **4**, imidazole ring; <sup>c</sup>Cg(2) denotes the phenyl ring

As depicted in Fig. 1a, the *p*-HOBA molecule has donated its carboxyl proton to the amino-nitrogen atom of diethylamine, resulting in molecule **1** consisting of a *p*-HOBAA<sup>-</sup> and a protonated diethylamine cation. The unit cell of **1** contains eight *p*-HOBAA<sup>-</sup>s and eight protonated diethylamine cations, which are connected together through hydrogen bonds and the electrostatic effect. After deprotonation, the two carboxyl C–O bond lengths in *p*-HOBAA<sup>-</sup> become similar (C(7)–O(2) 1.253(3) and C(7)–O(3) 1.264(3) Å) as opposed to the C–O bond lengths (1.322(2) and 1.228(2) Å) in an independent *p*-HOBA molecule,<sup>23</sup> indicating that the conjugative effect becomes stronger among the O(2), C(7) and O(3) atoms. This situation can also be found in **2–4**. In *p*-HOBAA<sup>-</sup>, the atoms O(1) and C(7) together with the phenyl ring define a plane *P*1. In the diethylamine cation, the atoms N(1), C(8), C(9) and C(10) define another plane *P*2. The dihedral angle between *P*1 and *P*2 is 78.01°. Through strong O(1)–H(2)···O(3) hydrogen bonds (see Table II for details), the *p*-HOBAA<sup>-</sup> molecules are connected to each other with a head-to-tail motif and thus, a zigzag 1D chain is formed, run-

ning along the *a*-axis direction (Figs. 1b and 1c). Between two adjacent 1D chains, a repeating unit exists which is composed of two pairs of *p*-HOBAA<sup>-</sup> molecules, which arrange in a parallel and antiparallel orientation, with the center-to-center distances between two parallel phenyl rings being 11.843 and 13.947 Å, respectively. The two non-parallel phenyl rings are almost perpendicular, with the dihedral angle being 89.23°. At each pair of inflexion points between two adjacent 1D chains, two *p*-HOBAA<sup>-</sup> molecules are held together by two diethylamine cations via N(1)–H(4)···O(2), N(1)–H(4)···O(3) and N(1)–H(10)···O(2) bonds (see Table II for details). As a result, a 2D network is formed, as depicted in Fig. 1b. These 2D undulated arrays (Fig. 1c) are further stabilized by four types of interlayer C–H··· $\pi$  interactions (see Table III for details).

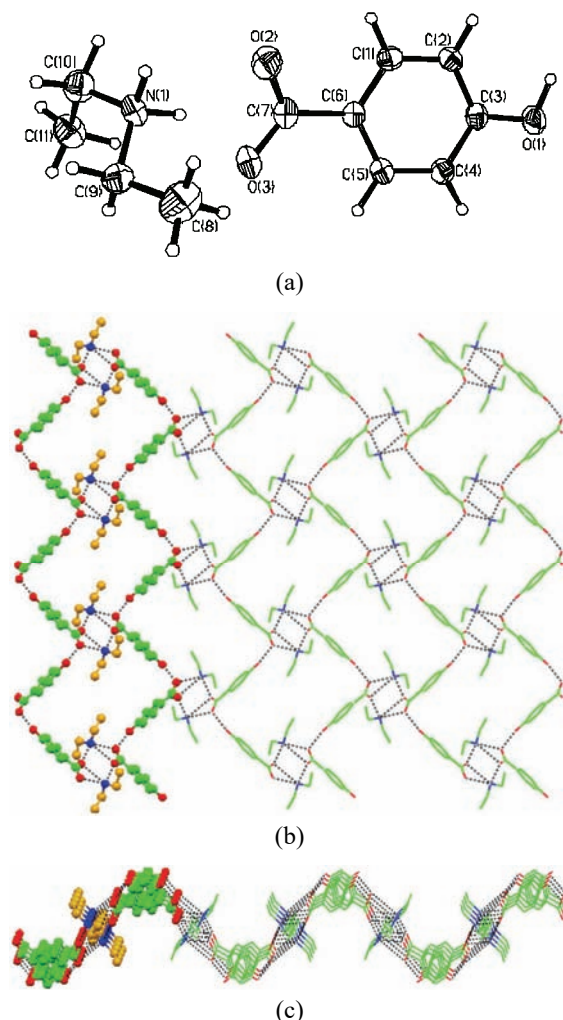


Fig. 1. a) Molecular structure of **1** with atomic numbering; 1D chain along the *a*-axis direction and perspective view in the *ac* plane (b) and in the *bc* plane (c).

### Molecular and supramolecular structure of **2**

Just as in compound **1**, *p*-HOBA molecule in **2** also transfers its carboxyl proton to the amino-nitrogen atom of *tert*-butylamine, resulting in molecule **2** consisting of a *p*-HOBAA<sup>-</sup> and a protonated *tert*-butylamine cation (Fig. 2a). A unit cell of **2** contains four pairs of *p*-HOBAA<sup>-</sup> and protonated *tert*-butylamine cation which connected together through hydrogen bonds and electrostatic effect. Similar to **1**, compound **2** also possesses abundant strong N–H···O and O–H···O hydrogen bonds. Primarily, the molecular assembly among *p*-HOBAA<sup>-</sup> occurs through O(3)–H(3B)···O(1) interactions, resulting in a zigzag 1D chain structure. Such a 1D chain runs along the *b*-axis with the *p*-HOBAA<sup>-</sup> moieties arranging in a head-to-tail motif (Fig. 2b). Between two contiguous 1D arrays, being similar to that in **1**, a repeating unit is found containing two pairs of *p*-HOBAA<sup>-</sup>, which

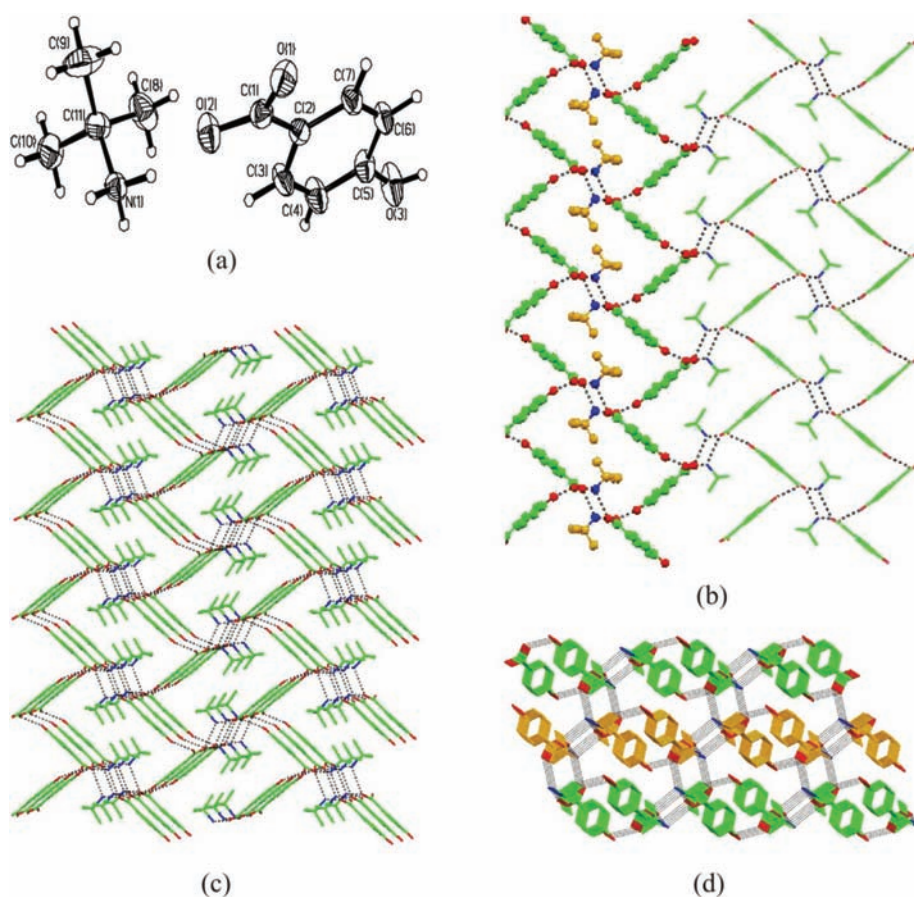


Fig. 2. a) Molecular structure of **2** with atomic numbering; b) 1D chain along the *b*-axis direction and perspective view in the *bc* plane; 3D architecture in the *bc* plane (c) and in the *ac* plane (d).

arrange in a parallel and antiparallel orientation (Fig. 2b), with the center-to-center distances between two parallel phenyl rings being 8.666 and 15.746 Å, respectively. The dihedral angle between two non-parallel phenyl rings is 81.64°. Then, these 1D chains are linked together by protonated *tert*-butylamine cations via N(1)–H(1)⋯O(2) and N(1)–H(2)⋯O(2) interactions (Table II). As depicted in Fig. 2b, two protonated *tert*-butylamine cations combine two *p*-HOBAAs molecules together at each pair of inflexion points between two adjacent 1D chains and thus, a 2D hydrogen-bonded net is given in the *bc* plane. Further analysis shows that these 2D layers adopt a parallel stack along the *a*-axis via N(1)–H(3)⋯O(1) and finally create a 3D supramolecular architecture (Figs. 2c and 2d), which is distinct from that of **1**. In addition, interlayer C(3)–H(3A)⋯O(3) and intra-layer C(9)–H(9B)⋯Cg(1) (Cg(1) denotes phenyl ring) (see Table II and Table III for details) forces also help to stabilize the whole supramolecular system.

#### *Molecular and supramolecular structure of 3*

Compound **3** comprises a *p*-HOBAAs and a protonated cyclohexylamine cation (Fig. 3a). The unit cell of **3** contains four pairs of *p*-HOBAAs and a protonated cyclohexylamine cation. The supramolecular constructions in **3** are very similar to those in **2**. Firstly, through O(3)–H(3A)⋯O(1) interactions, a zigzag 1D chain along the *b*-axis direction is formed of *p*-HOBAAs molecules in a head-to-tail fashion (Fig. 3b), and in the two neighboring 1D chains, two pairs of *p*-HOBAAs molecules array mutually parallel but reversed (Fig. 3b). Then, via N(1)–H(2)⋯O(2) and N(1)–H(3)⋯O(2) interactions, protonated cyclohexylamine cations join these 1D chains together at each pair of inflexion points to make a 2D layer network in the *bc* plane (Fig. 3b), with two protonated cyclohexylamine cations connecting two *p*-HOBAAs anions. Ultimately, the 2D layers stack along the *a*-axis via N(1)–H(1)⋯O(1) interactions to generate a 3D supramolecular architecture (Fig. 3c). However, opposed to **2**, in **3**, C(9)–H(9A)⋯O(3) forces exist in the same 2D layer, while C(14)–H(14B)⋯Cg(1) (see Table III) interactions are observed between neighboring 2D layers, both of which stabilize the supramolecular structure of **3**. In addition, in the contiguous 1D chains of **3**, the center-to-center distances between two pairs of parallel phenyl rings are 10.537 and 15.833 Å, respectively, both of which are larger than the corresponding values in **2**. The dihedral angle between two non-parallel phenyl rings is 46.23°, which is also different from that in **2**. These distinctions may be ascribed to the volume of the protonated cyclohexylamine cation being larger than that of the protonated *tert*-butylamine cation.

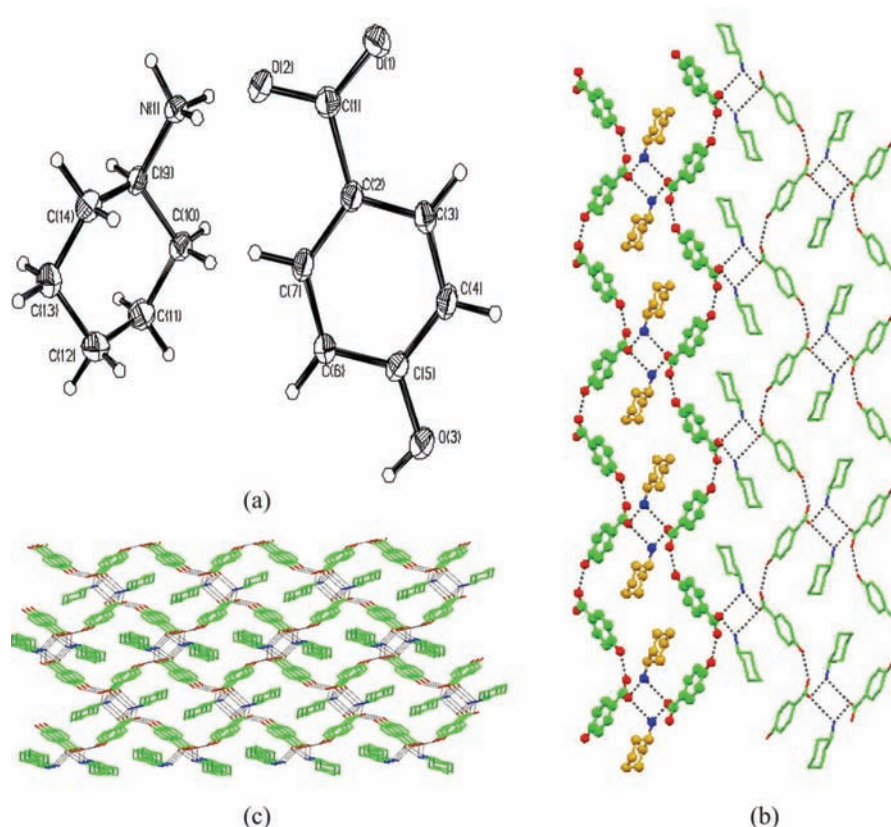


Fig. 3. a) Molecular structure of **3** with atomic numbering; b) 1D chain along the *b*-axis direction and perspective view in the *bc* plane; c) 3D structure viewed along the *a*-axis.

#### Molecular and supramolecular structure of **4**

Compound **4** (Fig. 4a) is made up of a *p*-HOBAA<sup>−</sup> and protonated imidazole cation. A unit cell contains four *p*-HOBAA<sup>−</sup>s and four protonated imidazole cations. With respect to the supramolecule building of **4**, similar to **1**, **2** and **3**, 1D zig-zag chains are primarily formed *via* O(3)–H(3A)⋯O(1) interactions between *p*-HOBAA<sup>−</sup> molecules with a head-to-tail motif (Fig. 4b). However, between the two neighboring 1D chains, as the repeat unit, two pairs of parallel *p*-HOBAA<sup>−</sup>s array in the same direction (Fig. 4b), respectively, which is a significant difference from those in **1**, **2** and **3**. In addition, for the repeat unit, both center-to-center distances between two pairs of parallel phenyl rings are the same and equal to 9.616 Å, and the dihedral angle between two non-parallel phenyl rings is 46.23°, which are also distinct to those in **1**, **2**, and **3**. As a consequence, when the 1D chains are held together by protonated imidazole cations through N(1)–H(1B)⋯O(1) and N(1)–H(1B)⋯O(2), as well as N(2)–H(2B)⋯O(1) interactions



(see Table II), a diverse 2D network is produced. In the 2D net, each inflexion point of each 1D chain connects with a pair of protonated imidazole cations and this pair of protonated imidazole cations couple with two inflexion points of another adjacent 1D chain synchronously. Further inspection of the lattice arrangement reveals that both C–H...O and face-to-face interactions stabilize the supramolecular architecture. Among them, C(9)–H(9A)...O(3) is intralayered, while C(10)—H(10A)...O(2) joins the interlayer acid and base components. Two types of  $\pi\cdots\pi$  stackings between phenyl ring-to-phenyl ring and phenyl ring-to-imidazole ring (see Table III for details) are also interlayer interactions.

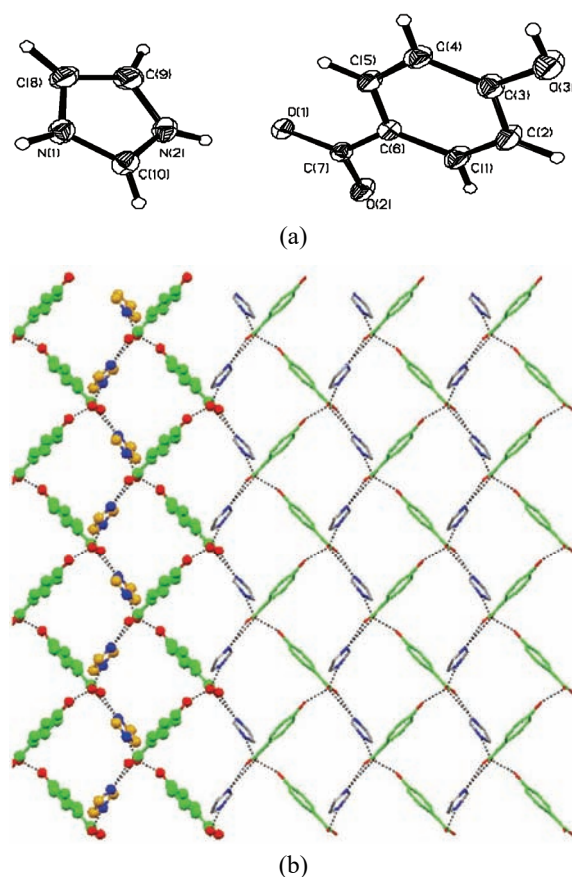


Fig. 4. a) Molecular structure of **4** with atomic numbering; b) 1D chain along the *b*-axis direction and 2D network viewed along the *c*-axis.

In view of the 2D structure of **4** being different from those of **1–3**, one can find that the organic base of imidazole in **4** has two important structural characteristics distinct from those of the organic bases used in **1–3**. One is that it is a rigid aromatic base and the other that it has two nitrogen atoms, which means that each protonated imidazole cation can form hydrogen bonds from two dif-

ferent directions of the molecule. On the contrary, in **1–3**, the organic bases are not rigid aromatic bases and they have only one nitrogen atom. It is possible that these two significant features of imidazole finally produce the unique 2D supramolecular building of **4**.

#### *Molecular and supramolecular structure of 5*

Opposed to **1–4**, co-crystallization of piperazine with *p*-HOBA yields the neutral molecular co-crystal **5**, in which *p*-HOBA does not transfer its carboxyl hydrogen atom to the piperazine molecule (Fig. 5a). Additionally, a lattice water solvent molecule is observed in **5**; hence compound **5** is built up of a *p*-HOBA, a piperazine and a water molecule. The unit cell contains four *p*-HOBA, two piperazine and four water molecules. In each *p*-HOBA, the bond distances of C–O are 1.259(3) and 1.273(2) Å, respectively, which are also different from those in an independent *p*-HOBA molecule.<sup>23</sup> As for the supramolecular building of **5**, first, each piperazine acts as a hydrogen-bonding connector, joining four *p*-HOBA subunits via strong pair-wise O(2)–H(1)⋯N(1) and N(1)–H(1B)⋯O(3) bonds (see Table II for details) and two *p*-HOBA molecules are linked to two piperazine molecules. Thus, a tape-like 1D supramolecular motif is formed, running along the *a*-axis direction, as shown in Fig. 5b. Then, each water molecule acts as a 3-connector to link with three *p*-HOBA molecules through O(1)–H(2)⋯O(1W), O(1W)–H(3)⋯O(2) and O(1W)–H(4)⋯O(3), which results in the 1D tapes being combined and a 3D hydrogen-bonding network being finally formed (Fig. 5c). Within the 3D network, an intermolecular C(8)–H(8B)⋯Cg(2) force is observed, which aids in the stabilization of the whole crystal structure.

#### *Melting point of compounds 1–5*

The melting point of *p*-HOBA is 213 °C. Of the five bases studied here, diethylamine, *tert*-butylamine and cyclohexylamine are all liquids and the melting points of imidazole and piperazine are 90 and 106 °C, respectively. The experimentally determined melting points for **1–5** are 215, 260, 220, 224 and 235 °C, respectively. It is evident that all the compounds **1–5** have higher melting points than their corresponding reactants, which may be because the hydrogen-bond types and numbers in **1–5** are greater than those in the corresponding reactants. For instance, the N–H⋯O hydrogen bond exists universally in **1–5**, while it cannot be found in any of the reactants used in this study. On the other hand, comparisons of the strength of the hydrogen bonds and the C–H⋯O, C–H⋯ $\pi$  and  $\pi$ ⋯ $\pi$  interactions (given in Tables II and III) and the melting points suggest that the melting points of the complexes are influenced not only by hydrogen bonds and other interactions. For instance, for **2**, **3** and **5**, although they all have four hydrogen bonds and one C–H⋯ $\pi$  interaction, and the distance C⋯Cg in **2** of 4.095 Å is the longest, the three of them have different melting points and the melting point of **2** is the highest. The maximum supramolecular number of interactions, including

six hydrogen bonds and three other interactions, exist in **4**, but the melting point of **4** is not the highest of the five complexes. Compound **1** contains four hydrogen bonds and four other interactions, which is more than in compounds **2**, **3** and **5**, however, its melting point is the lowest. Most important, the higher melting points suggest that compounds **1–5** are not the ordinary superposition of the reactants and that they become new materials different from the original reactants, and that they are more stable than the reactants, which might be useful information for further investigations on the synthesis of new pattern functional materials.

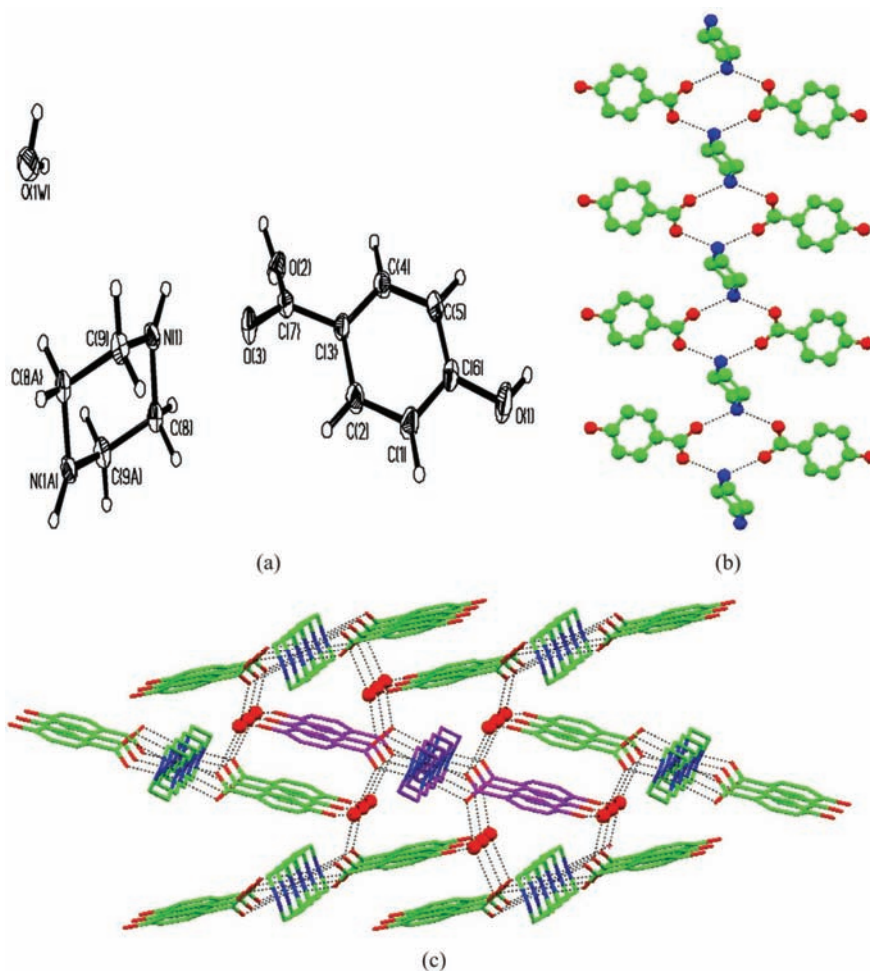


Fig. 5. a) Molecular structure of **5** with atomic numbering; b) 1D tape along the *a*-axis; c) 3D structure viewed along the *a*-axis.

## CONCLUSIONS

Five acid–base complexes were synthesized using *p*-hydroxybenzoic acid (*p*-HOBA) as the building block, which form 2D and 3D networks through hydrogen bonds and C–H...O, C–H... $\pi$  and  $\pi$ ... $\pi$  interactions. Determination of their melting points showed that the five compounds are more stable than their respective reactants, that they are not the ordinary superposition of the reactants and that they became new materials different from the original reactants.

*Supplementary material.* CCDC-652250 for **1**, 651984 for **2**, 651983 for **3**, 691985 for **4** and 651986 for **5** contain the supplementary crystallographic data for this paper. These data can be obtained free of charge at [www.ccdc.cam.ac.uk/conts/retrieving.html](http://www.ccdc.cam.ac.uk/conts/retrieving.html) (or from the Cambridge Crystallographic Data Centre (CCDC), 12 Union Road, Cambridge CB2 1EZ, UK; fax: +44(0)1222-336033; email: [deposit@ccdc.cam.ac.uk](mailto:deposit@ccdc.cam.ac.uk)).

*Acknowledgements.* This work was supported by the Natural Science Foundation of the Shandong Province (No. Z2007B01 and Y20 07B14) and by the Doctoral Fund of Qingdao, University of Science and Technology.

## ИЗВОД

ПРОЈЕКТОВАЊЕ КРИСТАЛА КИСЕЛИНСКО–БАЗНИХ КОМПЛЕКСА СА 2D И 3D ВОДНИЧНО ВЕЗАНИМ СИСТЕМИМА КОРИШЋЕЊЕМ *p*-ХИДРОКСИБЕНЗОЕВЕ КИСЕЛИНЕ КАО ГРАДИВНОГ БЛОКА

PU SU ZHAO, XIAN WANG, FANG FANG JIAN, JUN LI ZHANG и HAI LIAN XIAO

*New Materials and Function Coordination Chemistry Laboratory, Qingdao University of Science and Technology, Qingdao Shandong 266042, P. R. China*

*p*-Хидроксibenзоева киселина (*p*-НОВА) је изабрана као елемент за самоизградњу са пет база: диетиламином, *tert*-бутиламином, циклохексиламином, имидазолом и пиперазином градећи одговарајуће киселинско–базне комплексе **1–5**. Кристално–структурне анализе указују да се протон–трансфер са карбоксилног водоника на азотов атом базе може уочити код **1–4**, а само у **5** молекула из растварача воде коегзистира са *p*-НОВА и пиперазином. Водоничним везама О–Н...О, присутним у **1–4**, депротоновани *p*-хидроксibenзоатни анијони *p*-НОВАА<sup>–</sup> се једноставно повезују мотивом глава–реп градећи једnodимензионалне (1D) низове додатно проширене на разне дводимензионалне (2D) (за **1** и **4**) и тродимензионалне (3D) (за **2** и **3**) мреже путем Н–Н...О интеракција. Док су у **5** неутрална киселина и база повезане паровима О–Н...Н и Н–Н...О веза градећи 1D траку, комбинацијом 1D трака са молекулима воде креира се 3D мрежа. Неке С–Н...О, С–Н... $\pi$  и  $\pi$ ... $\pi$  интеракције изван и унутар слојева помажу стабилизовању супрамолекуларних творевина. Тачке топљења указују да 5 киселинско–базних комплекса нису обична суперпозиција реактаната и да су стабилнији од оригиналних реактаната.

(Примљено 16. априла, ревидирано 21. септембра 2009)

## REFERENCES

1. X. L. Zhang, X. M. Chen, *Cryst. Growth Des.* **5** (2005) 617
2. D. Y. Kong, J. L. McBee, A. Clearfield, *Cryst. Growth Des.* **5** (2005) 643
3. M. Du, Z. H. Zhang, X. J. Zhao, *Cryst. Growth Des.* **5** (2005) 1199

4. Z. J. Li, Y. Abramov, J. Bordner, J. Leonard, A. Medek, A. V. Trask, *J. Am. Chem. Soc.* **128** (2006) 8199
5. S. Wishkerman, J. Bernstein, M. B. Hickey, *Cryst. Growth Des.* **9** (2009) 3204
6. P. Gilli, L. Pretto, V. Bertolasi, G. Gilli, *Acc. Chem. Res.* **42** (2009) 33
7. L. S. Reddy, S. K. Chandran, S. George, N. J. Babu, A. Nangia, *Cryst. Growth Des.* **7** (2007) 2675
8. A. Nangia, *Cryst. Growth Des.* **8** (2008) 1079
9. M. Khan, V. Enkelmann, G. Brunklaus, *Cryst. Growth Des.* **9** (2009) 2354
10. A. M. Beatty, *Coord. Chem. Rev.* **246** (2003) 131
11. B. R. Bhogala, P. Vishweshwar, A. Nangia, *Cryst. Growth Des.* **2** (2002) 325
12. B. R. Bhogala, A. Nangia, *Cryst. Growth Des.* **3** (2003) 547
13. M. Eddaoudi, D. B. Moler, H. Li, B. Chen, T. M. Reineke, M. O'Keeffe, O. M. Yaghi, *Acc. Chem. Res.* **34** (2001) 319
14. P. J. Hagerman, D. Hagerman, J. Zubieta, *Angew. Chem., Int. Ed.* **38** (1999) 2638 and references therein
15. M. Du, Z. H. Zhang, X. G. Wang, H. F. Wu, Q. Wang, *Cryst. Growth Des.* **6** (2006) 1867
16. F. F. Jian, P. S. Zhao, Q. X. Wang, *Chin. J. Struct. Chem.* **24** (2005) 184
17. L. H. Wei, *Acta Crystallogr. E* **62** (2006) o4506
18. Y. Moritani, N. Sasahara, S. Kashino, M. Haisa, *Acta Crystallogr. C* **43** (1987) 154
19. H. Parshad, K. Frydenvang, T. Liljefors, H. O. Sorensen, C. Larsen, *Int. J. Pharm.* **269** (2004) 157
20. C. B. Aakeroy, G. S. Bahra, P. B. Hitchcock, Y. Patell, K. R. Seddon, *Chem. Commun.* (1993) 152
21. G. M. Sheldrick, *SHELXTL, v5 Reference Manual*, Siemens Analytical X-Ray Systems, Madison, WI, 1997
22. A. J. Wilson, *International Table for X-Ray Crystallography*, Vol. C, Kluwer Academic, Dordrecht, 1992, Tables 6.1.1.4 (pp. 500–502) and 4.2.6.8 (pp. 219–222)
23. M. Colapietro, A. Domenicano, C. Marciante, *Acta Crystallogr. B* **35** (1979) 2177.





*J. Serb. Chem. Soc.* 75 (4) 475–482 (2010)  
JSCS–3980

## Macrocyclic complexes: synthesis and characterization

DHARMPAL SINGH\* and KRISHAN KUMAR

Department of Chemistry, National Institute of Technology, Kurukshetra – 136 119, India

(Received 21 October 2009, revised 12 January 2010)

**Abstract:** A novel series of complexes of the type  $[M(C_{28}H_{24}N_4)X]X_2$ , where  $M = Cr(III), Fe(III)$  or  $Mn(III)$ ,  $X = Cl^-, NO_3^-, CH_3COO^-$  and  $(C_{28}H_{24}N_4)$  corresponds to the tetradentate macrocyclic ligand, were synthesized in methanolic media by the template condensation of 1,8-diaminonaphthalene and 2,3-butanedione (diacetyl) in the presence of trivalent metal salts. The complexes were characterized by elemental analyses, conductance and magnetic measurements, and UV/Vis and IR spectroscopy. Based on these studies, a five-coordinate square pyramidal geometry for all the prepared complexes is proposed. All the synthesized macrocyclic complexes were tested for their *in vitro* antifungal activity against some fungal strains viz. *Aspergillus niger* and *A. fumigatus*. The results obtained were compared with the standard antifungal drug fluconazole.

**Keywords:** antifungal activity; 2,3-butanedione; template synthesis; macrocyclic Schiff-base complexes.

### INTRODUCTION

A number of nitrogen donor macrocyclic derivatives have long been used in analytical, industrial and medical applications.<sup>1</sup> Macrocyclic compounds and their derivatives are interesting ligand system because they are good hosts for metal anions, neutral molecules and organic cation guests.<sup>2</sup> The metal-ion and host–guest chemistry of macrocyclic compounds are very useful in fundamental studies, e.g., in phase transfer catalysis and biological studies.<sup>3</sup> *In situ*, one pot template condensation reactions lie at the heart of macrocyclic chemistry.<sup>4</sup> Therefore, template reactions have been widely used for the synthesis of macrocyclic complexes,<sup>5</sup> where, generally, transition metal ions are used as the templating agent.<sup>6</sup> The metal ions direct the reaction preferentially towards cyclic rather than oligomeric or polymeric products.<sup>7</sup> Synthetic macrocyclic complexes mimic some naturally occurring macrocycles because of their resemblance to many natural macrocycles, such as metalloproteins, porphyrins and cobalamine.<sup>8,9</sup> Transition

\* Corresponding author. E-mail: dpsinghchem@yahoo.co.in  
doi: 10.2298/JSC091021028S

metal macrocyclic complexes have received great attention due to their biological activities, including antiviral, anticarcinogenic,<sup>9</sup> antifertile,<sup>10</sup> antibacterial and antifungal.<sup>11</sup> Macrocyclic metal complexes of lanthanides *e.g.*, Gd(III), are used as MRI (magnetic resonance imaging) contrast agents.<sup>12</sup> In a previous paper, the synthesis and characterization of macrocyclic complexes of Co(II), Ni(II), Cu(II), Zn(II) and Cd(II) derived from 1,8-diaminonaphthalene and diacetyl were reported.<sup>13</sup>

Prompted by these facts, in the present paper, the synthesis and characterization of Cr(III), Fe(III) and Mn(III) macrocyclic complexes derived from 1,8-diaminonaphthalene and diacetyl (2,3-butanedione) are discussed. Complexes were characterized using various physicochemical techniques, such as IR and UV/Vis spectroscopy, elemental analyses, and magnetic susceptibility and conductivity measurements.

All the synthesized macrocyclic complexes were tested for their *in vitro* antifungal activities against some fungal strains *viz.* *Aspergillus niger* (MTCC 282) and *A. fumigatus* (MTCC 870). The obtained results were compared with those for the standard antifungal drug fluconazole.

## EXPERIMENTAL

### Materials

All the chemicals and solvents used in this study were of AnalaR grade. 1,8-Diaminonaphthalene and 2,3-butanedione were procured from Acros, New Jersey, USA, the metal salts were purchased from S.D.-fine, Mumbai, India, Merck, Ranbaxy, India, and were used as received.

### Isolation of complexes

All the complexes were synthesized by the template method, *i.e.*, by condensation of 1,8-diaminonaphthalene and 2,3-butanedione in the presence of the respective trivalent metal salt. To a hot stirring methanolic solution ( $\approx 50 \text{ cm}^3$ ) of 1,8-diaminonaphthalene (10 mmol) was added trivalent chromium, manganese or iron salt (5.0 mmol) dissolved in the minimum quantity of MeOH ( $\approx 20 \text{ cm}^3$ ). The resulting solution was refluxed for 0.5 h. Subsequently, 2,3-butanedione (10 mmol) was added to the refluxing mixture and refluxing was continued for 8–10 h. The mixture was then concentrated to half its volume, cooled to room temperature and kept in a desiccator overnight, whereby dark-colored precipitates formed, which were filtered, washed with methanol, acetone and diethyl ether and dried *in vacuo*. The obtained yields were  $\approx 60$ – $70$  %. The complexes were soluble in DMF and DMSO. They were thermally stable up to 265–290 °C, after which decomposition occurred.

The template condensation of 1,8-diaminonaphthalene and 2,3-butanedione in the presence of trivalent metal salts, in the molar ratio 2:2:1 is represented in Scheme 1.

### Analytical and physical measurements

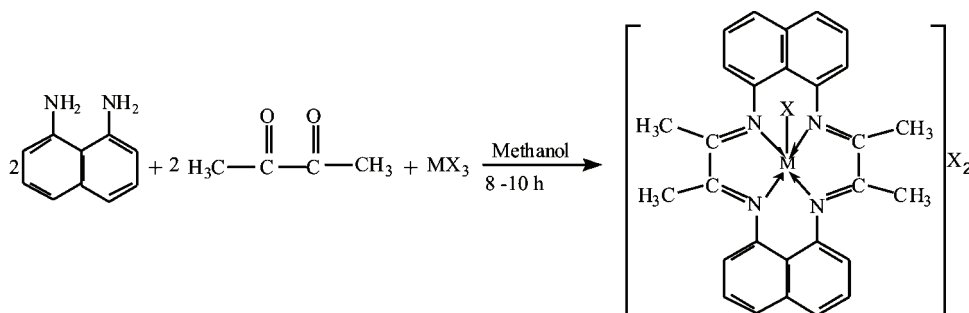
The microanalysis for C, H, and N were realized using an elemental analyzer (Perkin Elmer 2400) at SAIF, Punjab University, Chandigarh, India. The magnetic susceptibility measurements were made at SAIF, IIT Roorkee, on a vibrating sample magnetometer (Model PAR 155). The metal contents in the complexes were determined by literature methods.<sup>14</sup> The IR spectra were recorded on a FT-IR spectrophotometer (Perkin Elmer RX-I) in the range 4000–



200  $\text{cm}^{-1}$  using the Nujol Mull method. The electronic spectra (in DMSO) were recorded at room temperature on a Hitachi 330 spectrophotometer in the 200–850 nm range. The conductivity was measured on a digital conductivity meter (HPG system, G-3001). The melting points were determined in capillaries using a Swastika electric melting point apparatus.

#### In vitro antifungal activity

All the newly synthesized complexes were evaluated for their antifungal activities towards *A. niger* and *A. fumigatus* by the poison food technique.<sup>15</sup>



Scheme 1. Representation of the template condensation of 1,8-diaminonaphthalene and 2,3-butanedione in the presence of trivalent metal salts in the molar ratio 2:2:1 (M = Cr(III), Mn(III) or Fe(III) and X =  $\text{Cl}^-$ ,  $\text{NO}_3^-$  or  $\text{CH}_3\text{COO}^-$ ).

## RESULTS AND DISCUSSION

### Chemistry

The analytical data showed the suggested formula for macrocyclic complexes as:  $[\text{M}(\text{C}_{28}\text{H}_{24}\text{N}_4)\text{X}]\text{X}_2$ , where M = Cr(III), Fe(III) or Mn(III), X =  $\text{Cl}^-$ ,  $\text{NO}_3^-$  or  $\text{CH}_3\text{COO}^-$  and  $\text{C}_{28}\text{H}_{24}\text{N}_4$  corresponds to the tetradentate macrocyclic ligand. The measurements of molar conductance in DMSO showed that these chelates are 1:2 electrolytes<sup>16</sup> (conductance 155–185  $\Omega^{-1} \text{cm}^2 \text{mol}^{-1}$ ). Various attempts, such as crystallization using mixtures of solvents and low temperatures, were unsuccessful for the growth of a single crystal suitable for X-ray crystallography. However, the analytical, spectroscopic and magnetic data enabled the possible structure of the synthesized complexes to be predicted. All complexes gave satisfactory elemental analyses results, as shown in Table I.

### IR Spectra

It was noted that two bands present in the spectrum of 1,8-diaminonaphthalene at 3350 and 3390  $\text{cm}^{-1}$ , corresponding to the  $\nu(\text{NH}_2)$  group, were absent from the infrared spectra of all the complexes. Furthermore, no strong absorption band was observed near 1716  $\text{cm}^{-1}$  indicating the absence of the C=O group of the 2,3-butanedione (diacetyl) moiety. The disappearance of these bands and the appearance of a new strong absorption band in the range 1590–1629  $\text{cm}^{-1}$  confirms the condensation of the carbonyl group of 2,3-butanedione and the amino

group of diamionaphthalene and the formation of a macrocyclic Schiff's base,<sup>17</sup> as these bands may be assigned to  $\nu(\text{C}=\text{N})$  stretching vibrations.<sup>18</sup> The lower value of the frequency of  $\nu(\text{C}=\text{N})$  vibrations may be explained by a drift of the lone pair electron density of the azomethine nitrogen towards the metal atom,<sup>19</sup> indicating that coordination occurs through the nitrogen of the C=N groups. The medium intensity bands present in the region 2830–2950  $\text{cm}^{-1}$  may be assigned to the  $\nu(\text{C}-\text{H})$  stretching vibrations of the methyl group of the diacetyl moiety.<sup>20</sup> The various absorption bands in the region 1400–1588  $\text{cm}^{-1}$  may be assigned to  $\nu(\text{C}=\text{C})$  aromatic stretching vibrations of the naphthalene ring.<sup>21,22</sup> The bands in the region 740–785  $\text{cm}^{-1}$  may be assigned to the  $\nu(\text{C}-\text{H})$  out of plane bending of the aromatic ring.<sup>23</sup> The presence of the absorption bands at 1408–1440, 1290–1320 and 1010–1030  $\text{cm}^{-1}$  in the IR spectra of all the nitrate complexes suggest that the nitrate groups are coordinated to the central metal ion in a unidentate fashion.<sup>24</sup> The IR spectra of all the acetate complexes show an absorption band in the region 1650–1680  $\text{cm}^{-1}$  that is assigned to the  $\nu(\text{COO}^-)_{\text{as}}$  asymmetric stretching vibrations of the acetate ion and another in the region 1258–1290  $\text{cm}^{-1}$  that can be assigned to the  $\nu(\text{COO}^-)_{\text{s}}$  symmetric stretching vibration of the acetate ion. The difference between ( $\nu_{\text{as}}-\nu_{\text{s}}$ ) of around 390–370  $\text{cm}^{-1}$  is greater than 144  $\text{cm}^{-1}$ , which indicates the unidentate coordination of the acetate group with the central metal ion.<sup>25</sup>

TABLE I. Analytical data of the trivalent chromium, manganese and iron complexes derived from 1,8-diamionaphthalene and 2,3-butanedione

No.	Complex	Found (Calcd.), %				Color	Molecular weight
		M	C	H	N		
1	$[\text{Cr}(\text{C}_{28}\text{H}_{24}\text{N}_4)\text{Cl}]\text{Cl}_2$	8.96 (9.06)	58.52 (58.53)	4.10 (4.18)	9.68 (9.75)	Green	574
2	$[\text{Cr}(\text{C}_{28}\text{H}_{24}\text{N}_4)(\text{NO}_3)](\text{NO}_3)_2$	7.91 (7.95)	51.34 (51.37)	3.66 (3.67)	14.94 (14.98)	Yellowish green	654
3	$[\text{Cr}(\text{C}_{28}\text{H}_{24}\text{N}_4)(\text{OAc})](\text{OAc})_2$	8.01 (8.06)	63.21 (63.25)	5.10 (5.11)	8.64 (8.68)	Dark grey	645
4	$[\text{Mn}(\text{C}_{28}\text{H}_{24}\text{N}_4)(\text{OAc})](\text{OAc})_2$	8.47 (8.47)	62.92 (62.96)	5.03 (5.09)	8.63 (8.64)	Black	648
5	$[\text{Fe}(\text{C}_{28}\text{H}_{24}\text{N}_4)\text{Cl}]\text{Cl}_2$	9.63 (9.66)	58.10 (58.13)	4.10 (4.15)	9.66 (9.69)	Black	578
6	$[\text{Fe}(\text{C}_{28}\text{H}_{24}\text{N}_4)(\text{NO}_3)](\text{NO}_3)_2$	8.45 (8.49)	51.04 (51.06)	3.59 (3.65)	14.80 (14.89)	Dark grey	658
7	$[\text{Fe}(\text{C}_{28}\text{H}_{24}\text{N}_4)(\text{OAc})](\text{OAc})_2$	8.57 (8.60)	62.85 (62.86)	5.01 (5.08)	8.61 (8.63)	Reddish brown	649

The far infrared spectra show bands in the region 420–450  $\text{cm}^{-1}$  corresponding to  $\nu(\text{M}-\text{N})$  vibrations.<sup>26–28</sup> The bands in the spectra of all the complexes in the region 420–450  $\text{cm}^{-1}$  originate from (M–N) azomethine vibrational modes and identify coordination of the azomethine nitrogen.<sup>29</sup> The bands present in the

range 300–320  $\text{cm}^{-1}$  may be assigned to  $\nu(\text{M}-\text{Cl})$  vibration.<sup>26–28</sup> The bands present in the region 220–250  $\text{cm}^{-1}$  in all the nitrate complexes are related to the  $\nu(\text{M}-\text{O})$  stretching vibration.<sup>26,27</sup>

#### *Magnetic measurements and electronic spectra*

**Chromium complexes.** The magnetic moments of the chromium(III) complexes at room temperature were found in the range 4.25–4.50  $\mu_{\text{B}}$ , which are close to the predicted values for three unpaired electrons in the metal ion.<sup>15</sup> The electronic spectra of the chromium complexes show bands at  $\approx$  9010–9320, 13030–13350, 17460–18320, 27420–27850 and 34810  $\text{cm}^{-1}$ . These spectral bands cannot be interpreted in terms of either a four- or six-coordinated environment around the metal atom. However, the spectra are consistent with that of five-coordinated Cr(III) complexes, the structures of which were confirmed with the help of X-ray measurements.<sup>30</sup> Based on the analytical data, spectral studies and electrolytic nature of these complexes, a five-coordinated, square pyramidal geometry may be assigned to these complexes. Thus, assuming  $\text{C}_{4\text{V}}$  symmetry for these complexes,<sup>31,32</sup> the various spectral bands may be assigned as:  ${}^4\text{B}_1 \rightarrow {}^4\text{E}_a$ ,  ${}^4\text{B}_1 \rightarrow {}^4\text{B}_2$ ,  ${}^4\text{B}_1 \rightarrow {}^4\text{A}_2$  and  ${}^4\text{B}_1 \rightarrow {}^4\text{E}^b$ , respectively.

**Manganese complex.** The magnetic moment of the manganese(III) complex was found to be 4.89  $\mu_{\text{B}}$ , which indicates a high spin ( $d^4$ ) system.<sup>15</sup> The electronic spectra of the manganese complexes show three d–d bands, which lie in the range 12350–12590, 16050–18820 and 35420–35700  $\text{cm}^{-1}$ . The higher energy band at 35440–35750  $\text{cm}^{-1}$  may be assigned to charge transfer transitions. The spectra resemble those reported for five-coordinate, square pyramidal manganese complexes.<sup>31,32</sup> This idea is further supported by the presence of a broad ligand field band at 20400  $\text{cm}^{-1}$ , which is diagnostic for  $\text{C}_{4\text{V}}$  symmetry, and thus the various bands may be assigned as follows:  ${}^5\text{B}_1 \rightarrow {}^5\text{A}_1$ ,  ${}^5\text{B}_1 \rightarrow {}^5\text{B}_2$ , and  ${}^5\text{B}_1 \rightarrow {}^5\text{E}$ , respectively. The band assignment in a single electron transition may be given as:  $d_{z^2} \rightarrow d_{x^2-y^2}$ ,  $d_{xy} \rightarrow d_{x^2-y^2}$ , and  $d_{xz}$  and  $d_{yz} \rightarrow d_{x^2-y^2}$ , respectively, in order of increasing energy.

**Iron complexes.** The magnetic moments of iron complexes lie in the range 5.81–5.90  $\mu_{\text{B}}$ , corresponding to five unpaired electrons, which is close to the predicted high spin values for these metal ions.<sup>15</sup> The electronic spectra of the iron complexes show various bands at 9820–9970, 15520–15575 and 27550–27730  $\text{cm}^{-1}$ , which do not suggest octahedral or tetrahedral geometry around the metal atom. The spectral bands are, however, consistent with the range of spectral bands reported for five-coordinate, square pyramidal iron(III) complexes.<sup>32,33</sup> Assuming  $\text{C}_{4\text{V}}$  symmetry for these complexes, the various bands can be assigned as:  $d_{xy} \rightarrow d_{xz}$ , and  $d_{yz}$  and  $d_{xy} \rightarrow d_{z^2}$ . Any attempt to make an accurate assignment is thwarted due to interactions of the metal–ligand  $\pi$ -bond systems, which lifts the degeneracy of the  $d_{xz}$  and  $d_{yz}$  pair.

*Biological results and discussion*

The antifungal activities of all the complexes were determined against two fungal strains, *i.e.*, *A. niger* and *A. fumigatus* and then compared with the activity of the standard antifungal drug fluconazole. The antifungal activities (percentage inhibition) of the complexes and fluconazole are given in Table II. In the whole series, complex **1** showed the highest percentage inhibition against both fungal strains, whereas none of the tested compounds restricted the fungal growth excellently (Table II). However, of all the tested complexes, **2** and **7** showed nearly 50 % inhibition of mycelial growth against *A. niger*, whereas complexes **1** and **4** showed nearly 55 % inhibition of mycelial growth against *A. fumigatus* (Table II).

TABLE II. *In vitro* antifungal activities of the synthesized macrocyclic compounds determined by the poisoned food method

No.	Complexes	Mycelial growth inhibition, %	
		<i>A. niger</i>	<i>A. fumigatus</i>
<b>1</b>	[Cr(C <sub>28</sub> H <sub>24</sub> N <sub>4</sub> )Cl]Cl <sub>2</sub>	54	55.5
<b>2</b>	[Cr(C <sub>28</sub> H <sub>24</sub> N <sub>4</sub> )(NO <sub>3</sub> )](NO <sub>3</sub> ) <sub>2</sub>	49.6	32.5
<b>3</b>	[Cr(C <sub>28</sub> H <sub>24</sub> N <sub>4</sub> )(OAc)](OAc) <sub>2</sub>	(-) <sup>a</sup>	(-)
<b>4</b>	[Mn(C <sub>28</sub> H <sub>24</sub> N <sub>4</sub> )(OAc)](OAc) <sub>2</sub>	39.3	57.5
<b>5</b>	[Fe(C <sub>28</sub> H <sub>24</sub> N <sub>4</sub> )Cl]Cl <sub>2</sub>	(-)	(-)
<b>6</b>	[Fe(C <sub>28</sub> H <sub>24</sub> N <sub>4</sub> )(NO <sub>3</sub> )](NO <sub>3</sub> ) <sub>2</sub>	29.3	(-)
<b>7</b>	[Fe(C <sub>28</sub> H <sub>24</sub> N <sub>4</sub> )(OAc)](OAc) <sub>2</sub>	53.3	24.2
-	Fluconazole <sup>b</sup>	75.3	80.2

<sup>a</sup>No activity; <sup>b</sup>standard antifungal drug

## CONCLUSIONS

Based on various studies, such as elemental analyses, conductance measurements and magnetic susceptibilities, as well as IR, NMR and electronic spectral studies, a five-coordinate, square pyramidal geometry as shown in Scheme 1 may be proposed for all the synthesized complexes.

It has been suggested that chelation/coordination reduces the polarity of the metal ion mainly because of the partial sharing of its positive charge with the donor group within the whole chelate ring system.<sup>34</sup> Besides this, many other factors, such as solubility, dipole moment, conductivity influenced by the metal ion, may possibly explain the antifungal activities of these complexes.<sup>35</sup> It has also been observed that some moieties, such as azomethine linkage or heteroaromatic nucleus introduced into such compounds, exhibit extensive biological activities that may be a consequence of the increase in the hydrophobic character and liposolubility of the molecules in crossing the cell membrane of the microorganism and hence the enhanced biological utilization ratio and activity of the complexes.<sup>36</sup>

*Acknowledgements.* D. P. Singh thanks the University Grants Commission, New Delhi for financial support in the form of a Major Research Project [MRP-F. No. 32-196/2006(SR)]

and Krishan Kumar for the award of a Project Fellowship under the above project. Thanks are also due to the authorities of N.I.T., Kurukshetra for providing the necessary research facilities.

## ИЗВОД

## МАКРОЦИКЛИЧНИ КОМПЛЕКСИ: СИНТЕЗА И КАРАКТЕРИЗАЦИЈА

DHARMPAL SINGH и KRISHAN KUMAR

*Department of Chemistry, National Institute of Technology, Kurukshetra – 136 119, India*

Тепмплатном синтезом, полазећи од 1,8-диаминонафталена, 2,3-бутандиона и одговарајућих соли метала у метанолу као растварачу, синтетизована је серија нових комплекса типа  $[M(C_{28}H_{24}N_4)X]X_2$  ( $M = Cr(III), Fe(III)$  и  $Mn(III)$ ;  $X = Cl^-, NO_3^-, CH_3COO^-$ , док  $C_{28}H_{24}N_4$  представља одговарајући макроциклични лиганд). За карактеризацију добивених комплекса, поред елементарне микроанализе, кондуктометријских и магнетних мерења, употребљена је UV/Vis, и IR спектроскопија. На основу ових мерења нађено је да су добијени пентакоординовани комплекси имају квадратно-пирамидалну геометрију. Испитивана је *in vitro* антифунгална активност синтетизованих комплекса на следећим сојевима: *Aspergillus niger* и *Aspergillus fumigatus*. Добијени резултати су поређени са резултатима за стандардни антифунгални лек флуконазол.

(Примљено 21. октобра 2009, ревидирано 12. јануара 2010)

## REFERENCES

1. W. Ma, Y. P. Tian, S. Y. Zhang, J. Y. Wu, H. K. Fun, S. Chantrapromma, *Transition Met. Chem.* **31** (2006) 97
2. S. Chandra, A. Gautum, M. Tyagi, *Transition Met. Chem.* **32** (2007) 1079
3. L. Tusek-Bozic, E. Marotta, P. Traldi, *Polyhedron* **26** (2007) 1663
4. N. F. Curtis, *Coord. Chem. Rev.* **3** (1968) 3
5. M. S. Niasari, F. Daver, *Inorg. Chem. Commun.* **9** (2006) 175
6. R. N. Prasad, S. Gupta, S. Jangir, *J. Indian Chem. Soc.* **84** (2007) 1191
7. T. A. Khan, S. S. Hasan, A. K. Mohamed, M. Shakir, *Indian J. Chem.* **37A** (1998) 1123
8. S. Chandra, S. Sharma, *J. Indian Chem. Soc.* **83** (2006) 988
9. S. Chandra, M. Pundir, *Spectrochim. Acta A* **69** (2008) 1
10. S. Chandra, R. Gupta, N. Gupta, S. S. Bawa, *Transition Met. Chem.* **31** (2006) 147
11. S. Chandra, L. K. Gupta, S. Agrawal, *Transition Met. Chem.* **32** (2007) 558
12. D. P. Singh, R. Kumar, V. Malik, P. Tyagi, *J. Enzym. Inhib. Med. Chem.* **22** (2007) 177
13. D. P. Singh, K. Kumar, R. Kumar, J. Singh, *J. Serb. Chem. Soc.* **75** (2010) 217
14. A. I. Vogel, *A text book of quantitative chemical analysis*, 5<sup>th</sup> ed., Longman, London, 1989
15. D. P. Singh, K. Kumar, C. Sharma, *Eur. J. Med. Chem.* **44** (2009) 3299
16. R. Kumar, R. Singh, *Turk. J. Chem.* **30** (2006) 77
17. D. P. Singh, R. Kumar, P. Tyagi, *Transition Met. Chem.* **31** (2006) 970
18. D. P. Singh, N. Shishodia, B. P. Yadav, V. B. Rana, *Polyhedron* **16** (1997) 2229
19. S. Chandra, S. D. Sharma, *Transition Met. Chem.* **27** (2002) 732
20. R. Singh, P. Kumar, R. Shyam, V. Malik, S. Arya, *J. Indian Chem. Soc.* **83** (2006) 616
21. R. N. Prasad, M. Mathur, A. Upadhyay, *J. Indian Chem. Soc.* **84** (2007) 1202
22. J. Costamagna, G. Ferraudi, M. Villagran, E. Wolcan, *J. Chem. Soc. Dalton Trans.* (2000) 2631

23. D. P. Singh, N. Shishodia, B. P. Yadav, V. B. Rana, *J. Indian Chem. Soc.* **81** (2004) 287
24. S. Chandra, L. K. Gupta, *Spectrochim. Acta A* **60** (2004) 2767
25. K. Nakamoto, *Infrared and Raman spectra of inorganic and coordination compounds*, 5<sup>th</sup> ed., Wiley, New York, 1997
26. M. Shakir, O. S. M. Nasman, S. P. Varkey, *Polyhedron* **15** (1996) 309
27. M. Shakir, K. S. Islam, A. K. Mohamed, M. Shagufa, S. S. Hasan, *Transition Met. Chem.* **24** (1999) 577
28. S. Chandra, R. Kumar, *Transition Met. Chem.* **29** (2004) 269
29. V. B. Rana, D. P. Singh, P. Singh, M. P. Teotia, *Transition Met. Chem.* **7** (1982) 174
30. J. S. Wood, *Prog. Inorg. Chem.* **16** (1972) 227
31. D. P. Singh, R. Kumar, J. Singh, *Eur. J. Med. Chem.* **44** (2009) 1731
32. D. P. Singh, R. Kumar, *J. Serb. Chem. Soc.* **72** (2007) 1069
33. A. B. P. Lever, *Inorganic electronic spectroscopy*, 2<sup>nd</sup> ed., Elsevier, Amsterdam, 1984
34. Z. H. Chohan, H. Pervez, A. Rauf, K. M. Khan, C. T. Supuran, *J. Enzym. Inhib. Med. Chem.* **19** (2004) 417
35. Z. H. Chohan, A. Scozzafava, C. T. Supuran, *J. Enzym. Inhib. Med. Chem.* **17** (2002) 261
36. Z. H. Chohan, M. U. Hassan, K. M. Khan, C. T. Supuran, *J. Enzym. Inhib. Med. Chem.* **20** (2005) 183.



*J. Serb. Chem. Soc.* 75 (4) 483–495 (2010)  
JSCS–3981

## The importance of the accuracy of the experimental data for the prediction of solubility

SLAVICA ERIC<sup>1\*#</sup>, MARKO KALINIĆ<sup>1</sup>, ALEKSANDAR POPOVIĆ<sup>1</sup>, HALID MAKIĆ<sup>2</sup>,  
ELVISA CIVIĆ<sup>2</sup> and MEJRA BEKTAŠEVIĆ<sup>2</sup>

<sup>1</sup>Faculty of Pharmacy, University of Belgrade, Vojvode Stepe 450, 11000 Belgrade, Serbia and <sup>2</sup>Biotechnical Faculty, University of Bihać, Kulina Bana 2, 77000 Bihać, Bosnia and Herzegovina

(Received 9 August, revised 7 October 2009)

**Abstract:** Aqueous solubility is an important factor influencing several aspects of the pharmacokinetic profile of a drug. Numerous publications present different methodologies for the development of reliable computational models for the prediction of solubility from structure. The quality of such models can be significantly affected by the accuracy of the employed experimental solubility data. In this work, the importance of the accuracy of the experimental solubility data used for model training was investigated. Three data sets were used as training sets – data set 1, containing solubility data collected from various literature sources using a few criteria ( $n = 319$ ), data set 2, created by substituting 28 values from data set 1 with uniformly determined experimental data from one laboratory ( $n = 319$ ), and data set 3, created by including 56 additional components, for which the solubility was also determined under uniform conditions in the same laboratory, in the data set 2 ( $n = 375$ ). The selection of the most significant descriptors was performed by the heuristic method, using one-parameter and multi-parameter analysis. The correlations between the most significant descriptors and solubility were established using multi-linear regression analysis (MLR) for all three investigated data sets. Notable differences were observed between the equations corresponding to different data sets, suggesting that models updated with new experimental data need to be additionally optimized. It was successfully shown that the inclusion of uniform experimental data consistently leads to an improvement in the correlation coefficients. These findings contribute to an emerging consensus that improving the reliability of solubility prediction requires the inclusion of many diverse compounds for which solubility was measured under standardized conditions in the data set.

**Keywords:** aqueous solubility prediction; experimental data; model training; heuristic method.

\* Corresponding author. E-mail: seric@pharmacy.bg.ac.yu

# Serbian Chemical Society member.

doi: 10.2298/JSC090809022E

## INTRODUCTION

The solubility of drugs and drug-like compounds has been the subject of extensive studies aimed at finding a way to predict solubility from molecular structure. The aqueous solubility of a drug is an important factor that influences its absorption by, distribution in and elimination from the body.<sup>1</sup> Since poor pharmacokinetics is one of the major causes for late stage drug development failures,<sup>2</sup> it is clear that properties such as solubility need to be considered very early in the drug discovery process. Therefore, a reliable tool for the prediction of solubility from structure alone would be of great importance to help in the elimination of unsuitable candidates and reduction of overall development attrition rates.

A considerable number of *in silico* models for the prediction of solubility have been proposed over the past decade.<sup>3–22</sup> These utilize an ever-growing variety of approaches that differ in the way structure is represented, in the nature of the descriptors or properties that are derived from molecular structure and in the regression methods used. The sheer volume of publications on novel methods for the prediction of solubility seems to indicate that none of the existing models is fully satisfactory.<sup>23</sup> Consistent with this, very few of the proposed models for prediction of solubility have found practical implications in the drug discovery process, probably due to low prediction reliability. Whilst most of the published models perform satisfactorily with the test sets used for their validation, their performance with more diverse data plummet considerably.<sup>24</sup>

While significant progress has been made in developing new modelling techniques, there is, nevertheless, an emerging consensus that moving forward will require focusing on altogether different issues affecting the performance of existing models. Most of the recent reviews on solubility prediction indicate that solubility modelling efforts have suffered from some basic faults, such as training sets that are not drug-like, unknown or high experimental error, lack of structural diversity, incorrect tautomers or structures, neglect of ionization, no consideration of salt and/or common ion issues, avoidance of crystal packing effects and range of solubility data that is not pharmaceutically relevant.<sup>25</sup>

One of the issues is that the design of a good quality training set is something often overlooked.<sup>26</sup> It is worth noting that any model is only as good as the data used for its generation. A training set codifies the relationship between the relevant property and chemical structure; therefore, the applicability domain as well as model reliability will depend heavily upon the choice of the training set. The most limiting factor in the choice of a proper training set is the accuracy of the experimental solubility data. Katritzky *et al.* demonstrated that the average standard deviation for solubility measurements originating from different sources is as high as  $0.6 \log S$  units.<sup>27</sup> Occasionally, the solubility values reported for one compound may differ by 2–3 log units; this large difference may originate from different experimental protocols. There are differences in sample concentration,



co-solvent presence, co-solvent concentration, incubation times, thermodynamic methods, kinetic methods, *etc.*<sup>28</sup> In addition, inclusion of values that were not distinctly reported, such as those for intrinsic solubility, and other unintentional errors all contribute significantly to the overall experimental error that can plague a data set.<sup>29,30</sup> In a recent work by Taskinen and Norinder, in which over 30 models from the literature were reviewed, it was concluded that improving the accuracy and applicability will “require more consideration of the consistency of the experimental solubility data and the training set composition”.<sup>24</sup> Other authors also stressed that further development will require large, diverse sets of high-quality, uniformly determined experimental data.<sup>30,31</sup>

Despite the importance of this issue, there are very few published works dealing primarily with proposing carefully designed training sets. In one aspect this is understandable – consistent solubility data are not widely available and determining them for a “QSPR-significant” number of compounds would be a time-consuming, laborious and expensive endeavour. On the other hand, addressing the issue of a more selective collection of data from the literature is feasible. One such example is the data set proposed by Rytting *et al.*, who set out clear criteria for the inclusion of experimental data.<sup>32</sup>

Increasing interest in the importance of high-quality experimental data for modelling purposes was perhaps best exemplified in a recent paper by Llinas *et al.*, in which researchers were challenged to develop a model based on 100 reliable solubility measurements and to use it to predict the solubility of 32 additional molecules provided.<sup>33</sup> As the authors remarked, the findings of the challenge provided an overall perspective as to the current ability to estimate aqueous solubility.<sup>34</sup>

Based on the importance of this issue, the aim of this study was to investigate whether the implementation of solubility data obtained under standardized experimental conditions can make a significant contribution to the process of establishing new or optimizing existing QSPR models for the prediction of solubility.

## EXPERIMENTAL

### *Data sets*

The set of 322 structurally diverse “drug-like” molecules proposed by Rytting *et al.*<sup>32</sup> served as the basis for the first set used in this study (data set 1). The solubility data originated from various literature sources and were collected following several criteria: (i) the given compound is a drug or drug-like molecule, solid at room temperature; (ii) the reported value is that of the intrinsic solubility at around 25 °C; (iii) for solubility measurement, the equilibrium must have been achieved over time, excess solid must be present at the end of testing and acceptable analytical methods must have been used for quantification. Due to geometrical optimisation issues, three molecules were excluded from the Rytting set; hence, data set 1 consisted of 319 compounds. For the investigation of the implementation of experimental solubility data obtained under the uniform experimental conditions, the Sirius data set,<sup>35</sup>

consisting of 84 diverse drug molecules for which the solubility was determined using the Sirius CheqSol technique,<sup>36</sup> was used. This potentiometric method for the measurement of intrinsic solubility is very accurate and allows for rapid equilibration of the experiment and collection of the precipitate during the experiment for characterization.<sup>37</sup>

Data set 2 was created by substituting 28 solubility values from data set 1 with those from the Sirius data set. Data set 3 was created by adding the remaining 56 molecules from the Sirius data set to data set 2 (Table I). The Table with structures of all components included in the Sirius data set can be obtained on request.<sup>35</sup>

Table I. Data sets composition

Data set	Solubility values of compounds
1	319 from ref. 32
2	291 from ref. 32 and 28 from ref. 35
3	291 from ref. 32 and 84 from ref. 35

#### *Structure optimisation and descriptor calculation*

All structures were constructed using Spartan software.<sup>38</sup> Geometry optimisation was performed by the AM1 semi-empirical method implemented in the Spartan software. Calculation of descriptors was performed using the Codessa programme (comprehensive descriptors for structural and statistical analysis).<sup>39</sup> A total of 728 descriptors were calculated and divided into five groups: constitutional, topological, geometrical, electrostatic and quantum-chemical.

#### *Correlation analysis*

The heuristic method implemented in the Codessa software was used for the selection of the most significant descriptors for the prediction of solubility. The most significant descriptors were selected in each group of descriptors using the heuristic method. Heuristic 5-parameter analysis was also used for selection of the five most significant descriptors among all descriptors calculated, which were then used for establishing a QSPR (quantitative structure–property relationship) equation for each of the sets using the multiple linear regression (MLR) method. Prior to this, descriptor intercorrelation analysis was performed, so that no two descriptors appearing in the final equations have an intercorrelation coefficient larger than 0.5.

## RESULTS AND DISCUSSION

The potential limit of the accuracy of experimental data on the predictability of solubility models should be addressed before turning to the purely computational methods, therefore the Sirius data set was used to investigate the extent to which the implementation of solubility data measured under the same standardized method may influence the quality of the potential model training. The creation of data sets 1, 2 and 3 are described in the Experimental section.

The heuristic method was applied for the selection of the most significant descriptors for the prediction of solubility to all three data sets. The most significant descriptors for all three sets from each of the groups of descriptors obtained by the heuristic method are presented in Table II. The most highly correlated descriptor in all data sets was the partition coefficient ( $\log P$ ). Most of the selected electrostatic and quantum-chemical descriptors are derived from mole-

cular surface areas (H-donor/acceptor surface areas) and relative electrostatic charges. This would indicate that the descriptors selected using the heuristic method proved to be related to the solvation mechanism of the molecules.

Table II. The most significant descriptors among the five groups of descriptors, selected using the heuristic method

Descriptor <sup>a</sup>	Data set 1		Data set 2		Data set 3	
	$R^2$	$F$	$R^2$	$F$	$R^2$	$F$
Constitutional descriptors						
log $P$	0.5013	318.67	0.5337	362.77	0.5479	451.95
$N_{BR}$	0.3848	198.28	0.4116	221.73	0.4390	291.88
$R_C$	0.3587	177.33	0.3562	175.41	0.3289	182.81
$R_{BR}$	0.3133	144.65	0.3184	148.09	0.2978	158.16
$N_C$	0.3013	136.71	0.3294	155.70	0.3639	213.34
$N_R$	0.2651	114.34	0.2675	115.74	0.2765	142.53
$N_{AB}$	0.1885	73.63	0.2062	82.36	0.2686	136.97
$R_N$	0.1526	57.08	0.1570	59.05	–	–
$GI_{all}$	0.1351	49.53	0.1479	55.04	0.2051	96.23
MW	0.1283	46.65	0.1409	51.97	0.1962	91.05
Topological descriptors						
<sup>0</sup> ABIC	0.2833	125.31	0.2943	132.19	0.2526	126.06
<sup>0</sup> ACIC	0.2478	104.41	0.2661	114.94	0.2640	133.81
<sup>1</sup> ACIC	0.2196	89.22	0.2339	96.76	–	–
<sup>1</sup> ABIC	0.2072	82.83	0.2147	86.68	–	–
<sup>2</sup> ACIC	0.1949	76.73	0.2089	83.72	–	–
<sup>3</sup> Randic	0.1926	75.62	0.2038	81.12	0.2446	120.76
<sup>2</sup> CIC	0.1895	74.14	0.2224	90.68	0.2254	108.54
<sup>1</sup> K&H	0.1884	73.59	0.2061	82.31	0.2576	129.40
<sup>1</sup> Randic	0.1829	70.96	0.2023	80.39	0.2580	129.72
<sup>2</sup> Randic	–	–	0.1938	76.19	0.2426	119.49
<sup>0</sup> K&H	–	–	–	–	0.2327	113.13
<sup>2</sup> K&H	–	–	–	–	0.2199	105.16
Geometrical descriptors						
MSA	0.2312	95.31	0.2565	109.36	0.3125	169.57
XY Shadow	0.2259	92.50	0.2495	105.38	0.2978	158.17
$I_C$	0.2176	88.19	0.2289	94.11	0.2550	127.69
$I_B$	0.1778	68.55	0.1868	72.80	0.2142	101.66
MV	0.1613	60.99	0.1829	70.95	0.2378	116.35
$I_A$	0.1407	51.92	0.1500	55.93	0.1719	81.36
ZX Shadow	–	32.46	0.1104	39.34	0.1685	75.56
Electrostatic descriptors						
<sup>c</sup> FPSA-3	0.2603	111.56	0.2676	115.80	0.2759	142.10
<sup>ed</sup> HDSA-1/TMSA	0.2590	110.81	0.2678	115.96	0.2649	134.42
<sup>ed</sup> HDSA-2/TMSA	0.2555	108.82	0.2621	112.62	0.2554	127.93
<sup>c</sup> HASA-2/TMSA	0.2282	93.74	0.2401	100.17	0.2454	121.31
<sup>c</sup> HACA-2/TMSA	0.2189	88.82	0.2279	93.56	0.2333	113.48
<sup>ed</sup> HDSA-2/SQRT	0.2001	79.32	0.2037	81.09	–	–

TABLE II. Continued

Descriptor <sup>a</sup>	Data set 1		Data set 2		Data set 3	
	<i>R</i> <sup>2</sup>	<i>F</i>	<i>R</i> <sup>2</sup>	<i>F</i>	<i>R</i> <sup>2</sup>	<i>F</i>
Electrostatic descriptors						
<sup>ed</sup> HDCA-1/TMSA	0.1984	78.48	0.2072	82.86	0.2091	98.60
<sup>ed</sup> HDCA-2/TMSA	0.1979	79.20	0.2040	81.22	0.2040	95.57
<sup>c</sup> HASA-2/SQRT	0.1935	76.06	0.2035	81.01	–	–
<sup>c</sup> HASA-1/TMSA	0.1905	74.59	0.2026	80.54	0.2164	103.01
<sup>ew</sup> WNSA-1	–	–	–	–	0.2497	124.17
<sup>e</sup> TMSA	–	–	–	–	0.2437	120.18
Quantum-chemical descriptors						
ALFA-pol	0.2657	114.70	0.2873	127.79	0.3458	197.12
<sup>qd</sup> HDSA-1/TMSA	0.2579	110.18	0.2673	115.67	0.2642	133.95
<sup>qd</sup> HDSA-2/TMSA	0.2574	109.85	0.2645	113.99	0.2579	129.64
<sup>q</sup> HASA-2/TMSA	0.2282	93.74	0.2401	100.17	0.2454	121.31
<sup>q</sup> RNCG	0.2281	93.69	0.2393	99.72	0.2433	119.23
PMI <sub>C</sub>	0.2176	88.19	0.2289	94.11	0.2550	127.31
<sup>qd</sup> HDSA-2/SQRT	0.2005	79.52	0.2047	81.60	–	–
<sup>q</sup> HASA-2/SQRT	0.1935	76.06	0.2035	81.01	–	–
<sup>q</sup> HASA-1/TMSA	0.1905	74.59	0.2026	80.54	–	–
PMI <sub>C</sub> /#	0.1892	73.99	–	–	–	–
<sup>q</sup> TMSA	–	–	–	–	0.2437	120.16
Etot <sub>2-c ex</sub>	–	–	–	–	0.2385	116.80
<sup>qw</sup> WNSA-1	–	–	–	–	0.2274	109.80

<sup>a</sup>Symbols of descriptors used; **constitutional**: N<sub>BR</sub> – number of benzene rings, N<sub>C</sub> – number of C atoms, R<sub>BR</sub> – relative number of benzene rings, R<sub>C</sub> – relative number of C atoms, R<sub>N</sub> – relative number of N atoms, N<sub>R</sub> – number of rings, N<sub>AB</sub> – number of aromatic bonds, GI<sub>all</sub> – gravitational index (all bonds), MW – molecular weight; **topological**: <sup>0</sup>ACIC – average complementary information content (order 0), <sup>1</sup>ACIC – average complementary information content (order 1), <sup>2</sup>ACIC – average complementary information content (order 2), <sup>0</sup>ABIC – average bonding information content (order 0), <sup>1</sup>ABIC – average bonding information content (order 1), <sup>2</sup>ABIC – average bonding information content (order 2), <sup>1</sup>Randic – Randic index (order 1), <sup>2</sup>Randic – Randic index (order 2), <sup>3</sup>Randic – Randic index (order 3), <sup>0</sup>K&H – Kier & Hall index (order 0), <sup>1</sup>K&H – Kier & Hall index (order 1), <sup>2</sup>K&H – Kier & Hall index (order 2); **geometrical**: XY Shadow – area of the shadow of the molecule projected on a plane defined by X and Y axes, ZX Shadow – area of the shadow of the molecule projected on a plane defined by Z and X axes, MSA – molecular surface area, MV – molecular volume, I<sub>A</sub> – moment of inertia A, I<sub>B</sub> – moment of inertia B, I<sub>C</sub> – moment of inertia C; **electrostatic** (Zefirov's PC): <sup>q</sup>FPSA-3 – FPSA-3 fractional PPSA (PPSA-3/TMSA), <sup>ed</sup>HDSA-1/TMSA – HA dependent HDSA-1/TMSA, <sup>ed</sup>HDSA-2/TMSA – HA dependent HDSA-2/TMSA, <sup>ed</sup>HDSA-2/SQRT – HA dependent HDSA-2/SQRT(TMSA), <sup>ed</sup>HDCA-1/TMSA – HA dependent HDCA-1/TMSA, <sup>ed</sup>HDCA-2/TMSA – HA dependent HDCA-2/TMSA, <sup>q</sup>HASA-1/TMSA – HASA-1/TMSA, <sup>q</sup>HASA-2/TMSA – HASA-2/TMSA, <sup>q</sup>HASA-2/SQRT – HASA-2/SQRT(TMSA); <sup>q</sup>HACA-2/TMSA – HACA-2/TMSA, <sup>q</sup>TMSA – TMSA total molecular surface area, <sup>ew</sup>WNSA-1 – WNSA-1 weighted PPSA (PPSA-1\*TMSA/1000); **quantum-chemical**: ALFA-pol – ALFA polarizability (DIP), <sup>qd</sup>HDSA-1/TMSA – HA dependent HDSA-1/TMSA [Semi-MO PC], <sup>qd</sup>HDSA-2/TMSA – HA dependent HDSA-2/TMSA (semi-MO PC), <sup>qd</sup>HDSA-2/SQRT – HA dependent HDSA-2/SQRT(TMSA) (semi-MO PC), <sup>q</sup>HASA-1/TMSA – HASA-1/TMSA (semi-MO PC), <sup>q</sup>HASA-2/TMSA – HASA-2/TMSA (semi-MO PC), <sup>q</sup>HASA-2/SQRT – HASA-2/SQRT(TMSA) (semi-MO PC), PMI<sub>C</sub> – principal moment of inertia C, PMI<sub>C</sub>/# – principal moment of inertia C/# of atoms, <sup>q</sup>RNCG – RNCG relative negative charge (QMNEG/QTMINUS) (semi-MO PC), Eto<sub>2-c ex</sub> – total molecular 2-center exchange energy, <sup>q</sup>TMSA – TMSA total molecular surface area (semi-MO PC).

Comparing data sets 1 and 2, which differ only in the solubility values of 28 compounds, the order of the most significant descriptors selected by the heuristic method in the one-parameter correlation among each of the five groups of descriptors remained relatively unchanged. However, there was an increase in the correlation coefficient in all the descriptors involved. Comparing data sets 1 and 3, the order of the descriptors was slightly changed. Although the correlations of the individual descriptors decreased in a small number of instances, there was an overall improvement of the correlation in all descriptor groups. This would suggest that if no additional components are included in the set, with just the experimental data being altered, individual descriptors could retain their respective capacities for describing the correlation between solubility and structure. This does not hold true, however, when establishing a multi-parameter correlation, as is later demonstrated.

Inclusion of additional components in data set 3 increased the diversity of the set. This can result in a change of relative importance of different molecular properties governing solubility (within a set), which in turn affects the significance of selected molecular descriptors. In the present case, this was reflected in the reordering of closely related descriptors among each group of descriptors.

The present observations showed that changing the experimental data in multi-parameter correlations tended to have even a greater impact. A five-parameter heuristic correlation analysis and subsequent MLR yielded the following QSPR equations for data sets 1, 2 and 3, respectively:

$$\log S = -0.63647 \log P - 0.01454^q \text{HBCA} + 24.65157 I_C + 0.010761^2 \text{AIC} - 19.7268 R_{NR}, n = 319, R^2 = 0.6616 \quad (1)$$

$$\log S = -0.42352 \log P + 0.559774 \text{Etot}_{2-c \text{ ex}}/\# - 0.00756^q \text{DPSA-3} + 9.912633^q \text{RNCG} + 0.197134 \min(\# \text{HA}, \# \text{HD}), n = 319, R^2 = 0.6689 \quad (2)$$

$$\log S = -0.60863 \log P - 0.04033 N_{AB} - 14.2527 R_{NR} - 0.01145^q \text{DPSA-3} + 2.020366^q \text{RNCG}, n = 375, R^2 = 0.7045 \quad (3)$$

where:  $\log P$  – partition coefficient;

$q\text{HBCA}$  – HBCA H-bonding charged surface area (semi-MO PC);

$I_C$  – moment of inertia C;

$^2\text{AIC}$  – average information content (order 2);

$R_{NR}$  – relative number of rings;

$\text{Etot}_{2-c \text{ ex}}/\#$  – total molecular 2-center exchange energy/# of atoms;

$q\text{DPSA-3}$  – DPSA-3 difference in CPSAs (PPSA3-PNSA3) (semi-MO PC);

$q\text{RNCG}$  – RNCG relative negative charge (QMNEG/QTMINUS) (semi-MO PC);

$\min(\# \text{HA}, \# \text{HD})$  – minimum number of H-acceptors/donors;

$N_{AB}$  – number of aromatic bonds;

$R_{NR}$  – relative number of rings;

$q\text{DPSA-3}$  – DPSA-3 difference in CPSAs (PPSA3-PNSA3) (semi-MO PC);

*eRNCG* - RNCG Relative negative charge (QMNEG/QTMINUS).

The plots of the experimental *vs.* the predicted solubility values using these three equations for the three training sets are shown in Figs. 1–3.

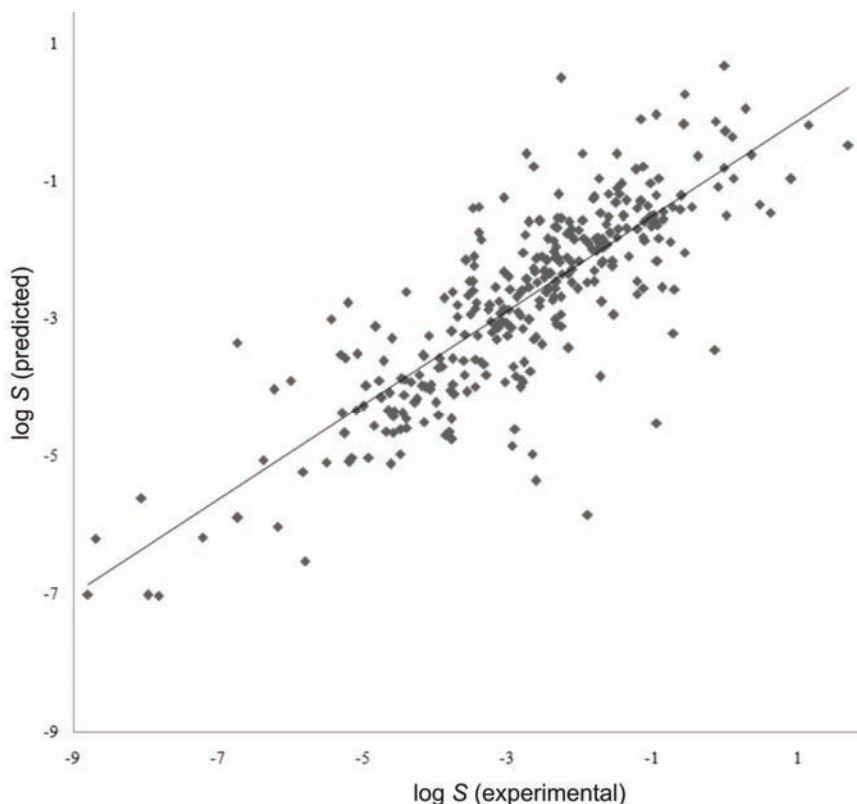


Fig. 1. The correlation between the experimental and predicted  $\log S$  values for data set 1 ( $n = 319$ ,  $R^2 = 0.6616$ ).

Equation (1), derived from data set 1 ( $n = 319$ ), has the smallest correlation coefficient of the three ( $R^2 = 0.6616$ ,  $RMSE = 0.9641$ ). In comparison, Eq. (2) shows a somewhat improved performance, with a slightly better correlation coefficient and a remarkable reduction in the root mean squared error ( $n = 319$ ,  $R^2 = 0.6689$ ,  $RMSE = 0.8623$ ). Equation (3), derived from the supplemented set ( $n = 375$ ), has the best correlation coefficient and a slightly reduced  $RMSE$ , compared to Eq. (1) ( $R^2 = 0.7045$ ,  $RMSE = 0.9382$ ). Introduction of uniform experimental data consistently leads to an increase in the correlation coefficient. This can be attributed to both the correction of outliers and the improvement of overall data consistency.

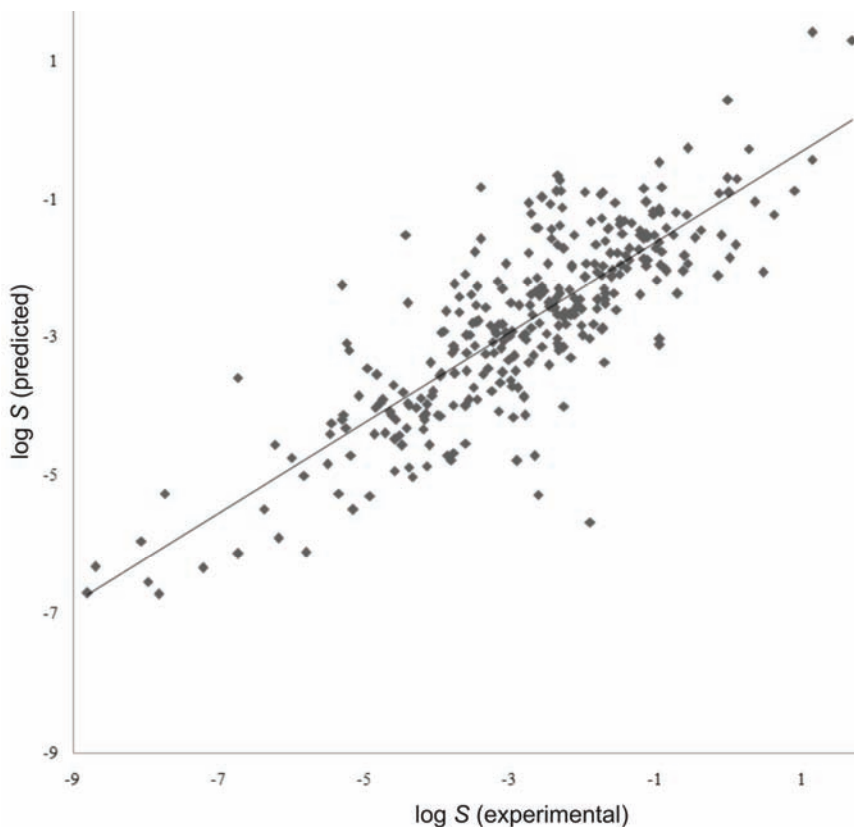


Fig. 2. The correlation between the experimental and predicted  $\log S$  values for data set 2 ( $n = 319$ ,  $R^2 = 0.6689$ ).

Moving from single to multi-parameter correlations, the difference in selection of the most significant descriptors using the three data sets became more evident. The equation corresponding to data set 1 is composed of 2 constitutional, 1 geometrical, 1 topological and 1 quantum-chemical descriptor. On the other hand, Eq. (2) was established using 1 constitutional and 4 quantum-chemical descriptors, which together account for several aspects of the solvation process, especially polar interactions and the possibility of H-bond formation. Thus, while the  $R^2$  values for Eqs. (1) and (2) are similar, the interpretability of these equations is significantly affected by the changes in the solubility values of the data set. On average, these values for the 28 substitutions made between data set 1 and 2 (Table III) differ by  $0.57\log S$ . This is largely consistent with observations made by Katritzky *et al.*<sup>27</sup> Differences in excess of  $1.5\log S$  are also present in some instances, *e.g.*, phenylbutazone, propranolol, sulfamerazine and notably terfenadine, for which the values differ by  $3\log S$ . Such large-scale differences can clearly affect the selection of the most significant descriptors. Data Set 3 is struc-

turally more diverse than the previous two, thus the corresponding Eq. (3) also features a different combination of descriptors. It is composed of 3 constitutional and 2 quantum-chemical descriptors. These descriptors encompass molecular properties that relate to hydrophobicity as well as those that facilitate solvation. In summary, both the structural diversity of the training set and the standardized experimental solubility data included in the training significantly influence not just the statistical performance but also the interpretability of a prospective model.

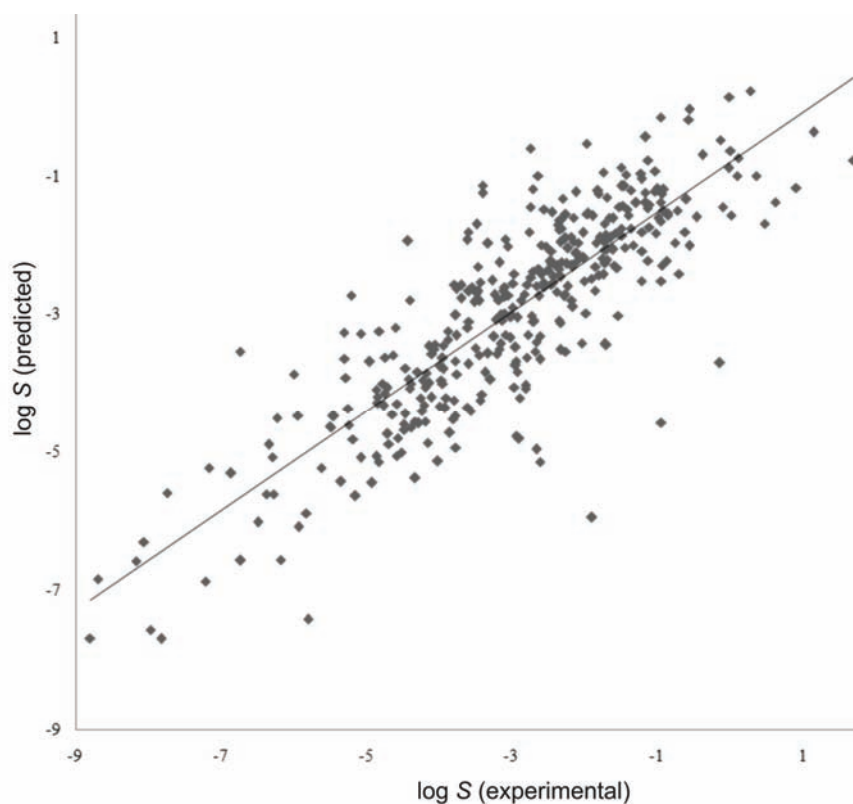


Fig. 3. The correlation between the experimental and predicted  $\log S$  values for data set 3 ( $n = 375$ ,  $R^2 = 0.7045$ ).

TABLE III. Rytting solubility data used in data set 1, substituted with Sirius solubility data used in data Set 2 (No. of compounds: 28)

Compound	$\log S$	
	Rytting (data set 1)	Sirius (data set 2)
Amitriptyline	-4.4560	-4.3900
Benzocaine	-2.6160	-2.2300
Benzoic acid	-1.5550	-1.6100
Chlorzoxazone	-2.8310	-2.6100



TABLE III. Continued

Compound	log <i>S</i>	
	Rytting (data set 1)	Sirius (data set 2)
Diclofenac	-5.0970	-5.4500
Flufenamic acid	-4.6230	-5.3500
Flurbiprofen	-3.7400	-4.1100
Folic acid	-5.4410	-5.3100
Haloperidol	-4.4290	-5.4700
Hydrochlorothiazide	-2.6890	-2.6800
Ibuprofen	-3.4200	-3.6100
Lidocaine	-1.7680	-1.8500
Metoclopramide	-3.1760	-3.5900
Nadolol	-1.0080	-1.5700
Naproxen	-4.1550	-4.1400
Nitrofurantoin	-3.4770	-3.3300
Norfloxacin	-3.0570	-2.7500
Paracetamol	-1.0740	-1.0000
Phenobarbital	-2.3660	-2.2800
Phenylbutazone	-2.6440	-4.3900
Prochlorperazine	-4.3980	-4.8700
Promethazine	-4.2600	-4.1900
Propranolol	-0.7140	-3.5000
Quinine	-2.7900	-2.8100
Sulfamerazine	-1.2180	-3.1000
Sulfathiazole	-2.8050	-2.7000
Sulindac	-5.0000	-4.5200
Terfenadine	-4.6740	-7.7400

## CONCLUSIONS

Solubility is a difficult property to predict, and one reason for this is the absence of a high-quality data set of reliable and reproducible solubility measurements. Hopefully, by measuring many compounds under standardized conditions, current predictive models can be improved. In this work, an attempt was made to demonstrate the importance of implementing such data to improve the confidence of the training of the models.

It was successfully shown that the usage of uniform experimental data can significantly improve the correlation in the training set. The results also showed that updating existing data sets with such data leads to changes in the selection of the most significant descriptor, which would require the given model to be additionally optimized. Continuously updated models would be a valuable tool for preliminary solubility screening and could be developed alongside solubility measurement devices as added value software.

*Acknowledgments.* This work was supported by the Ministry of Science and Technological Development of the Republic of Serbia under Project No 142071 and the Federal Ministry of Education of the Federation of Bosnia and Herzegovina under Project No. 03-39-159-13.

## ИЗВОД

ВАЖНОСТ ПРЕЦИЗНОСТИ ЕКСПЕРИМЕНТАЛНИХ ПОДАТАКА  
ЗА ПРОЦЕНУ РАСТВОРЉИВОСТИСЛАВИЦА ЕРИЋ<sup>1</sup>, МАРКО КАЛИНИЋ<sup>1</sup>, АЛЕКСАНДАР ПОПОВИЋ<sup>1</sup>, НАЛИД МАКИЋ<sup>2</sup>,  
ЕЛВИСА СИВИЋ<sup>2</sup> и МЕРЈА ВЕКТАШЕВИЋ<sup>2</sup><sup>1</sup>Фармацеутички факултет, Универзитет у Београду, Војводе Силеје 450, 11000 Београд и <sup>2</sup>Biotechnical Faculty, University of Bihać, Kulina Bana 2, 77000 Bihać, Bosnia and Herzegovina

Растворљивост лека у води је значајан фактор који утиче на више аспеката његовог фармакокинетичког профила. Бројне публикације презентују различите методологије за развој поузданих компјутерских модела за предвиђање растворљивости на основу структуре једињења. Квалитет модела за предвиђање растворљивости битно зависи од тачности експерименталних вредности за растворљивост које су коришћене за тренирање модела. У овом раду проучаван је значај примене експерименталних података добијених под стандардизованим, униформним условима за тренирање модела за предвиђање растворљивости. Коришћена су три сета података – испитивани сет 1 који је добијен одабиром експерименталних вредности за растворљивост под одређеним критеријумима из различитих литературних извора ( $n = 319$ ), затим испитивани сет 2 који је добијен заменом 28 вредности за растворљивост из испитиваног сета 1 вредностима за растворљивост добијеним стандардизованом експерименталном методом у једној лабораторији ( $n = 319$ ) и испитивани сет 3 који је добијен додатком још 56 компонената у испитивани сет 2, за које су вредности растворљивости такође одређене под стандардизованим условима у истој лабораторији ( $n = 375$ ). Затим је примењена хеурстичка метода за селекцију најзначајнијих дескриптора, коришћењем једнопараметарских и вишепараметарских анализа. Постављене су корелације између најзначајнијих дескриптора и растворљивости коришћењем мултилинеарне регресионе анализе за сва три испитивана сета података. Уочена је значајна разлика између једначина које су добијене коришћењем различитих сетова података, што указује на то да је након увођења нових експерименталних података неопходно додатно оптимизовати постојеће моделе. Показано је да коришћење униформних експерименталних података условљава побољшање коефицијената корелације. Ови резултати говоре у прилог све заступљенијем ставу да је за побољшање поузданости предвиђања растворљивости потребно користити сетове података великог броја различитих једињења чија је растворљивост мерена под стандардизованим условима.

(Примљено 9. августа, ревидирано 7. октобра 2009)

## REFERENCES

1. S. Stegemann, F. Leveiller, D. Franchi, H. de Jong, H. Lindén, *Eur. J. Pharm. Sci.* **31** (2007) 249
2. H. van de Waterbeemd, E. Gifford, *Nat. Rev. Drug Discovery* **2** (2003) 192
3. J. Huuskonen, *J. Chem. Inf. Comput. Sci.* **40** (2000) 773
4. W. L. Jorgensen, E. M. Duffy, *Bioorg. Med. Chem. Lett.* **10** (2000) 1155
5. I. V. Tetko, V. Y. Tanchuk, T. N. Kasheva, A. E. P. Villa, *J. Chem. Inf. Comput. Sci.* **41** (2001) 1488
6. P. Bruneau, *J. Chem. Inf. Comput. Sci.* **41** (2001) 1605
7. C. A. S. Bergström, U. Norinder, K. Luthman, P. Artursson, *Pharm. Res.* **19** (2002) 182
8. O. Engkvist, P. Wrede, *J. Chem. Inf. Comput. Sci.* **42** (2002) 1247
9. J. K. Wegner, A. Zell, *J. Chem. Inf. Comput. Sci.* **43** (2003) 1077
10. A. Cheng, K. M. Merz, *J. Med. Chem.* **46** (2003) 3572

11. J. S. Delaney, *J. Chem. Inf. Model.* **44** (2004) 1000
12. T. J. Hou, K. Xia, W. Zhang, X. J. Xu, *J. Chem. Inf. Model.* **44** (2004) 266
13. C. A. S. Bergström, C. M. Wassvik, U. Norinder, K. Luthman, P. Artursson, *J. Chem. Inf. Model.* **44** (2004) 1477
14. A. Yan, J. Gasteiger, M. Krug, S. Anzali, *J. Comput.-Aided Mol. Des.* **18** (2004) 75
15. C. Catana, H. Gao, C. Orrenius, P. F. W. Stouten, *J. Chem. Inf. Model.* **45** (2005) 170
16. A. Schwaighofer, T. Schroeter, S. Mika, J. Laub, A. ter Laak, D. Sülzle, U. Ganzer, N. Heinrich, K. R. Müller, *J. Chem. Inf. Model.* **47** (2007) 407
17. J. Wang, G. Krudy, T. Hou, W. Zhang, G. Holland, X. Xu, *J. Chem. Inf. Model.* **47** (2007) 1395
18. D. S. Palmer, N. M. O'Boyle, R. C. Glen, J. B. O. Mitchell, *J. Chem. Inf. Model.* **47** (2007) 150
19. J. Huuskonen, D. J. Livingstone, D. T. Manallack, *SAR QSAR Environ. Res.* **19** (2008) 191
20. L. Du-Cuny, J. Huwyler, M. Wiese, M. Kansy, *Eur. J. Med. Chem.* **43** (2008) 501
21. P. R. Duchowicz, A. Talevi, L. E. Bruno-Blanch, E. A. Castro, *Bioorg. Med. Chem.* **16** (2008) 7944
22. J. Wang, T. Hou, X. Xu, *J. Chem. Inf. Model.* **49** (2009) 571
23. B. Faller, P. Ertl, *Adv. Drug Delivery Rev.* **59** (2007) 533
24. J. Taskinen, U. Norinder, *Comprehensive Medicinal Chemistry II*, Vol. 5, Elsevier, Amsterdam, 2007, p. 627
25. S. R. Johnson, W. Zheng, *AAPS J.* **8** (2006) E27
26. J. Taskinen, J. Yliruusi, *Adv. Drug Delivery Rev.* **55** (2003) 1163
27. A. R. Katritzky, Y. Wang, S. Sild, T. Tamm, M. Karelson, *J. Chem. Inf. Comput. Sci.* **38** (1998) 720
28. D. Edwards, in *Proceeding of Phys. Chem. Forum 3*, Forest Row, UK, 2007, p. 10
29. K. V. Balakin, N. P. Savchuk, I. V. Tetko, *Curr. Med. Chem.* **13** (2006) 223
30. W. L. Jorgensen, E. M. Duffy, *Adv. Drug Delivery Rev.* **54** (2002) 355
31. C. A. S. Bergström, *Basic Clin. Pharmacol. Toxicol.* **96** (2005) 156
32. E. Rytting, K. A. Lentz, X. Q. Chen, F. Qian, S. Venkatesh, *AAPS J.* **7** (2005) E78
33. A. Llinàs, R. C. Glen, J. M. Goodman, *J. Chem. Inf. Model.* **48** (2008) 1289
34. A. J. Hopfinger, E. X. Esposito, A. Llinàs, R. C. Glen, J. M. Goodman, *J. Chem. Inf. Model.* **49** (2009) 1
35. K. Box, J. Mole, T. Gravestock, J. Comer, R. Allen, in *Proceedings of AAPS Annual Meeting*, San Diego, CA, 2007, T3104
36. M. Stuart, K. Box, *Anal. Chem.* **77** (2005) 983
37. G. Völgyi, K. Box, E. Baka, M. Stuart, K. Takács-Novák, J. Comer, *J. Pharm. Sci.* **95** (2006) 1298
38. *Spartan '02 for Linux*, Wavefunction, Inc. Irvine, CA, 2002
39. A. R. Katritzky, W. S. Lobanov, M. Karelson, *Codessa Reference Manual (version 2.0)*, Gainesville, FL, 1994, p. 2.





*J. Serb. Chem. Soc.* 75 (4) 497–504 (2010)  
JSCS–3982

Journal of  
the Serbian  
Chemical Society

JSCS@tmf.bg.ac.rs • www.shd.org.rs/JSCS

UDC 547.288.15+546.26-162-31:541.121:536.7

Original scientific paper

## Hexamethylenetetramine reaction with graphite oxide (GO) as a strategy to increase the thermal stability of GO: synthesis and characterization of a compound

ROBSON F. de FARIAS<sup>1\*</sup> and CLAUDIO AIROLDI<sup>2</sup>

<sup>1</sup>Departamento de Química, Universidade Federal do Rio Grande do Norte, Cx. Postal 1662,  
59078-970 Natal, Rio Grande do Norte and <sup>2</sup>Instituto de Química, UNICAMP,  
Cx. Postal 1664, 13083-97170 Campinas, São Paulo, Brazil

(Received 17 July, revised 23 September 2009)

**Abstract:** In this paper, the synthesis and characterization of a GO–hmta compound (GO – graphite oxide; hmta – hexamethylenetetramine) are presented. It is shown that the presence of hmta molecules inside the GO matrix, with very strong interactions, stabilize the GO matrix from a thermal point of view. Such a fact could be used to explore possible applications of GO matrix, especially in catalysis.

**Keywords:** graphite oxide; hexamethylenetetramine; thermal stability.

### INTRODUCTION

Graphite oxide (GO) can be defined/identified as an oxygen-rich carbogenic material that is typically derived by the strong oxidation of crystalline graphite and contains oxygen in the concentration range 30–40 % (w/w). This solid exhibits an extended lamellar structure with randomly distributed aromatic and aliphatic regions, as well as a high amount of hydroxyl/carboxyl functional groups embedded in its layers. Hence, GO is endowed with swelling, intercalation and ion exchange properties.<sup>1–7</sup> This layered solid decomposes at relatively low temperature (< 200 °C), releasing CO<sub>2</sub> and H<sub>2</sub>O. As a recent example of investigations on the chemistry of GO, the recently reported study of the intercalation of molecules of poly(ethylene oxide), poly(vinyl pyrrolidone), methyl cellulose, poly[oxymethylene(oxyethylene)], and poly[oligo(ethyleneglycol oxalate)] into GO can be mentioned.<sup>8</sup> Possible usages of GO in catalysis have also been reported.<sup>9</sup>

It was verified that the forces of attraction between the polymers and GO are primarily dipole–dipole and/or hydrogen bonding arising from the polar groups in the polymers and the functional groups (COC, COOH, COH, and CTO) in the

\* Corresponding author. E-mail: robsonfarias@pq.cnpq.br  
doi: 10.2298/JSC090717018D



GO.<sup>10</sup> Furthermore, it was verified that the addition of a small amount of dilute NaOH resulted in deprotonation of the acidic functionalities, which caused exfoliation of the layered structure.<sup>10</sup> It was shown<sup>10</sup> that GO is able to remove ammonia by two processes: intercalation and reactive adsorption. It was found that the total amount of adsorbed ammonia was significantly higher than that adsorbed on activated carbon. In an interesting interplay between GO and organosilanes (which are extensively used to modify amorphous or nanostructured oxide surfaces), there is report<sup>11</sup> of the preparation of intercalation compounds in which amino groups were inserted into the interlayer space of GO, using 3-aminopropylethoxysilanes. For such compounds, it was shown that the amino groups of 3-aminopropyltriethoxysilane were bonded to the hydroxyl groups of GO. It was also found that the temperature in which the intercalation occurred affected the interlayer distance, with larger distances been observed in products obtained at higher temperatures. On the other hand, it was shown that interactions with organic species can be used as a strategy to promote remarkable structural modifications in hybrid solids.<sup>12</sup>

In the present paper, the synthesis of a GO compound with hexamethylenetetramine (hmta) is reported.

#### EXPERIMENTAL

The graphite oxide was prepared as follows: 230 cm<sup>3</sup> of 96 % sulfuric acid was transferred to a 3.0 dm<sup>3</sup> Erlenmeyer flask which was cooled to 0 °C (ice bath). Graphite powder (10 g; Aldrich) was then added to the flask under mechanical stirring. KMnO<sub>4</sub> (30 g) was slowly added to the dark mixture with care being taken to maintain the reaction mixture below 20 °C. The reaction mixture was then allowed to cool to 2 °C and stirred at room temperature for 60 min. Then 230 cm<sup>3</sup> of deionized water was slowly added to the system, whereby a rapid increase in temperature was observed. The reaction mixture stirred for 45 min, after which 230 cm<sup>3</sup> of deionized water and 130 cm<sup>3</sup> of 31 % H<sub>2</sub>O<sub>2</sub> were added. Subsequently, deionized water was added to the system until a total volume of 2.0 dm<sup>3</sup> was achieved. After standing for 72 h, the GO particles settled to the bottom of the flask and the excess liquid was withdrawn. The remaining liquid and solid particles were transferred to centrifuge tubes and centrifuged at 6000 rpm for 3 min. All samples were washed several times with deionized water and the supernatant reacted with a solution of barium nitrate until a negative test for sulfate was achieved.

The wet powders were then dried at room temperature in a fume hood for 72 h and then at 30° for 3 h in an oven.

The GO intercalation compound was prepared by magnetically stirring (3 h) 2.0 g of GO with 50 cm<sup>3</sup> of an aqueous solution prepared by dissolution of 10.0 g of hexamethylenetetramine, hmta (Aldrich), C<sub>6</sub>H<sub>12</sub>N<sub>4</sub> (1,3,5,7-tetraazatricyclo[3.3.1.1<sup>3,7</sup>]decane)\*. The compound settled to the bottom of the flask and was filtered off, washed with deionized water and dried at room temperature for 72 h in a fume hood.

The CHN elemental analysis was performed using a Perkin–Elmer instrument, Bomem, model MB 102. The infrared (FTIR) spectra were recorded on a Bomem instrument using the

\* Hmta is also known under the names hexamine, methenamine and urotropine.

KBr disc technique. The thermogravimetric analysis was performed in a Shimadzu TGA-50 instrument under a dynamic nitrogen atmosphere ( $50 \text{ cm}^3 \text{ min}^{-1}$ ), in platinum sample holders at a heating rate of  $10 \text{ }^\circ\text{C min}^{-1}$ .

### RESULTS AND DISCUSSION

The elemental analysis results are summarized in Table I. Based on the nitrogen elemental analysis result, it can be calculated that the GO-hmta matrix contained 123 mmol of hmta per gram of sample.

TABLE I. Elemental analysis results (%) for GO and GO-hmta samples

Compound	C	H	N	O
GO	39.7	2.6	–	57.7
GO-hmta	53.0	3.3	6.9	36.8

The obtained FTIR spectra are shown in Fig. 1. In the spectrum of GO, bands at 3450 (OH stretching), 1654 (COOH), 1383 and  $1058 \text{ cm}^{-1}$  (COC/COH)

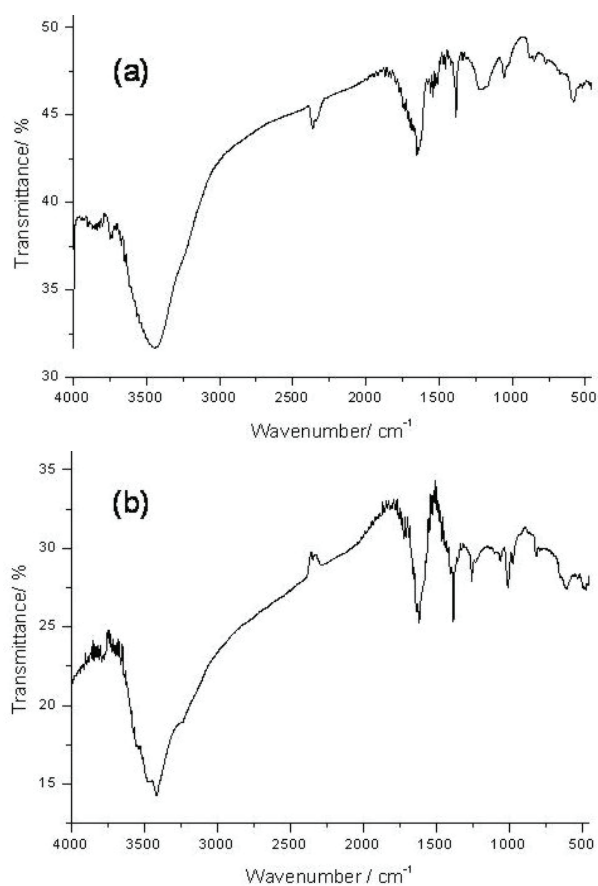


Fig. 1. FTIR Spectra for a) GO and b) GO-hmta.

can be observed. Such bands are, of course, not exhibited by graphite. The spectrum of GO-hmta exhibited respective bands at 3426, 1630, 1381 and 1015  $\text{cm}^{-1}$ . The significant shift to lower wave numbers of these bands, due to stretching of OH, COOH and COC/COH groups, shows that there were strong interactions between these groups and the hmta molecules, probably by hydrogen bonding. Taking into account the symmetric nature of hmta, the structure of which is shown in Fig. 2, it can interact simultaneously with many sites in the GO matrix.

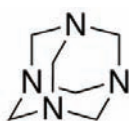


Fig. 2. Structural formula of hmta.

The thermogravimetric curves obtained for GO and the GO-hmta compound are shown in Fig. 3 and the TG data are summarized in Table II. The data given

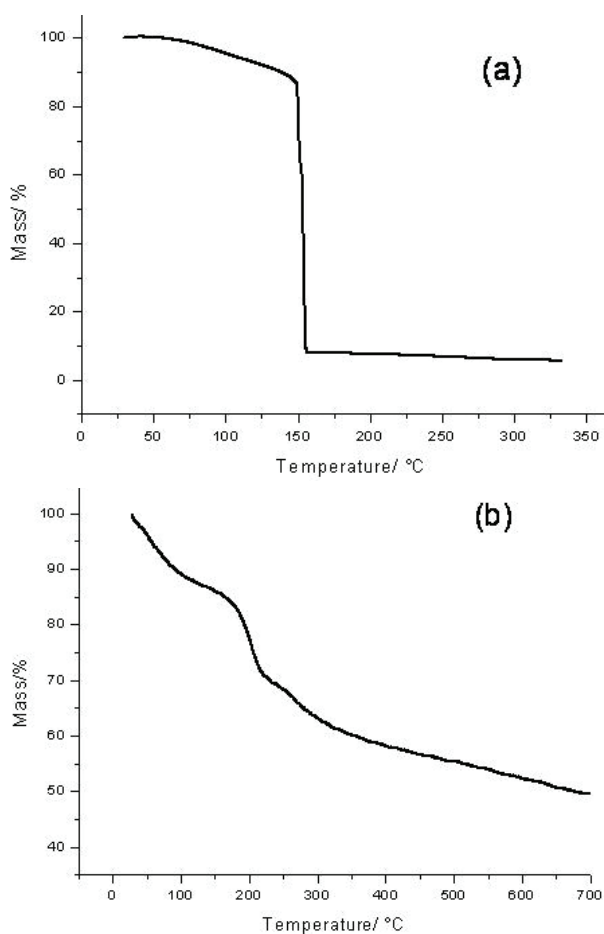


Figure 3. Thermogravimetric curves for a) GO and b) GO-hmta.



in Table II verify that the presence of hmta molecules inside the interlayer space of GO promoted stabilization of the matrix, since pure GO lost 80 % of its mass in the 150–160 °C range, whereas even with the hmta molecules, the mass loss in the 125 to 700 °C was only 39 %. The corresponding carbon residue increased from 8 % for GO to 49 % for the hybrid matrix.

TABLE II. Thermogravimetric data summary for GO and GO–hmta samples

Compound	Temperature range, °C	Mass loss, %	Process
GO	40–145	12	Release of physisorbed water molecules
	150–160	80	$2\text{C}_3\text{H}_3\text{O}_{4.5}(\text{s}) \rightarrow 6\text{CO} + 3\text{H}_2\text{O}$
GO–hmta	40–120	12	Release of physisorbed water molecules
	125–220	18	$2\text{C}_3\text{H}_3\text{O}_{4.5}(\text{s}) \rightarrow 6\text{CO} + 3\text{H}_2\text{O}$
	225–700	21	Release of hmta molecules and $2\text{C}_3\text{H}_3\text{O}_{4.5}(\text{s}) \rightarrow 6\text{CO} + 3\text{H}_2\text{O}$

It is noteworthy that the thermal degradation profile for GO shown in Fig. 3a, with two mass loss steps, is completely different from those previously presented.<sup>8</sup> In that study, three distinct mass loss steps were observed at 40, 185 and 433 °C, assigned to the release of water, CO and CO<sub>2</sub>, respectively, with a final residue of approximately 5 %. This discrepancy can be explained remembering that the elemental analysis results were also quite different in both cases: C, 47.16 %; H, 1.72 %, and O, 40.27 %, giving to the GO sample the formula C<sub>8</sub>H<sub>3.5</sub>O<sub>5.1</sub>,<sup>8</sup> whereas in the present work the results were C, 39.7 %; H, 2.6 %, and O, 57.7 %, giving the formula C<sub>4</sub>H<sub>3</sub>O<sub>4</sub>. Hence, the oxygen percentage of the matrix prepared in the present study surpassed the “usual” 30–40 % for GO. Such a difference in composition can be attributed to the larger volume of H<sub>2</sub>O<sub>2</sub> used in this study in comparison with the previously described preparation.<sup>8</sup> Thus, in the present GO compound there were equal amounts of C and O. However, if one takes into account the final carbon residue of 8 % after the thermal degradation and recalculates the carbon percentage based on this, the formulae C<sub>3</sub>H<sub>3</sub>O<sub>4.5</sub> is obtained, giving rise to the thermal degradation process:  $2\text{C}_3\text{H}_3\text{O}_{4.5}(\text{s}) \rightarrow 6\text{CO} + 3\text{H}_2\text{O}$ .

Analysis of the thermal degradation profile of the GO–hmta matrix gives more interesting results. The carbon percentage is increased from 39.7 (GO) to 53.0 % (GO–hmta), a difference of 13.3 %. However, after thermal degradation, the final carbon residues were 8 (GO) and 49 % (GO–hmta), a difference of 41 %. Hence, by comparison of the TG curves shown in Fig. 3, as well as on these carbon residues, it is clear that the presence of hmta molecules change, in a remarkable way, the thermal degradation profile of GO. This is a very uncommon effect in lamellar matrices. In lamellar MoO<sub>3</sub> for example,<sup>13–18</sup> after the release of the organic moiety, the lamellar matrix exhibits its “normal” degradation processes.

Taking into account that hmta sublimates in the range 285–295 °C,<sup>19</sup> it is valid to assume that in the temperature range covered by the TG curve, all the

hmta molecules had left the interlayer space. Hence, the mass loss steps observed in the TG curves for the GO–hmta matrix are assigned as shown in Table II. Such a proposal suggests that after the release of physisorbed water molecules, the release of CO and H<sub>2</sub>O from the GO matrix not interacting with hmta molecules commences but that this is interrupted when the decomposition of the GO parts that are interacting with the hmta molecules begins. Thus, the presence of hmta molecules inside the GO matrix, with very strong interactions, increases the thermal stability of the GO matrix. Such a fact could be explored to investigate possible applications of the GO matrix (in catalysis, for example). In the range 225–700 °C, hmta and GO decompose slowly: the GO parts decompose after the release of hmta molecules, *i.e.*, the main step (rate determining) of the thermal degradation is the release of hmta molecules.

The obtained X-ray diffraction patterns are shown in Fig. 4, from which it can be seen that the crystallinity of GO is enhanced after reaction with hmta. Fur-

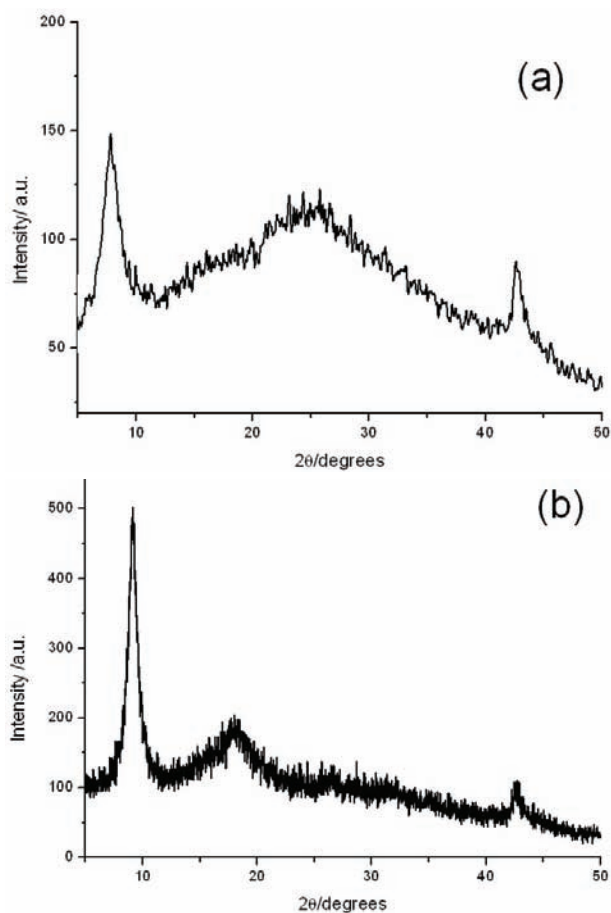


Fig. 4. X-Ray diffraction patterns for a) GO and b) GO–hmta.

thermore, the interlayer distance decreased from 1.13 nm (7.8°) to 0.96 nm (9.2°) after reaction with hmta – taking into account the (001) diffraction peaks. The peak at 18.4° can be assigned to the GO–hmta (002) diffraction peak.

Since the interlayer distance of GO decreased and did not increase after reaction with hmta, it can be concluded that the hmta molecules are not intercalated into the GO. However, it is possible to suppose that the insertion of hmta molecules into the GO interlayer space could provoke very intense interactions (*via* hydrogen bonds) between the layers, provoking the observed distance contraction. This second hypothesis is considered the most probable taking into account the increased thermal stability (Fig. 3 and Table II). The higher crystallinity of the hybrid matrix in comparison with pure GO also reinforces this hypothesis.

## ИЗВОД

РЕАКЦИЈА ХЕКСАМЕТИЛЕНТЕТРАМИНА СА ГРАФИТНИМ ОКСИДОМ (GO)  
КАО СТРАТЕГИЈА ПОБОЉШАЊА ТЕРМИЧКЕ СТАБИЛНОСТИ GO:  
СИНТЕЗА И КАРАКТЕРИЗАЦИЈА ЈЕДИЊЕЊА

ROBSON F. de FARIAS<sup>1</sup> и CLAUDIO AIROLDI<sup>2</sup>

<sup>1</sup>*Departamento de Química, Universidade Federal do Rio Grande do Norte, Cx. Postal 1662, 59078-970 Natal, Rio Grande do Norte* и <sup>2</sup>*Instituto de Química, UNICAMP, Cx. Postal 1664, 13083-970 Campinas, São Paulo, Brasil*

У раду је приказана синтеза и карактеризација оксид графита–хексаметилентетрамин (GO–hmta) једињења. Показано је да молекули хексаметилентетрамина у GO матрици имају врло јаку интеракцију што доводи до стабилизације и побољшања термичких особина GO матрице. Та чињеница отвара могућности примене GO матрице, посебно у катализи.

(Примљено 17. јула, ревидирано 23. септембра 2009)

## REFERENCES

1. R. F. de Farias, *Chemistry on modified oxide and phosphate surfaces – fundamentals and applications*, Academic Press, Amsterdam, 2009
2. I. Dákány, R. Krüger-Grasser, A. Weiss, *Colloid Polym. Sci.* **276** (1998) 570
3. A. B. Bourlinos, D. Gournis, D. Petridis, T. Szabó, A. Szeri, I. Dákány, *Langmuir* **19** (2003) 60505
4. A. Lerf, H. He, M. Forster, J. Klinowski, *J. Phys. Chem. B* **102** (1998) 4477
5. N. I. Kovtyukhova, P. J. Ollivier, B. R. Martin, T. E. Mallouk, S. A. Chizhik, E. V. Buzaneva, *Chem. Mater.* **11** (1999) 771
6. T. Szabó, A. Szeri, I. Dákány, *Carbon* **43** (2005) 87
7. T. Szabó, O. Berkesi, P. Forgó, K. Josepovits, Y. Sanakis, D. Petridis, *Chem. Mater.* **18** (2006) 2740
8. R. Bissessur, S. F. Scully, *Solid State Ionics* **178** (2007) 877
9. J. Bian, M. Xiao, S. J. Wang, Y. X. Lu, Y. Z. Meng, *Catal. Commun.* **10** (2009) 1529
10. M. Sereych, T. J. Bandosz, *Carbon* **45** (2007) 2126
11. Y. Matsuo, Y. Nishino, T. Fukutsuka, Y. Sugie, *Carbon* **45** (2007) 1384
12. R. F. de Farias, C. Airoidi, *J. Non-Cryst. Solids* **261** (2000) 181
13. R. F. de Farias, *Int. J. Inorg. Mater.* **3** (2001) 303

14. R. F. de Farias, *Int. J. Inorg. Mater.* **3** (2001) 931
15. R. F. de Farias, *J. Phys. Chem. Solids* **64** (2003) 2199
16. R. F. de Farias, *Mater. Chem. Phys.* **90** (2005) 302
17. R. F. de Farias, *J. Phys. Chem. Solids* **64** (2003) 1241
18. R. F. de Farias, M. S. Refat, H. A. Hashem, *J. Incl. Phenom. Macrocyc. Chem.* **61** (2008) 113
19. G. R. Maxwell, *Synthetic nitrogen products – a practical guide to the products and processes*, Springer, New York, 2006.



*J. Serb. Chem. Soc.* 75 (4) 505–512 (2010)  
JSCS–3983

## Digital holographic reconstruction detection of localized corrosion arising from scratches

LIANG WANG<sup>1</sup>, SHENHAO CHEN<sup>1,2\*</sup>, BOYU YUAN<sup>3</sup>, FANJIANG MENG<sup>2</sup>,  
JIANQIU WANG<sup>2</sup>, CHAO WANG<sup>2,4</sup> and LIANG LI<sup>4</sup>

<sup>1</sup>Department of Chemistry, Shandong University, Jinan 250100, <sup>2</sup>State Key Laboratory for Corrosion and Protection, Shenyang 110016, <sup>3</sup>Department of Physics, Xuzhou Normal University, Xuzhou 221116 and <sup>4</sup>Department of Chemistry, Xuzhou Normal University, Xuzhou 221116, P. R. China

(Received 27 June, revised 18 October 2009)

**Abstract:** In this study, electrochemical methods and the digital holographic reconstruction technique were combined to detect the localized scratch-induced corrosion process of Alloy 690 in 0.50 mol dm<sup>-3</sup> H<sub>2</sub>SO<sub>4</sub> containing 0.10 mol dm<sup>-3</sup> NaCl. The numerical reconstruction method has been proved to be an effective technique to detect changes of solution concentration. One can obtain direct information from the reconstructed images and capture subtle more revealing changes. It provides a method to detect localized corrosion arising from scratches.

**Keywords:** digital holography; numerical reconstruction; Alloy 690; scratch corrosion.

### INTRODUCTION

Alloy 690 is one of the most widely used nuclear materials and its corrosion has been studied for many years.<sup>1–6</sup> Localized corrosion is of particular interest because it can lead to a fast and fatal failure in engineering structures. Various experimental techniques have been employed to study localized corrosion, such as atomic force microscopy (AFM),<sup>7</sup> the acoustic emission technique (AET),<sup>8</sup> the optical interferometry technique (OIT),<sup>9</sup> electrochemistry impedance spectroscopy (EIS),<sup>10</sup> the electrochemical noise (EN)<sup>11</sup> technique, *etc.* Calvo *et al.*<sup>12</sup> examined *in situ* the localized corrosion of tinplate with a line scratch immersed in H<sub>2</sub>SO<sub>4</sub> solution by the scanning electrochemical microscopy (SECM) and indicated that the current over the scratch was markedly increased. However, it takes about 30 min to capture one image by SECM, during which time the surface status of the sample could change.

\* Corresponding author. E-mail: shchen@sdu.edu.cn  
doi: 10.2298/JSC090627016W

There is another method to study localized corrosion. In the 1990s, Habib<sup>13–15</sup> studied pitting corrosion by holographic interferometry. The method can be also used in microscopic structure measurements,<sup>16</sup> biology<sup>17,18</sup> and other fields. Li<sup>19</sup> investigated the pitting corrosion of aluminum induced by chloride ions by holographic microphotography. Using the in-line digital holography<sup>20</sup>, an amplitude-contrast and phase-contrast image of the specimen can be obtained simultaneously, which can yield useful information during electrochemical measurements. Yuan<sup>21</sup> introduced carrier-wave-recording into experiments and reconstructed the holograms, which can capture more revealing subtle changes. Digital holographic reconstruction can be applied to visualize the two-dimensional distribution of a concentration change at an electrode/solution interface.

The experimental principle is based on the relationships between the phase difference of an object wave ( $\Delta\Phi$ ), the refractive index of the solution ( $\Delta n$ ) and concentration ( $\Delta c$ ). Generally, several components are present in a solution. Thus, the net refractive index is the summation of the effect of the concentration of each species. The relationship is:<sup>22</sup>

$$\sum_i \Delta c_i = \sum_i k_i \Delta n_i = \frac{\lambda_0}{2\pi d} \sum_i k_i \Delta \Phi_i \quad (1)$$

where  $k_i$  is the concentrative refractivity;  $\lambda_0$  is the wavelength of the laser light and  $d$  is the geometrical path length where the refractive index variation exists. Thus, the measurement of concentration change can be transformed into the information of phase variation. Details about numerical reconstruction can be found in the literature.<sup>21</sup>

Electrochemical techniques, such as linear polarization and AC impedance spectroscopy<sup>23–24</sup> have been widely used to estimate the rate of general corrosion, but they suffer a major limitation in the measurement of the localized corrosion rate and distributions. In this study, an electrochemical technique and the digital holographic reconstruction method were combined to study localized corrosion arising from scratches. The results revealed that the method can be used to detect localized corrosion induced by scratches.

## EXPERIMENTAL

### *Electrochemical system*

An electrochemical cell consisting of a three-electrode system<sup>20</sup> was used. The working electrode was Alloy 690 (59.50 % Ni, 29.02 % Cr, 10.28 % Fe, 0.30 % Mn, 0.33 % Ti, 0.16 % Al, 0.018 % C, 0.31 % Si, 0.015 % Co, 0.01 % Cu and 0.009 % P) provided by the Electric Power Research Institute (EPRI). The counter electrode was a platinum sheet and the reference electrode was a saturated calomel electrode (SCE) with a Luggin capillary tip set at 2 mm from the working electrode surface.

The entire working electrode was sealed in a glass tube with a thin layer of epoxy resin, leaving the end exposed to the solution. An electrode having two scratches is shown in Fig. 1a, while the electrode used for comparison having no scratches is shown in Fig. 1b. Both

electrodes had the same area ( $0.046 \text{ cm}^2$ ). The scratch is  $100 \mu\text{m}$  in width and  $120 \mu\text{m}$  in depth. The working electrode material was cut from bulk material using an electric spark and polished with  $1.5 \mu\text{m}$  alumina paste. After ultrasonic cleaning in acetone, the samples were electropolished in methanol containing 30 % nitric acid.

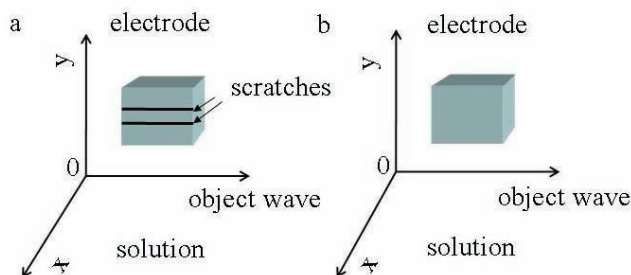


Fig. 1. The scheme of the electrode location. The  $x$ -axis is in the horizontal direction from the electrode surface toward the bulk electrolyte; the  $y$ -axis is in the vertical direction parallel to the surface of the electrode. The object wave and the scratch have the same direction.

In the experiments, the scratch-making device was self-made and it included a frequency converter, a straight-in feed electric engine, a scratching table and some conical heads. By adjusting the frequency converter to 10 Hz, a scratching speed of 9 mm/s was obtained. The geometry of the scratches was determined by the geometry of the conical heads. The conical head was fixed at the end of a micrometer and the scratching procedure was fixed in order to produce similar scratches.

To perform the  $I-t$  measurement, a polarization curve survey was first performed. All electrochemical measurements were measured using a CHI660B at room temperature. In this experiment, all potentials are referred to SCE.

#### Holography recording system

The measurement setup of the holographic recording system is shown in Fig. 2. The He-Ne laser with a wavelength of 632.8 nm is split by a beam-splitter into two beams, a reference wave and an object wave. Each beam is enlarged to a diameter of  $\approx 50 \text{ mm}$  by a beam ex-

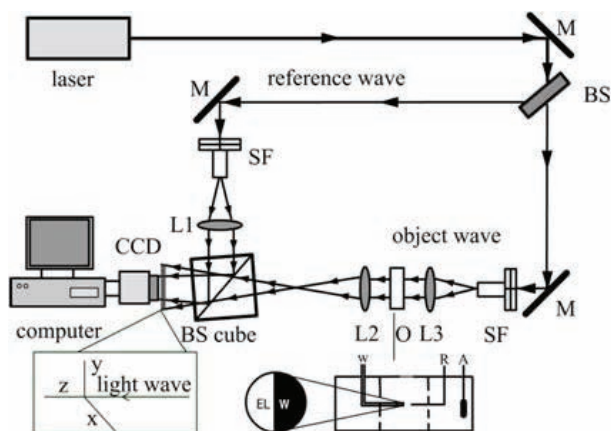


Fig. 2. Experimental setup of the digital holography recording system: M, mirrors; BS, beam-splitter; SF, spatial filter; L1, L2 and L3, lenses; O, object; BS Cube, beam-splitter cube; W, working electrode; R, reference electrode; A, counter electrode; EL, electrolyte.

pander including a spatial filter. The object wave, which carries the information of the electrode/solution interface, is combined with the reference wave by a beam-splitter cube. Thus, the two beams can interfere and produce a series of interference fringes. A Sony DSR-PD150P camera was used to record the interference fringes. The camera produces a standard CCIR video signal at 25 frames per second and the minimal phase difference detected was about 0.1 rad.

### RESULTS AND DISCUSSION

The polarization curve and  $I$ - $t$  curve of Alloy 690 in  $0.50 \text{ mol dm}^{-3} \text{ H}_2\text{SO}_4$  containing  $0.10 \text{ mol dm}^{-3} \text{ NaCl}$  solution at room temperature are shown in Figs. 3 and 4, respectively. In Fig. 4, some different time points were selected to reflect the corrosion process.

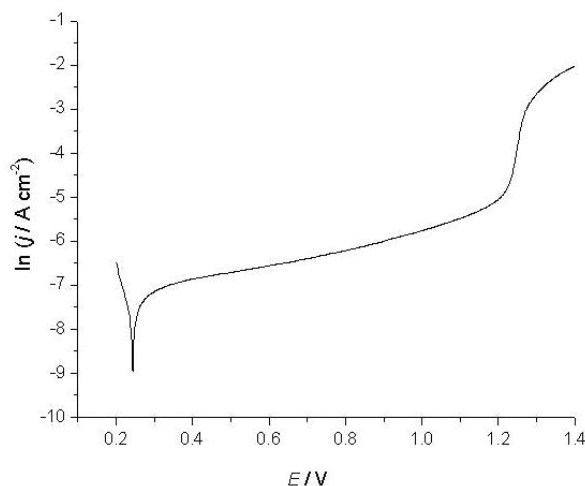


Fig. 3. The polarization curve of Alloy 690 in  $0.50 \text{ mol dm}^{-3} \text{ H}_2\text{SO}_4$  containing  $0.10 \text{ mol dm}^{-3} \text{ NaCl}$ , recorded at  $10 \text{ mV/s}$ .

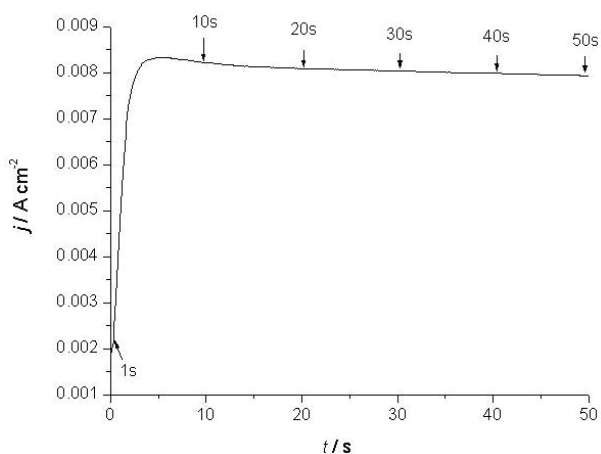


Fig. 4. The  $j$ - $t$  curve of Alloy 690 in  $0.50 \text{ mol dm}^{-3} \text{ H}_2\text{SO}_4$  containing  $0.10 \text{ mol dm}^{-3} \text{ NaCl}$ , with the potential controlled at  $1.26 \text{ V}$ .



Holograms were recorded simultaneously by the CCD camera and analyzed by the Fourier method<sup>25–26</sup> to abstract the information of phase difference. The Fourier analysis<sup>27</sup> method consists of Fourier transform, band-pass filtering and counter Fourier transform. The reconstructed images are shown in Fig. 5. In the images, the left part is the electrode, the right the solution and in between is the interface. The larger is the value of the phase difference ( $z$ -axis), the more intense is the concentration change. The green area indicates that the phase difference was zero or nearly zero. The phase differences are positive with increasing concentration changes from yellow to red. In the electrode area, the green level remained constant. In Fig. 5, the concentration change was very slight at 1 s. With passing time, two obvious yellow areas appeared at the electrode/electrolyte interface, which indicated that in both areas there were larger phase differences

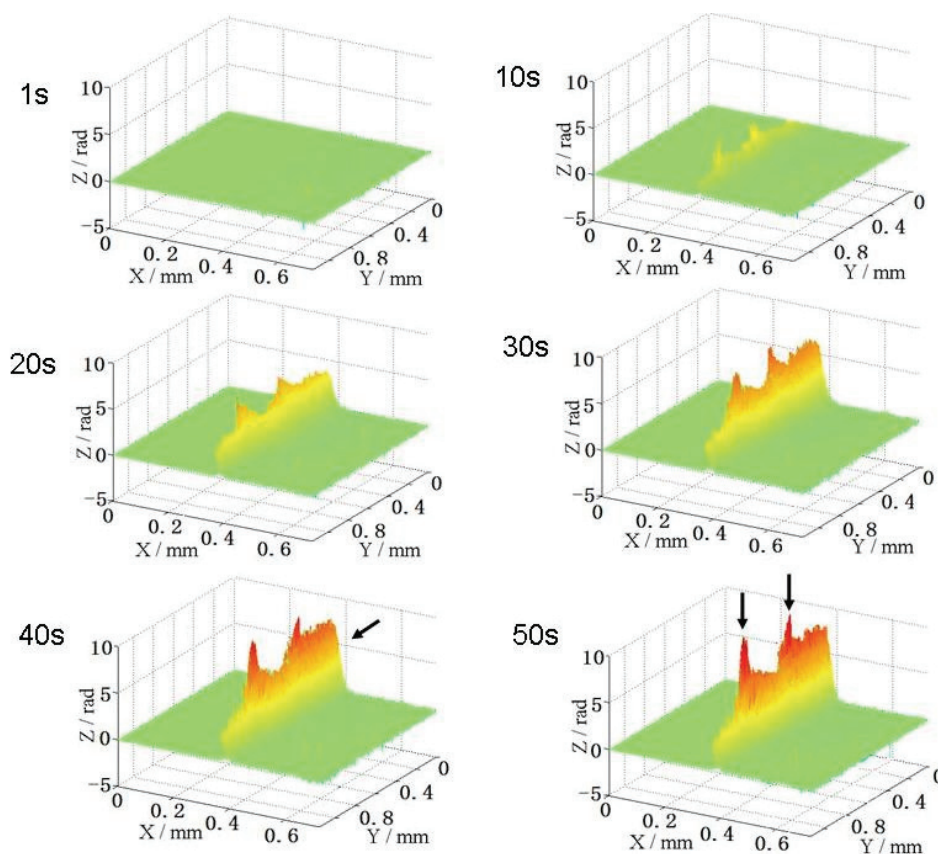


Fig. 5. Reconstructed three-dimensional images of the electrode/solution interface obtained at different times, shown in Fig. 4, for the scratched electrode. The  $x$ -axis is in horizontal direction from the electrode surface toward the bulk electrolyte while the  $y$ -axis in vertical direction is parallel to the surface of the electrode. The  $z$ -axis shows the phase changes.

than in other parts. The trait can be clearly seen in Fig. 5 at 50 s which has two prominent peaks (the position of the arrows). Because of the gravity,<sup>28</sup> the ions moved to the bottom of the electrode, hence the concentration at the bottom varied more greatly. In Fig. 5 at 40 s, the arrow indicates the bottom of the electrode.

To contrast to the above results, an electrode of the same size, but with no scratch, was used to detect the corrosion. The electrode schema is shown in Fig. 1b and the test conditions were the same as for the above measurements. From the reconstructed images shown in Fig. 6, the concentration changes at the electrode/electrolyte interface were well-proportioned. It can also be seen that the concentration at the bottom of the electrode increased markedly (see the arrow in Fig. 6 at 50 s).

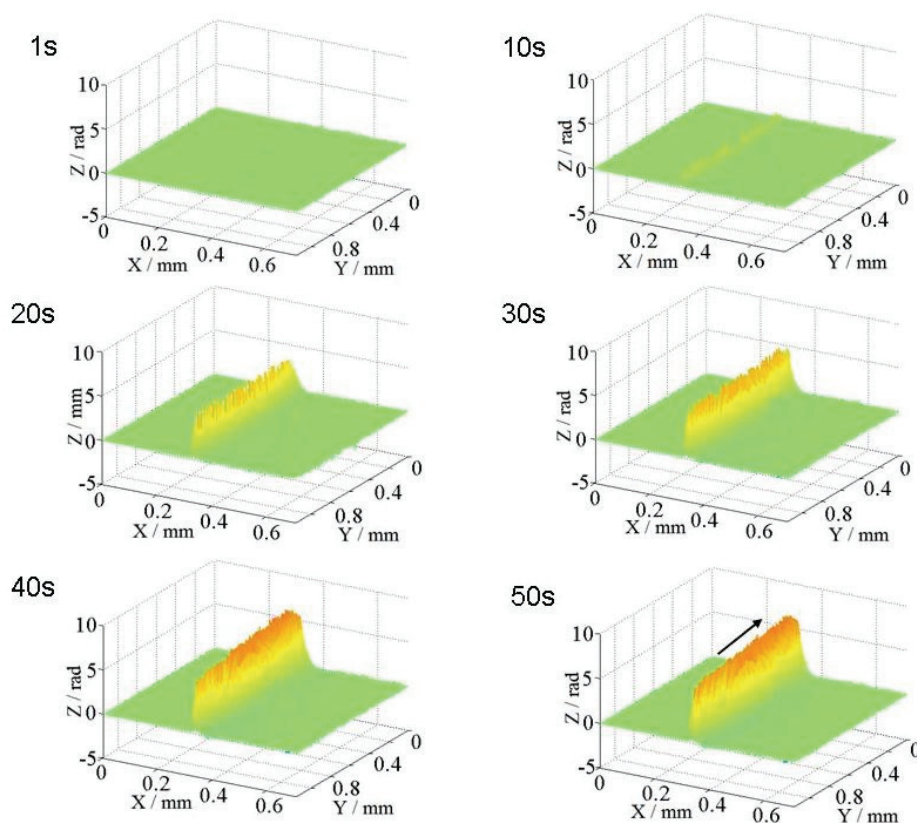


Fig. 6. The reconstructed three-dimensional images of the electrode without scratches during the electrochemical test. The meanings of the  $x$ -axis,  $y$ -axis and  $z$ -axis were the same as those in Fig. 5.

By comparing Figs. 5 and 6, it is clear that the increase of the concentration in the two peak areas was due to the existence of the scratches. The scratches can

be viewed as defects on the metal surface. When localized corrosion occurs, the corrosion over the scratches will be more severe, which can lead to the more dramatic increase in the concentration.<sup>28</sup> The larger concentration changes can induce major changes the phase differences. Hence, two prominent peaks are evident in Fig. 5. As can be seen from the results, the method effectively enables the detection localized corrosion due to the scratches.

#### CONCLUSIONS

A numerical processing method for digital holograms was proposed to study the scratch corrosion of Alloy 690. Digital holographic reconstruction was applied to visualize the two-dimensional distribution of the concentration change at the electrode/solution interface. The reconstructed images provide visual results and more useful information about the change in concentration at the interface can be obtained from the results. The method was able to evidence that corrosion over the scratch was more significant than over the unscratched areas. The reconstructed images supplied more visual information for a better analysis and understanding of the dynamic processes of concentration change in the solution.

*Acknowledgement.* The authors would like to thank the Special Funds for the Major State Basic Research Project (2006CB605004).

#### ИЗВОД

#### КОРИШЋЕЊЕ ДИГИТАЛНЕ ХОЛОГРАФСКЕ РЕКОНСТРУКЦИЈЕ ЗА ДЕТЕКЦИЈУ ЛОКАЛИЗОВАНЕ КОРОЗИЈЕ ИЗАЗВАНЕ ОГРЕБОТИНАМА

LIANG WANG<sup>1</sup>, SHENHAO CHEN<sup>1,2</sup>, BOYU YUAN<sup>3</sup>, FANJIANG MENG<sup>2</sup>,  
JIANQIU WANG<sup>2</sup>, CHAO WANG<sup>2,4</sup> И LIANG LI<sup>4</sup>

<sup>1</sup>Department of Chemistry, Shandong University, Jinan 250100, <sup>2</sup>State Key Laboratory for Corrosion and Protection, Shenyang 110016, <sup>3</sup>Department of Physics, Xuzhou Normal University, Xuzhou 221116 и <sup>4</sup>Department of Chemistry, Xuzhou Normal University, Xuzhou 221116, P. R. China

У раду су комбиноване електрохемијске методе и техника дигиталне холографске реконструкције у циљу детекције локализованог корозионог процеса легуре 690 који је индукован огреботинама у раствору 0,50 mol dm<sup>-3</sup> H<sub>2</sub>SO<sub>4</sub> и 0,10 mol dm<sup>-3</sup> NaCl. Показано је да је нумеричка реконструкција ефикасна техника за детекцију промена у концентрацији раствора. На основу реконструисаних слика могуће је добити директне и јасне информације из деликатних промена концентрације. Ово представља методу за детекцију локализоване корозије изазване огреботинама површине.

(Примљено 27. јуна, ревидирано 18. октобра 2009)

#### REFERENCES

1. Y. Y. Chen, L. B. Chou, H. C. Shih, *Mater. Chem. Phys.* **97** (2006) 37
2. H. T. Lee, J. L. Wu, *Corros. Sci.* **51** (2009) 733
3. Y. Y. Chen, L. B. Chou, H. C. Shih, *Mater. Sci. Eng. A* **396** (2005) 129
4. H. T. Lee, J. L. Wu, *Corros. Sci.* **51** (2009) 439

5. J. M. Zagal, H. F. López, O. Flores, J. L. Albarran, L. Martínez, *Corros. Sci.* **50** (2008) 3371
6. B. Peng, B. T. Lu, J. L. Luo, Y. C. Lu, H. Y. Ma, *J. Nucl. Mater.* **378** (2008) 333
7. R. E. Williford, C. F. Windisch Jr., R. H. Jones, *Mater. Sci. Eng. A* **288** (2000) 54
8. Y. P. Kim, M. Fregonese, *NDT and E Int.* **36** (2003) 553
9. K. Habib, K. Bouresli, *Electrochim. Acta* **44** (1999) 4635
10. C. F. Dong, A. Q. Fu, X. G. Li, Y. F. Cheng, *Electrochim. Acta* **54** (2008) 628
11. F. H. Cao, Z. Zhang, Y. L. Cheng, J. F. Li, J. Q. Zhang, J. M. Wang, C. N. Cao, *Acta Metal. Sin. (Engl. Lett.)* **16** (2003) 22
12. E. Völker, C. G. Inchauspe, E. J. Calvo, *Electrochem. Commun.* **8** (2006) 179
13. K. Habib, F. Al-Sabti, *Opt. Rev.* **4** (1997) 324
14. K. Habib, *Corros. Sci.* **40** (1998) 1435
15. K. Habib, F. Al-Sabti, *Corrosion* **53** (1997) 688
16. B. Rappaz, A. Barbul, A. Hoffmann, D. Boss, R. Korenstein, C. Depeursinge, P. J. Magistretti, P. Marquet, *Blood Cells Mol. Dis.* **42** (2009) 228
17. J. Schnekenburger, I. Bredebusch, W. Domschke, B. Kemper, P. Langehanenberg, G. V. Bally, *Med. Laser. Appl.* **22** (2007) 165
18. I. Bernhardt, L. Ivanova, P. Langehanenberg, B. Kemper, G. V. Bally, *Bioelectrochem.* **73** (2008) 92
19. L. Li, C. Wang, S. Chen, X. Hou, X. Yang, *J. Serb. Chem. Soc.* **73** (2008) 561
20. X. Yang, S. Chen, C. Wang, L. Li, *Electrochem. Commun.* **6** (2004) 643
21. B. Yuan, S. Chen, X. Yang, C. Wang, L. Li, *Electrochem. Commun.* **10** (2008) 392
22. B. Yuan, C. Wang, L. Li, S. Chen, *Electrochem. Commun.* **11** (2009) 1373
23. J. F. Li, Z. Q. Zheng, C. Y. Tan, S. C. Li, Z. Zhang, J. Q. Zhang, *Acta Metal. Sin. (Engl. Lett.)* **17** (2004) 894
24. X. T. Chang, Y. S. Yin, G. H. Niu, T. Liu, S. Cheng, S. B. Sun, *Acta Metal. Sin. (Engl. Lett.)* **20** (2007) 334
25. E. Cucho, F. Bevilacqua, C. Depeursinge, *Opt. Lett.* **24** (1999) 291
26. G. Pedrini, H. J. Tiziani, *Opt. Laser. Technol.* **29** (1997) 249
27. L. Li, C. Wang, B. Yuan, S. Chen, *Electrochem. Commun.* **10** (2008) 103
28. H. Jia, S. Chen, B. Yuan, C. Wang, L. Li, *J. Serb. Chem. Soc.* **74** (2009) 197.



*J. Serb. Chem. Soc.* 75 (4) 513–521 (2010)  
JSCS–3984

## Prediction of the retention of $\beta$ -diketonato complexes in TLC systems on silica gel by quantitative structure–retention relationships

RADA M. BAOŠIĆ\*, ANA D. RADOJEVIĆ and ŽIVOSLAV LJ. TEŠIĆ

*Faculty of Chemistry, University of Belgrade, Studentski trg 12,  
P.O. Box 158, 11000 Belgrade, Serbia*

(Received 25 February, revised 9 December 2009)

**Abstract:** Quantitative structure–retention relationships for a series of 30 mixed  $\beta$ -diketonato complexes of cobalt(III), chromium(III) and ruthenium(III) were derived by multiple linear regression analyses using molecular descriptors obtained by quantum chemical calculations. The retention parameters were obtained by thin layer chromatography on silica gel using mono and two-component solvent systems. The molecular descriptors included in the multiple linear regression analysis were molecular weight, molecular volume, surface area, hydrophilic–lipophilic balance, percent hydrophilic surface area, dipole moment, polarizability, refractivity, energy of the highest occupied molecular orbital and energy of the lowest unoccupied molecular orbital. High agreement between the experimental and predicted retention parameters was obtained when polarizability and the hydrophilic–lipophilic balance were used as the molecular descriptors. Comparison of the models with those established on polyacrylonitrile showed that the structure of the sorbent is responsible for the chromatographic behaviour of the same compounds. The presented models can be used for the prediction of the retention of new solutes in screening chromatographic systems.

**Keywords:** quantitative structure–retention relationship;  $\beta$ -diketonato complexes; molecular descriptors; thin layer chromatography.

### INTRODUCTION

Quantitative structure–retention relationships (QSRRs) are statistical models which quantify the relationship between the structure of a molecule and its chromatographic retention parameters in different kinds of chromatography.<sup>1–4</sup> Application of QSRRs allows the prediction of the retention of a new solute, identification of the most informative structural descriptors, elucidation of the mole-

\* Corresponding author. E-mail: rbaosic@chem.bg.ac.rs  
doi: 10.2298/JSC090225002B

cular mechanisms of separation in a given chromatographic system, evaluation of complex physicochemical properties of solutes and estimation of biological activities.<sup>5</sup> In recent QSRR studies, quantum chemical descriptors alone or in combination with conventional descriptors have been extensively applied. In this way, many of the electronic and geometric properties of molecules can be expressed.<sup>6</sup> The relationship between retention and the structural characteristics of a molecule explains the effect of chemical structure on the retention behaviour in a more accurate way.<sup>7-9</sup>

Metal–ligand complexes represent an important group of analytes. TLC is utilized as an analytical tool for metal ion analysis, metal speciation studies and characterization of metal complexes of pharmaceutical or industrial importance. Coordination complexes between metals and  $\beta$ -diketones are interesting in this field because of the possibility of making wide varieties of substitutions in the  $\beta$ -diketonato chelate ring.<sup>10</sup> These complexes provide models for different chemical processes and investigations ranging from synthetic, kinetic and structural topics to catalysis and many others, such as electron transfer processes relevant for biological activity.<sup>11-13</sup>

The objective of this study was to develop models for accurate quantitative relationships between molecular structure and retention parameters of mixed  $\beta$ -diketonato complexes on silica gel stationary phases based on their molecular properties and to identify molecular descriptors most sensitive to the retention parameter  $R_M$ . In addition, the obtained models were compared with those established on polyacrylonitrile as the sorbent. The elucidation of these relationships may promote a more profound understanding of chromatographic separation processes and be used to predict the retention behaviour of structurally similar compounds.

#### EXPERIMENTAL

The retention parameters,  $R_F$ , were extracted from a previous work<sup>14</sup> in which 30 mixed  $\beta$ -diketonato complexes of Co(III), Cr(III) and Ru(III) were chromatographed on silica gel with four mono- and five two-component mobile phases. They were converted to  $R_M$  values using the Bate-Smith and Westall Equation:  $R_M = \log((1/R_F) - 1)$ .

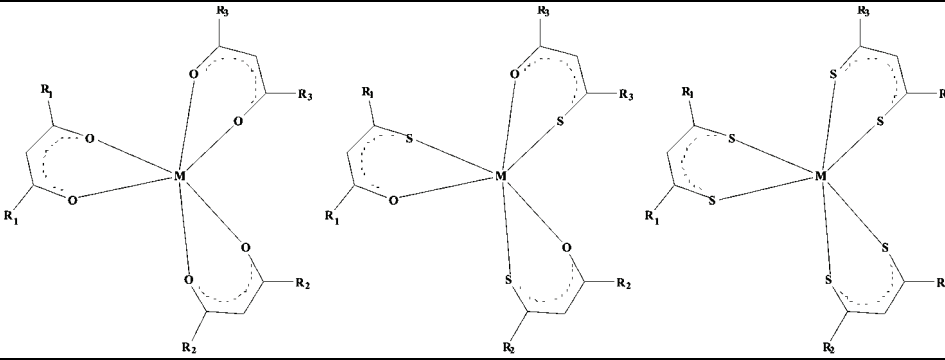
The geometry optimization of the molecules and calculation of molecular descriptors were realised with HyperChem 7.0 software.<sup>15</sup> Additional calculation of the descriptors was developed by the Molecular Modelling Program Plus software. The following descriptors were calculated: molecular weight ( $MW$ ), molecular volume ( $MV$ ), surface area ( $SA$ ), hydrophilic–lipophilic balance ( $HLB$ ), percent hydrophilic surface area ( $PHSA$ ), dipole moment ( $\mu$ ), polarizability ( $\alpha$ ), refractivity ( $R$ ), energy of the highest occupied molecular orbital ( $E_{HOMO}$ ) and energy of the lowest unoccupied molecular orbital ( $E_{LUMO}$ ). The QSRR equation was obtained by stepwise multiple linear regressions (MLR).<sup>15,16</sup> The significance level of the performed calculations was above 95 %.

#### RESULTS AND DISCUSSION

The structures of the 30 investigated compounds are shown in Table I. The calculated retention parameters,  $R_M$ , of these compounds are listed in Table II.

The compositions of the mobile phases are given in Table III. From Table II, it can be seen that substitution of a donor oxygen atom in the phacphac ligand with a less electronegative sulphur atom, to form the corresponding thio ligand, resulted in increased mobility of all the complexes.<sup>14</sup> Also, substitution of the acac ligands leads to decreased  $R_M$  values, *i.e.*, the mobility was higher.

TABLE I. The structures of the investigated complexes



		I		II		III	
Compound		Complex		R <sub>1</sub>	R <sub>2</sub>	R <sub>3</sub>	Type
(1) (11) (21)	[M(acac) <sub>3</sub> ] <sup>a,b</sup>	CH <sub>3</sub>	CH <sub>3</sub>	CH <sub>3</sub>	CH <sub>3</sub>	CH <sub>3</sub>	I
(2) (12) (22)	[M(acac) <sub>2</sub> (phacphac)] <sup>c</sup>	CH <sub>3</sub>	CH <sub>3</sub>	C <sub>6</sub> H <sub>5</sub>	C <sub>6</sub> H <sub>5</sub>	C <sub>6</sub> H <sub>5</sub>	I
(3) (13) (23)	[M(acac) <sub>2</sub> (phacphSac)] <sup>d</sup>	CH <sub>3</sub>	CH <sub>3</sub>	C <sub>6</sub> H <sub>5</sub>	C <sub>6</sub> H <sub>5</sub>	C <sub>6</sub> H <sub>5</sub>	II
(4) (14) (24)	[M(acac) <sub>2</sub> (phSacphSac)] <sup>e</sup>	CH <sub>3</sub>	CH <sub>3</sub>	C <sub>6</sub> H <sub>5</sub>	C <sub>6</sub> H <sub>5</sub>	C <sub>6</sub> H <sub>5</sub>	III
(5) (15) (25)	[M(acac)(phacphac) <sub>2</sub> ]	CH <sub>3</sub>	C <sub>6</sub> H <sub>5</sub>	C <sub>6</sub> H <sub>5</sub>	C <sub>6</sub> H <sub>5</sub>	C <sub>6</sub> H <sub>5</sub>	I
(6) (16) (26)	[M(acac)(phacphSac) <sub>2</sub> ]	CH <sub>3</sub>	C <sub>6</sub> H <sub>5</sub>	C <sub>6</sub> H <sub>5</sub>	C <sub>6</sub> H <sub>5</sub>	C <sub>6</sub> H <sub>5</sub>	II
(7) (17) (27)	[M(acac)(phSacphSac) <sub>2</sub> ]	CH <sub>3</sub>	C <sub>6</sub> H <sub>5</sub>	C <sub>6</sub> H <sub>5</sub>	C <sub>6</sub> H <sub>5</sub>	C <sub>6</sub> H <sub>5</sub>	III
(8) (18) (28)	[M(phacphac) <sub>3</sub> ]	C <sub>6</sub> H <sub>5</sub>	C <sub>6</sub> H <sub>5</sub>	C <sub>6</sub> H <sub>5</sub>	C <sub>6</sub> H <sub>5</sub>	C <sub>6</sub> H <sub>5</sub>	I
(9) (19) (29)	[M(phacphSac) <sub>3</sub> ]	C <sub>6</sub> H <sub>5</sub>	C <sub>6</sub> H <sub>5</sub>	C <sub>6</sub> H <sub>5</sub>	C <sub>6</sub> H <sub>5</sub>	C <sub>6</sub> H <sub>5</sub>	II
(10) (20) (30)	[M(phSacphSac) <sub>3</sub> ]	C <sub>6</sub> H <sub>5</sub>	C <sub>6</sub> H <sub>5</sub>	C <sub>6</sub> H <sub>5</sub>	C <sub>6</sub> H <sub>5</sub>	C <sub>6</sub> H <sub>5</sub>	III

<sup>a</sup>M = Co(III) (1–10) or Cr(III) (11–20) or Ru(III) (21–30); <sup>b</sup>acac = 2,4-pentanedionato ion; <sup>c</sup>phacphac = 1,3-diphenyl-1,3-propanedionato ion; <sup>d</sup>phacphSac = 3-mercapto-1,3-diphenyl-prop-2-en-1-one ion; <sup>e</sup>phSacphSac = 3-mercapto-1,3-diphenyl-prop-2-en-1-thione ion

The employed approaches were to find quantitative relationships between the intrinsic molecular structure and the physico-chemical properties of the compounds and to establish models that define the effects of molecular structure on the separation mechanisms. The structures of molecules were expressed numerically by quantitative molecular descriptors, which were in agreement with the structure of the compounds, as seen from Table IV.

For all investigated complexes, a correlation check for the descriptors was performed by a correlation matrix for the variables.<sup>17,18</sup> To find if the structural descriptors of the complexes significantly influence their retention parameters, MLR analysis was used. The best model was selected based on the multiple squared correlation coefficients ( $r^2$ ), the mean square error ( $MSE$ ) and the value of the

Fischer significance,  $F$ -value (a statistical parameter for assessing the overall significance). For all mobile phases used, the best fitted correlation equations were obtained with selected molecular descriptors, which included polarizability and the hydrophilic–lipophilic balance. The following equations for one mono- and one two-component mobile phase are given as examples.

Compounds **1–10**:

$$R_M = (0.993 \pm 0.533) - (0.024 \pm 0.002)\alpha + (0.134 \pm 0.125)HLB \quad (1)$$

$$r^2 = 0.951, F = 67.989, MSE = 0.013, n = 10$$

$$R_M = (1.372 \pm 0.313) - (0.030 \pm 0.001)\alpha + (0.141 \pm 0.073)HLB \quad (2)$$

$$r^2 = 0.989, F = 311.278, MSE = 0.005, n = 10$$

TABLE II.  $R_M$  values of the investigated compounds (the compositions of the mobile phases are given in Table III)

Compd.	Mobile phase								
	1	2	3	4	5	6	7	8	9
<b>1</b>	1.279	0.788	0	1.690	1.005	0.410	1.061	1.061	1.005
<b>2</b>	0.954	0.659	-0.140	0.753	0.525	0.269	0.954	0.954	0.659
<b>3</b>	0.525	0.477	-0.176	0.689	0.389	0	0.659	0.630	0.575
<b>4</b>	0.347	0.231	-0.231	0.524	0.327	-0.194	0.454	0.389	0.432
<b>5</b>	0.659	0.052	-0.288	0.431	0.269	-0.140	0.602	0.659	0.140
<b>6</b>	0.250	-0.122	-0.327	0.07	0.176	-0.308	0.308	0.368	-0.070
<b>7</b>	-0.194	-0.176	-0.347	-0.017	0.122	-0.550	0.231	0.213	-0.194
<b>8</b>	0.052	-0.368	-0.327	0.347	0.105	-0.689	0.231	0.308	-0.368
<b>9</b>	-0.308	-0.410	-0.368	-0.158	-0.213	0.753	-0.052	0	-0.575
<b>10</b>	-0.432	-0.501	-0.389	-0.194	-0.269	-0.908	-0.105	-0.052	-0.689
<b>11</b>	1.380	1.005	-0.017	1.996	0.826	0.250	1.195	0.826	0.788
<b>12</b>	0.575	0.720	-0.087	1.061	0.454	0.070	0.602	0.454	0.659
<b>13</b>	0.231	0.550	-0.140	0.602	0.158	-0.017	0.454	0.347	0.501
<b>14</b>	0	0.389	-0.176	0.140	0.105	-0.176	0.347	0.213	0.432
<b>15</b>	-0.140	0	-0.176	0.308	0.213	-0.250	0.213	0.176	0.140
<b>16</b>	-0.250	-0.231	-0.213	-0.070	-0.158	-0.327	0.176	0.070	-0.194
<b>17</b>	-0.432	-0.368	-0.250	-0.194	-0.327	-0.410	0.105	-0.017	-0.389
<b>18</b>	-0.308	-0.454	-0.250	-0.035	0.052	-0.720	0.070	0.017	-0.368
<b>19</b>	-0.454	-0.501	-0.269	-0.194	-0.432	-0.788	-0.105	-0.017	-0.501
<b>20</b>	-0.602	-0.602	-0.308	-0.432	-0.753	-0.865	-0.231	-0.140	-0.689
<b>21</b>	1.996	1.279	0.070	1.690	1.005	0.368	1.279	0.908	0.954
<b>22</b>	1.279	0.659	-0.158	1.005	0.410	0.035	0.954	0.788	0.525
<b>23</b>	0.550	0.431	-0.176	0.389	0.347	-0.158	0.659	0.659	0.410
<b>24</b>	0.368	0.231	-0.194	0.070	0.105	-0.432	0.454	0.477	0.250
<b>25</b>	0.550	-0.070	-0.194	0.213	0.231	-0.327	0.659	0.525	0.052
<b>26</b>	0.269	-0.194	-0.213	-0.140	0.105	-0.410	0.213	0.432	-0.052
<b>27</b>	-0.176	-0.454	-0.250	-0.327	-0.347	-0.865	0.070	0.250	-0.368
<b>28</b>	-0.194	-0.410	-0.231	-0.194	0.052	-0.659	0.087	0.035	-0.368
<b>29</b>	-0.432	-0.550	-0.250	-0.525	-0.288	-0.865	-0.140	-0.035	-0.550
<b>30</b>	-0.788	-0.575	-0.288	-0.826	1.195	-1.061	-0.308	-0.231	-0.659



TABLE III. Mobile phases used

No.	Composition	Proportions (v/v)
1	Toluene	–
2	Dichloromethane	–
3	Chloroform	–
4	Xylene	–
5	1,2,3,4-tetrahydronaphthalene	–
6	<i>n</i> -Butyl acetate–carbon tetrachloride	40:60
7	Chloroform–carbon tetrachloride	50:50
8	Chloroform–carbon tetrachloride	30:70
9	Dichloromethane–carbon tetrachloride	80:20

Compounds **11–20**:

$$R_M = (1.097 \pm 0.699) - (0.029 \pm 0.003)\alpha + (0.175 \pm 0.148)HLB \quad (3)$$

$$r^2 = 0.953, F = 70.687, MSE = 0.020, n = 10$$

$$R_M = (0.836 \pm 0.717) - (0.027 \pm 0.003)\alpha + (0.196 \pm 0.151)HLB \quad (4)$$

$$r^2 = 0.942, F = 57.160, MSE = 0.021, n = 10$$

Compounds **21–30**:

$$R_M = (0.620 \pm 1.037) - (0.030 \pm 0.004)\alpha + (0.322 \pm 0.246)HLB \quad (5)$$

$$r^2 = 0.924, F = 42.467, MSE = 0.036, n = 10$$

$$R_M = (0.435 \pm 0.474) - (0.027 \pm 0.002)\alpha + (0.300 \pm 0.112)HLB \quad (6)$$

$$r^2 = 0.978, F = 158.351, MSE = 0.007, n = 10$$

Equations (1), (3) and (5) present the QSRR models for dichloromethane and Eqs. (2), (4) and (6) for dichloromethane–carbon tetrachloride as mobile phases.

By interpreting the descriptors in the regression models, it is possible to gain some insight into factors affecting the affinity of the investigated compounds for the stationary phase. It is known that, under the conditions of adsorption chromatography on silica gel, hydrogen bonds formed with the silanol groups of the sorbent, dipole–dipole and other electrostatic interactions determine the retention of the analysed compounds.<sup>19</sup>

Polarizability as a quantum-chemical descriptor of a molecule depends on the symmetry of the various covalent bonds in the molecule.<sup>20</sup> Highly polarisable compounds are expected to have strong attractions with the sorbent, resulting in shorter migration distance as seen from Tables II and IV. The repulsive steric interactions between the surface of silica gel and the phenyl rings of the complexes are reflected by the *HLB* descriptor on the QSRR models. A molecule with a high *HLB* has a high ratio of hydrophilic groups to lipophilic groups and *vice versa*. The *HLB* values are determined by calculating the values for different regions of a molecule.<sup>21</sup> The proposed nonlinear QSRR models exhibit a high degree of correlation between the experimental and predicted retention factors. The obtained statistical results are presented in Table V.

TABLE IV. The calculated molecular descriptors

Compd.	$MW^a$	$MV^b$ Å <sup>3</sup>	$SA^c$ Å <sup>2</sup>	$HLB^d$	$PHSA^e$	$\mu^f$ D	$\alpha^g$ Å <sup>3</sup>	$R^h$ Å <sup>3</sup>	$E_{HOMO}^i$ eV	$E_{LUMO}^j$ eV
<b>1</b>	356.26	173.62	23.94	4.066	24.02	0.384	28.60	81.99	-6.870	5.110
<b>2</b>	480.40	239.36	30.43	3.931	23.44	0.724	44.25	122.13	-6.738	4.885
<b>3</b>	480.40	239.81	30.49	3.961	23.57	5.119	46.62	128.57	-6.587	4.401
<b>4</b>	513.54	252.28	31.98	3.613	22.06	2.522	46.62	135.01	-6.506	3.826
<b>5</b>	604.54	304.87	36.83	3.824	22.97	0.317	59.90	162.26	-6.727	4.925
<b>6</b>	636.68	317.50	38.36	4.170	24.48	5.621	64.63	175.14	-6.251	3.616
<b>7</b>	670.83	332.61	40.46	3.470	21.44	4.168	64.63	188.03	-5.791	1.474
<b>8</b>	728.69	370.07	43.26	3.742	22.62	1.195	75.55	202.39	-6.705	4.797
<b>9</b>	776.89	389.80	45.63	4.216	24.68	5.628	82.64	221.72	-5.650	1.223
<b>10</b>	828.11	411.52	48.34	3.204	20.28	9.492	82.64	241.05	-6.170	1.990
<b>11</b>	349.32	175.94	24.45	4.409	25.52	0.356	28.60	81.99	-2.213	5.854
<b>12</b>	473.47	241.39	30.86	4.175	24.50	1.596	44.25	122.13	-2.222	4.866
<b>13</b>	489.54	247.40	31.61	4.389	25.43	5.480	46.62	128.57	-2.347	4.540
<b>14</b>	506.61	254.53	32.49	3.875	23.19	3.932	46.62	135.01	-2.267	3.554
<b>15</b>	597.61	306.72	37.27	4.015	23.81	0.949	59.90	162.26	-2.234	4.937
<b>16</b>	629.74	318.70	38.73	4.364	25.32	5.858	64.63	175.14	-2.387	4.470
<b>17</b>	663.89	333.13	40.56	3.563	21.84	5.706	64.63	188.03	-2.184	3.441
<b>18</b>	721.75	372.10	43.67	3.903	23.32	1.030	75.55	202.39	-2.152	4.976
<b>19</b>	769.95	389.93	45.81	4.330	25.17	6.935	82.64	221.72	-2.046	4.412
<b>20</b>	821.17	412.91	48.85	3.380	21.04	8.302	82.64	241.05	-2.935	2.790
<b>21</b>	398.40	174.38	23.90	4.045	23.94	0.865	28.60	81.99	-0.926	6.487
<b>22</b>	522.54	239.54	30.27	3.851	23.09	1.618	44.25	122.13	-0.912	4.915
<b>23</b>	538.61	245.69	31.00	4.080	24.09	6.081	46.62	158.57	-1.057	4.516
<b>24</b>	555.68	251.55	31.88	3.690	22.39	3.348	46.62	135.01	-1.099	3.710
<b>25</b>	646.68	305.12	36.71	3.759	22.69	2.037	59.90	162.26	-0.863	4.869
<b>26</b>	678.81	317.12	38.13	4.087	24.12	6.916	64.63	175.14	-1.308	4.334
<b>27</b>	712.96	329.56	39.96	3.438	21.29	2.604	64.63	188.03	-1.272	3.697
<b>28</b>	770.82	370.70	43.15	3.693	22.40	2.469	75.55	202.39	-0.809	4.809
<b>29</b>	819.02	388.77	45.29	4.122	24.27	8.280	82.64	221.72	-1.476	4.119
<b>30</b>	870.25	411.94	48.69	3.360	20.96	10.770	82.64	241.05	-1.755	2.580

<sup>a</sup>Molecular weight; <sup>b</sup>molecular volume; <sup>c</sup>surface area; <sup>d</sup>hydrophilic-lipophilic balance; <sup>e</sup>percent hydrophilic surface area; <sup>f</sup>dipole moment (1 D = 3.336×10<sup>-30</sup> C m); <sup>g</sup>polarizability; <sup>h</sup>refractivity; <sup>i</sup>energy of the highest occupied molecular orbital; <sup>j</sup>energy of the lowest unoccupied molecular orbital

TABLE V. Statistical results obtained

Compd.	Mobile phase	Intercept	Slope	$r^2$	$F$	$MSE$
<b>1-10</b>	2	0.003 (±0.034)	0.951 (±0.076)	0.951	155.732	0.011
	9	0.001 (±0.020)	0.989 (±0.037)	0.989	709.096	0.004
<b>11-20</b>	2	0.002 (±0.041)	0.953 (±0.075)	0.953	161.270	0.017
	9	0.002 (±0.042)	0.942 (±0.082)	0.942	130.611	0.017
<b>21-30</b>	2	0.003 (±0.054)	0.924 (±0.094)	0.924	96.926	0.029
	9	0.0005 (±0.025)	0.978 (±0.051)	0.978	362.727	0.006

The relationships between the experimental and predicted  $R_M$  values together with their residuals (difference between predicted and experimental value), for the Cr(III) complexes are shown in Fig. 1 as an example.

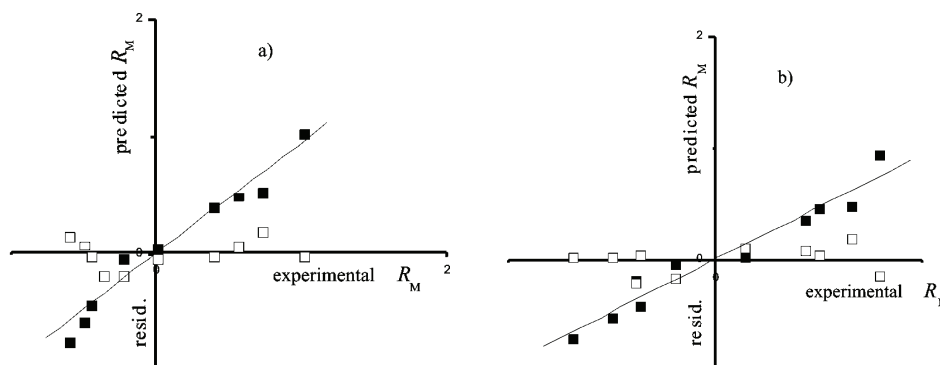


Fig. 1. Relationship between the experimental and predicted  $R_M$  values together with their residuals, for Cr(III) complexes; a) dichloromethane, b) dichloromethane-carbon tetrachloride.

The distribution of the residuals on both sides of the zero line indicates that there is no systematic error in the obtained models. Fig.1 reflects the actual predictive power of the established models.

Analysis of these results indicates that the proposed models can correctly represent the relationship between the retention parameters of the investigated compounds on silica gel and the molecular descriptors calculated solely from molecular structure. These models are suitable for prediction of the retention of structurally similar compounds under the same chromatographic conditions.

Finally, the obtained models were compared with those established on polyacrylonitrile sorbent.<sup>15</sup> In the established QSRR models for these sorbents, the retention behaviours are described by different molecular descriptors. This comparison showed that different aspects of the molecular structure are responsible for the separation of the analytes. This is a quantitative confirmation of the previously established separation mechanisms of the investigated compounds on silica gel<sup>14</sup> and polyacrylonitrile.<sup>22</sup> Hence, it is clear that differences in the structure of the sorbent determine the chromatographic behaviour of analytes, *e.g.*, the type of the sorbent-molecule interactions. In addition, these QSRR models can be used for selection of the corresponding chromatographic system for separation of structurally similar compounds.

#### CONCLUSIONS

A QSRR study of a series of mixed  $\beta$ -diketonato complexes of Co(III), Cr(III) and Ru(III) on a thin layer of silica gel has been presented. The established two-parameter models show satisfactory correlation and predictive po-

wer. The main factors influencing retention on silica gel for all employed mobile phases are polarizability and the hydrophilic–lipophilic balance. The QSRR models quantitatively describe the retention of analytes, based on their molecular descriptors, which reflect structural differences between the compounds. A good correlation between the experimental and predicted retention parameters was observed when polarizability and *HLB* were used as the molecular descriptors. The correlations obtained between the retention and the molecular descriptors were highly significant and might be used to predict the retention behaviour of structurally similar compounds with a considerable degree of confidence when the molecules are new or when the experimental determination is rather difficult or subject to large uncertainties. This study gives a quantitative assessment of the relative importance of specific interactions.

*Acknowledgements.* This study was supported by Grant No. 142062 from the Ministry of Science and Technological Development of the Republic of Serbia.

## ИЗВОД

ПРЕДВИЂАЊЕ РЕТЕНЦИЈЕ  $\beta$ -ДИКЕТОНАТО КОМПЛЕКСА У TLC СИСТЕМИМА  
НА СИЛИКА-ГЕЛУ ПРИМЕНОМ КВАНТИТАТИВНОГ ОДНОСА  
СТРУКТУРЕ И РЕТЕНЦИЈЕ

РАДА М. БАОШИЋ, АНА Д. РАДОЈЕВИЋ И ЖИВОСЛАВ Љ. ТЕШИЋ

*Хемијски факултет, Универзитет у Београду, Студентски тирг 12, б.бр. 158, 11000 Београд*

У овом раду квантификован је однос структуре и ретенције 30 мешовитих  $\beta$ -дикетонато комплекса кобалта(III), хрома(III) и рутенијума(III) применом мултилинеарне регресионе анализе коришћењем молекулских дескриптора, који су добијени помоћу квантно-хемијских израчунавања. Ретенциони параметри су добијени танкослојном хроматографијом на силика-гелу применом моно- и двокомпонентних растварача. Молекулски дескриптори који су укључени у мултилинеарну регресиону анализу су молекулска тежина, молекулска запремина, површина, хидрофилни–липофилни баланс, проценат хидрофилне површине, диполни моменат, поларизабилност, рефрактивност, енергија највише заузете молекулске орбитале и енергија најниже празне молекулске орбитале. Добијена је задовољавајућа корелација између експерименталних ретенционих параметара и ретенционих параметара предвиђених постављеним моделима, који садрже поларизабилност и хидрофилни–липофилни баланс као дескрипторе. Поређења ових модела са моделима добијеним на полиакрилонитрилном сорбенту, за иста једињења, показују да је структура сорбента одговорна за хроматографско понашање. Ови модели се могу користити за предвиђање ретенције нових једињења у датим хроматографским системима.

(Примљено 25. фебруара, ревидирано 9. децембра 2009)

## REFERENCES

1. K. Heberger, *J. Chromatogr. A* **1158** (2007) 273
2. L. Komsta, *Anal. Chim. Acta* **629** (2008) 66
3. S. Sremac, B. Škrbić, A. Onjia, *J. Serb. Chem. Soc.* **70** (2005) 1291
4. H. Y. Xu, J. W. Zou, Y. J. Jiang, G. X. Hu, Q. S. Yu, *J. Chromatogr. A* **1198** (2008) 202

5. R. Put, Q. S. Xu, D. L. Massart, Y. V. Heyden, *J. Chromatogr. A* **1057** (2004) 11
6. R. Put, C. Perrin, F. Questier, D. Coomans, D. L. Massart, Y. V. Heyden, *J. Chromatogr. A* **988** (2003) 261
7. R. Siavash, R. G. Mohammad, P. Estam, N. Paviz, *Chromatographia* **67** (2008) 1612
8. C. Sarbu, D. Casoni, M. Darabantu, C. Maioreanu, *J. Pharm. Biomed. Anal.* **35** (2004) 213
9. M. Ačanski, *J. Serb. Chem. Soc* **68** (2003) 163
10. T. Lockyer, R. L. Martin, in *Progress in Inorganic Chemistry*, S. J. Lippard, Ed., Wiley, New York, 1980, p. 223
11. J. Leipoldt, S. Basson, G. Vanzyl, G. Steyn, *J. Organomet. Chem.* **418** (1991) 241
12. C. Glidewell, C. Zakaria, *Acta Crystallogr. C* **50** (1994) 1673
13. P. Viswanathamurthi, K. Natarajan, *Transition Met. Chem.* **25** (2000) 311
14. R. Baošić, D. Milojković-Opsenica, Ž. Tešić, *J. Planar Chromatogr.* **17** (2004) 250
15. R. Baošić, A. Radojević, Ž. Tešić, *Chromatographia* **68** (2008) 797
16. J. Ghasemi, S. Saaidpour, *Anal. Chim. Acta* **604** (2007) 99
17. W. Ma, F. Luan, H. Zhang, X. Zhang, M. Liu, Z. Hu, B. Fan, *J. Chromatogr. A* **1113** (2006) 140
18. B. Xia, W. Ma, B. Zheng, X. Zhang, B. Fan, *Eur. J. Med. Chem.* **43** (2008) 1489
19. M. Aleksić, D. Agbaba, R. Baošić, D. Milojković-Opsenica, Ž. Tešić, *J. Serb. Chem. Soc.* **66** (2001) 39
20. T. Körtvélyesi, M. Görgényi, K. Héberger, *Anal. Chim. Acta* **428** (2001) 73
21. E. A. Tehrani, F. Fournier, S. Desobry, *J. Food Eng.* **77** (2006) 135
22. Ž. Tešić, R. Baošić, D. Milojković-Opsenica, *J. Chromatogr. A* **847** (1999) 303.





*J. Serb. Chem. Soc.* 75 (4) 523–535 (2010)  
JSCS–3985

## Fluidized bed combustion of pesticide-manufacture liquid wastes

ZORANA ARSENIJEVIĆ<sup>1\*</sup>, ŽELJKO GRBAVČIĆ<sup>2</sup>, BOŠKO GRBIĆ<sup>1</sup>,  
NENAD RADIĆ<sup>1</sup>, RADMILA GARIĆ-GRULOVIC<sup>1</sup>, SAŠA MILETIĆ<sup>3</sup>,  
GORDAN SAVČIĆ<sup>3</sup> and BOJANA ĐORĐEVIĆ<sup>3</sup>

<sup>1</sup>*Institute of Chemistry, Technology and Metallurgy – Department of Catalysis and Chemical Engineering, University of Belgrade, Njegoševa 12, Belgrade,* <sup>2</sup>*Faculty of Technology and Metallurgy, University of Belgrade, Karnegijeva 4, Belgrade and* <sup>3</sup>*Galenika – Fitofarmacija A.D., Batajnički drum bb, Belgrade, Serbia*

(Received 20 August, revised 4 November 2009)

**Abstract:** Industrial liquid wastes can be in the form of solutions, suspensions, sludges, scums or waste oil and have organic properties. The objective of this work was to demonstrate the technical feasibility of a fluidized bed as a clean technology for burning liquid waste from a pesticide production plant. The combustion of liquid waste mixtures, obtained from realistic samples, was investigated in a pilot scale fluidized bed with quartz sand particles of 0.63–1.25 mm in diameter and 2610 kg/m<sup>3</sup> in density at 800–950 °C. To ensure complete combustion of liquid waste and additional fuel, the combustion chamber was supplied with excess air and the  $U/U_{mF}$  (at ambient temperature) was in between 1.1 and 2.3. In the fluidized bed chamber, liquid waste, additional liquid fuel and air can be brought into intense contact sufficient to permit combustion in bed without backfire problems. The experimental results show that the fluidized bed furnace offers excellent thermal uniformity and temperature control. The results of the combustion tests showed that degradation of liquid wastes can be successfully realized in a fluidized bed with no harmful gaseous emissions by ensuring that the temperatures of both the bed and the freeboard are not lower than 900 °C.

**Keywords:** fluidized bed incinerator; liquid waste; pesticide production plant; design; operating experience.

### INTRODUCTION

Pesticide manufacture, formulation, and packaging facilities produce significant amounts of hazardous materials, including raw materials and intermediate/final products. The handling, storage, and transportation of these materials should be managed properly to avoid or minimize their environmental and health im-

\* Corresponding author. E-mail: zorana@tmf.bg.ac.rs  
doi: 10.2298/JSC090820024A

pacts.<sup>1</sup> Unused dilute pesticide formulations and equipment rinse water contain high levels of pesticides that can lead to contamination of soil and eventually of water resources if not properly managed.<sup>2</sup>

The accumulation and bad management of various pesticides and other hazardous chemicals constitute a threat for health and the environment, locally, regionally and globally. Estimates indicate that large amounts of obsolete pesticides are accumulated globally, especially in developing countries. A considerable amount of the accumulated obsolete pesticides are persistent organic pollutants that possess toxic properties, resist degradation, bio-accumulate and are transported, through air, water and migratory species, across international boundaries and deposited far from their place of origin, where they accumulate in terrestrial and aquatic ecosystems. Organochlorine pesticide residues have been detected in air, water, soil, sediments, fish and birds even more than one decade after being banned and it is reasonable to believe that contaminated sites and mixed waste still represent locally and regionally important on-going primary source inputs of hazardous compounds to the global environment.

Several international environmental conventions aim to protect human health and the environment through measures that will destroy and irreversible transform hazardous chemicals and reduce and/or eliminate emissions and discharges of pesticides and persistent organic pollutants. The hazardous waste has mainly been transported to developed countries for high-temperature incineration in dedicated facilities, a practice that does not stimulate development of local solutions and capacity building. In addition, this approach involves higher costs and increased risks of accidents and spills. These international conventions acknowledge that there is an urgent need for environmentally sound disposal of hazardous chemicals and that developing countries and countries with economies in transition need to strengthen their national capabilities for chemical management, *i.e.*, of special relevance is the stimulation and development of local treatment of hazardous wastes.<sup>3,4</sup>

The pesticide manufacturing industry started already in the 1970s to explore possible treatment options for obsolete pesticides and pesticide wastes and combustion was soon considered as the prominent method. In order to treat these wastes, destruction in high temperature incinerators was established by Environmental Protection Agency (EPA), after extensive expert and public reviews, to be the best-demonstrated available technology for most organic hazardous wastes. This is because incineration safely and effectively destroys the hazardous constituents in the waste.<sup>5</sup>

To achieve complete thermal destruction, a sufficiently high temperature, oxygen supply, residence time and mixing conditions are required. The combustion temperature and residence time needed for mixed hazardous wastes cannot be readily calculated and are often determined empirically. Some common sol-



vents, such as alcohols and toluene, can be easily combusted at lower temperatures, while other more complex organic halogens require more stringent conditions, such as incineration criteria of 2 s residence time at 1200 °C and 3 % excess oxygen in the stack gas,<sup>6</sup> or incineration of waste criteria of 1100 °C for at least 2 s if more than 1 % of halogenated organic substances are to be incinerated.<sup>4,7</sup>

The main advantages of the incineration of industrial hazardous wastes are the following: 1) the marked reduction of the organic part of the wastes by oxidation reactions with the oxygen in the air supplied, 2) the complete elimination of the hazardous properties in the wastes and 3) recovery of the heat released by the incineration of the waste.

Many different types of incinerators have been tested. Among them, suitable equipment for the thermal treatment of industrial hazardous wastes is the fluidized bed type of incinerator. A fluidized bed incinerator provides all the advantageous characteristics of gas–solid fluidization technologies. First, the particle sizes in industrial liquid wastes (suspension, sludge, *etc.*) are usually small and uniform; therefore, they have relatively large contact areas with the oxygen in the air for carbon oxidation to be realized. Second, the waste particles are suspended by means of the fluidizing air; therefore, further contact between the waste particles and the fluidizing air is obtained. Third, the fluidization promotes the mixing of the waste and the bed of sand particles; consequently, a uniform combustion temperature is achieved in the fluidized bed.

Other significant advantages of fluidized bed combustors over conventional combustors include their compact furnace, simple design, and effective burning of a wide variety of wastes and fuels. Fluidized bed combustors can be designed to combust almost any solid, semi-solid or liquid fuel without the use of supplement fuel, as long as the heating value is sufficient to heat the fuel, drive off the moisture and preheat the combustion air.<sup>8</sup>

The objective of this work was to demonstrate the technical feasibility of a fluidized bed as a clean technology for the burning of a liquid waste from pesticide manufacturing process. Sunflower oil was used as an additional fuel for the combustion of high moisture liquid wastes. The combustion efficiency and the flue gas composition were investigated using a pilot scale unit.

This paper provides an overview of the thermal decomposition of a pesticide manufacturing liquid waste in a fluidized bed incinerator.

#### EXPERIMENTAL

The technological scheme of the pilot scale unit for liquid waste combustion is given in Fig. 1.

The main part of the pilot unit is the fluidization column of 124 mm in diameter in the lower part and 150 mm in diameter in the upper part, with overall column height of 1800 mm. The atmospheric pressure fluidized bed incinerator was made of stainless steel. The air dis-

tributor plate was placed at the column bottom (1a). The column was filled with quartz sand, size fraction 0.63–1.25 mm and density 2610 kg/m<sup>3</sup> (1b). The static height of sand bed was 200 mm. This unit was designed to operate at temperatures up to 950 °C with a fluidizing air velocity of 0.5–2 m/s at ambient temperature. Liquid waste was fed onto the bed surface from a sealed reservoir (9) and the flow rate was controlled by a peristaltic pump (10). The supplement liquid fuel (sunflower oil) was fed onto the bed surface from a reservoir (6) using a pump (7) and twin fluid nozzle-gas/liquid ejector (8), located 80 mm from the column bottom. The residence time in the fluidized bed incinerator varied between 0.6 and 0.8 s.

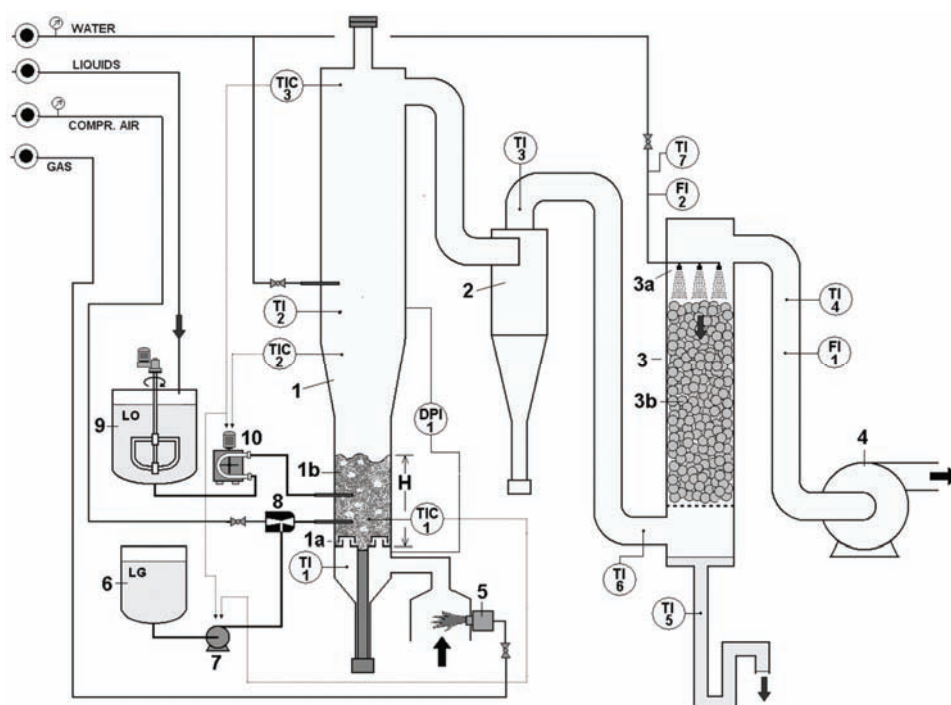


Fig. 1. Technological scheme of the pilot scale unit for liquid waste combustion in a fluidized sand bed (1-fluidized column, 1a-air distributor, 1b-sand, 2-cyclone, 3-scrubber, 3a-water nozzles, 3b-packing, 4-blower, 5-gas burner, 6-additional liquid fuel reservoir (LG), 7-pump for additional liquid fuel, 8-twin fluid nozzle-gas/liquid ejector, 9-liquid waste reservoir (LO), 10-pump for liquid waste, H-bed height, TIC1–TIC3-temperature indication and control, TI1–TI7-temperature indication, FI1-air flowrate indicator, FI2-water flowrate indicator, DPI1-indication of the differential pressure difference in the fluidized column).

Three tubes with manholes, covered with hardened quartz glass, placed above the dynamic sand bed height (2 manholes) and at the top of the fluidized bed chamber (1 manhole), enabled visual observations during the combustion experiments.

The other constitutional parts of the pilot unit were a cyclone (2) of 100 mm in diameter and scrubber (3) of 124 mm in diameter and 800 mm in height. Aluminum Rashig rings (3b) with dimensions 20×20 mm were employed in the scrubber. An air blower (4) was placed at

the end of the process line, in such way the pilot unit operated under vacuum with respect to the atmospheric pressure.

In order to limit heat losses, all constitutional parts of the pilot unit as well as the pipe lines were thermally isolated with mineral wool of thickness 50 to 100 mm.

The bed temperature, freeboard temperature and other characteristic temperatures were measured by means of sheathed Ni/Cr–Ni thermocouples. Combustion gas samples were obtained from a sampling port located at the scrubber exit. Only the VOCs and NO<sub>x</sub> concentrations were measured, while measurements of the CO concentrations were neglected due to the sufficiently high process temperatures and high oxygen concentration. The concentration of the total hydrocarbons at the outlet of the system was measured by an on-line gas chromatograph (Perkin–Elmer 3920B) equipped with a flame ionization detector (FID). The concentration of nitrogen oxides (NO<sub>x</sub>) was analyzed by a NO–NO<sub>2</sub>–NO<sub>x</sub> analyzer (Thermo Electron Model 44). The air and gas flow rates were measured by calibrated rotameters.

*Process control.* After startup of the pilot unit, the gas burner (5) was turned on. The fuel used for heating the fluidizing air was a commercial propane–butane mixture (50–50 %), supplied in pressurized bottles with a nominal heat capacity of 45.8 MJ/kg.<sup>9,10</sup> When the temperature in the middle of the bed (TIC1) reached the value of 600 °C, the additional liquid fuel pump was turned on and the feeding process begun by the twin fluid nozzle (8). The additional fuel was sunflower oil with a nominal heat capacity of 39.6 MJ/kg.<sup>11</sup> The temperature controllers TIC1 and TIC3 controlled the feeding pump for additional liquid fuel in such manner that the pump operated in the on/off mode, *i.e.*, the pump was turned on if the temperature in the middle of the bed (TIC1) was below 880 °C and if the temperature at the top of the fluidization column (TIC3) was below 950 °C. The temperature controllers TIC2 and TIC3 controlled the feeding pump for liquid waste (10) in such manner that the pump operated in the on/off mode, *i.e.*, the pump was turned on if the temperature above the fluidized bed (TIC2) was 800 °C at least and the pump was turned off if the temperature at the top of the fluidization column (TIC3) exceeded 950 °C. After the stationary state was attained, the pilot unit operation was fully automatic.

The flue gases were exhausted at the top of the fluidized bed chamber, and were passed to a cyclone, to capture any elutriated particles of the bed material. The effluent gases from the cyclone were passed through the scrubber to cool out and to eliminate the finest particles and odors. In all runs, the cooling water flowrate in the scrubber was 2.8 L/min. The cooling water flowrate was chosen in order to keep the outlet cooled air temperature (TI4) below 65 °C and the wastewater temperature (TI5) below 75 °C. In all runs, the air flow rate in the stationary state (calculated for 20 °C) was between 35 and 40 m<sup>3</sup>/h.

The employed bed material was quartz sand. The main characteristics of the bed are presented in Table I.

TABLE I. Characteristics of the bed material

Quartz sand, granulation $d_p$	0.63–1.25 mm
Mean particle diameter, $d_{p-avg}$	0.94 mm
Sand density, $\rho_s$	2610.00 kg/m <sup>3</sup>
Sand bulk density, $\rho_{s-bulk}$	1488.00 kg/m <sup>3</sup>
Sand bed height (static), $H_s$	0.20 m
Superficial air velocity at minimum fluidization (at 20 °C), $U_{mf}$	0.64 m/s
Superficial terminal air velocity (at 20 °C), $U_t$	7.93 m/s
Mass of the sand, $M_s$	3.59 kg

Six realistic samples, *i.e.*, different rinsates from a pesticide production plant, the specifications of which are given in Table II, as well as three different mixtures, *i.e.*, mixture 1 (samples 1, 2 and 5 in volume proportions 1:1:1), mixture 2 (samples 3, 4 and 6 in volume proportions 1:1:1), mixture 3 (samples 1, 2 and 6 in volume proportions 1:1:1), were used in combustion experiments.

TABLE II. Rinsates after different products from the pesticide production plant

Sample	Product type	Active matter	Washing fluid
1	Herbicide	Atrazine	Water
2	Herbicide	Paraquat	Water
3	Herbicide	2,4-D	Water
4	Fungicide	Carbendazim	Water
5	Herbicide	Acetochlore	Water
6	Fungicide	Tebuconazol (carrier: sunflower oil, colored with Basonyl Red)	Water

## RESULTS AND DISCUSSION

Wastewater from pesticide formulation and packaging operations typically has low levels of organics and the pH is generally neutral. The level of toxicity and biodegradability depends on the presence of chemicals such as pesticide residues, organic solvents and other auxiliary substances that may be toxic to aquatic organisms.

The main aim of these experimental investigations was to determine the operating regimes that enable satisfactory combustion of the propane–butane mixture (50–50 %), additional oil and liquid waste, the oxidation of combustibles in the fluidized bed incinerator to be as high as possible and, at the same time, to avoid fouling of the incinerator walls, and sintering and agglomeration of the bed material.

All available data supplied by the pesticide production company indicated to variability in the quality and quantities of wastewaters and other liquid wastes to be treated. Therefore, the identification of a profound solution that would not be sensitive to these factors was important.

Supplementary fuel consumption, air flow and specific solution consumption for the three chosen representative test runs are given in Table III.

TABLE III. Flow rates of liquid waste, supplementary fuels (propane–butane mixture 50–50 %, sunflower oil) and air

Run	Propane–butane $Q_{\text{gas}} / \text{kg h}^{-1}$	Sunflower oil $Q_{\text{LG}} / \text{L h}^{-1}$	Liquid waste $Q_{\text{LO}} / \text{L h}^{-1}$	$G_{\text{air}} / \text{kg h}^{-1}$	Liquid waste mixture
1	0.728	0.971	2.442	70.0	1: Samples 1,2,5 (1:1:1)
2	0.728	0.611	2.532	74.6	2: Samples 3,4,6 (1:1:1)
3	0.760	0.291	2.536	75.0	3: Samples 1,2,6 (1:1:1)

The samples 1 to 6, according to the specification given in Table II, were investigated. In addition, mixtures of these samples were also investigated, *i.e.*, mixture 1 (samples 1, 2 and 5 in volume proportions 1:1:1), mixture 2 (samples 3, 4 and 6 in volume proportions 1:1:1) and mixture 3 (samples 1, 2 and 6 in volume proportions 1:1:1). The duration of each run was up to 3 h. All information about the liquid waste composition is the property of the factory for pesticide manufacture and, therefore, these data are not presented.

During system heat up, with air in excess, the combustion was least efficient at the lowest temperatures, with relatively high total hydrocarbons concentrations. As the bed heated up, the total concentration of hydrocarbons dropped rapidly to below the limit of detection (below 1 ppm). In an idealized combustion process, all chemical and thermal steps have to occur in the bubbling bed only. According to the fluidized bed geometry and operational conditions, it is possible that a fluidized bed exhibits a slugging behavior. It was visually observed that the fluidized bed showed uniform bubbling behavior after attaining steady-state conditions. Micro-explosions were noted during the experiments over a wide temperature range (up to 800 °C); they were associated with acoustic effects, detectable by the ear, and oscillations of the temperature. The light released during the explosions was clearly visible from the top of the column as flashes. It was not possible to distinguish clearly if the micro-explosions occurred within the bed or in the freeboard. Therefore, there is possibility that the most of the burn off occurred above the bed.

When hazardous wastes with high moisture contents are added into the incinerator, the moisture evaporates instantaneously due to the amount of heat stored in the bed sand without any change of the combustion temperature. Once the moisture evaporation of the wastes is complete, then combustion follows. The sand bed will absorb the heat released during the combustion. This type of heat recirculation in the fluidized bed maintains a uniform total heat content.<sup>13</sup>

A typical diagram of the temperature variations as a function of time during combustion tests in the pilot scale unit is given in Fig. 2.

The test mixture 2 (samples 3, 4 and 6 in the volume proportions 1:1:1) contained component 6, containing a high percent of mineral oil with a high combustion capacity. It can be seen from Fig. 3 that the consumption of auxiliary liquid fuel required to maintain the desired temperature values in the bed was lower in comparison with the combustion of mixture 1. After steady operation was attained, the feeding of the propane-butane mixture 50–50 % was stopped, which was followed with a sudden T11 temperature drop. It can be seen from Fig. 3 that the heating value of mixture 2 was sufficient to maintain combustion at the desired temperatures in the fluidized bed chamber. There was no significant temperatures drop due to released heat from combustion of mixture 2 after 170 min. In the runs

with the liquid waste with a high energy potential (*i.e.*, sample 6), the additional liquid fuel consumption was very low.

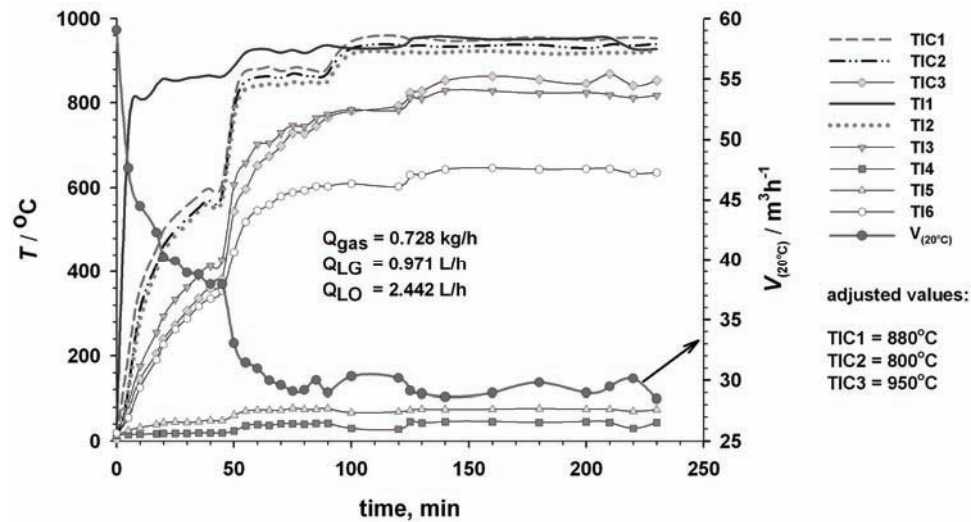


Fig. 2. Typical temperature profiles and exit air volumetric flowrate ( $V_{(20^{\circ}\text{C})}$ ) in the pilot fluidized bed incinerator under turbulent bed conditions (Run 1).

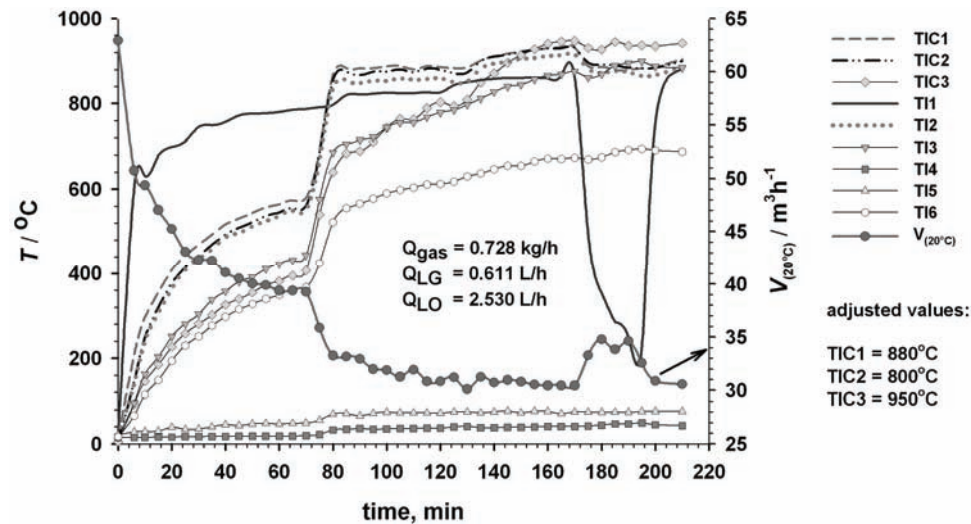


Fig. 3. Temperature profiles and exit air volumetric flowrate ( $V_{(20^{\circ}\text{C})}$ ) in the pilot fluidized bed incinerator under turbulent bed conditions (Run 2).

The hot fluidizing air flows into the fluid bed zone of the incinerator and fluidizes the inert bed of sand. The turbulence of the fluid bed zone serves to disperse the liquid waste and additional liquid fuel. The large surface area of the

fluidized sand particles results in the efficient heat transfer from the fluidizing air to the sand and from the sand to the feeds.

Primary combustion occurs in the bed zone. The freeboard height (above the fluidized sand bed) is an important factor, since volatiles released from the bed will continue burning in the freeboard region. The proper choice of the freeboard height provides the necessary residence time. The residence time in the pilot scale unit was about 0.6 to 0.8 s, which is well below the recommended value for a combustion system, *i.e.*, 2 s at 1100 °C.<sup>2,7</sup>

When the temperature at the top of the column (TIC3) was above 900 °C, the overall hydrocarbons concentration (expressed as xylene concentration) at the system outlet was below the detection limits of the gas chromatograph, as illustrated in Fig. 4, while the NO<sub>x</sub> concentrations were low (< 25 ppm). NO<sub>x</sub> can be formed by two paths, from the combustion of nitrogen containing compounds from the liquid waste and as consequence of elevated temperatures. Under the proper temperature profile along the fluidized bed incinerator (TIC3 > 900 °C), despite the short residence time, the detected levels of hydrocarbons and NO<sub>x</sub> in effluent gasses indicated that the combustion efficiency was very high.

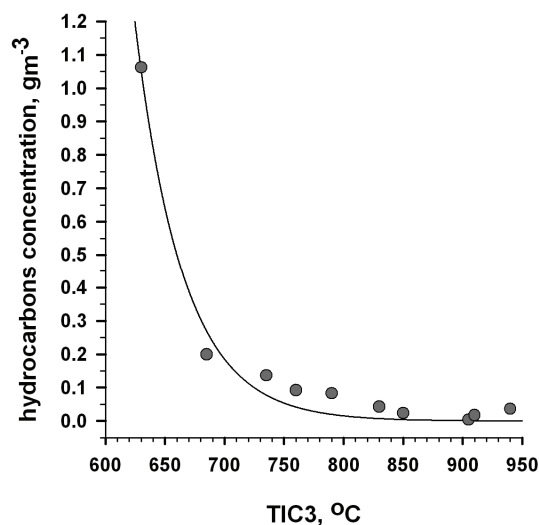


Fig. 4. Gas chromatography analysis of the outlet gases from the fluidized bed incinerator (Run 3).

It should be emphasized that in the runs in which the freeboard temperature was below 900 °C, only partial combustion of the supplementary fuel and organic compounds in the waste solution occurred. This resulted, to some extent, in fouling of the walls above the bed of the fluidized bed incinerator and the appearance of soot in the exit gases and in the exit scrubber water. The lower freeboard temperatures resulted in higher emissions in the flue gasses.

In fluidized bed incinerators, incomplete combustion, *i.e.*, generation of CO, can be caused by “bad-burning” (the combustion conditions are deteriorated, *i.e.*, the combustion is frozen because of a temperature drop despite an abundant air supply) or “over-burning” (combustion becomes excessive relative to the air supply, *i.e.*, the liquid mixture is not homogeneous and clusters of high fuel concentration gas appear in the freeboard).<sup>12</sup> Hence, it is necessary to ensure stable combustion by preventing over-combustion or bad combustion. However, even if operations are performed under stable conditions, changes in emissions concentrations in the output gases could occur due to changes in the quality of the liquid waste and other factors.

In several runs, the “over-burning” phenomenon occurred, *i.e.*, an open flame above the sand bed was visually observed. This was confirmed by fluctuating and higher concentration of organics.

As the gas velocity increases, the bed of solid particles goes through the states of minimum fluidization, bubbling, turbulent to fast fluidization, and eventually become a transport reactor when the gas velocity exceeds the terminal velocity of the sand particles. The regime under which the system is operated is an important factor. The minimum fluidizing velocity ( $U_{mF}$ ) for the sand particles ranged between 0.42 and 0.44 m/s under dense bed conditions (TIC2, TIC3 = 900–950 °C). The  $U/U_{mF}$  ratio ranged between 6.4 and 6.8 under steady state conditions, the regime was turbulent, which was consistent with the visual observation through the viewing manholes on the combustion chamber. In this manner, the finest sand particles were carried over during the experiment, which was confirmed by the continuous pressure drop in the sand bed with time. This effect was much more pronounced in the preliminary experiments conducted in the fluidized bed chamber with a shorter freeboard zone.

Defluidization of the bed is particularly critical in the combustion of industrial wastes. A high risk of agglomeration might occur in the area where mixing is not perfect or when local over-heat zones exist in the bed. Bed sintering symptoms were not noticed during the combustion tests. Although the experiments were conducted at much lower temperatures (up to 950 °C) than the critical temperature for the transformation of quartz to cristobalite (around 1400 °C),<sup>14</sup> results are inconclusive with respect to the cumulative effect in long term operation. Additional investigations regarding defluidization caused by sintering are required in order to obtain reliable data for an industrial plant project.

The first priority for any waste management strategy should be practices that prevent or at least minimize generation of waste and promote recycling of materials. If reuse and recycling are not feasible options, then treatment technologies must be employed.

This study was specifically focused on the experimental development of a treatment for rinsates that cannot be recycled or reused for production of “ready to use” products. In addition, an important fact that had to be considered was the



higher energy input as a consequence of the high water content in the liquid waste. Recovering the calorific value of the used solvents and other organic compounds present in liquid wastes refers to the proposed “waste to energy” concept rather than just co-incineration. Since the energy released during the process might be utilized to generate hot water and steam, the disadvantage of high-energy consumption of the chosen treatment technology is mainly compensated.

The organics content (expressed as xylene of 5.33 vol. %) and the liquid waste flowrate of about 60 kg/h (150 m<sup>3</sup>/year) were adopted for preliminary calculations of an industrial unit. According to these calculations, the size of sand particles in the fluidized bed has no effect on the heat balance, but has effect on the column diameter and residence time (Fig. 5). With finer sand particle granulation, the residence time is longer, which is preferable, but at the same time, the column diameter is larger. The sand particles size and column diameter have to be chosen in order to meet the recommended values for the combustion system, *i.e.*, minimum 2 s at 1100 °C.<sup>7</sup> According to the preliminary design of the industrial plant for the chosen operating conditions, the plant would operate for about 100 days only during the winter period, with the basic concept of utilizing the heat released during the combustion for heating within the factory.

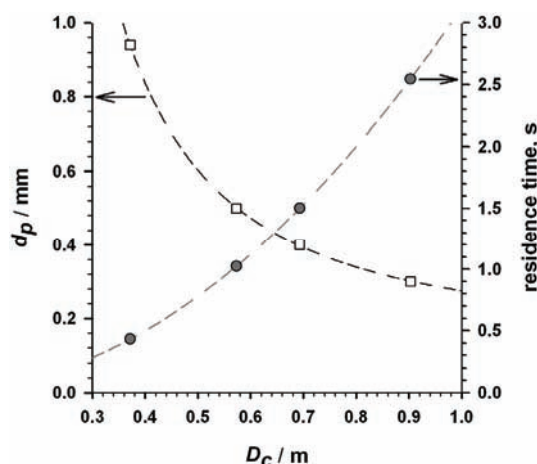


Fig. 5. The effect of the size of the sand particles ( $d_p$ ) in the fluidized bed on the column diameter ( $D_c$ ) and residence time.

The main objectives were achieved: the liquid waste was safely decomposed; fouling problems and emission levels could be eliminated under proper operating conditions. Doubtless, the industrial unit will be more efficient, since the freeboard residence time will be longer and temperatures will be higher.

#### CONCLUSIONS

The results of experimental investigations the disintegration of liquid waste (generated in a pesticide production plant) in a fluidized bed incinerator are given in this paper.

The obtained results indicate that this technology can be used for this purpose since it enables good control of temperature, which was found to be the most critical parameter. The main conclusions derived after these investigations are as follows:

1. The pilot scale unit operation was stable; bed sintering symptoms were not noticed.

2. In all runs, with sufficient excess air, where the temperature at the top of the column (TIC3) was above 900 °C, the overall hydrocarbons concentration at the system outlet was below the detection limits of the gas chromatograph, while the NO<sub>x</sub> concentrations were negligible. It should be noted that the residence time in the pilot scale unit was nearly 0.8 s, which is below the recommended value for combustion systems (2 s at 1100 °C). As different molecules might be present in the wastewater, including those containing chlorine, in order to prevent toxic emissions, high enough temperatures, residence times and turbulence in the combustion chamber should be ensured in order to prevent emissions of dioxins and furans. In addition, the temperature profile should be carefully controlled to prevent re-formation during cooling or starting-up.

3. The consumption of the propane-butane mixture was 0.72 kg/h, the consumption the additional liquid fuel (LG, sunflower oil) varied between 0.3 and 0.97 L/h, depending on the energy potential of liquid waste, and the liquid waste (LO) combustion capacity was in range of 2.2 to 2.5 L/h.

4. In the runs with the liquid waste with a high energy potential (sample 6, the consumption of the additional liquid fuel was negligible.

5. The obtained test results were used for a preliminary design of an industrial plant for incinerating 150 m<sup>3</sup>/year of these liquid wastes.

*Acknowledgements.* This study was supported by the Ministry of Science and Technological Development of the Republic of Serbia (Project No. 142014G and Project No. 451-01-00065/2008-01/10).

#### ИЗВОД

#### САГОРЕВАЊЕ ТЕЧНОГ ОТПАДА ФАБРИКЕ ПЕСТИЦИДА У ФЛУИДИЗОВАНОМ СЛОЈУ

ЗОРАНА АРСЕНИЈЕВИЋ<sup>1</sup>, ЖЕЉКО ГРБАВЧИЋ<sup>2</sup>, БОШКО ГРБИЋ<sup>1</sup>, НЕНАД РАДИЋ<sup>1</sup>,  
РАДМИЛА ГАРИЋ-ГРУЛОВИЋ<sup>1</sup>, САША МИЛЕТИЋ<sup>3</sup>, ГОРДАН САВЧИЋ<sup>3</sup> И БОЈАНА ЂОРЂЕВИЋ<sup>3</sup>

<sup>1</sup>Институт за хемију, технологију и металургију – Центар за катализу и хемијско инжењерство,  
Универзитет у Београду, Нjegoшева 12, Београд, <sup>2</sup>Технолошко-металуршки факултет, Универзитет у  
Београду, Карнегијева 4, Београд и <sup>3</sup>Галеника – Фармација А.Д., Бајбањички друм 66, Београд

Индустријски течни отпад може бити у облику раствора, суспензија, муља, пене, отпадног уља и генерално садржи различите органске компоненте. Предмет овог рада је демонстрација третмана течног отпада са високим садржајем загађујућих материја фабрике за производњу пестицида методом термичке деструкције у флуидизованом слоју песка као технички практичне и оптималне технологије. Испитивања сагоревања реалних течних отпад-

них смеша фабрике пестицида су извршена у полуиндустријском-демонстрационом постројењу, тј. у флуидизационој колони са слојем кварцног песка гранулације 0,63–1,25 mm и густине 2610 kg/m<sup>3</sup> на 800–950 °C. У циљу обезбеђења потпуног сагоревања течног отпада, у флуидизационој колони је увођен ваздух у вишку и однос  $U/U_{mf}$  (на температури околине) је износио између 1,1 и 2,3. У флуидизационој колони се течни отпад, додатно течни гориво и ваздух могу довести у стање интензивног контакта што омогућава стабилно и хомогено сагоревање у слоју. Резултати експерименталних испитивања показују да се у флуидизованом слоју песка остварује веома добра термичка униформност и контрола температура. Резултати испитивања сагоревања су показали да се течни отпад са високим садржајем загађујућих материја може успешно термички третирати у флуидизованом слоју песка без емисије штетних продуката сагоревања, под условом да су у слоју и изнад слоја обезбеђене температуре изнад 900 °C.

(Примљено 20. августа, ревидирано 5. новембра 2009)

#### REFERENCES

1. *Environmental, Health and Safety Guidelines for Pesticide Manufacturing, Formulation, and Packaging*, [http://www.ifc.org/ifcext/sustainability.nsf/AttachmentsByTitle/gui\\_EHSGuidelines2007\\_Pesticides/\\$file/Final+-+Pesticides.pdf](http://www.ifc.org/ifcext/sustainability.nsf/AttachmentsByTitle/gui_EHSGuidelines2007_Pesticides/$file/Final+-+Pesticides.pdf) (06 April, 2009)
2. A. S. Felsot, K. D. Racke, D. J. Hamilton, *Rev. Environ. Contam. Toxicol.* **177** (2003) 123
3. *Stockholm Convention on Persistent Organic Pollutants*, [http://chm.pops.int/Portals/0/Repository/convention\\_text/unep-pops-cop-convttext-full.English.pdf](http://chm.pops.int/Portals/0/Repository/convention_text/unep-pops-cop-convttext-full.English.pdf) (06 April, 2009)
4. K. H. Karstensen, *The Potential of using Cement Kilns for Environmentally Sound Destruction of Obsolete Pesticides in Developing Countries*, [http://www.coprochem.com/documents/19potential\\_cement\\_kilns\\_in\\_developing\\_countries.pdf/view](http://www.coprochem.com/documents/19potential_cement_kilns_in_developing_countries.pdf/view) (06 April, 2009)
5. *Hazardous Waste Incineration: Advanced Technology to Protect the Environment*, <http://www.vessa.eu/images/hazardous%20waste%20incineration.pdf> (06 April, 2009)
6. *Federal Register Environmental Documents*, <http://www.epa.gov/fedrgstr/1999.htm> (06 April, 2009)
7. *Official Journal of the European Communities: Directive 2000/76/EC of the European Parliament and of the Council on the incineration of waste*, [http://www.wbcsd.org/web/projects/cement/tf2/2000-76\\_en.pdf](http://www.wbcsd.org/web/projects/cement/tf2/2000-76_en.pdf) (06 April, 2009)
8. S. Patumsawad, K. R. Cliffe, *Energ. Convers. Manage.* **43** (2002) 2329
9. R. Natarajana, N. S. Karthikeyana, A. Agarwaala, K. Sathiyarayanan, *Renew. Energ.* **33** (2008) 2423
10. J. B. Kandpal, R. C. Maheshwari, T. C. Kandpal, *Energ. Convers. Manage.* **36** (1995) 1067
11. *Vegburner Report: Vegetable Oil as a Fuel*, <http://vegburner.co.uk/report.html> (06 April, 2009)
12. Y. Miyamoto, Y. Kurosaki, H. Fujiyama, E. Nanbu, *Control Eng. Pract.* **6** (1998) 1159
13. J. C. H. Chu, *Korean J. Chem. Eng.* **16** (1999) 795
14. R. Yan, D. T. Liang, L. Tsen, *Energ. Convers. Manage.* **46** (2005) 1165.





*J. Serb. Chem. Soc.* 75 (4) 537–549 (2010)  
JSCS–3986

## Polyaniline–multi-wall-carbon nanotube nanocomposites as a dopamine sensor

REZA EMAMALI SABZI<sup>1,2\*</sup>, KAMRAN REZAPOUR<sup>1</sup> and NASER SAMADI<sup>1</sup>

<sup>1</sup>Department of Chemistry, Faculty of Science, Urmia University, Urmia and

<sup>2</sup>Institute of Biotechnology, Urmia University, Urmia, Iran

(Received 27 May, revised 6 November 2009)

**Abstract:** A composite of polyaniline with multi-wall-carbon nanotubes (PANi/MWCNTs) was synthesized by an *in situ* chemical oxidative polymerization method. The PANi nanoparticles were synthesized chemically using aniline as the monomer and ammonium peroxydisulfate as the oxidant. The nanocomposites were prepared as a carbon paste using functionalized MWCNTs and PANi nanoparticles. The PANi–MWCNTs were characterized physically using scanning electron microscopy (SEM) and the electrochemical behavior of the composites in acidic solution (HCl) was investigated using cyclic voltammetry. The PANi/MWCNT composite electrode was used for studying dopamine (DA) as an electroactive material. The cyclic voltammetric results indicated that multi-wall carbon nanotubes (MWCNTs) significantly enhanced the electrocatalytic activity in favor of the oxidation of DA. The kinetics of the catalytic reaction was investigated using the chronoamperometry technique whereby the average value of the diffusion coefficient ( $D$ ) and the catalytic rate constant ( $k$ ) for DA were determined to be  $(7.98 \pm 0.8) \times 10^{-7} \text{ cm}^2 \text{ s}^{-1}$  and  $(8.33 \pm 0.072) \times 10^4 \text{ dm}^3 \text{ mol}^{-1} \text{ s}^{-1}$ , respectively.

**Keywords:** multi-wall-carbon nanotubes; dopamine; nanocomposite; polyaniline; sensor.

### INTRODUCTION

Carbon nanotubes (CNTs) are an important group of nanomaterials with unique electronic and chemical properties. Since CNTs were discovered in 1991 by Iijima *et al.*,<sup>1</sup> there has been a growing interest in nanotubes for several applications.<sup>2–6</sup> CNT-modified electrodes promote electron transfer due to their conductivity and mechanical properties. Composites of a conducting polymer and CNTs show synergistic effects and have been made for different applications. The two types of CNTs, single-wall carbon nanotubes (SWNT) and multi-wall

\* Corresponding author. E-mail: rezasabzi@yahoo.com

doi: 10.2298/JSC090527012S

carbon nanotubes (MWCNTs), have considerable potential in the field of polymer composites.<sup>7,8</sup> Functionalized nanotubes are also more easily dispersed in organic solvents, leading to an improved dispersion and homogeneity of the MWCNT within the polymer composite. For this reason, the MWCNTs prepared in these studies were treated with a mixture of concentrated  $\text{H}_2\text{SO}_4:\text{HNO}_3$ .<sup>9</sup>

Dopamine (DA) is an important neurotransmitter of the central nervous system. Variations in DA levels may result in brain disorders, such as Parkinson's disease, and also have impacts on learning and memory.<sup>10</sup> Hence, there is considerable interest in developing simple and accurate electrochemical techniques for measuring the chemical behaviors of DA.<sup>11-14</sup>

The advantages of using conducting polymers as opposed to the historically used inorganic materials are their diversity and ease of synthesis. Conducting polymers have also been studied intensively for their transducing properties.<sup>15-18</sup> Among those studied, PANi is one of the more important polymers due to its electrical conductivity and stability. Furthermore, it exhibits significant redox behavior. The conducting form of polyaniline is the protonated polyemeraldine or the green-colored polyemeraldine salt with a conductivity of approximately  $15 \text{ S cm}^{-1}$ .

PANi may be synthesized either chemically or electrochemically. The chemical synthesis involves mixing aniline with an acidic medium, such as HCl or  $\text{H}_2\text{SO}_4$ , and an oxidant, such as ammonium peroxydisulfate, whereas the electrochemical synthesis of PANi may be performed using galvanostatic, potentiostatic or potentiodynamic methods. Recently, the manufacture of CNTs in polymer materials, particularly composites based on polymers and nanotubes, have attracted much attention due their superior properties.<sup>19-21</sup>

Chemical polymerization is a simple and robust strategy for the large scale production of PAN. When performing chemical polymerization, oxidizing agents, such as ammonium peroxydisulfate, ammonium vanadate, potassium iodate and potassium dichromate, are employed.

There are many articles reporting experimentation concerning the determination of the concentration of DA. Compared with other electrodes<sup>22,23</sup> used for detection of DA, the proposed sensor shows a long lifetime, a linear dynamic range and good performance. In addition this sensor shows good stability and involves a simple construction. In this study, the electrochemical behavior of a PANi-MWCNTs composite prepared by chemical polymerization was assessed for the measurement of DA.

## EXPERIMENTAL

### *Chemicals and reagents*

Multi-wall carbon nanotubes (specific surface area,  $250 \text{ m}^2 \text{ g}^{-1}$ , diameter, 10 nm, length, 10–20  $\mu\text{m}$ ) made by chemical vapor deposition (CVD) were provided by the Petroleum Research Institute of Iran. The purity of the pristine MWCNT was 97 %. Dopamine, aniline mo-

monomer and ammonium peroxydisulfate were purchased from Merck and used for PANi preparation. All other chemicals and solvents were of analytical grade and were used without any further purification.

#### *Apparatus*

All electrochemical experiments were performed at  $25 \pm 1$  °C using a potentiostat/galvanostat Autolab, system type III. A conventional three-electrode cell was used for the electrochemical experiments. Ag/AgCl, platinum wire and PANi–MWCNT composite electrodes were used as the reference, auxiliary and working electrode, respectively. A centrifuge system (Eppendorf, Germany) was used for the physical separation of the MWCNTs.

Microstructure characterization of the PANi–MWCNT composites was performed using a Philips–XL30 low vacuum scanning electron microscope located in Tarbiat Modres University, Tehran, Iran.

#### *Carboxyl group functionalized MWCNTs*

Formation of carboxylic acid groups at the defective sites of the MWCNTs improved their solubility in HCl solution. The prepared MWCNTs were treated ultrasonically using a 3:1 mixture of 6 M  $\text{H}_2\text{SO}_4$  and  $\text{HNO}_3$  at 50 °C for 4 h. The dark suspension was then centrifuged for 30 min at 4000 rpm, washed with distilled water and dried at 50 °C.

#### *Synthesis of the PANi–MWCNTs nanocomposite*

The nanocomposite of protonic acid doped polyaniline with functionalized NTs (c-MWCNT) was synthesized using *in situ* chemical oxidation polymerization. This procedure entailed dissolving 0.10 g of c-MWCNT in 50 mL of 0.50 M HCl solution under stirring. The dark c-MWCNT suspension was then added to a solution composed of 0.70 g aniline monomer dissolved in 50 mL of 0.50 M HCl in an ice bath at 0–4 °C and stirred. Ammonium peroxydisulfate (APS) was added drop-wise into the c-MWCNT/aniline solution, and the resulting green suspension was then filtered and dried at 50 °C for 2 h.

For optimization of the modifier, different quantities of MWCNT (0.040, 0.080, 1.0 and 1.4 g) were used while keeping the weight of aniline monomer constant at 0.70 g. Optimization was also attempted using different amounts of aniline monomer (0.30, 0.50, 0.70 and 0.90 g) with a constant amount of CNT (0.10 g). Experimental results showed that a steep rise in peak current occurred when the amount of CNT incorporated into the mixture was increased up to a value of 1.0 g. Any further increases in the amount of CNT added to the mixture resulted in a linear rise in peak current but with a lower slope. Increasing the aniline monomer weight had the effect of increasing the peak current. But, when the aniline monomer weight reached or exceeded 0.70 g, a constant peak current was observed. Based on these results, 1.0 g of CNT and 0.70 g of aniline monomer were used in all experiments.

#### *Electrode preparation*

A composite electrode was prepared by carefully homogenizing (using slow rubbing) a mixture of 0.35 g graphite powder, 0.050 g PANi–MWNTs, precipitated with 7:1 weight ratio, and 2 drops of paraffin oil, for 15 min. The resulting paste was then packed into a polyethylene tube. The electrode surface ( $0.048 \text{ cm}^2$ ) was renewed by extrusion of approximately 0.5 mm carbon paste from the holder and smoothed with filter paper.

## RESULTS AND DISCUSSION

*Voltammetric behavior of the PANi–MWCNTs electrode*

Cyclic voltammetry was used for the study of PANi–MWCNTs modified chemically with polymerized aniline. The cyclic voltammograms obtained for both PANi and PANi–MWCNT composite electrodes at a scan rate of  $50 \text{ mV s}^{-1}$  in the potential range  $-0.20$  to  $1.0 \text{ V}$  are shown in Fig. 1. Three identifiable anodic peaks with cathodic counter parts are observed for the PANi–MWCNT composite electrode but not for the PANi composite electrode. Here, it is also important to take note of the role played by the CNT in the PANi composite.

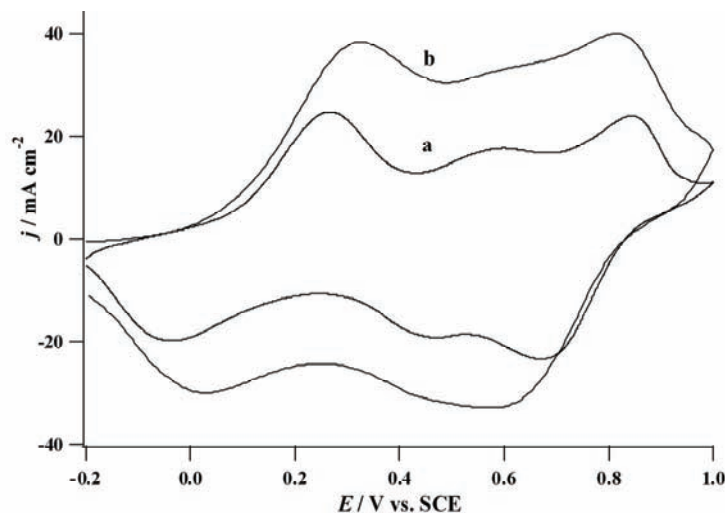


Fig. 1. Cyclic voltammograms of a) PANi–MWCNTs and b) PANi composite electrodes in  $0.50 \text{ M HCl}$  at a scan rate of  $50 \text{ mV s}^{-1}$ .

As can be seen in Fig. 1, the cyclic voltammograms have a defined peak at approximately  $200 \text{ mV}$ , corresponding to the formation of radical cations, a second peak at  $500 \text{ mV}$ , corresponding to the oxidation of benzoquinone (a hydrolysis product), and a third peak at  $700 \text{ mV}$ , corresponding to the oxidation of radical cations to diamine and formation of quinoid. Surface coverage ( $\Gamma$ ) could be evaluated from the area under the first anodic peak of the cyclic voltammograms for the PANi–MWCNT composite electrode. The surface coverage for PANi–MWCNTs was calculated according to Eq. (1):<sup>25</sup>

$$\Gamma = Q/nFA \quad (1)$$

where  $Q$  is the charge obtained by integration of the current vs. time for the first anodic peak,  $A$  is the surface area of the anodic peak, and  $n$  is the number of electrons transferred. Using this equation, the surface coverage,  $\Gamma = 2.369 \times 10^{-8} \text{ mol cm}^{-2}$ , was calculated.



The peak-to-peak separations ( $\Delta E = E_{pa} - E_{pc}$ ) were calculated for a PANi/MWCNT composite electrode using scan rates of up to  $50 \text{ mV s}^{-1}$  in the presence of HCl as the supporting electrolyte. At higher scan rates,  $\Delta E$  increased, indicating a limitation arising from the kinetics of the charge transfer.

Laviron derived general expressions for the linear potential sweep voltammetric response for the case of surface-confined electroactive species.<sup>23</sup> According to Laviron, the standard rate constant ( $k_s$ ) in 0.50 M HCl as the supporting electrolyte was calculated to be  $6.9 \times 10^{-8} \text{ mol}^{-1} \text{ dm}^3 \text{ s}^{-1}$  when a scan rate of  $30 \text{ mV s}^{-1}$  was applied and using values for  $\Delta E_p > 200/n$  (mV) with  $\alpha = 0.42$ .

#### *Morphology of the PANi-MWCNTs composite*

PANi was obtained by polymerization in the presence of 15 mass % c-MWCNTs. The scanning electron microscopy (SEM) technique was used for studying the morphology of the MWCNTs coated with PANi and the results are shown in Fig. 2. SEM Revealed a uniform deposition of PANi onto the MWCNTs, whereby the diameter of the PANi-coated MWCNTs was estimated to be in the range 80–120 nm.

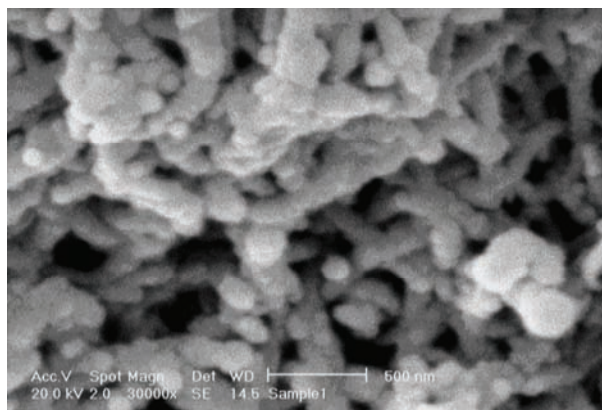


Fig. 2. SEM Image of a PANi/MWCNT nanocomposite.

#### *FTIR Results*

The FTIR spectra obtained for MWCNTs and c-MWCNTs are presented in Fig. 3. The peaks at  $1190$  and  $1720 \text{ cm}^{-1}$  correspond to the stretching modes of the carboxylic acid groups, and thus confirm the formation of carboxylic acid groups on the walls of the MWCNTs at defect sites.

#### *Thermal stability of the electrodes*

The thermal stability of the electrode was verified by subjecting it to different temperatures ( $15$ ,  $25$ ,  $35$  and  $45 \text{ }^\circ\text{C}$ ) for 2 h under dry conditions. The shapes of voltammetric curves were maintained and only a 6.5 % decrease of initial peak current was observed at the highest temperature ( $45 \text{ }^\circ\text{C}$ ). The good thermal sta-

bility of the PANi–MWCNTs composite may be attributed to the stability of PANi itself and the protective effect of PANi against desorption of MWCNTs from the composite.

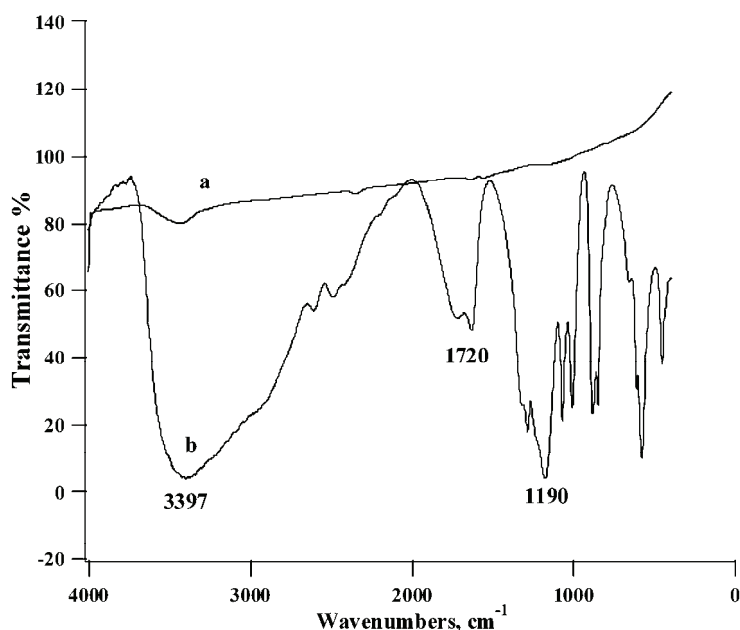


Fig. 3. The FTIR spectra of a) MWCNTs and b) c-MWCNTs.

#### *Response time, reversibility and reproducibility of the electrode*

The electrode response time was less than 20 s. The inset of Fig. 4 shows the calibration graph. The long-term response of the electrode for DA determination under hydrodynamic conditions was evaluated at 30-min intervals. The experimental results show that there was no appreciable change in the response for DA determination over time suggesting that the electrode remains stable even under stirring and, hence, may be used as a sensor for the determination of DA in flow systems. The response of the modified electrode remained reproducible and stable for almost one month without the need for its reactivation or remodification.

To characterize the reproducibility of the preparation of the PANi–MWCNTs composite, repetitive preparations of PANi–MWCNTs composite were made and tested. The relative standard deviation in the accompanying electrode signal for 5 successive preparations on different days was 6.8 %, indicating that successive preparations of PANi–MWCNTs yields a reproducible electrode activity. The modified electrode also exhibited high stability. For example, only a 5.4 % drop in the electrode signal from its initial response was observed when the electrode was used successively during a 1-day period.

Reproducibility of the PANi–MWCNTs composite modified electrodes stored in air or phosphate buffer at room temperature were investigated by measuring their current responses under both storage conditions at weekly intervals. The experimental results show that during a 4-week storage period of electrodes in a 0.10 M phosphate buffer solution and in air, the response currents of the PANi/MWCNTs composite modified electrodes decreased gradually to 12 and 19 % of their initial values, respectively.

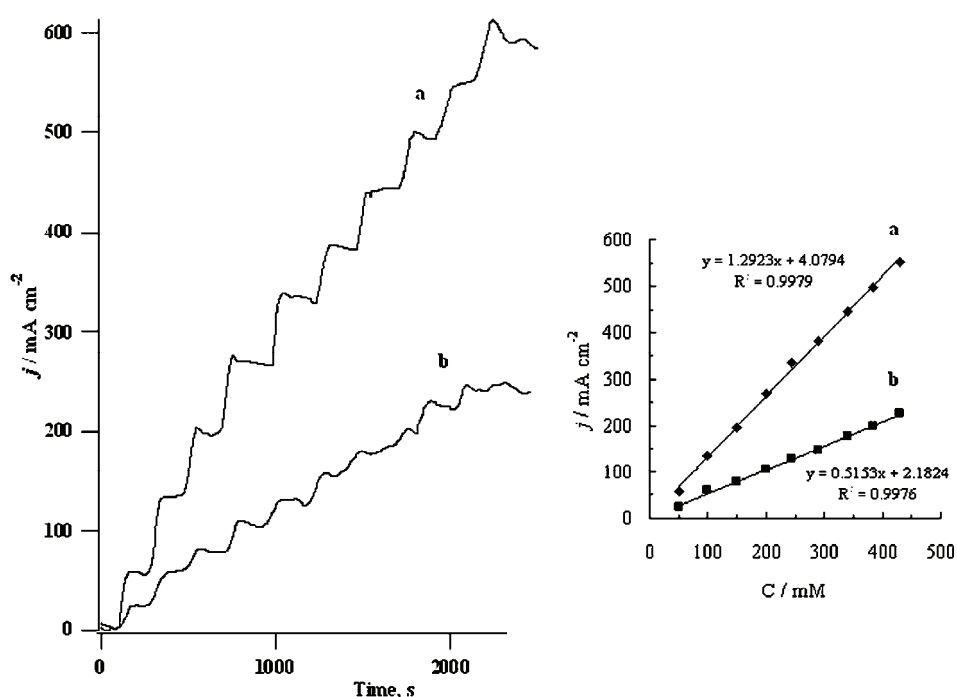


Fig. 4. Amperometric current response curves resulting from experiments with a) a PANi–MWCNTs nanocomposite electrode and b) a PANi carbon paste electrode. The points on the curves follow successive additions of 50  $\mu$ M DA in 0.10 M phosphate buffer at pH 7.0 and 0.70 V (the corresponding calibration curves are given in the inset).

#### *Electrocatalysis of dopamine oxidation*

*Amperometric studies.* Typical current–time plots for the PANi–MWCNT and PANi composites upon successive addition of 50  $\mu$ M dopamine under stirred conditions at 0.70 V are illustrated in Fig. 4. The PANi–MWCNT composites attained 95 % of the steady-state current within a reaction time of 15 s. The calibration curve of dopamine at the PANi–MWCNT composite electrode is shown in Fig. 4 (inset). The composite electrode exhibited a linear response to DA in the

range from 50.0 to 385  $\mu\text{M}$  with a correlation coefficient of 0.9979. The electrode was found to have a low detection limit of 38  $\mu\text{M}$ .

**Cyclic voltammetry studies.** Cyclic voltammetry was performed to study the electrocatalytic behavior of PANi–MWCNTs toward the oxidation of DA in 0.10 M phosphate buffer (pH 7.0) and to compare to different composite electrodes. The cyclic voltammograms of PANi–MWCNTs, PANi, MWCNTs and carbon paste electrodes in the presence of 3.7 mM of DA are shown in Fig. 5. Experiments with PANi–MWCNTs resulted in pronounced electrocatalytic activity for the oxidation of DA in comparison to those using a PANi electrode alone, MWCNT or a carbon paste electrodes (Fig. 5). The peak current enhancement for DA oxidation ( $2.56 \text{ mA cm}^{-2}$ ) at a low oxidation potential ( $E_{\text{pa}} = 269 \text{ mV vs. SCE}$ ) is clearly observed. The enhanced current peak and the negative shift (see Table I) in the oxidation overvoltage for DA oxidation indicates enhanced electrocatalytic activity associated with the PANi–MWCNTs electrode. The observed shift in the oxidation overvoltage for DA oxidation may be related to kinetic and transport effects of DA at the PANi–MWCNT interface. A substantial increase in the electron transfer rate at an electrode may promote enhancement of the oxidation of DA.

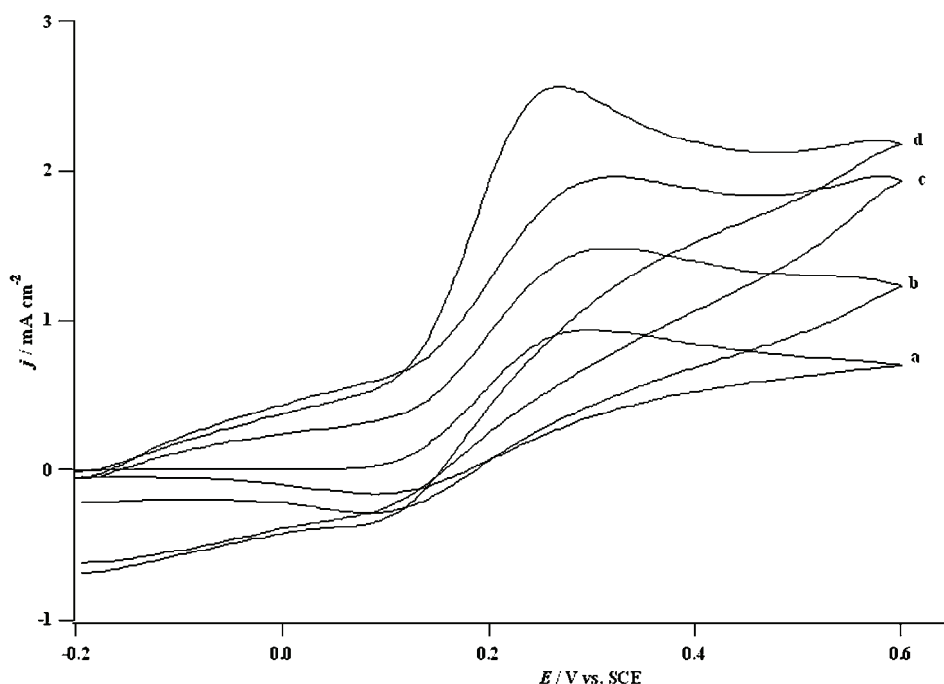


Fig. 5. Cyclic voltammograms of a) a carbon paste electrode, b) PANi, c) MWCNTs and d) PANi–MWCNTs in the presence of 3.7 mM DA.

Table I. Oxidation potential of DA using different electrodes

Composite electrode	DA oxidation potential, mV vs. SCE
Carbon paste	313
MWCNTs	308
PANi	300
PANi-MWCNTs	269

*Chronoamperometric studies.* Chronoamperometry was used to calculate the diffusion coefficient of DA. The well-defined chronoamperograms acquired for PANi-MWCNT modified electrodes at applied potential steps of 0.50 and 0.0 V for the forward and backward chronoamperometry, respectively, both in the absence and presence of 1.66 and 2.85 mM DA, are shown in Fig. 6. The forward and backward potential step chronoamperometry of the composite electrode in the absence of DA shows very symmetrical chronoamperograms with an equal charge consumed for the oxidation and reduction of the surface-confined PANi-MWCNT sites. For electro-active materials with a diffusion coefficient  $D$ , the current corresponding to the electrochemical reaction (under diffusion control) is described by the Cottrell Law:<sup>26</sup>

$$I = nFAD^{1/2}c(\pi t)^{-1/2} \quad (2)$$

where  $D$  and  $c$  are the diffusion coefficient ( $\text{cm}^2 \text{s}^{-1}$ ) and bulk concentration ( $\text{mol cm}^{-3}$ ), respectively. Thus, a plot of  $I$  vs.  $t^{-1/2}$  should be linear and from its slope, the value of  $D$  can be obtained.

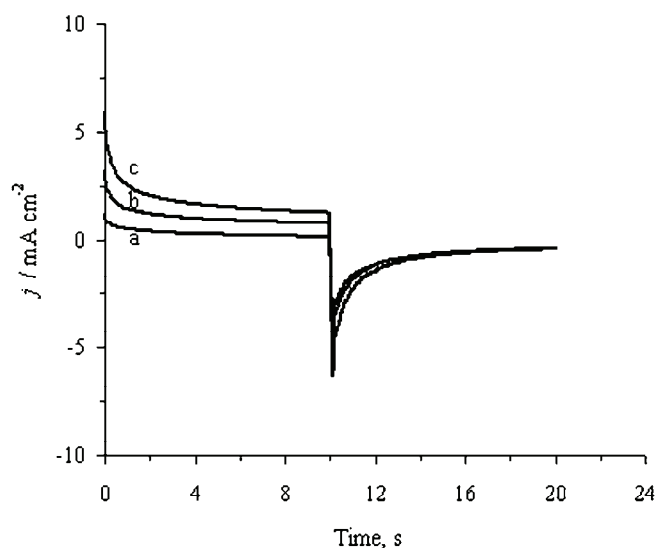


Fig. 6. Chronoamperograms acquired with a PANi-MWCNT composite electrode in 0.10 M phosphate buffer, pH 7.0, in a) the absence, b) presence of 1.66 mM DA and c) presence of 2.85 mM DA.

The mean value of  $D$  was found to be  $(7.98 \pm 0.8) \times 10^{-7} \text{ cm}^2 \text{ s}^{-1}$  (for 5 repetitions and at the 95 % confidence limit). Chronoamperometry also can be used to evaluate the kinetics of a reaction. At intermediate times (0.1–5 s in the present work), the catalytic current ( $I_{\text{cat}}$ ) is dominated by the rate of electron cross-exchange between the PANi–MWCNT redox sites and DA. The rate constant in this time limit was determined according to Eq. (3) as described in the literature:<sup>27</sup>

$$I_{\text{cat}}/I_{\text{L}} = \gamma^{1/2} \pi^{1/2} = \pi^{1/2} k c_0 t \quad (3)$$

where  $k$ ,  $c_0$ ,  $t$ ,  $I_{\text{cat}}$  and  $I_{\text{L}}$  are the catalytic rate constant ( $\text{dm}^3 \text{ mol}^{-1} \text{ s}^{-1}$ ), analyte concentration ( $\text{mol dm}^{-3}$ ), time elapsed (s), and current of the PANi–MWCNT composite electrodes in the presence and absence of DA, respectively. From the slope of the  $I_{\text{cat}}/I_{\text{L}}$  vs.  $t^{1/2}$  plot, the value of  $k$  for a given concentration of DA can be calculated. According to the experimental data, the value of  $k$  was found to be  $(8.33 \pm 0.072) \times 10^4 \text{ dm}^3 \text{ mol}^{-1} \text{ s}^{-1}$  (for 6 repetitions and at the 95 % confidence limit).

#### *Study of interferences*

The possible interferences from substances such as ascorbic acid, AA, and uric acid, UA, were evaluated using the Differential Pulse Voltammetry (DPV) technique. Oxidation of DA on a PANi–MWCNTs electrode in 0.10 M phosphate buffer solution (pH 6.0) occurred at 0.10 V vs. SCE. The oxidation of ascorbic acid at the same concentration and pH resulted in a peak at 0.18 V vs. SCE in 0.10 M phosphate buffer (pH 6.0). Under identical solution conditions (0.10 M phosphate buffer, pH 6.0), uric acid produced a peak at 0.32 V vs. SCE. According to the experimental results, the amount of DA can be determined in the presence of ascorbic acid or uric acid by adjusting the pH.

According to the experimental results obtained using the PANi–MWCNTs electrode, the peak separation of DA vs. ascorbic acid realized by the DPV technique is less than 0.10 V. A similar investigation with DA and uric acid identified a peak separation of 0.22 V. Typical amounts in grams of DA determined by the DPV method in the presence of ascorbic acid or uric acid are shown in Fig. 7, from which it can be seen that successive additions of uric acid or ascorbic acid causes an increase in the peak current. From this, it can be concluded that the determination of the amount of DA in the presence of ascorbic acid or uric acid is possible using this electrode.

#### *Analytical application to real samples*

The applicability of the modified electrode was evaluated by measuring the concentration of DA in pharmaceutical injection samples. The injection samples were diluted with phosphate buffer solution (pH 6.0) without any further treatment. The DPVs for a DA sample in phosphate buffer solution were recorded.

An oxidation peak at 0.10 V was observed, which was assigned to the oxidation of DA. To check that the observed oxidation peak at 0.1 V did in fact originate from DA, a secondary experiment was performed in which the sample was spiked with specific amounts of a DA standard solution and the corresponding DPVs were recorded. The obvious increase in the peak current after addition of DA to the injection sample is a clear sign that the observed peak corresponded to the oxidation of DA.

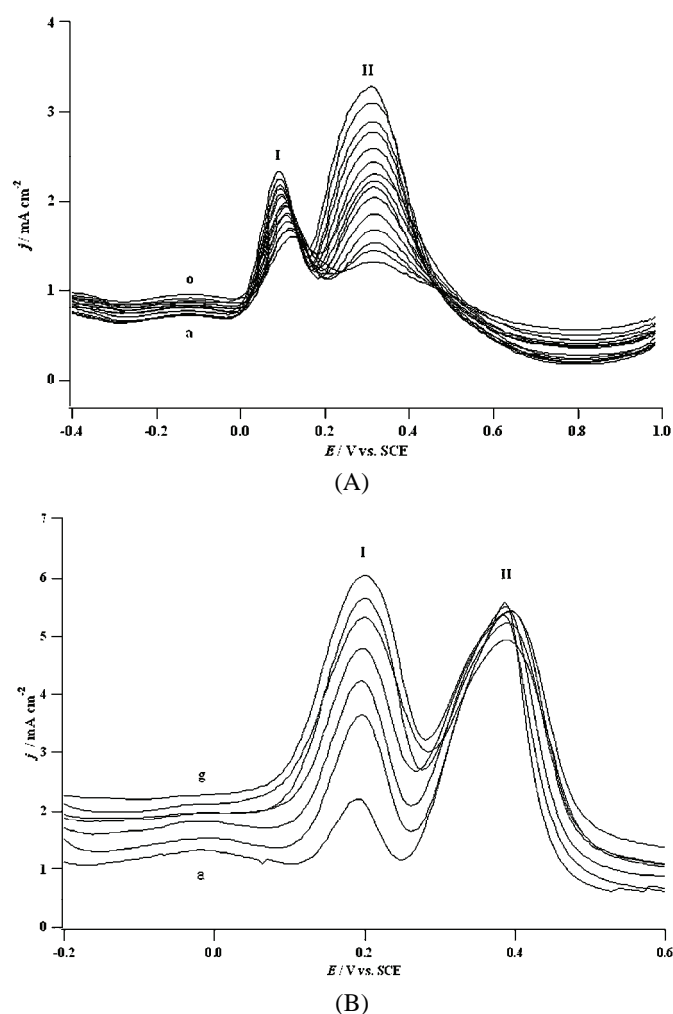


Fig. 7. DPV Voltammograms of a PANi-MWCNT electrode for A) peak I- 50  $\mu\text{M}$  of DA and peak II - different concentrations of UA (a-n: 15, 20, 25, 30, 35, 40, 45, 50, 55, 60, 65, 70, 75 and 80  $\mu\text{M}$ ) and B) peak I - different concentrations of DA (a-g: 40, 50, 60, 70, 80, 100 and 120  $\mu\text{M}$ ) and peak II - 50  $\mu\text{M}$  of AA in phosphate buffer (pH 6.0).

The relative recoveries of DA for some injection samples were investigated. For this purpose, an analytical curve was constructed using hydrodynamic voltammetry. Thus, a voltage 0.30 V vs. SCE was applied to the electrode and the samples were analyzed using a calibration plot. In addition, a definite quantity of standard DA solution was added to the corresponding injection samples in order to test for DA recovery. Typical results are shown in Table II. The recovery was acceptable, showing that the proposed methods could be efficiently employed for the quantification of DA in pharmaceutical injection samples. The recoveries of DA observed after spiking pharmaceutical injection samples ( $n = 3$ ) with a fixed quantity of DA solution varied from 97 to 99 % (Table II) using the proposed sensor.

Table II. Results of the determination of DA in pharmaceutical injection samples (DA spiking,  $50.0 \times 10^{-5} \text{ mol dm}^{-3}$ )

Sample	DA Found, $10^{-5} \text{ mol dm}^{-3}$	Recovery, %
1	49.5	99
2	48.5	97
3	48.5	97

#### CONCLUSIONS

The preparation of PANi–MWCNTs and their employment for the measurement of the electrocatalytic activity of DA have been described. The PANi–MWCNT nanocomposites were prepared using an *in situ* chemical polymerization reaction between MWCNTs and PANi monomer. The presence of functionalized MWCNT composites caused an increase in the DA oxidation current. The morphology of the PANi–MWCNTs was studied by the SEM technique and FTIR spectroscopy confirmed the incorporation of carboxylic acid groups into the MWCNTs.

#### ИЗВОД

#### НАНОКОМПОЗИТ ПОЛИАНИЛИНА И УГЉЕНИЧНИХ НАНОЦЕВИ КАО ДОПАМИНСКИ СЕНЗОР

REZA EMAMALI SABZI<sup>1,2</sup>, KAMRAN REZAPOUR<sup>1</sup> и NASER SAMADI<sup>1</sup>

<sup>1</sup>Department of Chemistry, Faculty of Science, Urmia University, Urmia u <sup>2</sup>Institute of Biotechnology, Urmia University, Urmia, Iran

Композитни материјал полианилина и вишеслојних угљеничних наноцеви (PANi–MWCNT) је синтетисан методом *in situ* хемијске оксидативне полимеризације. Наночестице полианилина су синтетисане хемијским путем коришћењем анилина као мономера и амонијум-пероксодисулфата као оксидационог средства. Наноконтролитни материјал је припремљен коришћењем функционализованих вишеслојних угљеничних наноцеви и наночестица полианилина у виду угљеничне пасте. Композит PANi–MWCNT је карактерисан скенирајућом електронском микроскопијом, док је његово електрохемијско понашање у киселом раствору (HCl) испитано цикличном волтаметријом. Електрода направљена од компо-



зита PANi-MWCNT је коришћена за испитивање допамина као електроактивне врсте. Резултати цикличне волтаметрије су показали да вишеслојне угљеничне наноцеви значајно побољшавају електрокаталитичку активност за оксидацију допамина. Кинетика ове реакције је испитивана методом хроноамперометрије. Одређена је средња вредност коефицијента дифузије ( $(7,98 \pm 0,8) \times 10^{-7} \text{ cm}^2 \text{ s}^{-1}$ ) и константа брзине каталитичке оксидације допамина ( $(8,33 \pm 0,072) \times 10^4 \text{ dm}^3 \text{ mol}^{-1} \text{ s}^{-1}$ ).

(Примљено 27. маја, ревидирано 6. новембра 2009)

#### REFERENCES

1. S. Iijima, T. Ichihashi, *Nature* **363** (1993) 603
2. Z.-H. Wang, Q.-L. Liang, Y.-M. Wang, G.-A. Luo, *J. Electroanal. Chem.* **540** (2003) 129
3. S. N. Marinković, *J. Serb. Chem. Soc.* **73** (2008) 891
4. N. Rastkari, R. Ahmadkhaniha, M. Yunesian, *J. Chromatogr. B* **877** (2009) 1568
5. G. Nechifor, S. I. Voicu, A. C. Nechifor, S. Garea, *Desalination* **241** (2009) 342
6. H. Yu, X. Quan, S. Chen, H. Zhao, Y. Zhang, *J. Photochem. Photobiol. A* **200** (2008) 301
7. T.-M. Wu, Y.-W. Lin, C.-S. Liao, *Carbon* **43** (2005) 734
8. E. V. Shlyakhova, N F. Yudanov, Yu. V. Shubin, L. I. Yudanov, L. G. Bulusheva, A. V. Okotrub, *Carbon* **47** (2009) 1701
9. S.-H. Baek, B. Kim, K.-D. Suh, *Colloids Surf. A* **316** (2008) 292
10. M. Wightman, L. J. May, A. C. Michael, *Anal. Chem.* **60** (1988) 769A
11. K. Wu, J. Fei, S. Hu, *Anal. Biochem.* **318** (2003) 100
12. B. J. Venton, R. M. Wightman, *Anal. Chem.* **75** (2003) 414A
13. P. Zhang, F.-H. Wu, G.-C. Zhao, X.-W. Wei, *Bioelectrochem.* **67** (2005) 109
14. G. Alarcon-Angeles, B. Perez-Lopez, M. Palomar-Pardave, M. T. Ramirez-Silva, S. Alegret, A. Merkoci, *Carbon* **46** (2008) 898
15. J. Yuan, D. Han, Y. Zhang, Y. Shen, Z. Wang, Q. Zhang, L. Niu, *J. Electroanal. Chem.* **599** (2007) 127
16. T. Del Castillo-Castro, M. M. Castillo-Ortega, I. Villarreal, F. Brown, H. Grijalva, M. Perez-Tello, S. M. Nuno-Donlucas, J. E. Puig, *Composites A* **38** (2007) 639
17. T.-M. Wu, Y.-W. Lin, *Polymer* **47** (2006) 3576
18. M. Guo, J. Chen, J. Li, B. Tao, S. Yao, *Anal. Chim. Acta* **532** (2005) 71
19. T.-M. Wu, Y.-W. Lin, *Polymer* **47** (2006) 3576
20. P. K. Khanna, M. V. Kulkarni, N. Singh, S. P. Lonkar, V. V. V. S. Subbarao, A. Kasi Viswanath, *Mater. Chem. Phys.* **95** (2006) 24
21. M. Guo, J. Chen, J. Li, B. Tao, S. Yao, *Anal. Chim. Acta* **532** (2005) 71
22. B. Fang, S. Jiao, M. Li, H. Tao, *Anal. Bioanal. Chem.* **386** (2006) 2117
23. P. Zhang, F. H. Wu, G. C. Zhao, X. W. Wei, *Bioelectrochem.* **67** (2005) 109
24. A. J. Bard, L. R. Faulkner, *Electrochemical Methods, Fundamentals and Application*, Wiley, New York, 2001
25. E. Laviron, *J. Electroanal. Chem.* **101** (1979) 19
26. Z. Galus, *Fundamentals of Electrochemical Analysis*, Ch. 10, Ellis Horwood, New York, 1976, p. 313.





*J. Serb. Chem. Soc.* 75 (4) 551–564 (2010)  
JSCS–3987

## Hexavalent chromium removal by waste mycelium of *Aspergillus awamori*

VELIZAR K. GOCHEV<sup>1\*</sup>, ZDRAVKA I. VELKOVA<sup>2</sup>  
and MARGARITA S. STOYTICHEVA<sup>3</sup>

<sup>1</sup>Department of Biochemistry and Microbiology, Paisii Hilendarski University of Plovdiv,  
Tzar Asen Str. 24, Plovdiv 4000, <sup>2</sup>Department of Inorganic and Physical Chemistry,  
University of Food Technologies, Maritza Boulevard 26, Plovdiv 4000, Bulgaria and  
<sup>3</sup>University of Baja California, Mexicali, Mexico

(Received 31 March, revised 15 July 2009)

**Abstract:** In this study, the Cr(VI) removal potential of waste mycelium from the industrial xylanase-producing strain *Aspergillus awamori* was evaluated. It was determined by FTIR analysis that amino groups from the major fungal wall constituents, chitin and chitosan, played a key role in the metal binding process. The effect of pH, initial ion concentration, temperature and amount of biomass on the removal was also studied. The removal efficiency increased with decreasing pH and increasing temperature and amount of biomass. The mechanism of Cr(VI) removal by *A. awamori* can be explained by a two-stage process involving an initial adsorption stage followed by a reducing stage. The removal process was described by a second-order polynomial and the optimal process parameters for attaining  $R_{\max}$  94.4 % in 48 h were predicted, *i.e.*, pH 1.5 and  $t = 40$  °C. From both economic and ecological points of view, a promising possibility for the utilization of waste industrial mycelium of *A. awamori* as a low-cost Cr(VI) removal agent was proposed.

**Keywords:** *Aspergillus awamori*; Cr(VI) removal; waste fungal mycelium.

### INTRODUCTION

Due to the accelerated development of various industries, constantly increasing amounts of pollutants are annually discharged into ecosystems. Environmental pollution with industrial wastewaters contaminated with heavy metals has become one of the major ecological problems. One such heavy metal is Cr(VI). Due to its carcinogenic, mutagenic, teratogenic and tissue damaging potential, Cr(VI) is known to be very toxic to both plants and animals and has been classified in Group A of human carcinogens.<sup>1–4</sup> The high risk of Cr(VI) bioaccumulation through the food chain and the disadvantages of traditional chemical

\* Corresponding author. E-mail: vgochev2000@yahoo.com  
doi: 10.2298/JSC090331008G

methods for metal removal have led scientific attention to be focused on non-conventional, biological methods for Cr(VI) removal by various biomaterials, such as bacteria, yeast, algae, seaweed, filamentous fungi and agricultural waste biomass.<sup>5–20</sup> On the one hand, compared to living and resting cells, non-living cells possess higher metal removal capacities.<sup>11,21–23</sup> On the other hand, from both economic and ecological points of view, it is very important to utilize inexpensive and waste biomaterials as metal removal agents. Many of the cited studies for Cr(VI) removal were not realized with waste fungal biomasses, but with especially cultivated fungal strains that were then killed. Filamentous fungi belonging to genera *Aspergillus*, *Penicillium* and *Rhizopus* are intensively used in fermentation industries for producing enzymes, antibiotics and other bioproducts, which means large amounts of waste fungal mycelium are produced annually. Only Fourest and Roux<sup>24</sup> and Gulati *et al.*<sup>25</sup> have studied the biosorption of Cu, Ni, Zn, Cd and Pb by waste fungal mycelium of *A. terreus* and *R. arrhizus* obtained as by-products from industrial fermentation processes. To the best of our knowledge, no articles considering Cr(VI) removal using waste fungal mycelium from industrial fermentations exist in the literature.

The aim of this study was to evaluate for the first time the potential of waste mycelium of the industrial xylanase-producing strain *A. awamori* for Cr(VI) removal from aqueous solutions. The cell surface binding groups before and after Cr(VI) removal were detected. The effects of pH, initial Cr(VI) concentration, amount of biomass and temperature on metal removal from aqueous solutions were studied in a batch system. The activation energy of the process was calculated and Cr(VI) removal was explained by a pseudo-first order kinetic model.

## EXPERIMENTAL

### *Preparation of the biosorbent*

Waste mycelium of the industrial strain *A. awamori* was harvested by filtration at the end of the fermentation process for the industrial production of a complex enzyme preparation with a leading xylanase activity.<sup>26,27</sup> The waste mycelium was killed by autoclaving at 121 °C for 20 min, washed thoroughly with deionized water and dried in an oven at 80 °C for 10 h. Then it was powdered to particles of uniform size of about 100 µm. This powdered biomass was used in the further biosorption experiments.

### *Chemical modification of the amino groups*

Formaldehyde and sodium iodoacetate treatment were performed as described by Park *et al.*<sup>28</sup> Acetic anhydride treatment was performed as described by Bai *et al.*<sup>11</sup> At the end of the treatment procedures, biosorbent was separated, washed with deionized water and dried in an oven at 80 °C for 10 h.

### *Preparation of the Cr(VI) solution*

A stock solution (1000 mg L<sup>-1</sup>) of Cr(VI) was prepared by dissolving the adequate amount of K<sub>2</sub>Cr<sub>2</sub>O<sub>7</sub> (Merck, Darmstadt, Germany) in deionized water. For metal biosorption experiments, Cr solutions of different concentrations (25, 50 and 100 mg L<sup>-1</sup>) were prepared by appropriate dilution of the stock solution with deionized water.

#### *Analysis of the Cr concentration*

The residual Cr(VI) concentration after biosorption was determined spectrophotometrically (Camspec, UK) at 540 nm using 1,5-diphenylcarbazide as the complexing agent in acidic solution.<sup>29</sup> To estimate the total chromium concentration, Cr(III) was first converted to Cr(VI) at 130–140 °C by the addition of excess of KMnO<sub>4</sub> prior to the 1,5-diphenylcarbazide reaction. The Cr(III) concentration was calculated from the difference between the total chromium and the Cr(VI) concentration. The detection limit was 0.03 mg L<sup>-1</sup>.

#### *Biosorption studies*

In order to evaluate the effect of pH, initial Cr(VI) concentration, amount of biosorbent and temperature, a series of biosorption experiments were performed in a batch system. The pH of the metal solution was adjusted to values between 1.5 and 4.0 using 1.0 M HCl or 1.0 M NaOH. Biosorption of Cr was realized at temperatures ranging from 20 to 40 °C. The effect of the quantity of biosorbent was studied at concentrations ranging from 1 to 20 g L<sup>-1</sup>. A known amount of biosorbent was added to 100 mL Cr(VI) solution of the desired concentration and pH in 250 mL Erlenmeyer flasks. The flasks were placed on a rotary shaker at the desired temperature and 150 rpm for 48 h. At the end of the biosorption process, the biosorbent was separated from the solution by filtration and residual Cr(VI) concentration was measured as given above. To eliminate the probable influence of glassware and filter papers on the metal sorption capacity, the Cr(VI) concentration was measured under the same batch experimental conditions (pH, temperature, duration and agitation) without using biosorbent.

All experiments were performed in triplicate. For all graphical representation, the mean values of three independent experiments were considered and standard deviations within the triplicates were too small to be plotted as error bars (< 1 %).

#### *Removal efficiency of Cr(VI)*

The removal efficiency was calculated as:

$$R = 100 \frac{c_i - c_f}{c_i} \quad (1)$$

where:  $c_i$  and  $c_f$  denote respectively the initial concentration of Cr(VI) and final residual concentration of Cr(VI) at the moment  $t$ , in mg L<sup>-1</sup>.

#### *Fourier transform infrared spectroscopy*

The chemical characteristics of the biosorbent surface before and after Cr(VI) adsorption were analyzed and interpreted by FTIR spectroscopy of the biomass in KBr pellets using a Perkin–Elmer Spectrum One, FT-IR spectrometer equipped with software Spectrum, v. 5.0.2, for interactive interpretation of possible structure units.

## RESULTS AND DISCUSSION

#### *FTIR Analysis of the biosorbent*

Biosorption is defined as the property of microorganisms to accumulate metal ions by adsorption on the cell surface. The major constituents of fungal cell wall are carbohydrates chitin (3–39 %) and chitosan (5–33 %), polyuronide and polyphosphates (2–12 %), lipids (2–7 %) and proteins (0.5–2.5 %) and there are marked variations in the wall composition between different fungal taxonomic groups.<sup>23,24</sup> For this reason, to study the mechanism of Cr(VI) removal by waste

mycelium of xylanase-producing *A. awamori*, the active chemical groups on the cell surface before and after Cr(VI) removal were evaluated by FTIR spectroscopy. The obtained results are shown in Fig. 1.

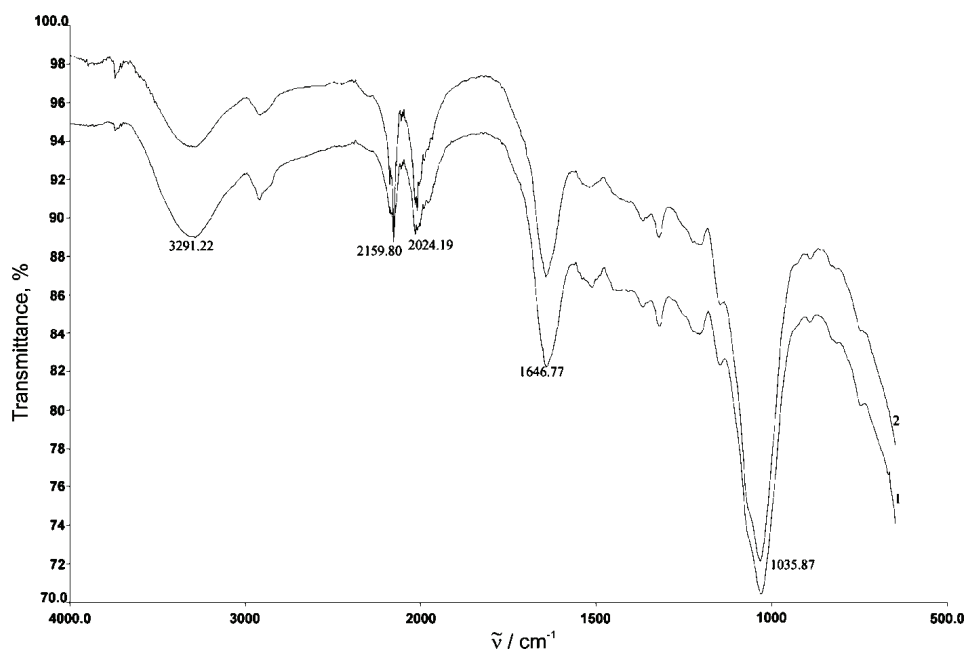


Fig. 1. FTIR Spectra of waste *A. awamori* biomass before (1) and after (2) Cr(IV) adsorption.

The FTIR spectroscopic analysis indicated broad absorption bands at 3291  $\text{cm}^{-1}$ , representing the  $-\text{OH}$  groups of glucose and the  $-\text{NH}$  stretching of the proteins and the acetamido group of chitin. The absorption bands at 2159 and 2024  $\text{cm}^{-1}$  can be assigned to  $\text{C}=\text{O}$  and  $\text{C}=\text{N}$  groups. The absorption band at 1646  $\text{cm}^{-1}$  can be attributed to the amide bond in the *N*-acetyl glucosamine polymer of the protein peptide bond. The strong absorption band at 1035  $\text{cm}^{-1}$  could be assigned to the  $-\text{CN}$  stretching vibrations of the chitin–chitosan and protein fractions. The spectral analysis before and after Cr(VI) binding indicated that  $-\text{NH}$  group were involved in the binding process because there were substantial changes in the absorption intensity of the  $-\text{NH}$  bending (1646  $\text{cm}^{-1}$ ) and  $-\text{NH}$  stretching (3291  $\text{cm}^{-1}$ ) bands after Cr(VI) adsorption. As chitin and chitosan are the major constituents of the fungal cell wall and major donors of  $-\text{NH}$  groups, their key role in the Cr(VI) removal process can be assumed. The results obtained were in accordance with published FTIR spectra of untreated *Rhizopus nigricans* biomass before and after Cr(VI) adsorption and the active groups involved in the metal binding process and major fungal cell wall constituents.<sup>11,23,24</sup>

### Chemical modification of amino groups

To elucidate the role of amino groups in Cr(VI) removal, they were modified by chemical treatment with a mixture of formaldehyde and formic acid, acetic anhydride and sodium iodoacetate. The chromium removal capacity of the chemically treated biosorbent was compared to that of untreated biosorbent. The results are shown in Fig. 2.

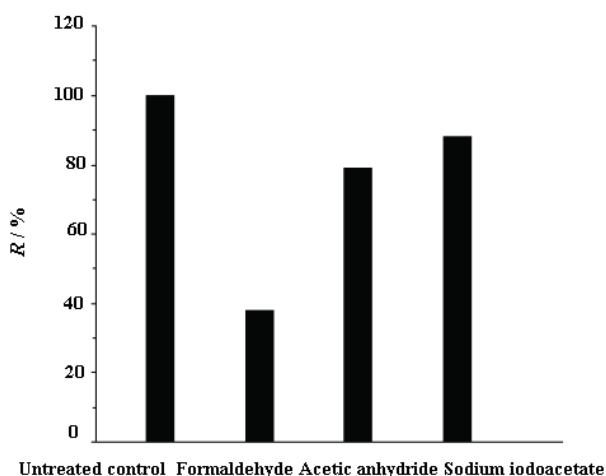


Fig. 2. Effect of chemical modification of the amino groups on the Cr(VI) removal capacity of waste *A. awamori* biomass.

As shown, Cr(VI) removal from the aqueous solution was dependent on the chemical treatment of the biosorbent. Formaldehyde treatment caused methylation of the amino groups and reduced the number of positively charged sides on the biosorbent surface, which significantly reduced Cr(VI) removal by about 42 % compared to untreated biosorbent. An about 21 % reduction in Cr(VI) removal by the acetic anhydride-treated biosorbent in comparison to the untreated was determined. Acetic anhydride caused acetylation of the amino groups and in this way also reduced the number of positively charged groups on the surface of the biosorbent.<sup>11</sup> Treatment of the biosorbent with sodium iodacetate caused a 12 % reduction in Cr(VI) removal compared to that of the native biosorbent. Sodium iodacetate attaches to and neutralizes amino groups at low pH values by introducing carboxyl groups.<sup>28</sup> The obtained results confirmed our assumption that positively charged amino groups play a key role in Cr(VI) removal from aqueous solutions by waste mycelium of *A. awamori*. Among the tested treatment procedures, replacement of amino groups with carboxyl groups demonstrated the smallest negative effect on the removal process, which means that carboxyl groups may also participate in the Cr(VI) removal process. The results obtained are in accordance with data published by other authors.<sup>11,28</sup>

### Effect of pH

The pH of the metal solution is one of the major factors affecting the Cr(VI) removal process.<sup>10,22</sup> The effect of the initial pH on Cr(VI) removal by waste *A. awamori* biomass was evaluated in the range from 1.5 to 4. The results are shown in Fig. 3.

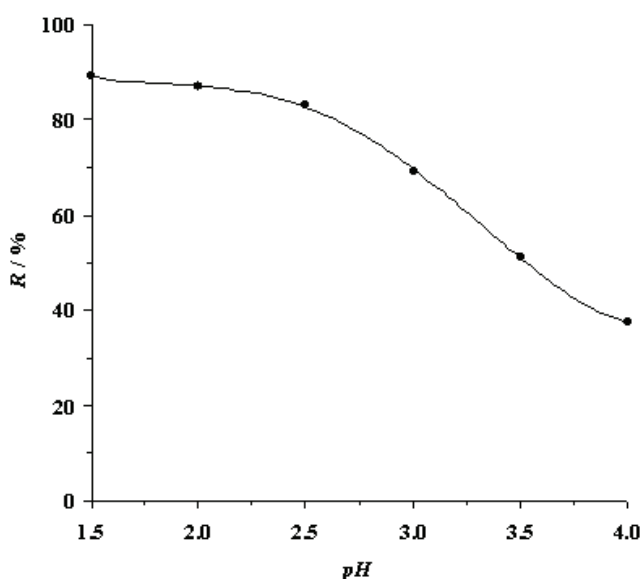


Fig. 3. Effect of pH on Cr(VI) removal by waste *A. awamori* biomass ( $c_0 = 25 \text{ mg L}^{-1}$ ,  $V = 100 \text{ mL}$ ,  $W = 1 \text{ g L}^{-1}$ ,  $\tau = 48 \text{ h}$ ).

Increasing the initial pH of the solution from 1.5 to 4 decreased Cr(VI) removal by *A. awamori* from 89.26 to 27.50 %. The effect of pH can be explained by its influence on the protonation of the functional groups on the cell surface.<sup>11,29</sup> At the pH values 1.5 and 2, functional groups such as amino groups are protonated ( $\text{NH}_3^+$ ) and chromate ions are in the forms  $\text{Cr}_2\text{O}_7^-$  and  $\text{HCr}_2\text{O}_4^-$ . The negatively charged dichromate ions are electrostatically attracted by the positively charged amino groups but at these pH values, Cr(VI) is also rapidly reduced to Cr(III).<sup>10,31–33</sup> During and after the Cr(VI) removal process, the pH was almost constant and varied in a very narrow interval between 2.00–2.12, which means that the removal mechanism is not ion exchange. The removal of Cr(VI) from aqueous solution by waste mycelium of *A. awamori* is probably due to a combination of two processes: Cr(VI) adsorption by the biomass and its reduction to the less toxic Cr(III). Park *et al.* published that the contact time for Cr(VI) removal is a pH dependent process and at pH 2.0 and an initial concentration of  $25 \text{ mg L}^{-1}$ , Cr(VI) was removed completely by dead *Aspergillus niger* biomass in about 30 h.<sup>31</sup> In the present study, a Cr(VI) removal of 89.26 % was reached at pH 2.0 after 48 h. Based on the performed experiments, pH 2.0 was selected as



the most appropriate pH value for Cr(VI) removal by waste mycelium of *A. awamori* and all of the following experiments were performed at pH 2.0.

#### *Effect of the initial Cr(VI) concentration and the amount of biomass*

The effect of the initial Cr(VI) concentration on the effectiveness of the removal process was studied at three concentrations: 25, 50 and 100 mg L<sup>-1</sup> and the results are shown in Fig. 4.

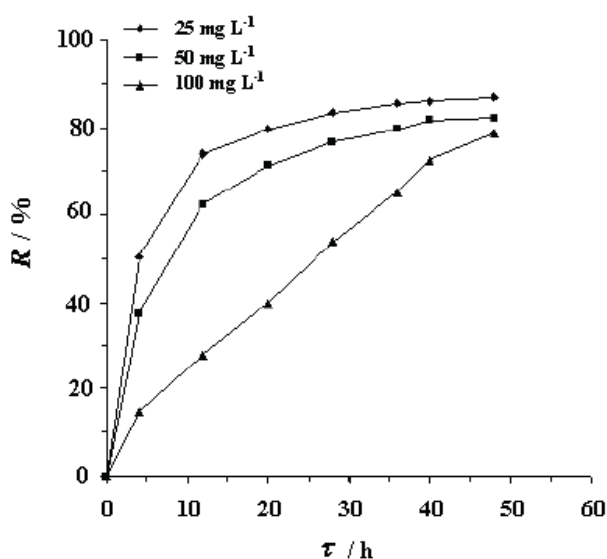


Fig. 4. Effect of initial Cr(VI) concentration on the removal efficiency of waste *A. awamori* biomass ( $V = 100$  mL,  $W = 1$  g L<sup>-1</sup>,  $\tau = 48$  h).

As shown, after a 48-h contact time, 87.0, 82.4 and 78.6 % removal was attained for initial Cr(VI) concentrations of 25, 50 and 100 mg L<sup>-1</sup>, respectively. Thus, lowering the initial Cr(VI) concentration increased the % metal removed for a 48-h contact time. According to Park *et al.*, increasing the initial metal ion concentration prolonged the process for complete Cr(VI) removal.<sup>10,31</sup>

To evaluate the effect of the biomass concentration, experiments were performed in which the biomass concentration was varied from 0.5 to 2 g/100 mL and the results are shown in Fig. 5.

The obtained results indicate that increasing the biomass concentration increased the Cr(VI) removal. This fact may be attributed to the higher number of active groups available for Cr(VI) adsorption and reduction because of the increased amount of *A. awamori* biomass.

#### *Effect of temperature*

Another major factor affecting both processes the adsorption and reduction processes is temperature. The effect of temperature on the Cr(VI) removal pro-

cess by waste biomass of *A. awamori* at three temperatures: 20, 30 and 40 °C was studied and the results are shown in Fig. 6.

Increasing of temperature increased the Cr(VI) removal. According to Witbrodt and Palmer, increased temperature induces and accelerates the rate of redox reactions.<sup>34</sup>

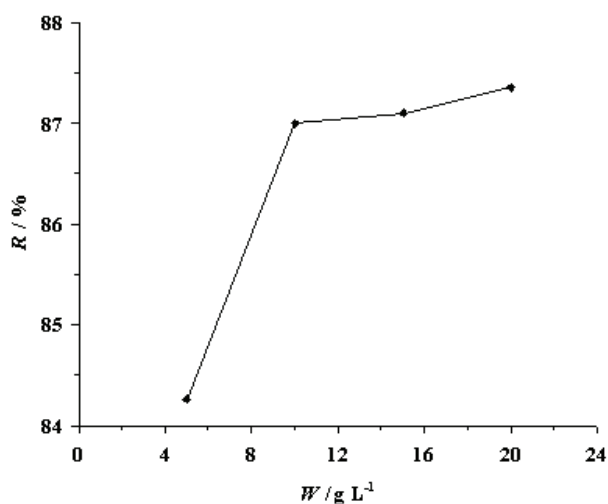


Fig. 5. Effect of biomass concentration on Cr(VI) removal by waste *A. awamori* biomass ( $c_0 = 25 \text{ mg L}^{-1}$ ,  $V = 100 \text{ mL}$ ,  $\tau = 48 \text{ h}$ ).

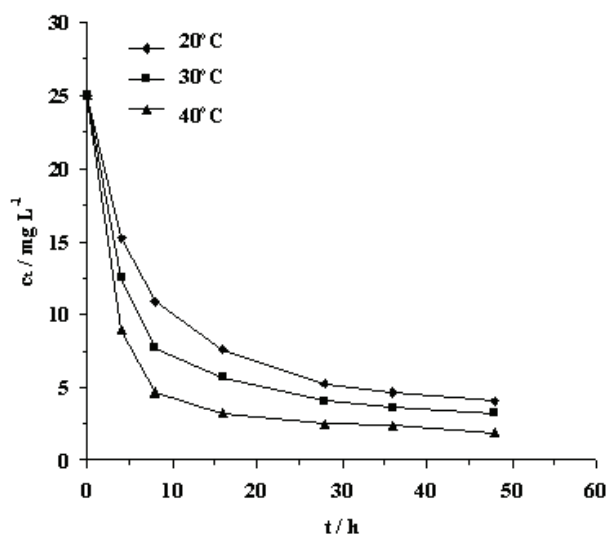


Fig. 6. Effect of temperature on Cr(VI) removal by waste *A. awamori* biomass ( $c_0 = 25 \text{ mg L}^{-1}$ ,  $V = 100 \text{ mL}$ ,  $\tau = 48 \text{ h}$ ).

A pseudo-first order equation with respect to the Cr(VI) concentration was used:

$$\log (c_{\tau} - c_f) = -\frac{kt}{2.303} + \log c_0 \quad (2)$$

where  $c_{\tau}$ ,  $c_f$  and  $c_0$  are the concentration of Cr(VI) at the moment  $t$ , and the final and the initial Cr(VI) concentrations, respectively, and  $k$  is the rate constant.

In order to determine the reaction rate constants,  $\log (c_{\tau} - c_f)$  was plotted vs. time (Fig. 7). The calculated rate constants and the correlation coefficients are shown in Table I.

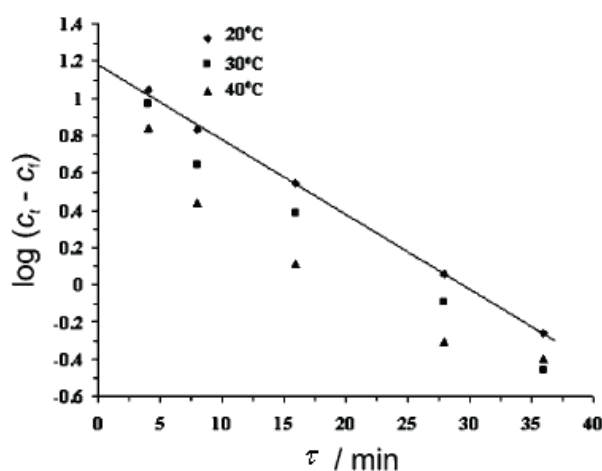


Fig. 7. Pseudo-first kinetic model for Cr(VI) removal by waste *A. awamori* biomass ( $c_0 = 25 \text{ mg L}^{-1}$ ,  $V = 100 \text{ mL}$ ,  $W = 1 \text{ g.L}^{-1}$ ,  $\tau = 48 \text{ h}$ ).

TABLE I. Reaction rate constants and correlation coefficients for Cr(VI) removal at different temperatures

$t / ^\circ\text{C}$	$k / \text{h}^{-1}$	$R$
20	0.0949	0.998
30	0.0956	0.992
37	0.1075	0.987

The activation energy for the Cr(VI) removal process was determined by the Arrhenius Equation. The activation energy of Cr(VI) removal by waste biomass of *A. awamori* was calculated to be  $5.15 \text{ kJ mol}^{-1}$ . Park *et al.* reported an activation energy of  $7.8 \text{ kJ mol}^{-1}$  for the same temperature interval for Cr(VI) removal by dead biomass of *A. niger*, which means that the removal process realized with *A. awamori* will be faster.<sup>31</sup>

#### Mechanism of Cr(VI) removal

In an attempt to explain the mechanism of Cr(VI) removal by waste biomass of *A. awamori*, decreasing Cr(VI) concentrations and increasing Cr(III) concentrations in time were studied. The results are shown in Fig. 8.

As can be seen, the Cr(VI) concentration decreased with time. Cr(III) was not observed in the solution at the beginning of the removal process but it appeared with time. Probably during the first stage, when Cr(III) was absent (first 8 hours), Cr(VI) adsorbed to protonated active groups on the biomass surface. Then, during the second stage, some of the Cr(VI) was easily or spontaneously reduced to Cr(III), as reported by Lytle *et al.*<sup>31</sup>. After 48 h, the concentration of Cr(III) reached  $7.25 \text{ mg L}^{-1}$ . The results obtained demonstrated that both processes, adsorption and reduction, were involved in the removal process and were described well by the two stage Cr(VI) removal mechanism proposed by Park *et al.*<sup>10,31</sup> Taking into consideration the previously obtained experimental data, a model based on a second degree polynomial was chosen to describe the dependences between  $R = f(\text{pH})$  and  $R = f(T)$ , *i.e.*:

$$z = a + bx + cy + dy^2 \quad (3)$$

where  $z$  is the removal efficiency,  $x$  is the pH of the solution and  $y$  is the temperature.

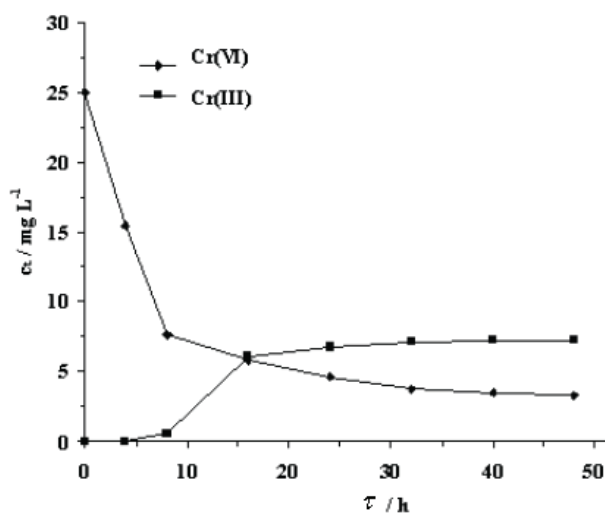


Fig. 8. Time curves of Cr(VI) and Cr(III) concentrations (pH 2.0,  $c_0 = 25 \text{ mg L}^{-1}$ ,  $V = 100 \text{ mL}$ ,  $W = 1 \text{ g L}^{-1}$ ).

The inputs of the model were the temperature and pH, and the output was the removal efficiency. The coefficients  $a$ ,  $b$ ,  $c$  and  $d$  of the postulated polynomial model were determined by means of the D-optimum composition plan.<sup>35</sup> The independent factors were varied as follow:  $1.5 < \text{pH} < 4.0$  and  $20 \text{ }^\circ\text{C} < t < 40 \text{ }^\circ\text{C}$ . The experimental matrix of the DOE, applied for the modelling and optimisation of the  $R$  of Cr(VI) by waste *A. awamori* biomass is shown in Table II.

The mathematical analysis of the results led to a suitable response model according to the following equation:

$$(z / \%) = 59.547 + 23.468\text{pH}^2 + 0.461(t / \text{ }^\circ\text{C}) \quad (6)$$

The values of statistics  $r^2$  and  $r^2_{\text{adjusted}}$  were 0.9891 and 0.9874, respectively. The model is shown in graphical form in Fig. 9.

Maximization of the model allowed the optimal set of parameters for reaching maximum removal to be predicted, *i.e.*,  $R_{\text{max}} = 94.4\%$ , pH 1.5 and  $t = 40\text{ }^\circ\text{C}$ .

TABLE II. Experimental matrix of DOE applied for the modelling and optimisation of the removal of Cr(VI) from aqueous solutions by waste *A. awamori* biomass ( $V = 100\text{ mL}$ ,  $c_0 = 25\text{ mg L}^{-1}$ ,  $\tau = 48\text{ h}$ ,  $W = 1\text{ g.L}^{-1}$ )

No.	pH	$t / ^\circ\text{C}$	$R / \%$	No.	pH	$t / ^\circ\text{C}$	$R / \%$	No.	pH	$t / ^\circ\text{C}$	$R / \%$
1	1.5	20	84.79	11	3.5	25	49.68	21	2.5	35	85.84
2	2	20	83.64	12	4	25	35.88	22	3	35	72.04
3	2.5	20	79.72	13	1.5	30	89.26	23	3.5	35	54.04
4	3	20	65.92	14	2	30	87	24	4	35	40.24
5	3.5	20	47.92	15	2.5	30	83.10	25	1.5	40	94.38
6	4	20	34.12	16	3	30	66.26	26	2	40	92.32
7	1.5	25	86.76	17	3.5	30	51.25	27	2.5	40	88.40
8	2	25	85.40	18	4	30	37.50	28	3	40	74.60
9	2.5	25	81.48	19	1.5	35	91.84	29	3.5	40	59.28
10	3	25	67.68	20	2	35	89.76	30	4	40	42.80

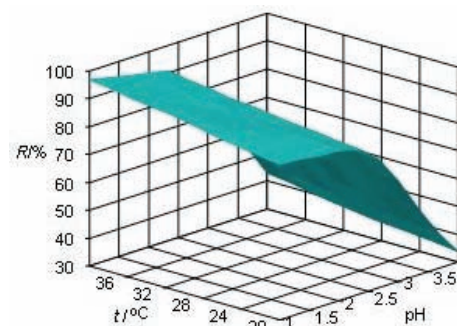


Fig. 9. Removal efficiency of Cr(VI) by waste *A. awamori* biomass as a function of pH and temperature ( $c_0 = 25\text{ mg L}^{-1}$ ,  $\tau = 48\text{ h}$ ).

Usually for comparing the biosorption potential of various biosorbents, the sorption capacity of the biomaterial, expressed as mg or mol metal ion adsorbed per gram of biomass, is used. The results obtained in the present study and those published by Park *et al.*<sup>10,31</sup>. and Lytle *et al.*<sup>32</sup>. unambiguously proved that Cr(VI) removal from aqueous solutions is not pure biosorption, but rather a combination of biosorption and reduction. For this reason, it was decided to compare the studied biosorbent with other Cr(VI) biosorbents based on removal capacity not on specific sorption capacity (Table III). As can be seen, waste mycelium of *A. awamori* is competitive with other fungal biosorbents, because using an about five times shorter contact time, relatively high Cr(VI) removal was reached. For the same contact time, only the removal capacity of the biosorbent from *Rhizopus oryzae* exceeded the removal capacity of waste mycelium of *A. awamori*. The major advantage of *A. awamori* mycelium over other fungal

biosorbents is not only the high Cr(VI) removal capacity and relatively short contact time, but also its low cost, because it is a waste product from enzyme production. Most of the other published Cr(VI) fungal biosorbents were specially cultivated and then killed for preparation of the biosorbent, which inevitably increases the total costs of the removal process, especially if large amounts of polluted solutions are to be treated. Real industrial wastewaters are multicomponent systems containing various organic and inorganic compounds that can negatively influence the metal removal process.<sup>36</sup> According to Gadd, one of the major disadvantages of the currently published research in the sphere of biosorption is the lack of information concerning the applicability of the results in real industrial effluents and scale-up of the removal process to the industrial scale.<sup>37</sup> For these reasons, the present results for the removal of Cr(VI) from aqueous solutions by waste mycelium of *A. awamori* cannot be applied directly to real wastewaters and additional experiments are a necessity.

TABLE III. Cr(VI) removal capacity of various fungal biosorbents (pH 2.0,  $W = 5 \text{ g L}^{-1}$ )

Biosorbent	$c_0 / \text{mg L}^{-1}$	$\tau / \text{h}$	Cr(VI) Removal, %	Reference
<i>Aspergillus awamori</i>	50	48	85.46	Current study
<i>Rhizopus oryzae</i>	50	48	100	22
<i>Aspergillus niger</i>	50	218	100	22
<i>Penicillium chrysogenum</i>	50	218	100	22
<i>Saccharomyces cerevisiae</i>	50	254	100	22
<i>Aspergillus sp.</i>	500	24	36	30

### CONCLUSIONS

It was demonstrated by FTIR analysis and chemical treatment of the biosorbent that amino groups from the major fungal wall constituents, chitin and chitosan, played a key role in the Cr(VI) removal process. The effectiveness of the removal process depended mainly on pH followed by temperature, amount of biomass and initial Cr(VI) concentration. The process can be explained by an indirect two-stage mechanism involving first an adsorption stage and then a reducing stage. The activation energy of Cr(VI) removal by waste biomass of *A. awamori* was lower than that of the same process based using dead biomass from *A. niger*. The removal process could be described by a second-degree polynomial and the optimal process parameters for attaining an  $R_{\text{max}}$  of 94.4 % in 48 h were predicted (pH 1.5 and  $t = 40 \text{ }^\circ\text{C}$ ). Based on the performed experiments and the obtained results, it can be summarized that waste mycelium from the industrial xylanase-producing strain *A. awamori* is a prospective, competitive and low-cost biomaterial with possible application in Cr(VI) removal. Further experiments for application of the current results and waste mycelium of *A. awamori* for Cr(VI) removal from real industrial wastewaters and a study of the process in a column bioreactor are in progress.

*Acknowledgment.* The present study was financially supported by the NSFB project GAMA DO 02-70 11/12/2009 of the Bulgarian Ministry of Education.

## ИЗВОД

УКЛАЊАЊЕ ШЕСТОВАЛНЕТНОГ ХРОМА ОТПАДНИМ МИЦЕЛИЈУМОМ  
ГЉИВЕ *Aspergillus awamori*VELIZAR K. GOCHEV<sup>1</sup>, ZDRAVKA I. VELKOVA<sup>2</sup> и MARGARITA S. STOYTCHIEVA<sup>3</sup>

<sup>1</sup>Department of Biochemistry and Microbiology, Paisii Hilendarski University of Plovdiv, Tzar Asen Str. 24, Plovdiv 4000, <sup>2</sup>Department of Inorganic and Physical Chemistry, University of Food Technologies, Maritza Boulevard 26, Plovdiv 4000, Bulgaria и <sup>3</sup>University of Baja California, Mexicali, Mexico

У овом раду је процењен потенцијал уклањања Cr(VI) отпадним мицелијумом индустријског соја *Aspergillus awamori* који се користи за производњу ксиланазе. FTIR Анализом је одређено да су аминок групе основних састојака ћелијског зида гљиве, цитина и цитозана, играле кључну улогу у процесу везивања метала. Такође је испитиван и утицај рН, почетне концентрације јона, температуре и количине биомасе на процес уклањања. Механизам уклањања Cr(VI) гљивом *A. awamori* може бити објашњен процесом у два ступња, који се састоји од почетног адсорпционог ступања за којим следи ступањ редукције. Процес уклањања описан је полиномом другог реда, а утврђени су и оптимални параметри за постизање  $R_{\max}$  од 94,4 % за 48 h, тј. рН 1,5 и  $t = 40$  °C. Предложена је обећавајућа могућност употребе отпадног индустријског мицелијума гљиве *A. awamori* као јефтиног агенса за уклањање Cr(VI) са економског и еколошког гледишта.

(Примљено 31. марта, ревидирано 15. јула 2009)

## REFERENCES

1. M. Costa, *Toxicol. Appl. Pharmacol.* **188** (2003) 1
2. D. Park, Y. S. Yun, J. M. Park, *Ind. Eng. Chem. Res.* **45** (2006) 2405
3. C. Pellerin, S. M. Booker, *Environ. Health Persp.* **108** (2000) 402
4. M. V. Subbaiah, S. Kalyani, G. S. Reddy, V. M. Boddu, A. Krishnaiah, *E.-J. Chem.* **5** (2008) 499
5. K. Vijayaraghavan, Y. S. Yun, *Biotechnol. Adv.* **26** (2008) 266
6. J. Wang, C. Chen, *Biotechnol. Adv.* **24** (2006) 427
7. V. K. Gupta, A. K. Shrivastava, N. Jain, *Water Res.* **35** (2001) 4075
8. D. Park, Y. S. Yun, H. Y. Cho, J. M. Park, *Ind. Eng. Chem. Res.* **43** (2004) 8226
9. D. Park, Y. S. Yun, J. M. Park, *Environ. Sci. Technol.* **3** (2004) 4860
10. D. Park, Y. S. Yun, J. M. Park, *J. Microbiol. Biotechnol.* **15** (2005) 786
11. S. R. Bai, T. E. Abraham, *Water Res.* **36** (2002) 1224
12. K. K. Deepa, M. Sathishkumar, A. R. Binuprya, G. S. Murugesu, K. Swaminathan, S. E. Yun, *Chemosphere* (2006) 833
13. R. Kumar, N. R. Bishnoi, G. Bishnoi, K. Bishnoi, *Chem. Eng. J.* **135** (2008) 202
14. J.-G. S. Mala, B. U. Nair, R. Puvanakrishnan, *J. Gen. Appl. Microbiol.* **52** (2006) 179
15. D. Park, Y. S. Yun, J. H. Jo, J. M. Park, *Ind. Eng. Chem. Res.* **45** (2006) 5059
16. Y. Sağ, *Separ. Purif. Res.* **30** (2001) 1
17. S. Srivastava, I. S. Thakur, *Curr. Microbiol.* **53** (2006) 232
18. J. M. Tobin, C. White, G. M. Gadd, *J. Ind. Microbiol.* **13**(1994) 126
19. S. Tunal, I. Kiran, T. Akar, *Mineral Eng.* **18** (2005) 681

20. L. Chung, C. Hongzhang, L. Zuohu, *Process Biochem.* **39** (2004) 1
21. Y. Khambhaty, K. Mody, S. Basha, B. Jha, *Environ. Eng. Sci.* **26** (2009) 1
22. D. Park, Y. S. Yun, J. M. Park, *Proc. Biochem.* **40** (2005) 2559
23. S. M. Siegel, M. Galun, B. Z. Siegel, *Water Air Soil Pollut.* **53** (1990) 335
24. E. Fourest, J.-C. Roux, *Appl. Microbiol. Biotechnol.* **37**(1992) 399
25. R. Gulati, R. K. Saxena, R. Gupta, *World J. Microbiol. Biotechnol.* **18** (2002) 397
26. A. Atev, S. Ilieva, BG Patent No. 94361 (1991)
27. S. Ilieva, N. Bakalova, S. Petrova, A. Atev, *Biotechnol. Biotechnol. Eq.* **16** (2002) 98
28. D. Park, Y. S. Yun, J. M. Park, *Chemosphere* **60** (2005) 1356
29. A. D. Eaton, L. S. Clesceri, A. E. Greenberg, *Standard methods for the examination of water and waste water*, American Health Association (APHA), AWWA, Washington DC, 1995, p. 4
30. M. Sen, M. G. Dastidar, *Iran. J. Environ. Health Sci. Eng.* **4** (2007) 9
31. D. Park, Y. S. Yun, J. H. Jo, J. M. Park, *Water Res.* **39** (2005) 533
32. C. M. Lytle, F. W. Lytle, N. Yang, J. H. Qian, D. Hansen, A. Zayed, N. Terry, *Environ. Sci. Technol.* **32** (1998) 3087
33. L. Dupont, E. Guillon, *Environ. Sci. Technol.* **37** (2003) 4235.
34. P. R. Wittbrodt, C. D. Palmer, *Environ. Sci. Technol.* **30** (1996) 2470
35. V. V. Fedorov, *Theory of optimal experiments*, Academic Press, New York, 1972, p. 12
36. V. Prigione, M. Zerlottin, D. Refosco, V. Tigini, A. Anastasi, G. C. Varese, *Biores. Technol.* **100** (2009) 2770
37. G. M. Gadd, *J. Chem. Technol. Biotechnol.* **84** (2009) 13.





*J. Serb. Chem. Soc.* 75 (4) 565–573 (2010)  
JSCS–3988

## Removal of organochlorine pesticides from water using virgin and regenerated granular activated carbon

MIRJANA B. NINKOVIĆ<sup>1</sup>, RADA D. PETROVIĆ<sup>2\*</sup> and MILA D. LAUŠEVIĆ<sup>2#</sup>

<sup>1</sup>Belgrade Waterworks and Sewerage, Deligradska 28, 11000 Belgrade and <sup>2</sup>Faculty of Technology and Metallurgy, Karnegijeva 4, 11000 Belgrade, Serbia

(Received 15 June, revised 3 September 2009)

**Abstract:** Public water systems use granular activated carbon in order to eliminate pesticides. After saturation, the used activated carbon is regenerated and reused in order to reduce the costs of water production and minimize waste. In this study, the adsorption of 10 different chlorinated pesticides from water using columns packed with commercial virgin and regenerated granular activated carbon was simulated in order to compare their adsorption capacities for different chlorinated pesticides. The breakthrough curves showed that chlorinated pesticides from the group of hexachlorocyclohexane (HCH) were poorly adsorbed, followed by cyclodiens as averagely adsorbed and the derivatives of halogenated aromatic hydrocarbons (DDT) as strongly adsorbed. However, the adsorption capacity of regenerated granular activated carbon was considerably lower for tested pesticides compared to the virgin granular carbon. In addition, rinsing of the pesticides after the saturation point is a far more efficient process on regenerated carbon.

**Keywords:** granular activated carbon; adsorption; organochlorine pesticides; gas chromatography.

### INTRODUCTION

Pesticides are artificially synthesized, toxic bioaccumulative agents. The on-growing and uncontrolled use of pesticides to fight pests and improve agricultural production constitutes a risk for water quality. Thus, pesticides have been detected by monitoring surface and underground waters. According to the European Union Directives and Regulations for drinking water hygiene,<sup>1</sup> the maximum allowed concentration of total pesticides is 0.5  $\mu\text{g dm}^{-3}$ . Different types of pesticides can be found in water. The most frequently found pesticides are derivatives of urea, pyridazinone, phenoxy acetic acid, tryazin and the group of chlo-

\* Corresponding author. E-mail: radaab@tmf.bg.ac.rs

# Serbian Chemical Society member.

doi: 10.2298/JSC090615014N

rinated pesticides. Chlorinated pesticides are divided according to their chemical structure into 3 basic groups: derivatives of DDT, hexachlorocyclohexanes (HCH) and aldrin. Derivatives of DDT are halogenated aromatic hydrocarbons, while hexachlorocyclohexanes (HCH) and derivatives of aldrin are halogenated alicyclic hydrocarbons. The main characteristic of halogenated hydrocarbons is their huge chemical stability and consequential persistence in water and soil. The second important characteristic of chlorinated pesticides is their very poor solubility in water, due to their lipophilic character.

Pesticides can be eliminated from water in different ways, most frequently by adsorption on granular activated carbon (GAC) and/or by ozonization.<sup>2</sup> When GAC is saturated, it is usually regenerated and reused. In the majority of cases, spent GAC is thermally regenerated either on-site or transported to a thermal regeneration facility. During regeneration, the contaminants are transformed into less toxic byproducts and the sorption capacity of the carbon is re-established; thus, increasing the useful life of the GAC is increased and the costs of water treatment are reduced.

Many studies concerning the adsorption capacities of selected types of pesticides on commercial activated carbons, as well as on other carbon materials, have been published recently.<sup>3-5</sup> Gerard and co-workers<sup>3</sup> examined the adsorption of diuron, MCPA, atrazine and chlorydazon on Chemviron's coal-based commercial granular activated carbon. They came to the conclusion that the strongest adsorption was achieved for diuron and the weakest for MPCA. A study of the impact of temperature and size of the molecule on adsorption on commercial activated carbon<sup>4</sup> showed that the adsorption at higher temperatures was enhanced and smaller molecules were better adsorbed. Martin-Gullon<sup>5</sup> compared the adsorption of atrazine on commercial activated carbon Norit GAC 1240 and carbon fibers Donacarbo and found that the efficiency was several times higher on the carbon fibers.

The aim of the present study was to compare the adsorption capacities and removal efficiency of virgin and regenerated granular activated carbon for different chlorinated pesticides. The test columns used in the experiments were filled with virgin commercial granular activated carbon as well as with regenerated activated carbon. Both GAC materials are used in the public water system that supplies Belgrade with drinking water.

## EXPERIMENTAL

### *Materials*

Commercial activated carbon Trayal K-81/B was used in all experiments, as virgin or regenerated. Both GAC materials are used in the public water supply system in Belgrade and were taken directly from the filters of the plant for the preparation of drinking water. The characteristics of the virgin and regenerated GAC are given in Table I.

All organic solvents were of chromatographic purity as supplied by JT Baker and Fluka. Water of high quality ( $0.054 \mu\text{S cm}^{-1}$ ) was obtained by deionization through a Milli-Q system (Millipore water). The mixture of pesticides was supplied by Supelco. The main physical and chemical data of the analyzed pesticides are given in Table II.

TABLE I. Characteristics of the employed virgin and regenerated GAC Trayal K-81/B

Parameter	Carbon samples	
	Virgin Trayal K-81/B	Regenerated Trayal K-81/B
Total pore volume, $\text{cm}^3 \text{g}^{-1}$	1.0	0.8
Specific surface BET, $\text{m}^2 \text{g}^{-1}$	1237	950
Micropore volume, $\text{cm}^3 \text{g}^{-1}$	0.50	0.39
Iodine number, $\text{mg g}^{-1}$	1239	998
Methylene Blue index, $\text{cm}^3$	22	17
Apparent density, $\text{kg m}^{-3}$	462	492
Granule size, mm	Granule size distribution, %	
> 1.6 mm	4.1	4.0
0.8 – 1.6 mm	91.5	90.8
< 0.8 mm	4.4	5.2

TABLE II. Main physical and chemical data of the tested pesticides

Group	Pesticide	Formula	$M_r$ $\text{g mol}^{-1}$	Solubility in water (25 °C) $\text{mg dm}^{-3}$	$\log K_{ow}$ <sup>a</sup>	Maximum limit of concentration $\mu\text{g dm}^{-3}$
Hexachloro- cyclohexane	$\alpha$ -HCH	$\text{C}_6\text{H}_6\text{Cl}_6$	287.86	2.0	3.08	n.r. <sup>b</sup>
	$\beta$ -HCH	$\text{C}_6\text{H}_6\text{Cl}_6$	287.86	1.5	3.78	n.r.
	$\gamma$ -HCH	$\text{C}_6\text{H}_6\text{Cl}_6$	287.86	10	2.67	0.1
Chlorinated alicyclic hydrocarbon	$\alpha$ -endosulfan	$\text{C}_9\text{H}_6\text{Cl}_6\text{O}_3\text{S}$	403.82	0.32	3.83	n.r.
	$\beta$ -endosulfan	$\text{C}_9\text{H}_6\text{Cl}_6\text{O}_3\text{S}$	403.82	0.33	3.62	n.r.
	Heptachlor epoxide	$\text{C}_{10}\text{H}_5\text{Cl}_7$	369.82	0.056	5.44	0.03
Aromatic chlorinated hydrocarbon	Dieldrin	$\text{C}_{12}\text{H}_8\text{Cl}_6\text{O}$	377.87	0.19	3.69	0.03
	4,4'-DDT	$\text{C}_{14}\text{H}_9\text{Cl}_5$	354.49	0.025	6.91	0.1
	4,4'-DDD	$\text{C}_{14}\text{H}_{10}\text{Cl}_4$	320.05	0.090	6.02	n.r.
	Methoxychlor	$\text{C}_6\text{H}_{15}\text{Cl}_3$	345.65	0.045	4.68	n.r.

<sup>a</sup>Partition coefficient; <sup>b</sup>not recommended

### Methods

On column experiments were based on the use of test columns<sup>6</sup> filled with virgin or regenerated GAC, in order to determine their adsorption capacities for pesticides. A mixture of pesticides, listed in Table II, was spiked into Millipore water to obtain a concentration of  $2 \mu\text{g dm}^{-3}$  of each pesticide and passed through the columns at room temperature using a flow rate of  $0.15 \text{ cm}^3 \text{ min}^{-1}$ . The experimental conditions on the test columns are given in Table III.

Preconcentration of the pesticides from the effluent water was achieved by solid phase<sup>7,8</sup> extractions on Chromabond cartridges C8 (500 mg,  $6 \text{ cm}^3$ ). The cartridges were conditioned with  $3 \text{ cm}^3$  of methanol and rinsed with  $2 \text{ cm}^3$  of Millipore water. Using a vacuum manifold, the effluent water was drawn through the cartridge at a flow rate of  $5 \text{ cm}^3 \text{ min}^{-1}$ . Subsequently, the column was rinsed with  $1 \text{ cm}^3$  of Millipore water and the pesticides were eluted

with 1.5 cm<sup>3</sup> of solvent mixture, hexane:diethyl ether. The solution was evaporated and then reconstructed to 1 cm<sup>3</sup>.

TABLE III. Experimental conditions on the test columns

Carbon sample	<i>m</i> / g	Bed height mm	Bed volume cm <sup>3</sup>	Influent flow cm <sup>3</sup> min <sup>-1</sup>	Contact time, min
Virgin Trayal GAC K-81/B	0.400	7	0.95	0.15	6.5
Regenerated Trayal GAC K-81/B	0.400	6	0.90	0.15	6.5

An Agilent gas chromatograph 6890, equipped with an electron capture detector,<sup>9,10</sup> was used for quantification of the pesticides. The chromatographic separation of pesticides was realized on a capillary column (30 m×0.32 mm) coated with 5 % diphenylmethylsiloxane film, 0.25 μm thick. High quality nitrogen was used as the supporting (1.8 cm<sup>3</sup> min<sup>-1</sup>) and the make up gas (30 cm<sup>3</sup> min<sup>-1</sup>). The injector and detector temperatures were 250 and 320 °C, respectively. The sample splitless injection volume was 1 μl. The initial column temperature of 100 °C was maintained for 2 min, then programmed to 160 °C at a heating rate of 15 °C min<sup>-1</sup> and held for 10 min at 160 °C. Subsequently, the temperature was raised to 220 °C at a heating rate of 5 °C min<sup>-1</sup>, held for 2 min and the raised to the final temperature of 270 °C at a heating rate of 10 °C min<sup>-1</sup>.

#### RESULTS AND DISCUSSION

The analyzed pesticides (Table II) were divided in three groups according to their chemical properties and structure. The concentrations of the effluent solutions (*c<sub>e</sub>*) from the test columns for each group of pesticides are presented in Figs. 1–3, in which breakthrough curves are apparent.

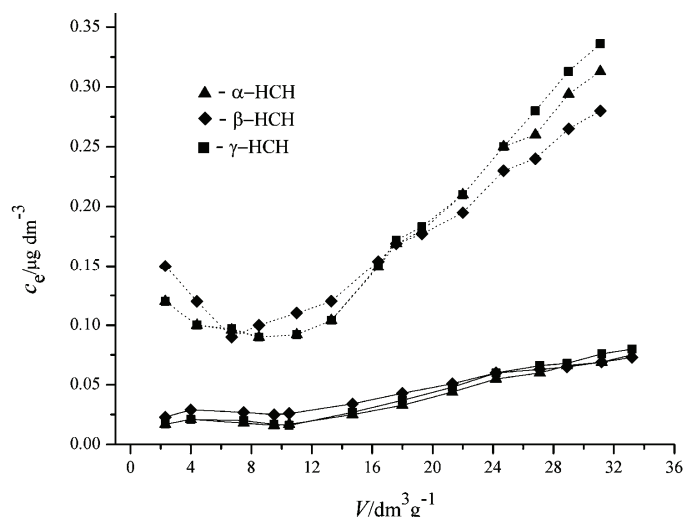


Fig. 1. Breakthrough curves for the chlorinated cyclohexane pesticide mixture in Millipore water (*c<sub>e</sub>* – pesticide concentration in the effluent, *V* – effluent volume per unit mass of GAC) on virgin (—) and regenerated (---) GAC. Pesticide concentration in the influent was 2 μg dm<sup>-3</sup>.

The starting concentration ( $2 \mu\text{g dm}^{-3}$ ) of each pesticide was thoroughly reduced to approximately  $0.02 \mu\text{g dm}^{-3}$  for all pesticides tested on the column with virgin GAC at saturation point, confirming that the adsorption on activated carbon is a very efficient technique for the removal of pesticides from water. However, it is not a destructive process. The pollutants pass from one medium (water) to another (carbon), thus producing a new pollution problem. When the columns are saturated, rinsing of pollutants commences, as is visible in Figs. 1–3. The adsorption efficiency depends on both the surface properties and porosity of the GAC as well as on the chemical assets and geometry of the pesticides. The most soluble pesticides (HCH) are very efficiently rinsed from the saturated column containing virgin GAC. However, derivatives of DDT, due to their highest partition coefficient (Table II), were firmly bound to the virgin GAC column with minor rinsing observed during the experiment, predominantly for the methoxychlor derivative. Chlorinated alicyclic hydrocarbons showed intermediate behavior compared to the HCH and DDT derivatives. Thus, pesticide solubility in water is in reverse correlation to the adsorption affinity of the activated carbon.

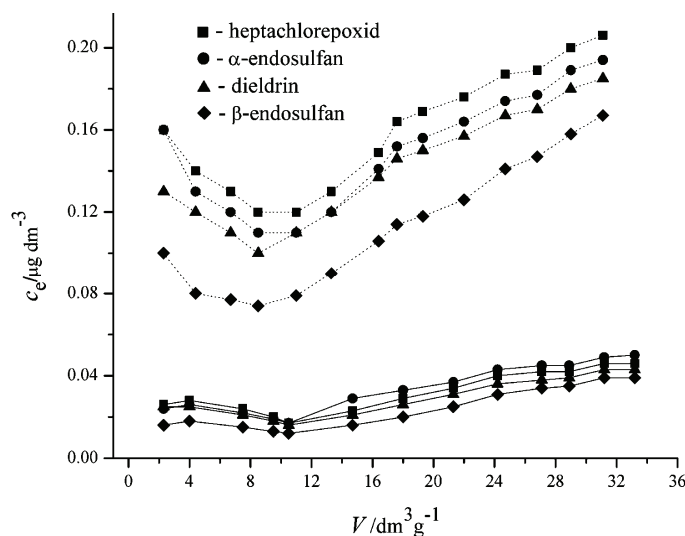


Fig. 2. Breakthrough curves for the chlorinated alicyclic hydrocarbon pesticide mixture in Millipore water ( $c_e$  – pesticide concentration in the effluent,  $V$  – effluent volume per unit mass of GAC) on virgin (—) and regenerated (---) GAC. Pesticide concentration in the influent was  $2 \mu\text{g dm}^{-3}$ .

Based on the appearances of the breakthrough curves displayed in Figs. 1–3, it is evident that both virgin and regenerated activated carbon exhibit similar adsorption affinities towards the examined pesticide: highest for DDT derivatives and lowest for HCH. However, the concentration of the pesticides in the effluent from the regenerated GAC column was several times higher compared to the

effluent from the virgin GAC. The adsorption properties of regenerated GAC could be adversely affected by incomplete carbon regeneration and by surface deterioration during heating. Table I clearly shows the deterioration of surface properties of GAC after regeneration. The specific surface area, total pore volume<sup>11</sup> and micropore volume were reduced by approximately 20 %. Consequently, the iodine number and Methylene Blue index were reduced in the same proportion. These results are consistent with other studies on regeneration of GAC using a variety of regeneration methods.<sup>12-14</sup>

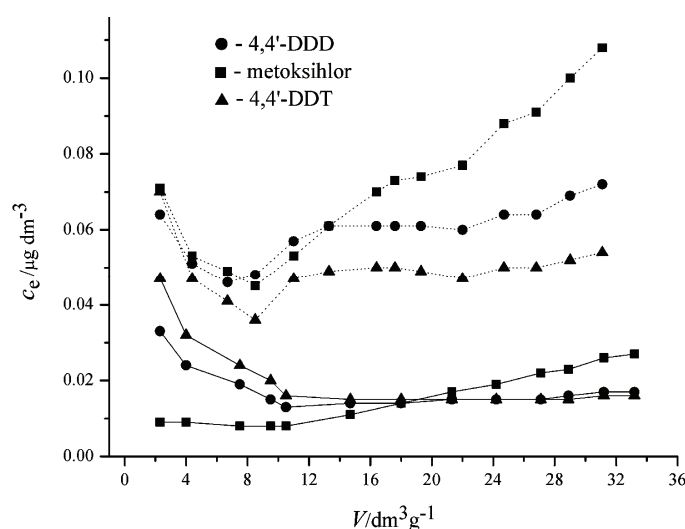


Fig. 3. Breakthrough curves for the aromatic chlorinated hydrocarbon pesticide mixture in Millipore water ( $c_e$  – pesticide concentration in the effluent,  $V$  – effluent volume per unit mass of GAC) on virgin (—) and regenerated (- - -) GAC. Pesticide concentration in the influent was  $2 \mu\text{g dm}^{-3}$ .

The adsorption of the tested pesticides on the regenerated GAC was affected by regeneration. The differential factors of the pesticides (weighted against the firmly adsorbed 4,4'-DDT) on virgin and regenerated activated carbon, after transmitting  $30 \text{ dm}^3 \text{ g}^{-1}$  of the standard organochlorine pesticide mixture ( $2 \mu\text{g dm}^{-3}$ ) are listed in Table IV. The differential factors for each pesticide adsorbed on virgin activated carbon were higher than these on regenerated carbon. According to Gerard,<sup>3</sup> compounds with a differential factor less than 0.40 are poorly adsorbed, compounds with a differential factor in range from 0.40 to 0.80 are averagely adsorbed, while compounds with a differential factor higher than 0.80 are considered as strongly adsorbed on GAC. Thus, 4,4'-DDT and 4,4'-DDD are strongly adsorbed pesticides, methoxychlor and  $\beta$ -endosulfan are averagely adsorbed pesticides and  $\alpha$ -HCH,  $\beta$ -HCH,  $\gamma$ -HCH,  $\alpha$ -endosulfan, heptachlorepoxide and dieldrin are considered as poorly adsorbed pesticides on virgin GAC. After

regeneration of GAC, 4,4'-DDT remained the only strongly adsorbed pesticide, methoxychlor and 4,4'-DDD averagely but all the remaining pesticides were poorly adsorbed. The discrepancy between the differential factors before and after regeneration was 20 to 30 %.

TABLE IV. Pesticide differential factors compared to 4,4'-DDT. Effluent concentration ratio through regenerated ( $c_r$ ) and virgin ( $c_v$ ) GAC

Pesticide	Differential factor for virgin GAC	Differential factor for regenerated GAC	$c_r/c_v$
$\alpha$ -HCH	0.23	0.17	4.5
$\beta$ -HCH	0.23	0.19	4.1
$\gamma$ -HCH	0.21	0.16	4.4
$\alpha$ -endosulfan	0.33	0.28	4.0
$\beta$ -endosulfan	0.41	0.32	4.3
Heptachlorepoxyde	0.35	0.26	4.4
Dieldrin	0.37	0.29	4.3
4,4'-DDT	1	1	3.3
4,4'-DDD	0.94	0.75	4.2
Methoxychlor	0.62	0.50	4.2

The effluent concentration ratio after passing  $30 \text{ dm}^3 \text{ g}^{-1}$  of standard pesticide mixture through the test columns with regenerated ( $c_r$ ) and virgin GAC ( $c_v$ ) are also given in Table IV. The influent flow was adequately adjusted so that the contact time of 6.5 min was sufficient for adsorption of the organic compounds on GAC according to the suggestions of the U.S. Environmental Protection Agency. The astonishing result was that the concentrations of pesticides in the effluent from the column with regenerated GAC were 3.3 (for DDT) up to 4.5 (for  $\alpha$ -HCH) times higher, depending mostly on the rinsing efficiency.

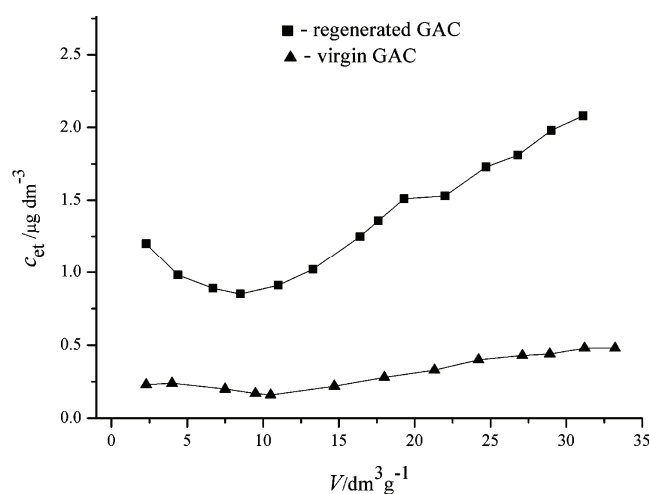


Fig. 4. Cumulative breakthrough curves for pesticides ( $c_{et}$  – total pesticide concentration in the effluent,  $V$  – effluent volume per unit mass of GAC) on virgin and regenerated GAC. Total pesticide concentration in the influent is  $20 \mu\text{g dm}^{-3}$ .

The cumulative breakthrough curves for the total pesticides are shown in Fig. 4, which clearly indicates that the regeneration process adversely affected the adsorption affinity of GAC towards the tested pesticides by limiting the sorption sites and the quantity of pesticides that could be absorbed. In this respect, this study indicates the potential risk of reusing regenerated GAC.

#### CONCLUSIONS

From the results obtained on the test columns with virgin and regenerated granular activated carbon, it is possible to compare the adsorption affinity towards selected pesticides. Activated carbon adsorption is an efficient treatment for the majority of the studied pesticides. The concentration in the effluent was reduced to 1 % of initial concentration for all pesticides at the breakthrough point on the column with virgin carbon. Derivatives of DDT were the firmly adsorbed on activated carbon, derivatives of aldrine were moderately adsorbed, while the hexachlorocyclohexanes (HCH) were poorly bound and labile to rinsing after saturation.

The adsorption capacity of regenerated carbon was reduced during the conventional heating process due to blockage of the porous structure, the reduced number of active sites and, probably, incomplete removal of the adsorbed matter. Differential factors for all tested pesticides were 20 to 30 % lower and rinsing of all pesticides after saturation into the effluent was several times higher from regenerated GAC as compared to virgin GAC. The activated carbon used in the present experiments was regenerated a few times, whereby the adsorption properties decreased gradually with subsequent regeneration cycles. Therefore, this study indicates to a potential risk of reusing regenerated carbon.

*Acknowledgment.* The authors acknowledge the financial support of the Ministry of Science and Technological Development of the Republic of Serbia (Project No. 142002).

#### ИЗВОД

#### УКЛАЊАЊЕ ПЕСТИЦИДА ИЗ ВОДЕ НА ГРАНУЛИСАНОМ АКТИВНОМ УГЉУ

МИРЈАНА Б. НИНКОВИЋ<sup>1</sup>, РАДА Д. ПЕТРОВИЋ<sup>2</sup> и МИЛА Д. ЛАУШЕВИЋ<sup>2</sup>

<sup>1</sup>Београдски водовод и канализација, Делиградска 28, 11000 Београд и

<sup>2</sup>Технолошко-механички факултет, Карнегијева 4, 11000 Београд

Постројења за припрему воде у многим земљама користе гранулисани активни угљ за уклањање остатака пестицида. Уобичајено је да се активни угљ регенерише и поново користи да би се смањили трошкови производње воде за пиће и да би се смањила количина отпада. У овом раду смо испитивали адсорпцију органохлорних пестицида из воденог раствора 10 различитих пестицида на колонама испуњеним комерцијалним свежим и регенерисаним гранулисаним активним угљем. Утврђене су адсорпционе способности гранулисаниог угља за различите пестициде. Криве пробоја на овим колонама показују да се органохлорни пестициди из групе хексахлороциклохексана најслабије адсорбују, затим хлоровани циклодиени, а најјаче пестициди из групе ДДТ. Утврђено је да је адсорпциони капа-



цитет регенерисаног активног угља знатно мањи од адсорпционог капацитета свежег активног угља, а испирање пестицида је много ефикасније после регенерације.

(Примљено 15. јуна, ревидирано 3. септембра 2009)

## REFERENCES

1. Council Directive 98/83/EC, Official Journal L330, 05/12/1998, pp. 0032–0054
2. M. P. Ormad, N. Miguel, A. Claver, J. M. Matesanz, J. L. Ovelleiro, *Chemosphere* **71** (2008) 97
3. M. C. Gerard, J. P. Barthelemy, *Biotechnol. Agron. Soc. Environ.* **7** (2003) 79
4. B. Schreiber, T. Brinkmann, V. Schmalz, E. Worch, *Water Res.* **39** (2005) 3449
5. J. Martin-Gullon, R. Font, *Water Res.* **35** (2001) 516
6. J. C. Crittenden, K. Vaitheeswaran, D. W. Hand, E. W. Howe, E. M. Aieta, C. H. Tate, M. J. McGuire, M. K. Davis, *Water Res.* **27** (1993) 715
7. L. Ruiz-Gil, R. Romero-Gonzales, A. Garrido Frenich, J. L. Martinez Vidal, *J. Sep. Sci.* **31** (2008) 151
8. I. Vassilakis, D. Tsipi, M. Scoullou, *J. Chromatogr. A* **823** (1998) 49
9. C. Aguilar, F. Borull, R. M. Marce, *J. Chromatogr. A* **771** (1997) 221
10. a) L. S. Clescerl, A. E. Greenberg, A. D. Eaton, *Standard methods for the examination of water and wastewater*, 20<sup>th</sup> ed., American Water Works Association, 1998; b) C. Aguilar, F. Borull, R. M. Marce, *J. Chromatogr. A* **771** (1997) 221
11. D. R. U. Knappe, V. L. Snoeyink, P. Roche, M. J. Prados, M. Bourbigot, *Water Res.* **31** (1997) 2899
12. F. K. Yuen, B. H. Hameed, *Adv. Colloid Interface Sci.* **149** (2009) 19
13. C. Liang, Y.-T. Lin, W.-H. Shin, *J. Hazardous Mat.* **168** (2009) 187
14. S. G. Huling, E. Kan, C. Wingo, *Appl. Catal. B* **89** (2009) 651.





*J. Serb. Chem. Soc.* 75 (4) 575–586 (2010)  
JSCS–3989

## Purification of waters and elimination of organochloric insecticides by means of active coal

DRAGAN MARINOVIĆ<sup>1\*</sup>, MARINA STOJANOVIĆ<sup>2</sup> and DANILO POPOVIĆ<sup>2</sup>

<sup>1</sup>Public Health Institute, Slobodana Penezića 16, 36000 Kraljevo and <sup>2</sup>Faculty of Occupational Safety, University of Niš, Čarnojevića 10a, 18 000 Niš, Serbia

(Received 2 June, revised 7 October 2009)

**Abstract:** Pollution of water and the determination of the degree of its pollution with numerous physical, chemical and biological pollutants have become general, ever increasing social and health related problems. Within this study, the concentrations of some most frequently used organochloric insecticides (OCI):  $\alpha$ -hexachlorocyclohexane ( $\alpha$ -HCH),  $\gamma$ -hexachlorocyclohexane (lindane), heptachlor, aldrin, dieldrin, endrin, dichlorodiphenyl trichlorethane (DDT) were investigated. OCI are highly toxic substances for the human population and their effective elimination from the environment is of paramount interest. To determine the OCI concentration in water samples, the EPA–608 method and the liquid–liquid extraction principle were applied. A procedure for OCI elimination was realized by passing the water over four columns filled with various active coals: KRF, K-81/B, NORIT ROW-0.8 and AQUA SORB CS. These active coals are carbonized coconut shells activated by different procedures. The obtained results indicated that best purification of potable and waste water achieved using a column with Norit Row-0.8 filling. Research proved that small quantities of OCI can also be effectively removed using a Norit Row-0.8 active coal filled column, without altering the organoleptic properties of the water, which meets the requirements of water purification processes.

**Keywords:** potable (drinking) water; waste water; organochloric insecticides; waters purification; active coal; gas chromatography.

### INTRODUCTION

The process of environment pollution was particularly initiated with the modern development of agriculture, cattle breeding and industry. The consequences thereof have become increasingly visible in the biosphere, the thin shell around the earth, where 90 % of the entire life persists between 3000 m above sea level to 90 m under the sea surface.

\* Corresponding author. E-mail: dragan.marinovic@zjzkv.org.rs  
doi: 10.2298/JSC090602013M

As the population of the earth increases, the problems of water quantity and quality are encountered and the problem of how to provide a sufficient quantity of good quality water for food production and the needs of the population must be addressed. The solutions seem to be the more efficient use of the water resources and the prevention of their pollution.<sup>1</sup>

Pollution of potable, surface and wastewaters has increased. Waters have become more and more polluted with both organic and inorganic matters. The most frequent polluters of organic origin are oil derivatives, organochloric insecticides (OCI), polychlorinated biphenyls and others. Jovančićević with collaborators has contributed substantially to the management of the issue of environmental pollution, primarily of waters and sediments.<sup>2-4</sup> They made quite a big contribution in the isolation, evidencing and determination of oil derivatives in various samples.

One of the major factors of water pollution is the application of synthetic toxic OCI in agriculture. Separate attention has been paid to their production and efficient application. Their degradation products have, however, been neglected, although they can produce detrimental effects for months and years after application of the insecticides.

The ever increasing application of organochloric insecticides and their stability in nature demand the need for the isolation, evidencing and determination of these active materials in various types of samples.

Due to their many-year production and wide and uncontrolled application, residues of organochloric insecticides can be found in samples from the ecosystem. Residues of these toxicants have been detected in different parts of the biosphere, confirming their presence and cycling in the environment.<sup>5</sup>

The degree of waters pollution is particularly high. In Serbia, according to regulations and by-laws, the maximal allowed concentration of total pesticides in drinking water is 0.5 µg/l.<sup>6-10</sup>

Some of most frequently used OCIs in agricultural production were tested in this study.  $\alpha$ -HCH is an organochloric insecticide used for the protection of forests. Lindane is a wide spectrum insecticide used for agricultural and non-agricultural purposes, including the treatment of seeds and soils, trees, trunks and stocked materials, animals against ectoparasites and in the area of medical protection. Heptachlorine has been used for over 30 years as a stomach and contact insecticide, mainly for the control of termites and earth insects. Aldrine is an organochloric insecticide previously used for termination of insects, *e.g.*, termites and hoppers, for the protection of crops such as potatoes and corn. This chemical is laboratory made and cannot be found in nature. Dieldrin is an organochloric insecticide used against termites, textile and agricultural pests and insects-spread diseases. It was mainly used for the protection of corn, cotton and potatoes. Endrin is an organochloric insecticide that has been used since used 1950 against a

large number of agricultural pests, primarily for the protection of cotton, rice, sugar cane, corn and other crops. DDT is the first chlorated insecticide used in agriculture, forestry and medical protection.<sup>11,12</sup>

The physicochemical properties of the analyzed OCIs are given in Table I.<sup>11,12</sup>

TABLE I. Physicochemical characteristics of the analyzed organochloric insecticides

Insecticide	Formula	Density ( $t / ^\circ\text{C}$ ), $\text{g}/\text{cm}^3$	Melting point, $^\circ\text{C}$	Solubility in water ( $t / ^\circ\text{C}$ ) $\text{mg}/\text{l}$
$\alpha$ -HCH	$\text{C}_6\text{H}_6\text{Cl}_6$	1.87 (20)	158	2 (28)
Lindane	$\text{C}_6\text{H}_6\text{Cl}_6$	1.85 (40)	112.8	10 (20)
Heptachlor	$\text{C}_{10}\text{H}_5\text{Cl}_7$	1.65–1.67 (25)	135–145	0.056 (20)
Aldrin	$\text{C}_{12}\text{H}_8\text{Cl}_6$	1.54 (20)	104–104.5	0.027 (25)
Dieldrin	$\text{C}_{12}\text{H}_8\text{Cl}_6\text{O}$	1.62 (20)	175–176	0.186 (20)
Endrin	$\text{C}_{12}\text{H}_8\text{Cl}_6\text{O}$	1.64 (20)	226–230	0.230 (25)
4,4-DDT	$\text{C}_{14}\text{H}_9\text{Cl}_5$	–	108.5–109.0	0.003 (20)

Pesticides, such as organochloric insecticides, are frequently removed from water by adsorption on active coal. The adsorption mechanism is of a physical nature (van der Waals attraction forces). The degree of adsorption is dependent on the structure and shape of the adsorbate molecules, the structure and size of the active coal pores, the adsorbate polarity, dissociation, temperature and pH value.

A number of papers<sup>13–15</sup> analyze the adsorption of certain kinds of pesticides onto commercially available active coals and onto carbon fibers. Gerard and collaborators<sup>13</sup> studied the adsorption of diurone, MCPA, atrazine and chloridazone onto Chemviron's F 400 coal and came to the conclusion that highest adsorption was that of diurone and lowest of MCPA. Martin-Gullon<sup>14</sup> compared the adsorption of atrazine on commercial Norit GAC 1240 and on Donacarbon carbon fiber and found that the adsorption efficiency was several times higher onto the carbon fibers. Schreiber and collaborators<sup>15</sup> studied the influence of temperature and molecule size on adsorption onto F 300 active coal and came to the conclusion that adsorption at elevated temperatures was better and that the adsorption of smaller molecules was favored.

Most studies were aimed at investigating the adsorption of individual pesticides from the derivatives groups comprising urea, pyridazinone, phenoxy acetic acid and triazine, with a much smaller number considering members of the group of chlorinated pesticides. Various types of pesticides are, however, simultaneously present in waters.

It is therefore of both theoretical and practical significance to investigate the adsorption capabilities of commercially available active coals for the simultaneous elimination of various types of pesticides, especially of OCI.

The present research was aimed at developing satisfactory procedures for the purification of waters contaminated with OCI, without changing the organoleptic properties of the waters. For this purpose, samples of both potable and waste water were used.

## EXPERIMENTAL

*Materials and analytical methods*

In this work, potable and waste waters sampled at the following locations were investigated:

1. Potable water from the tap at the Public Health Institute in Kraljevo and non-chlorinated water from the Konarevo pumping station, from where the City of Kraljevo is supplied with potable water.

2. Wastewaters from the Agricultural–Industrial Plant (PIK) Takovo and the Agricultural Cooperative (ZZ) Lunovo Selo.

PIK Takovo and ZZ Lunovo Selo both produce alcoholic and non-alcoholic products; hence, their waste waters are similar. Waste waters from PIK Takovo are discharged into the town collector from where they are led to the purification plant, purified and finally discharged into the Despotovica River.

Wastewaters from the Agricultural Cooperative Lunovo Selo are discharged into the Lužnica River (which is not categorized) that flows into the Skrapež River and later into the Zapadna Morava River.

The water samples were prepared according to the literature<sup>16</sup> or by means of modified standard methods.

Physicochemical analyses of the water samples were realized by volumetric methods (consumption of  $\text{KMnO}_4$ , content of Ca and Mg), electrochemical methods (pH value) and spectrophotometric methods (contents of nitrate, ammonium, Fe, chemical demand in oxygen (COD), biological demand in oxygen (BOD<sub>5</sub>), suspended matter, total organic carbon (TOC) and surface agents (detergents, DBS).

The instruments employed were a pH-meter (Hanna), a spectrophotometer (Lambda 2, Perkin Elmer) and a pastel UV (Secoman Analyzer).

The determinations of the organochloric insecticides, *i.e.*,  $\alpha$ -HCH, lindane, heptachlor, aldrin, dieldrin, endrin and DDT, were realized according to the Rule Book on the Hygienic Acceptability of Potable Water, FRY (Official Gazette No. 42/98 and 44/99).

The standards organochloric insecticides investigated in this work,  $\alpha$ -HCH, lindane, heptachlor, aldrin, dieldrin, endrin and DDT, were obtained from Dr. Ehrenstorfer GmbH (Augsburg, Germany).

The organochloric insecticides present were prepared according to the appropriate EPA-608 method, by liquid–liquid extraction. The method is equally applicable for the determination of organochloric insecticides in both potable and waste waters. The water sample was extracted with dichloromethane and the obtained extract was dried and concentrated to 1 cm<sup>3</sup>. The extract is evaporated in nitrogen flow and than 1 cm<sup>3</sup> of *n*-hexane is added. The tested organochloric insecticides were detected by gas chromatography using a Perkin Elmer 8500 instrument with an electron capture detector (ECD) and either a glass 1.5 % OV-17+1.95 % OV-210 or a capillary SPB-5 (30 m length) column. The oven temperature was maintained isothermally at 230 °C for the glass column or 250 °C for the capillary column.

Samples of potable and wastewaters were spiked with a standard mixture of organochloric insecticides and passed through the columns. The standard mixture consisted of  $\alpha$ -HCH, lindane, heptachlor, aldrin, dieldrin, endrin and DDT, which was diluted to a concentration that could be detected by the ECD.

Four columns, 60 cm high and 12 cm in diameter, containing different active coals were used for the elimination of OCI from the water samples. The columns were filled with active coal up to two thirds: Column 1 (K1) – active coal KRF, Column 2 (K2) – active coal K-81/B, Column 3 (K3) – active coal NORIT ROW-0.8 and Column 4 (K4) – active coal Aqua Sorb

CS. The active coals KRF and K-81/B are domestic productions (Miloje Zakić, Kruševac), while Norit Row-0.8 is a Dutch production, and Aqua Sorb CS is Swedish. The specifications of the adsorbing characteristics of these coals are presented in Table II.

TABLE II. Characteristics of the investigated active coals

Coal property	Active coal			
	KRF	K-81/B	Norit Row-0.8	Aqua Sorb CS
Total pores volume, cm <sup>3</sup> /g	0.8–1.0	0.8–1.0	–	0.62
Specific surface (BET), m <sup>2</sup> /g	1200	1200	1150	1100
Micro pores volume, cm <sup>3</sup> /g	0.45–0.5	0.45–0.50	–	–
Iodine number, mg/g	1150–1250	1150–1250	1050	1050
Methylene Blue index, cm <sup>3</sup>	16–18	16–18	22	–
Filling mass, kg/ m <sup>3</sup>	420–470	420–460	–	–

After filtering through qualitative filter paper REF 235 produced by Albert to remove the coarser impurities, the water samples were passed through all four columns, at a flow rate of 10 cm<sup>3</sup>/min. They were previously filtered.

#### RESULTS AND DISCUSSION

Based on the set investigation goal, results were obtained by testing the samples of potable water (tap water at the Public Health Institute in Kraljevo and from the Konarevo pumping station) and waste water (PIK Takovo and ZZ Lunovo Selo).

##### *Physicochemical analyses of the waters*

The physicochemical parameters of the waters were analyzed prior to and after passage through the columns.

Physicochemical characteristics of the water samples before passage through the columns are presented in Table III.

Physicochemical analyses of the potable water samples taken from the Public Health Institute and from the Konarevo pumping station show that these waters meet the standards set in the Rule Book FRY<sup>6</sup> on the hygienic acceptability of potable water (Table III).

The quality of the waste water from PIK Takovo is standardized by the Rule Book on prescribed values of dangerous and toxic matters discharged in the Municipality of Gornji Milanovac.<sup>17</sup> The standards of the Gornji Milanovac Municipality are extremely high in relation to the European ones and have to be harmonized accordingly.

In ZZ Lunovo Selo, they do not have any standards for their wastewater discharge into the non-categorized Lužnica River that flows into the Skrapež River and later into the Zapadna Morava River. The only quality-related criterion is that wastewaters must not alter the quality of the recipient into which they are discharged.

TABLE III. Physicochemical characteristics of the examined water samples

Parameter	Tap water <sup>a</sup>	Pumping station <sup>b</sup>	MAC <sup>1c</sup>	w.w. Takovo <sup>d</sup>	MAC <sup>2e</sup>	w.w. Lunovo S. <sup>f</sup>
pH value	7.8	8.0	6.8–8.5	4.9	6.5–9.0	5.0
Nitrates conc., mg/l	13.4	12.9	50.0	–	50.0	–
NH <sub>3</sub> conc., mg/l	0.038	0.050	0.100	1.70	50.0	6.892
Consumption of KMnO <sub>4</sub> , mg/l	5.4	6.0	8.0	183	–	118
COD, mg/l	–	–	–	305	460	146
BOD <sub>5</sub> , mg/l	–	–	–	74	300	69
Suspended matters, mg/l	–	–	–	246	500	180
Calcium conc., mg/l	40.1	44.1	200	50.0	–	76.2
Magnesium conc., mg/l	0.60	0.60	50	3.0	–	1.8
Iron conc., mg/l	0.061	0.052	0.30	–	–	–
TOC, mg/l	–	–	–	55	20	49
DBS, mg/l	–	–	–	3.6	–	9.0

<sup>a</sup>Potable water tap at the Public Health Institute in Kraljevo; <sup>b</sup>water taken at the Konarevo pumping station; <sup>c</sup>according to Book of Rules on hygienic adequacy of potable water FRY (Official Gazette no. 42/98 and 44/99); <sup>d</sup>waste waters taken at the Agricultural Industrial Plant Takovo; <sup>e</sup>according to the Gornji Milanovac Rule Book on prescribed values of dangerous and toxic matters discharged; <sup>f</sup>waste waters taken at the Agricultural Cooperative Lunovo Selo

The physico-chemical analyses revealed reduced pH values and increased concentrations of total organic carbon (Table III).

After passage through the columns, the water samples were subjected to physicochemical analyses. The results obtained with potable waters are presented in Table IV and with waste waters in Table V.

TABLE IV. Results of the physicochemical analyses of potable water, sampled at the Public Health Institute and at the Konarevo pumping station prior to and after passage through the active coal-containing columns

Parameter	Tap water					Pumping station					MAC
	Sample	Column				Sample	Column				
		K1	K2	K3	K4		K1	K2	K3	K4	
pH value	7.8	9.73	9.74	6.85	8.99	8.05	9.52	9.62	6.90	9.19	6.8–8.5
Nitrates conc., mg/l	13	1.6	2.3	<1.0	4.6	13	1.6	1.3	<1.0	3.7	50
NH <sub>3</sub> conc., µg/l	58	20	25	17	42	50	27	33	18	17	100
Consumption of KMnO <sub>4</sub> , mg/l	5.37	5.16	4.32	3.05	3.79	6.00	5.68	5.43	2.37	4.10	8.00
Calcium, mg/l	40.1	28.0	32.1	20.0	22.0	44.1	24.1	28.0	22.1	20.0	200
Magnesium, mg/l	0.60	0.21	0.60	0.21	0.41	0.60	0.25	0.41	0.28	0.30	50
Iron, µg/l	61	44	40	32	61	52	38	29	20	44	300

After passage of the water samples through the columns K1, K2 and K4, pH values measured were higher than allowed by the a.m. Rule Book. The ranges of the other tested physical and chemical parameters were within the limits pre-



scribed by the Rule Book. On passing the samples through K3 column filled with Norit Row-0.8 active coal, no change in the pH value was observed that exceeded the range set in the Rule Book (Table IV).

Passage of the waste waters of PIK Takovo and ZZ Lunovo Selo through the K1, K2, K3 and K4 columns, resulted in a high degree of purification in all cases. However, only the purified waste water from the K3 column had a pH value that was not above the maximum allowed value (Table V).

TABLE V. Results of the physicochemical analyses of the waste waters from PIK Takovo and Lunovo Selo, prior to and after passage through the active coal-containing columns

Parameter	w.w. Takovo						w.w. Lunovo S.				
	Sample	Column				MAC	Sample	Column			
		K1	K2	K3	K4			K1	K2	K3	K4
pH value	4.9	9.6	9.8	7.6	9.0	6.5–9.0	5.0	9.3	9.6	6.9	9.1
NH <sub>3</sub> conc., mg/l	1.7	0.083	0.050	0.020	0.22	50	6.9	0.34	0.13	0.12	0.64
Consumption of KMnO <sub>4</sub> , mg/l	183	36.3	39.5	23.4	25.8	–	118	19.8	41.4	18.4	25.8
COD, mg/l	305	3.6	6.4	2.2	3.5	460	146	7.9	25	5.6	8.3
BOD <sub>5</sub> , mg/l	74	1.3	2.6	0.9	1.5	300	69	3.3	12	2.5	3.7
Suspended maters, mg/l	246	29	38	8	12	500	180	44	62	11	15
Ca, mg/l	50	40	28	12	8.0	–	76	28	32	20	30
Mg, mg/l	3.0	1.8	1.8	1.6	1.8	–	1.8	1.8	1.4	0.60	0.60
TOC, mg/l	55	<1.0	1.9	1.0	1.0	20	49	2.7	8.1	2.4	2.5
DBS, mg/l	3.6	<1.0	<1.0	<1.0	<1.0	–	9.0	<1.0	1.1	<1.0	<1.0

#### OCI analysis of the waters

In the investigated waters, as well as in the spiked potable and waste waters, the contents of organochloric insecticides were determined prior to and after their passage through the active coal-containing columns.

The investigated organochloric insecticides were detected by means of gas chromatography, with the following detection limits:  $\alpha$ -HCH (0.0012  $\mu$ g/l), lindan (0.0015  $\mu$ g/l), heptachlor (0.0012  $\mu$ g/l), aldrin (0.0024  $\mu$ g/l), dieldrin (0.0014  $\mu$ g/l), endrin (0.0012  $\mu$ g/l) and DDT (0.0054  $\mu$ g/l).

The results obtained for the potable waters are presented in Tables VI and VII for the tap and pumping station water, respectively.

The total concentrations of OCI in the tap water (0.257  $\mu$ g/l) (Table VI) and in the pumping station water (0.294  $\mu$ g/l) (Table VII) meet the norm of the Rule Book on the hygienic acceptability of potable water that allows a maximum total content of pesticides of 0.5  $\mu$ g/l.

TABLE VI. The results of gas chromatographic analysis of OCl in potable and spiked potable water sampled from the tap at the Public Health Institute in Kraljevo, prior to and after having it passed through active coal containing columns

OCl, $\mu\text{g l}^{-1}$	Sample	Columns				Standard	Sample + standard	Columns				MAC <sup>a</sup>	
		K1	K2	K3	K4			K1	K2	K3	K4		
$\alpha$ -HCH	0.0	0.0	0.0	0.0	0.0	0.10	0.0	0.0	0.0	0.0	0.0	0.0	/
Lindane	0.043	0.038	0.039	0.023	0.035	0.10	0.12	0.058	0.067	0.050	0.054	0.054	0.20
Heptachlor	0.093	0.081	0.020	0.0	0.0	0.10	0.167	0.12	0.096	0.026	0.10	0.10	0.03
Aldrin	0.053	0.034	0.032	0.016	0.025	0.10	0.16	0.030	0.021	0.012	0.022	0.022	0.03
Dieldrin	0.028	0.004	0.017	0.000	0.025	0.10	0.18	0.0	0.045	0.0	0.0	0.0	0.03
Endrin	0.040	0.010	0.039	0.0	0.0	0.20	0.20	0.0	0.055	0.0	0.0	0.0	—
DDT	0.0	0.0	0.0	0.0	0.0	0.50	0.50	0.0	0.011	0.0	0.026	0.026	0.10
$\Sigma$	0.26	0.17	0.15	0.039	0.085	1.20	1.35	0.21	0.30	0.088	0.20	0.20	—
Adsorption, %	—	35.0	42.8	84.8	66.9	—	—	84.3	78.2	93.5	85.1	85.1	—

<sup>a</sup>According to Book of Rules on hygienic adequacy of potable water SRY (Official Gazette no. 42/98 and 44/99)

TABLE VII. The results of gas chromatographic analysis of OCl in potable and spiked potable water sampled from Konarevo pumping station, prior to and after having it passed through active coals containing columns

OCl, $\mu\text{g l}^{-1}$	Sample	Columns				Standard	Sample + standard	Columns				MAC <sup>a</sup>	
		K1	K2	K3	K4			K1	K2	K3	K4		
$\alpha$ -HCH	0.0	0.0	0.0	0.0	0.0	0.10	0.11	0.0	0.0	0.0	0.0	0.0	—
Lindane	0.057	0.0	0.050	0.0	0.0	0.10	0.15	0.10	0.095	0.070	0.095	0.095	0.20
Heptachlor	0.11	0.10	0.055	0.0	0.067	0.10	0.19	0.14	0.091	0.025	0.11	0.11	0.03
Aldrin	0.060	0.055	0.053	0.035	0.066	0.10	0.14	0.076	0.030	0.028	0.063	0.063	0.03
Dieldrin	0.0	0.0	0.0	0.0	0.0	0.10	0.089	0.0	0.0	0.0	0.0	0.0	0.03
Endrin	0.064	0.035	0.054	0.025	0.052	0.20	0.23	0.082	0.13	0.025	0.11	0.11	/
DDT	0.0	0.0	0.0	0.0	0.0	0.50	0.49	0.0	0.070	0.0	0.030	0.030	0.10
$\Sigma$	0.29	0.19	0.21	0.060	0.18	1.2	1.4	0.40	0.42	0.15	0.41	0.41	—
Adsorption, %	—	35.4	27.9	79.6	37.1	—	—	71.4	70.3	89.4	70.8	70.8	—

<sup>a</sup>According to Book of Rules on hygienic adequacy of potable water SRY (Official Gazette no. 42/98 and 44/99)

The analyses results obtained for the total and individual OCI in the water sampled at the Public Health Institute in Kraljevo after passage through the columns showed that best purification results were achieved with the K3 column (84.8 % removed).

Confirmation of purification efficiency was achieved by adding known concentrations of the corresponding OCI standards. The overall purification effect was even better, ranging from 78 to 93 %. The best purification efficiency (93.50 %) was exhibited with the K3 column (Table VI).

The obtained results of the total and individual OCI analyses in the water sampled at the Konarevo pumping station after its passage through the columns showed that the best purification results were obtained with the K3 column (79.60 %).

Confirmation of the purification efficiency was achieved by adding known concentrations of the corresponding OCI standards. The overall purification efficiency was even better and ranged from 70 to 89 %. The best purification effect (89.43 %) was achieved with the K3 column (Table VII).

The obtained analyses results for the examined waste waters are presented in Tables VIII and IX.

Determination of the elimination of the total and individual OCI from the waste waters from PIK Takovo and ZZ Lunovo Selo showed that the best purification of both waters was achieved with the K3 column with the removal efficiency ranging from 92 to 96 %.

The purification efficiency was confirmed by the addition of known concentrations of the corresponding OCIs standards (Tables VIII and IX).

#### CONCLUSIONS

The results obtained for two potable water samples and two waste water samples enabled the adsorption abilities of various types of commercially available active coals.

For both examined potable water samples (taken from the tap at the Public Health Institute in Kraljevo and from the Konarevo pumping station), which had similar physical properties and chemical compositions, as well both waste waters from two companies (PIK Takovo and ZZ Lunovo Selo), which had similar physical properties and chemical compositions, the best purification, *i.e.*, attainment of acceptable physical and chemical parameters and removal of the organochloric insecticides present, was achieved using the active coal of Swedish production - Norit Row-0.8.

Further research should be directed towards confirmation of the obtained results and finding a model for the efficient application of active coals with the ultimate goal of quality preservation of water resources.

The achievement of the prescribed physical and chemical parameters and the removal of organochloric insecticides present in potable waters and, especially, in

TABLE VIII. The results of gas chromatographic analysis of OCl waste water in spiked waste water sample taken at PIK Takovo, prior to and after having it passed through active coals containing columns

OCl, $\mu\text{g l}^{-1}$	Sample	Columns				Standard	Sample + standard	Columns			
		K1	K2	K3	K4			K1	K2	K3	K4
$\alpha$ -HCH	0.0	0.0	0.0	0.0	0.10	0.12	0.074	0.025	0.0	0.092	
Lindane	0.0	0.0	0.0	0.0	0.10	0.12	0.10	0.045	0.0	0.023	
Heptachlor	0.60	0.14	0.46	0.034	0.41	0.62	0.12	0.11	0.050	0.10	
Aldrin	0.11	0.020	0.085	0.0	0.066	0.20	0.065	0.081	0.037	0.055	
Dieldrin	0.382	0.065	0.095	0.010	0.12	0.48	0.065	0.15	0.0	0.13	
Endrin	0.12	0.040	0.035	0.0	0.052	0.29	0.074	0.040	0.0	0.055	
DDT	0.0	0.0	0.0	0.0	0.50	0.48	0.11	0.20	0.0	0.10	
$\Sigma$	1.20	0.24	0.67	0.044	0.64	2.31	0.61	0.65	0.087	0.56	
Adsorption, %	–	80.0	44.2	96.4	46.5	–	73.7	71.8	96.2	75.8	

TABLE IX. The results of gas chromatographic analysis of OCl waste water in spiked waste water sample taken from ZZ Lunovo Selo, prior to and after having it passed through active coals containing columns

OCl, $\mu\text{g l}^{-1}$	Sample	Columns				Standard	Sample + standard	Columns			
		K1	K2	K3	K4			K1	K2	K3	K4
$\alpha$ -HCH	0.51	0.11	0.14	0.061	0.18	0.58	0.034	0.052	0.015	0.089	
Lindane	0.0	0.0	0.0	0.0	0.10	0.075	0.066	0.056	0.025	0.045	
Heptachlor	0.46	0.18	0.22	0.025	0.14	0.55	0.14	0.071	0.015	0.12	
Aldrin	0.11	0.030	0.040	0.010	0.060	0.19	0.057	0.075	0.030	0.045	
Dieldrin	0.0	0.0	0.0	0.0	0.10	0.095	0.0	0.0	0.0	0.0	
Endrin	0.095	0.020	0.035	0.0	0.052	0.28	0.025	0.050	0.010	0.031	
DDT	0.0	0.0	0.0	0.0	0.50	0.45	0.0	0.0	0.0	0.0	
$\Sigma$	1.18	0.34	0.43	0.096	0.43	2.22	0.32	0.30	0.095	0.34	
Adsorption, %	–	70.7	63.4	91.9	63.3	–	85.5	86.3	95.7	84.9	

waste waters will be increasingly required if Serbia wished to join Europe and meet the European standards of waste water discharge into city collectors and rivers. The European standards are much stricter than the Serbian ones, which will impose the necessity of increased efficiency in waste waters purification.

## ИЗВОД

## ПРЕЧИШЋАВАЊЕ ВОДА И УКЛАЊАЊЕ ОРГАНОХЛОРИНИХ ИНСЕКТИЦИДА АКТИВНИМ УГЉЕМ

ДРАГАН МАРИНОВИЋ<sup>1</sup>, МАРИНА СТОЈАНОВИЋ<sup>2</sup> И ДАНИЛО ПОПОВИЋ<sup>2</sup>

<sup>1</sup>Завод за јавно здравље, Слободана Пенезића 16, 36000 Краљево и <sup>2</sup>Факултет заштитне на раду, Универзитет у Нишу, Чарнојевића 10а, 18 000 Ниш

Истраживања у овом раду односила су се на налажење задовољавајућих поступака пречишћавања вода контаминираних органохлорним инсектицидима, а да се, при томе, не промене органолептичка својства воде. У том циљу, за анализу су коришћени узорци пијаћих и отпадних вода. За одређивање концентрације ОНИ у узорцима воде коришћена је EPA-608 метода и принцип течно–течне екстракције. Поступак одстрањивања органохлорних инсектицида урађен је пропуштањем воде преко четири колоне, напуњене различитим активним угљевима: KRF, K-81/B, Norit Row-0.8 и Aqua Sorb CS. Ови активни угљеви су карбонизоване љуске кокосовог ораха активирани различитим поступцима. Добијени резултати указују на то да се најбољи ефекат пречишћавања пијаћих и отпадних вода постиже коришћењем колоне са Norit Row-0.8 пуњењем. Истраживања показују да се коришћењем колоне напуњене активним угљем Norit Row-0.8 могу ефикасно уклонити и мале количине органохлорних инсектицида, а да се при том не промене органолептичка својства воде, што задовољава захтеве процеса пречишћавања вода.

(Примљено 2. јуна, ревидирано 7. октобра 2009)

## REFERENCES

1. M. Kristoforović Plić, M. Radovanović, L. Vajagić, Z. Jeftić, R. Folić, S. Krnjetin, R. Obrknezev, *Communal Hygiene*, Prometej, Novi Sad, 1998, p. 13 (in Serbian)
2. B. Jovančičević, M. Antić, T. Solević, M. Vrvic, A. Kronimus, J. Schwarzbauer, *Environ. Sci. Pollut. Res.* **12** (2005) 205
3. M. Antić, B. Jovančičević, M. Ilić, M. Vrvic, J. Schwarzbauer, *Environ. Sci. Pollut. Res.* **13** (2006) 320
4. B. Jovančičević, M. Vrvic, J. Schwarzbauer, H. Wehner, G. Scheeder, D. Vitorović, *Water Air Soil Pollut.* **183** (2007) 225
5. D. R. Soldatović, *Toxicology of pesticides with analytics*, Economic Review, Belgrade, 1980, p.53 (in Serbian)
6. *Regulations on Hygienic Acceptability of Potable Water*, Official Gazette FRY, No. 42/98, 44/99, 1999 (in Serbian)
7. *Decision on the Maximum Allowed Concentrations of Radionuclides and Dangerous Matters in Inter-Republican Water Flows, Inter-State Waters and Waters of the Coastal Sea of Yugoslavia*, Official Gazette SFRY, No. 8/78, 1978 (in Serbian)
8. *Regulations on Dangerous Matters in Water*, Official Gazette of SR Serbia, No. 31/82, 1982 (in Serbian)

9. *By-Law on the Classification of Waters of Inter-Republican Water Flows, Inter-State Waters and Waters of Coastal Sea of Yugoslavia*, Official Gazette SFRY, No. 6/78, 1978 (in Serbian)
10. *By-Law on Water-Flow Categorization*, Official Gazette of SR Serbia, No. 5/68, 1968 (in Serbian)
11. B. Jovančičević, *Persistent Organic Pollutants, POPs*, Department of Chemistry, University of Belgrade, 2006 (in Serbian)
12. N. Mitić, *Pesticides in Agriculture and Forestry in Yugoslavia*, Economic Review, Belgrade, 1994, p. 90 (in Serbian)
13. M. C. Gerard, *Biotechnol. Agron. Soc. Environ.* **7** (2003) 79
14. M. Gullon, R. Font, *Water Res.* **35** (2001) 516
15. B. Schreiber, T. Brinkmann, V. Schmalz, E. Worch, *Water Res.* **39** (2005) 3449
16. B. Poček, *Potable Water, Standard Methods for Hygienic Acceptability Investigation*, Economic Review, Belgrade, 1990, p.179 (in Serbian)
17. *Rule Book on prescribed values for discharging dangerous and toxic matter*, Official Gazette of the Municipality of Gornji Milanovac, No. I/92, 1992 (in Serbian).



*J. Serb. Chem. Soc.* 75 (4) 587–594 (2010)



Journal of  
the Serbian  
Chemical Society

JSCS@tmf.bg.ac.rs • www.shd.org.rs/JSCS

UDC 543+061.3(4)

*EuCheMS news*

DIVISION OF ANALYTICAL CHEMISTRY  
EUROPEAN ASSOCIATION FOR CHEMICAL AND  
MOLECULAR SCIENCES

EUCHEMS NEWS

**European Analytical Column no. 38 from the Division of Analytical Chemistry (DAC) of the European Association for Chemical and Molecular Sciences (EuCheMS), January 2010**

(January 2010)

BO KARLBERG<sup>1</sup>, PAUL WORSFOLD<sup>2</sup> and JENS E. T. ANDERSEN<sup>3\*</sup>

<sup>1</sup>*Department of Analytical Chemistry, Stockholm University, SE-10691 Stockholm, Sweden,*

<sup>2</sup>*School of Geography, Earth and Environmental Sciences, University of Plymouth, Plymouth*

*PL4 8AA, UK and* <sup>3</sup>*Department of Chemistry, Technical University of Denmark, Building 207, DK-2800 Lyngby, Denmark*

A MESSAGE FROM THE CHAIRMAN OF DAC: "A FOCUS ON  
CONFERENCE FRAGMENTATION"

The Euroanalysis conference series constitutes the cornerstone activity of the Division of Analytical Chemistry (DAC) of the European Association for Chemical and Molecular Sciences (EuCheMS). Hence this column reports on the last Euroanalysis conference held in Innsbruck, Austria, in September 2009. The present column also follows up the pattern from the previous two columns; namely to invite a European analytical chemist to give his or her view on a certain topic of interest. This time Professor Paul Worsfold gives his personal view on water quality in the developing world.

The Euroanalysis conferences are organised every second year and the event in Innsbruck in 2009 was the 15<sup>th</sup> in the series. Euroanalysis conferences cover all aspects of Analytical Chemistry and doubts have been raised about organising such broad based conferences at a time when specialised and topic focused conferences are very popular. The discipline of Analytical Chemistry has long been subjected to fragmentation in that the formation of groups, clusters, societies or clubs is a common occurrence. Thus, experts in a particular area of analytical chemistry have a tendency to focus on their own specialisation. This is to some extent understandable but it is also a danger since new paradigms very often arise

\* Corresponding author. E-mail: jeta@dac-euchems.org; jeta@kemi.dtu.dk



when several scientific areas meet in a combined effort to solve a specific problem. So, consider the question “What kind of area-focused conference should the following analytical chemist attend?” This analytical chemist is working with beverages trying to develop methods for the determination of pesticides using advanced sampling, sample pre-treatment and separation methods, mass spectrometry detection and chemometrics to treat the data. There are specialised conferences for all these individual areas within analytical chemistry and also for specific applications such as beer, wine and pesticides. In addition, there are national and international divisions and/or societies focussed on, *e.g.*, “food”, “environment” and “chemometrics” that would be relevant and welcome this analytical chemist as a member and appreciate their contribution on advanced analytical techniques. Therefore why not go to a broad analytical chemistry conference such as Euroanalysis instead? The last Euroanalysis conference in Innsbruck attracted more than 700 attendees, demonstrating that this conference concept is still very viable and has a bright future.

The Division of Analytical Chemistry is open to all analytical chemists. Within this conference the existing “sub-groups” are welcome to organise thematic sessions so that experts can meet and disseminate their knowledge and at the same time be inspired by experts representing other sub-groups. The next Euroanalysis conference will be in Belgrade, Serbia, 11–15 September, 2011 (see <http://www.euroanalysis2011.rs>) and we really look forward to seeing you there! The year 2011 is also the International Year of Chemistry (see <http://www.chemistry2011.org>) which will add to the occasion.

#### PERSONAL VIEW

##### *Water Quality in the Developing World – Challenges for Analytical Chemistry*

In the previous European Analytical Column the challenges for Analytical Chemistry in the context of the European Union Policy for Sustainable Development were highlighted.<sup>1</sup> The key thematic areas considered were air quality, water quality and quantity, climate change and global poverty and development cooperation. Analytical Chemistry has a pivotal role to play in all of these areas over the next decade. With regard to water quality, for example, there is a growing need for *in situ* sensor technologies that can provide high temporal and spatial resolution data in real time, with an appropriate standard of data quality, to supplement techniques and methods for laboratory analysis.

##### *Water quality*

Water quality can be defined by its chemical, physical, and biological characteristics and needs to be considered in the context of whether it is fit for purpose. This will depend on its intended use, *e.g.*, agriculture, manufacturing, mining, human consumption, food production, recreation or for broader human and



ecosystem health. Water quality is impacted by natural processes (*e.g.*, seasonal trends, underlying geology and hydrology, weather and climate) and human activities (*e.g.*, agriculture, industry, environmental engineering). In order to achieve effective water quality management, a balance must be met between socio-economic pressures and environmental sustainability/protection. Good environmental monitoring operating within a robust legislative framework is an essential prerequisite for achieving that balance. Poor water quality can lead to lower agricultural yields and higher treatment costs for good quality potable water and water used by industry. In addition to having systems in place for water quality monitoring, the sources, transport, fate and persistence of chemical contaminants in the aquatic environment also need to be understood within local, national and international contexts. Key processes that impact on water quality include:

- eutrophication, *i.e.*, elevated nutrient concentrations leading to excessive algal growth and deoxygenation, due to diffuse run-off from agricultural land and point source discharges from wastewater treatment plants;
- diffuse and point source discharges/drainage from mining activities that increase acidity and dissolved metal concentrations;
- localised discharges of organic micropollutants, metals, radionuclides and nutrients from specific industries and domestic wastewater;
- saline intrusion into groundwater in coastal areas;
- erosion and sedimentation from, *e.g.*, deforestation, rainfall events (which are temporally and spatially highly variable) and engineering projects.

#### *Eutrophication*

Taking eutrophication as a specific example, there are many ecological and socio-economic drivers that require the reliable measurement of nutrients in natural waters. The oceans (coastal, shelf and open ocean waters) have been estimated to contribute ~21 trillion US\$ per year to human welfare (compared with a global GNP of ~25 trillion US\$).<sup>2</sup> Catchments and coastal waters of industrialised countries have received elevated inputs of nutrients for decades, in many cases giving rise to cultural eutrophication, *i.e.*, the anthropogenic enrichment of the environment with nutrients and the concomitant production of undesirable effects. Enhanced nutrient concentrations do not irrevocably lead to changes in the trophic status of natural water systems, but they are the primary cause where this occurs. Many areas of the globe are undergoing cultural eutrophication because of continuing population growth, urbanisation and industrialisation. Many undesirable effects resulting from nutrient enrichment have been documented, ranging from localised high concentrations of suspended algae to marked dissolved oxygen depletion and death of biota. The economic costs of these effects are potentially large, but are infrequently assessed. In addition, our understanding of the role of nutrients in the sequestration of atmospheric carbon by oceans is far

from complete. For example, subtropical oligotrophic (low nutrient and low biomass) areas of the ocean represent nearly half of the Earth's surface. These oceanic habitats, once thought to be homogenous and constant in time, exhibit transient pulses of carbon sequestration in response to episodic nutrient inputs. The significance of this phenomenon to carbon cycling is not known. Nutrient measurements in these environments are challenging because of the generally very low concentrations encountered. Furthermore, oceanic nutrient datasets have insufficient spatial and temporal coverage to satisfactorily test biogeochemical models of the global ocean.

Legislation and guidelines designed to protect vulnerable marine and freshwater environments has been introduced nationally and internationally. For example, the Paris, Helsinki and Barcelona Conventions, EU Directives (*e.g.*, Species and Habitats, Nitrates, Urban Wastewater and Water Framework), and USEPA guidelines. Remediation strategies require nutrient measurements to assess their efficacy, including the use of diagnostic models. Therefore nutrient measurements are critical, whether they are undertaken in a "monitoring" context, *i.e.*, mapping of the affected environment spatially and/or temporally, or used to examine key nutrient transport and cycling processes. The measurement of nutrients should include all of those fractions (dissolved inorganic and organic, particle-associated) that may be bioavailable within the timeframe(s) of the system's dynamics. Any effective decision support tool (conceptual model) for determining the causes and effects of eutrophication needs to link bottom-up causes with top-down consequences. The former requires information on nutrient inputs and biogeochemical cycling which, in turn, necessitates reliable analytical techniques.

#### *In situ analytical technologies*

There is a plethora of analytical methods for the determination of nutrients, particularly nitrogen and phosphorus species, in the aquatic environment. In recent years techniques such as flow injection analysis have become popular because of their portability, which allows remote (*in situ*) deployment in order to provide high quality analytical data with good temporal and spatial resolution.<sup>3</sup> The key requirements for *in situ* technologies include:

- easy to use, rugged and automated instrumentation;
- on-line or in-line devices to minimise contamination;
- sensitive and selective detection;
- elimination of matrix interferences;
- system stability (*e.g.*, reagents, standards, pumps, detector);
- on-board filtration and prevention of bio-fouling;
- remote calibration, validation and maintenance.

*Water quality in the developing world*

The challenges for providing good water quality are particularly acute in parts of the developing world, *e.g.*, in Africa. Increasing population growth and demand for water from food production and industry, loss of surface and ground-water resources and climate change, combined with a lack of stringent environmental safeguards, has led to serious concerns about water quality (and quantity), which threaten human health and the environment. To help address these concerns, increasing Africa's capacity in analytical chemistry is imperative. In order to support chemical monitoring and management activities there is an urgent need for scientifically qualified and practically trained personnel in relevant advanced analytical chemistry techniques. Thus, it is essential to create and support centres of excellence in analytical chemistry that involve a critical mass of experts in African universities (and other organisations).

The status of instrumentation in African Higher Education institutions is a critical issue which urgently needs to be addressed, not only at a government level, by the provision of funds to enable universities to access and maintain the required equipment but also, most importantly, by facilitating and sustaining the training of analytical chemists and associated staff. Optimisation of resources is crucial if funds are to be used wisely, *e.g.*, by establishing national and regional centres of excellence, with shared research facilities, as part of this effort.

The Pan Africa Chemistry Network,<sup>4</sup> co-ordinated by the Royal Society of Chemistry, is a good example of capacity building activities in this area. Activities include the commissioning, installation and maintenance of analytical instrumentation, facilitating networking activities of African and non-African scientists in water research and management and the provision of analytical training courses for researchers across Africa. The ultimate aim is to develop well-equipped chemical research communities by creating regional centres of excellence. It is important that these centres are supported, promoted and continuously funded.

The Division of Analytical Chemistry within the European Association for Chemical and Molecular Sciences (DAC-EuCheMS) is part of a network of European chemical societies and has members working in all fields of Analytical Science. One of its aims is to develop close links with related organisations all over the world. As part of this remit, support for capacity building in Analytical Science in the developing world would make an important contribution to tackling global issues such as water quality (and quantity) and climate change.

## INFORMATION FROM THE EUCHEMS DIVISION OF ANALYTICAL CHEMISTRY

Innsbruck was the venue of Euroanalysis 15<sup>5</sup> organised by Wolfgang Buchberger and Wolfgang Lindner. Despite much anxiety due to the global economic situation, the Conference was well attended, with over 700 participants from 53 countries presenting 130 lectures and 640 posters under the theme "The Impact

of Analytical Chemistry on the Quality of Life". Contributions were made from many areas of analytical chemistry and EUROANALYSIS maintained its position as one of the most important international broad spectrum analytical science conferences. Slavica Ražić is the Conference Chair for Euroanalysis 16 in Belgrade, Serbia, in 2011<sup>6</sup> with the motto "Challenges in Modern Analytical Chemistry". At the Annual Meeting of EuCheMS DAC in Innsbruck it was decided that Euroanalysis 17 will be held in Warsaw, Poland, on August 23–25, 2013. In the near future, analytical science will also be well represented at the 3<sup>rd</sup> EuCheMS Chemistry Congress on August 29 – September 2, 2010, in Nuremberg, Germany.<sup>7</sup>

At Euroanalysis 15 the Robert-Kellner Lecture sponsored by Springer-Heidelberg was awarded to Boris Mizaikoff, University of Ulm. The Robert-Kellner Lecture was established by EuCheMS DAC in memory of the late Prof. Robert Kellner of Vienna University of Technology, and the Robert-Kellner Lecture is awarded to scientists who qualify according to the statute: "This award shall distinguish a person who has made a substantial contribution to the advancement of Analytical Chemistry in research or education". The Austrian Society of Analytical Chemistry honoured two outstanding scientists with the prestigious awards: the Pregl Medal and the Emich Plaque. The Pregl Medal was awarded to Prof. Friedrich Lottspeich (Max-Planck-Institute, Martinsried, Germany), and the Emich Plaque to Prof. Harald Fuchs (University Muenster, Germany). Furthermore, Prof. Lindner was presented with the Martin Gold Medal of the Chromatographic Society.

Reiner Salzer offers a template for the development of a shared set of case studies which is available from the DAC/EuCheMS website. Scientists are encouraged to contribute case studies that are well suited to teaching in higher education. A new initiative was started to facilitate the formation of national or international consortia for education in Analytical Chemistry. The focus is on two aspects: *i*) achieving the highest scientific standard of education in Analytical Chemistry and *ii*) improving the employability of graduates from such programmes. Details can be found at *Anal. Bioanal. Chem.* **394** (2009) 649–653.

Hendrik Emons is the EuCheMS DAC liaison person to CITAC and he reported on new initiatives in legislation. In Germany, new legislation on accreditation was introduced as a result of harmonisation with new EU legislation. He also raised awareness of ISO Guide 99 on concepts and terminology of metrology which contains a lot of information relevant to analytical chemists. This guide, also known as VIM 3, is freely available at the BIPM webpage.<sup>9</sup> It is also important to enlighten students about the topic.

George Horvai of the DAC Bioanalytics Study Group reported that it is necessary to search ways to bring the analytical and bioanalytical chemistry communities closer together. Several analytical journals have moved strongly in the direction of bioanalytical chemistry, and a significant fraction of authors pub-

lishing bioanalytical papers in analytical chemistry journals come from outside traditional analytical workplaces. Moreover, important journals which have historically covered areas other than analytical chemistry have moved strongly into the analytical field. This report should initiate much debate on the position, development and teaching of Bioanalytics, which is one of the largest single subject areas within the range of analytical disciplines. The challenges include proteomics and analysis of GMOs. It should be stressed that the approaches and procedures used in Analytical Chemistry also apply to Bioanalytics. The Delegates expressed concern about a lack of formal education in Chemistry for those working in the Bioanalytics field, which may pose a problem in the interpretation of results obtained by analytical chemistry methodologies.

Bioanalytical chemistry is also considered one of the emerging issues of the Analytical Chemistry Division (ACD) of IUPAC. Indeed at the 2009 IUPAC Congress in Glasgow there was a high proportion of biochemistry presentations. In the Analytical Chemistry Division, work on a new edition of the Orange Book has just started and Jose Pingarron and Jan Labuda are responsible for a chapter on bioanalytical methods in the methodological section of the Orange Book. Jan Labuda, a titular member of the Analytical Chemistry Division of IUPAC (2006–2009) and chair of the task group of IUPAC project No. 2006-026-1-500 entitled “Electrochemical DNA-based biosensors: terms and methodology“, organised a project workshop in Seville, Spain, on 6 September, 2008 and lead the preparation of an IUPAC technical report on the subject.

It was reported by IRMM of the European Commission that calls have been announced on the CORDIS webpage for topics in the areas of Problem Solving, Decision Making, Method Development, Competitiveness, Fundamentals and Environment, and funding of 400 M Euro has been allocated for Metrology over the next seven years. There is no specific Analytical Chemistry call. Electrochemistry topics, including those that are analytical chemistry orientated, are funded by 35 M Euro per year in a three year programme. Calls under Energy are closing in November 2010. Positions are available for young scientists at IRMM. Moreover, analytical laboratories which can execute appropriate validated methods can apply for participation in IRMM’s reference material programme (<http://irmm.jrc.ec.europa.eu>).

Bo Karlberg announced his retirement as Chair of EuCheMS DAC in 2010, and encourages the Delegates of member societies to nominate candidates to be elected at the Annual Meeting in Nuremberg in conjunction with the 3<sup>rd</sup> EuCheMS Conference on Chemistry.<sup>7</sup> The website of EAConweb will continue to be maintained by DAC/Bo Karlberg with the support of the Swedish Chemical Society.

## REFERENCES

1. European Analytical Column No. 37, DAC-EuCheMS, January 2009, <http://www.dac-euchems.org/dac> (March 2010)
2. R. Costanza, R. d'Arge, R. de Groot, S. Farber, M. Grasso, B. Hannon, K. Limberg, S. Naeem, R. V. O'Neill, J. Paruelo, R.G. Raskin, P. Sutton, M. van den Belt, *Nature* **387** (1997) 253
3. S. Gray, G. Hanrahan, I. McKelvie, A. Tappin, F. Tse, P. Worsfold, *Environ. Chem.* **3** (2006) 3
4. *Royal Society of Chemistry*, <http://www.rsc.org/Membership/Networking/International-Activities/PanAfrica/> (March 2010)
5. *Euroanalysis 2009 Conference*, <http://www.euroanalysis2009.at> (March 2010)
6. *Euroanalysis 2011 Conference*, <http://www.euroanalysis2011.rs> (March 2010)
7. *3<sup>rd</sup> EuCheMS Chemistry Congress*, <http://www.euchems-congress2010.org> (March 2010)
8. *Austrian Society of Analytical Chemistry*, <http://www.asac.at> (March 2010)
9. *Bureau International des Poids et Mesures*, <http://www.bipm.org> (March 2010)
10. *Department of Analytical Chemistry, Stockholm University*, <http://www.anchem.su.se/euchems/countries.asp> (March 2010).